

INHIBITORS OF *MYCOBACTERIUM TUBERCULOSIS* DOSRST SIGNALING AND
PERSISTENCE

By

Huiqing Zheng

A DISSERTATION

Submitted to
Michigan State University
in partial fulfillment of the requirements
for the degree of

Microbiology and Molecular Genetics – Doctor of Philosophy

2017

ABSTRACT

INHIBITORS OF *MYCOBACTERIUM TUBERCULOSIS* DOSRST SIGNALING AND PERSISTENCE

By

Huiqing Zheng

Tuberculosis (TB) is one of the most deadly infectious diseases in human history and is caused by the bacterium *Mycobacterium tuberculosis* (Mtb). Current TB therapy requires 6-9 months of treatment with four different antibiotics, including isoniazid, rifampin, ethambutol and pyrazinamide. However, due to the long course of TB therapy and the evolution of drug-resistant Mtb strains, first-line anti-mycobacterial drugs are not sufficient to control the TB epidemic. Therefore, it is urgent to develop new drugs with novel targets to shorten the course of therapy, control the spread of drug-resistant TB and eradicate this deadly disease.

In response to host immune cues, Mtb modulates its metabolism to establish a state of low metabolic activity called non-replicating persistence (NRP). DosRST is a two-component regulatory system that plays an essential role to establish and maintain NRP in Mtb. It is induced by host immune stimuli, such as hypoxia, carbon monoxide and nitric oxide, through the histidine kinase sensors DosS and DosT. The response regulator DosR regulates about 50 genes in the dormancy regulon. NRP bacilli are problematic because 1) they are insensitive to several anti-mycobacterial agents and drive the long course of TB therapy; and, 2) they can resuscitate for growth once the immune system weakens for infectious transmission of the Mtb. Therefore, inhibiting the DosRST pathway may help reduce the population of NRP bacteria during infection and thus function to reduce drug tolerance and shorten TB treatment.

This dissertation presents a whole-cell phenotypic high-throughput screen of a ~540,000 compound small-molecule library. The screen employed a DosR-dependent,

hypoxia-inducible fluorescent reporter strain, CDC1551(*hspX::GFP*), and successfully identified six distinct, novel chemical inhibitors of DosRST signaling, named HC101A-106A. Physiological and mechanistic studies were performed to characterize HC101-104 and HC106A. All five inhibitors are shown to inhibit genes of the DosRST regulon and persistence-associated physiologies, such as triacylglycerol accumulation. HC101A, HC102A, HC103A and HC106A also reduce Mtb survival when cultured under strongly hypoxic conditions. UV-visible spectroscopy studies show that HC101A (artemisinin) and HC106A target the heme group of sensor kinases DosS/T via distinct mechanisms. For example, artemisinin modulates the redox status of DosS/T and alkylates the heme to form artemisinin-heme adducts, whereas HC106A interacts with DosS heme. In contrast, HC102A and HC103A do not target the heme group, but instead inhibit sensor kinase autophosphorylation activity. Electrophoretic mobility assays suggest that HC104A functions by directly inhibiting DosR DNA binding activity. Overall, this dissertation provides proof-of-concept that multiple components of the DosRST pathway can be targeted by small molecules to inhibit Mtb persistence and antibiotic tolerance.

Additionally, this dissertation presents the discovery of a new chemical inhibitor, HC2091, that kills Mtb by targeting the mycolic acid transporter MmpL3. MmpL3 is an essential protein that functions to transport trehalose monomycolate across mycomembranes for trehalose dimycolate biosynthesis. HC2091 is bactericidal against Mtb in a dose- and time-dependent manner *in vitro*. It also has activity against Mtb inside of macrophages. Whole genome sequencing spontaneous mutants resistant to HC2091 identified five single nucleotide variants primarily located in the C-terminus of MmpL3, and HC2091-treated Mtb exhibits decreased mycolic acid synthesis, thus supporting that MmpL3 is the target of HC2091.

I dedicate this work to
my parents Jiahe Zheng and Aiyu Huang,
and to my wife Annie Yang

ACKNOWLEDGEMENTS

First, I would like to thank my mentor Robert B. Abramovitch for having me in the lab to work on such wonderful projects that have kept my interests for the duration of my studies. As well, he has provided me guidance and mentorship throughout my graduate career at Michigan State University and has been so supportive of me throughout my graduate career. His positive attitude has always encouraged me to be in the field of science and made me enthusiastic about science. I have been trained critically and scientifically through his time and effort.

Second, I would like to thank Bob R. Hausinger, Lee Kroos, Linda S. Mansfield and Chris M. Waters for being on my guidance committee and providing helpful suggestions each time we had committee meetings. I am also grateful for Mark Farrugia for his assistance with UV-visible spectroscopy assay, Lijun Chen for her help with mass spectrometry analyses, and Chris Colvin and Ben Johnson for their support and data collection in the high-throughput screens, that identified the compounds studied in this dissertation. I would like to thank our collaborators, Scott D. Larsen, Paul D. Kirchhoff, Michael Wilson, and Edmund Ellsworth for their contributions to these studies.

Third, I would like to thank my fellow lab mates, Jake Baker, Javiera Ortiz, Rajni Goyal, Garry Coulson, Uma Gautam, Shelby Dechow, and John Williams for their support and our regular scientific discussions that helped accelerate my research and created such a friendly and joyful work environment. Special thanks also go to undergraduate students I mentored, Katriana Jorgensen-Muga, Marilyn Werner, Sharon-Rose Nartey, and Ryan Borchert for their assistance with these projects. Our work together advanced these projects and really taught me how to be a good mentor.

Fourth, I would like to thank the Biomolecular Science program for bringing me to MSU, and the MMG department for always backing me up whenever I ran into problems. Staff in the MMG office have been always helpful to keep my studies on track. I would like to acknowledge the Bill and Melinda Gates Foundation, the National Institutes of Health, a G.D. Edith Hsiang and Margaret Everett Kimball Scholarship, and a Dissertation Completion Fellowship for financial support for my research, without which I would have been be unable to conduct this research.

Last, but not least, my family. My heartfelt gratitude to my parents for their endless care throughout my life. Although they can't fully understand my work, they are always with me wherever I go, and give me spiritual support for whatever I am doing. After we immigrated to the US, they worked tirelessly to support me and my brother to pursue the higher education that they couldn't have. I am very proud of myself to be the first college student, and now the first Ph.D. in my entire family. Without their support, I wouldn't be able to move to the stage where I am today. Also, I am grateful that I met and married my wife Annie Yang during graduate school. I am very lucky to have her standing side by side with me and aiding me through my graduate school life.

TABLE OF CONTENTS

LIST OF TABLES	x
LIST OF FIGURES	xi
KEY TO ABBREVIATIONS.....	xiv
CHAPTER 1 - Strategies for controlling bacterial persistence	1
Introduction.....	1
Therapeutic strategies to control bacterial persistence	2
Modulation of metabolism reverts persisters to an antibiotic susceptible state.....	2
Reactive oxygen species sensitize persister cells to antibiotic treatment	4
Enhancing antibiotic uptake promotes killing of persisters.....	8
Targeting stationary phase respiration to inhibit persisters	9
Targeting bacterial proteases to kill persisters.....	11
Modulating intracellular ATP levels to kill persisters	13
Disrupting membrane integrity to kill persisters	14
Inhibition of cell envelope biosynthesis potentiates killing of persisters by antibiotics...	16
Targeting two-component regulatory systems to inhibit bacterial persistence.....	18
Concluding remarks	23
REFERENCES	25
CHAPTER 2 - Inhibitors of <i>Mycobacterium tuberculosis</i> DosRST signaling and persistence ...	35
Summary	36
Introduction.....	37
Results.....	38
Discovery of DosRST regulon inhibitors	38
Artemisinin, HC102A and HC103A disrupt persistence.....	46
Artemisinin targets DosS and DosT sensor kinase heme	50
HC103A inhibits DosS and DosT autophosphorylation.....	56
Discussion	58
Materials and methods	60
Bacterial strains and growth conditions.....	60
High-throughput screening assay and data analysis	61
Transcriptional profiling and data analysis.....	63
Real-time PCR assays.....	64
Triacylglycerol accumulation analysis	64
NRP survival and antibiotic tolerance assays	65
DosS and DosT protein purification	66
UV-visible spectroscopy assay and mass spectrometry.....	67
DosS and DosT autophosphorylation assay.....	67
Structural modeling of DosT and the G85L and G115L substituted proteins	68
Chemical synthesis of HC102A (CCG-232500) and HC103A (CCG-257424).....	69

Acknowledgments.....	69
APPENDIX.....	70
REFERENCES	86

CHAPTER 3 - Chemical inhibition of the *Mycobacterium tuberculosis* DosRST two-component regulatory system by targeting sensor kinase heme and response regulator DNA binding 93

Summary	94
Introduction.....	95
Results.....	97
Inhibition of the DosR regulon by HC104A and HC106A.....	97
Inhibition of Mtb persistence-associated physiologies.....	103
HC104A inhibits DosR DNA binding.....	104
HC106A modulates DosS heme.....	108
Synergistic interactions between DosRST inhibitors.....	109
Structure-activity relationship study for HC104A and HC106.....	112
Discussion.....	114
Materials and methods.....	118
Bacterial strains and growth conditions.....	118
EC ₅₀ assays.....	118
Transcriptional profiling and data analysis.....	119
Real-time PCR assays.....	119
TAG biosynthesis.....	120
NRP survival assays.....	120
DosR protein purification.....	121
Electrophoretic mobility assay.....	121
UV-visible spectroscopy assay.....	122
Checkboard synergy studies.....	122
Autophosphorylation assay.....	123
Kinetic solubility assay.....	123
Acknowledgments.....	123
APPENDIX	125
REFERENCES	144

CHAPTER 4 - HC2091 kills *Mycobacterium tuberculosis* by targeting the MmpL3 mycolic acid transporter 149

Summary	150
Introduction.....	151
Results.....	152
HC2091 kills Mtb <i>in vitro</i> and in macrophages.....	152
HC2091 resistant strains have mutations in <i>mmpL3</i>	157
Inhibition of mycolic acid biosynthesis by HC2091.....	159
Transcriptional analysis of Mtb treated with HC2091 and SQ109.....	159
HC2091 has no effect on Mtb membrane potential.....	160
Structure-activity relationship studies.....	163
Discussion.....	165
Materials and methods	167

Bacterial strains and growth conditions.....	167
EC ₅₀ determination and spectrum of activity in other mycobacteria and non-mycobacteria	167
Bactericidal activity of HC2091	168
Activity of HC2091 against intracellular Mtb	169
Whole genome sequencing to identify the target of HC2091	169
Mycolic acid accumulation analysis	169
Transcriptional profiling and data analysis.....	169
Membrane potential	169
Structure activity relationship (SAR) and eukaryotic cytotoxicity of HC2091	170
Kinetic solubility assay	170
Acknowledgments.....	172
APPENDIX.....	173
REFERENCES	181
CHAPTER 5 - Concluding Remarks	187
REFERENCES	194

LIST OF TABLES

Supplementary Table 2.1. GFP fluorescence inhibition and eukaryotic cytotoxicity by DosR regulon inhibitors.....	73
Supplementary Table 2.2. Small molecule screening data.....	74
Supplementary Table 3.1. Structure and properties of HC104 series.....	127
Supplementary Table 3.2. Initial SAR studies of the HC106 series.....	128
Supplementary Table 3.3. Initial Topliss Tree evaluation of “A-ring” aniline of series HC106.....	129
Table 4.1. Identification of HC2091 resistance mutations.....	158
Table 4.2. HC2091 Structure activity relationship study.....	164
Supplementary Table 4.1. Spectrum of activity of HC2091.....	175
Supplementary Table 4.2. Cytotoxicity of HC2091 analogs.....	176
Supplementary Table 4.3. Solubility of HC2091 analogs.....	177

LIST OF FIGURES

Figure 1.1. Summary of major pathways that can be targeted to kill persisters.	6
Figure 1.2. Structures of different classes of select inhibitors that kill persister cells.....	7
Figure 2.1. Discovery of inhibitors of the DosRST pathway.	44
Figure 2.2. Transcriptional profiling shows artemisinin, HC102A and HC103A inhibit the core genes of the DosRST regulon during hypoxia.....	45
Figure 2.3. Artemisinin, HC102A and HC103A inhibit TAG synthesis, survival and isoniazid tolerance.....	49
Figure 2.4. Artemisinin directly inhibits DosS and DosT by targeting sensor kinase heme.	54
Figure 2.5. Amino acid substitutions in DosS or DosT promote resistance to artemisinin.....	55
Figure 2.6. HC103A inhibits DosS and DosT autophosphorylation.....	57
Supplementary Figure 2.1. Statistical analysis of HTS controls.	75
Supplementary Figure 2.2. Identification of inhibitors of the DosRST pathway.	76
Supplementary Figure 2.3. Transcriptional profiling shows artemisinin, HC102A and HC103A inhibit the core genes of the DosRST regulon during hypoxia.....	77
Supplementary Figure 2.4. Artemisinin, HC102A and HC103A inhibit TAG synthesis, survival and isoniazid tolerance during NRP.	78
Supplementary Figure 2.5. Artemisinin directly modulates DosS and DosT (G85L) heme in a dose-dependent manner.	79
Supplementary Figure 2.6. HC102A and HC103A do not modulate DosS redox.	80
Supplementary Figure 2.7. Substitutions in DosT provide resistance to artemisinin.	81
Supplementary Figure 2.8. Modulation of DosS and DosT kinase activities by HC102A and HC103A.	82
Figure 3.1. HC104A and HC106A inhibit DosRST reporter fluorescence.	100
Figure 3.2. Transcriptional profiling shows HC104A and HC106A inhibited DosR regulon during hypoxia.....	101

Figure 3.3. Inhibition of DosR regulon and persistence-associated physiologies by HC104A and HC106A.	102
Figure 3.4. Inhibition of DosR DNA-binding by HC104A.	106
Figure 3.5. Interactions between HC106A and DosS heme.	107
Figure 3.6. Synergistic interactions between DosRST inhibitors.	111
Supplementary Figure 3.1. Inhibition of the DosR regulon by HC104 and HC106A during hypoxia.	130
Supplementary Figure 3.2. TLC of TAG reduction in Mtb treated with HC104A and HC106A.	131
Supplementary Figure 3.3. Autoradiograph examining the impact of HC104A and HC106A on DosS autophosphorylation.	132
Supplementary Figure 3.4. Investigation of interaction between HC104A and DosS.	133
Supplementary Figure 3.5. The impact of virstatin on DosR DNA-binding and DosRST signaling in Mtb.	134
Supplementary Figure 3.6. Investigating the interaction between HC106A and DosS heme.	135
Supplementary Figure 3.7. Checkerboard assays examining paired interactions of DosRST inhibitors.	136
Supplementary Figure 3.8. Synthetic scheme for the HC106 analogs.	138
Supplementary Figure 3.9. Comparison between artemisinin, HC103 and HC106 for interactions.	139
Figure 4.1. HC2091 is bactericidal to Mtb.	155
Figure 4.2. HC2091 is active against intracellular Mtb and inactive against non-replicating Mtb ...	156
Figure 4.3. HC2091 inhibits TDM accumulation.	161
Figure 4.4. Shared transcriptional profiles between HC2091 and SQ109.	162
Supplementary Figure 4.1. Dose-response curves for HC2091 resistant mutants.	178
Supplementary Figure 4.2. The map of HC2091 resistance substitutions on the MmpL3 protein.	

.....	179
Supplementary Figure 4.3. Impact of HC2091 on Mtb membrane potential.	180

KEY TO ABBREVIATIONS

ADEP	Acyldepsipeptides
Art	Artemisinin
CCCP	Carbonyl cyanide <i>m</i> -chlorophenyl hydrazone
CFU	Colony forming units
CI	Combination Index
DCM	Dichloromethane
DHA	Dihydroartemisinin
DMF	Dimethylformamide
DMSO	Dimethyl sulfoxide
DTN	Dithionite
EC ₅₀	Half maximal effective concentration
EMSA	Electrophoretic mobility shift assay
ETC	Electron transport chain
FI	Fluorescence inhibition
GFP	Green fluorescence protein
GI	Growth inhibition
HTS	High-throughput screen
INH	Isoniazid
LC/MS	Liquid chromatography/mass spectrometry
MRSA	Methicillin-resistant <i>Staphylococcus aureus</i>
MSSA	Methicillin-sensitive <i>Staphylococcus aureus</i>

Mtb *Mycobacterium tuberculosis*
NRP Non-replicating persistence
OADC Oleic acid, albumin, dextrose, catalase
OH• Hydroxyl radical
PMF Proton motive force
ROS Reactive oxygen species
Sar structure-activity relationship
TAG Triacylglycerol
TDM Trehalose dimycolate
THF Tetrahydrofuran
TMM Trehalose monomycolate
TB Tuberculosis
TLC Thin-layer chromatography
WT WILD TYPE

CHAPTER 1 - Strategies for controlling bacterial persistence

Introduction

During the golden era of antibiotic discovery, between 1940 and 1960, many new antibiotics were discovered that are still currently in use to treat different infectious diseases (1). However, over time, antibiotics have become less effective at controlling bacterial infections. Treatment failure is due, in part, to the rise of drug resistant strains that have acquired genetic elements to inactivate or efflux antibiotics or strains with mutations in drug targets that modulate drug-target interactions. Another factor driving treatment failure is the phenomenon of bacterial persistence, which was first described by Hobby *et al.* in 1942 (2). At that time, scientists noticed that there was always a small fraction of a treated *Staphylococcus aureus* population that tolerated killing by penicillin. Pre-treatment of bacteria under stressful conditions, such as cold, or acidic pH, arrested bacterial replication and enhanced tolerance to antibiotics (2, 3). These populations of bacteria were referred to as persister cells.

Biphasic killing is often observed for bacterial cultures exposed to antibiotics under growth permissive conditions (4). Treatment with antibiotics initiates rapid killing of the majority of bacteria in a population, however, a population of persister cells will often remain that are completely tolerant to the antibiotic. These persister cells are responsible for phenotypic tolerance to antibiotics. There are two different classes of bacterial persistence observed: Class I persistence is driven by a small sub-population of dormant bacteria (<0.1%) that naturally tolerates antibiotics (5); Class II persistence is induced when the bacterial population responds to stress conditions, such as hypoxia, acidic pH, or nutrient starvation (6). Class II bacterial persistence is also observed

during infections where bacteria in the host are exposed to stressful conditions that trigger a population of bacteria to cease replication and become persistent. Both classes of bacterial persistence cause antibiotic tolerance and treatment failure. For example, *Mycobacterium tuberculosis* (Mtb) requires a 6-month long course of therapy. This long course is driven, in part, by the difficulty of killing all of the persistent, drug-tolerant bacteria that are naturally associated with tuberculosis (TB) infection. Recent studies have advanced our understanding of bacterial persistence, and have highlighted different strategies to target each class. This introduction will survey recent approaches to controlling bacterial persistence with an emphasis on Mtb and other select Gram-negative and Gram-positive bacteria. The reader is directed to other recent reviews for additional information on mechanisms of controlling bacterial persistence (6, 7).

Therapeutic strategies to control bacterial persistence

Modulation of metabolism reverts persisters to an antibiotic susceptible state

Bacteria have evolved to maintain a sub-population of dormant cells that are naturally tolerant to antibiotic treatment, known as class I persisters. One signature of these dormant bacteria is their partially inactive metabolism. Antibiotics usually can kill the majority of cells by targeting essential cellular functions required for growth, such as transcription, protein synthesis, and cell wall synthesis. The reduced activity of these essential cellular processes in non-growing cells can diminish the effectiveness of antibiotics and induce phenotypic antibiotic tolerance. Therefore, this subpopulation can function to prevent eradication of the population during drug treatment.

One approach to target the class I persister population is by making them susceptible to antibiotics by re-initiating their metabolism. Allison *et al.* have reported that providing additional

metabolites is a strategy to eradicate persisters (8). Adding glucose, mannitol, or fructose, carbon sources that feed glycolysis, potentiates gentamicin killing of *Escherichia coli* and *S. aureus* persisters (Fig. 1.1). The killing is facilitated by the generation of a proton-motive force (PMF) by stimulation of metabolism and the electron transport chain (ETC). NADH produced from central metabolism is oxidized by the enzymes of the ETC, and thus activates the PMF required for the uptake of gentamicin. Interestingly, even though these exogenous metabolites stimulate metabolism, the growth of the persisters is not resumed. Therefore, other antibiotics that target cell-wall biosynthesis and DNA replication are still ineffective to kill persisters together with these metabolites. In a separate study glucose was also shown to potentiate class I *S. aureus* persister killing by daptomycin. However, this killing is not through a PMF-dependent mechanism (9). It is postulated that glucose triggers carbohydrate transport proteins to potentiate daptomycin activity or induces daptomycin-specific lysis of cells. However, further experiments are needed to determine the mode of action.

Enhancement of antibiotic killing by addition of metabolites supports a model of overcoming persistence by “waking up” the dormant persister cells. Once the cells are replicating they may be more susceptible to antibiotics. For example, Marques *et al.* have shown that treating *E. coli* or *Pseudomonas aeruginosa* persisters with the fatty acid signaling molecule *cis*-2-decenoic acid stimulates dormant cells into a metabolically active state, and activates transcription and increases protein synthesis (10). In combination with antimicrobials, such as ciprofloxacin, tobramycin, or tetracycline, *cis*-2-decenoic acid causes decreased cell viability when treated with antimicrobials and a reduction of persister cells in *E. coli* and *P. aeruginosa*. Therefore, reprogramming the metabolism of persister cells to become active can function to control persisters. Stimuli that jump-start different metabolic activities, such as activating RNA

transcription, protein synthesis machinery, or cell wall synthesis, may selectively potentiate specific classes of antibiotics to eradicate persister cells.

Reactive oxygen species sensitize persister cells to antibiotic treatment

Persister cells that are present within a bacterial population have enhanced survival under a variety of stress conditions (11). However, numerous reports have shown that persisters are sensitive to specific intracellular stress signals, such as reactive oxygen species (ROS) (Fig. 1.1). Morones-Ramirez *et al.* reported that ionic silver (Ag^+) is not only bactericidal to a broad spectrum of Gram-negative and Gram-positive bacteria, but also kills class I bacterial persister cells when a non-bactericidal dose of Ag^+ is used in combination with different classes of antibiotics, such as gentamicin, ofloxacin and ampicillin (Fig. 1.1) (12). Mechanistic studies show that Ag^+ induces hydroxyl radical ($\text{OH}\bullet$) production via Fenton chemistry. This is further supported by increasing Fe^{2+} release as a result of disturbance of iron hemostasis by disrupting Fe-S clusters. Furthermore, TCA cycle knockout mutants, including $\Delta icdA$, $\Delta sucB$, Δmdh , and $\Delta acnB$, are all less susceptible to Ag^+ treatment due to reduced production of $\text{OH}\bullet$, suggesting generation of $\text{OH}\bullet$ is likely driven by disruption of metabolic pathways. By using a fluorescent dye, propidium iodide, impermeable to cell membrane, it was found that Ag^+ treatment increases membrane permeability by destabilizing cell envelope to facilitate uptake of antibiotics.

Another report by Grant *et al.* also shows that increasing ROS in *Mycobacterium smegmatis*, by incubating the culture under aerobic conditions with dissolved-oxygen saturation of 95%, potentiates killing of class I persisters by antibiotics (13). The oxygen-dependent phenotype is rescued by adding the $\text{OH}\bullet$ scavenger thiourea, suggesting that persisters are sensitive to ROS. Supporting this model, treating *M. smegmatis* persister cells with the $\text{OH}\bullet$ producing

antibiotic clofazimine eradicates persisters. A similar phenomenon is also observed in *M. tuberculosis*. Treating *M. tuberculosis* with high concentrations of vitamin C completely sterilizes the cultures (Fig. 1.1) (14). The killing is driven by increasing ROS production through Haber-Weiss and Fenton reactions. A high concentration of vitamin C also increases the level of ferrous ion through reduction of ferric ion. Ferrous ion reacts with oxygen to produce ROS, and causes DNA damage, lipid alterations and redox stress. Isoniazid (INH) cannot sterilize a culture due to the presence of persisters, however, when INH is used in combination with vitamin C, at sub-lethal doses, INH can sterilize the culture. Furthermore, a recent report by Vilcheze *et al.* demonstrates that treating *M. tuberculosis* with cysteine and INH sterilizes the bacterial culture (Fig. 1.1) (15). Cysteine functions as a reductant like vitamin C that can quickly reduce ferric ion to ferrous ion, which leads to increased accumulation of ROS in the presence of oxygen. Addition of cation scavengers, such as the iron chelator deferoxamine, diminishes sterilization, and the combination of cysteine and rifampin causes no additional killing to Mtb cultures grown in anaerobic conditions. These findings indicate that potentiation of killing by addition of cysteine is dependent on cations and oxygen. Lastly, treating cultures with cysteine and INH increases oxygen consumption of non-respiring cells, as well as shifting the balance of menaquinol/menaquinone towards menaquinol, which has been shown to control the Mtb respiration rate, thus providing evidence that cysteine and INH can increase cellular respiration. Therefore, it is possible that cysteine can revert persister cells to metabolically active cells by stimulating their respiration. Together, these data support the hypothesis that modulating ROS production and respiration is a strategy to control persisters in mycobacterial species.

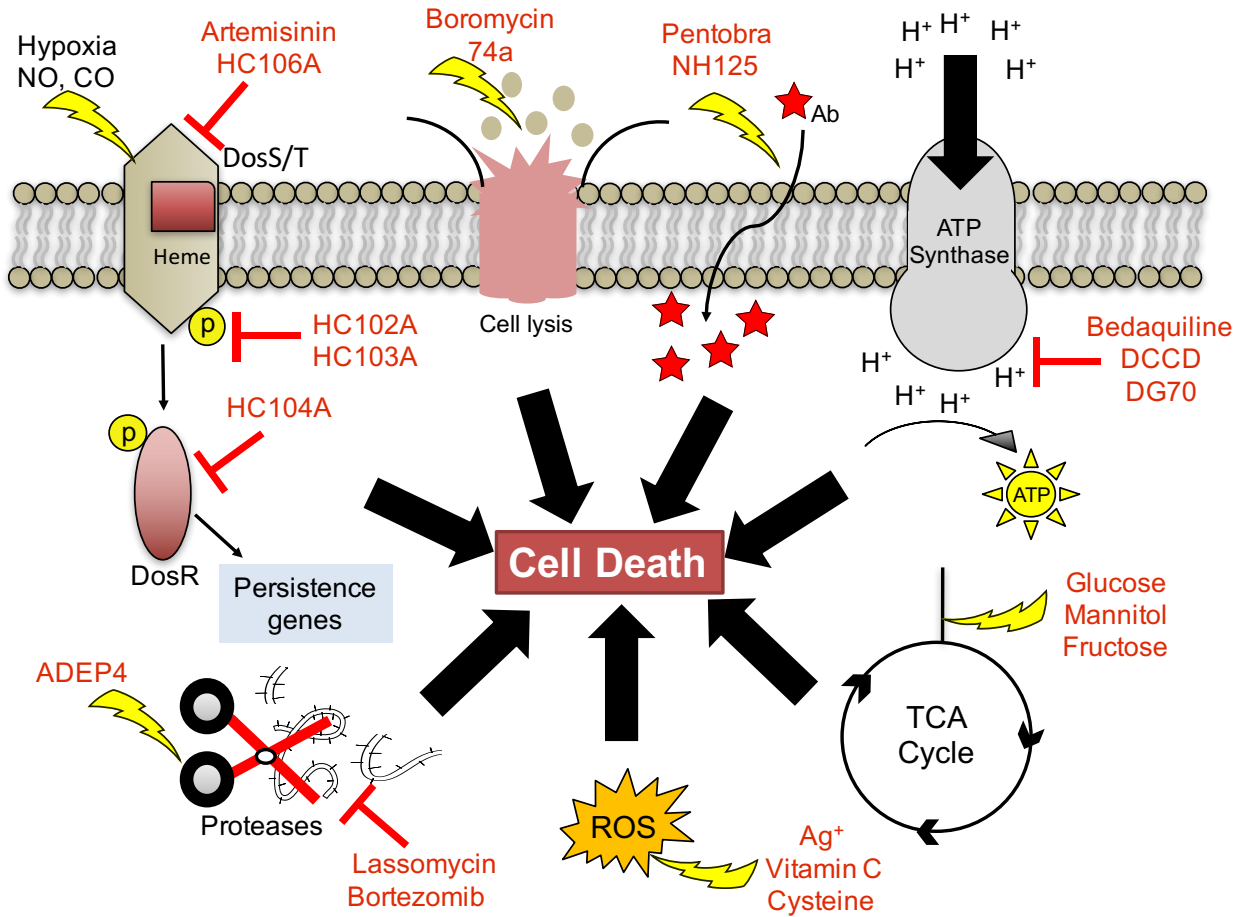


Figure 1.1. Summary of major pathways that can be targeted to kill persisters. Pathways that can be targeted include: 1) reactivation of metabolic pathways with supplement of metabolites; 2) induction of intracellular ROS overproduction; 3) increase of cytoplasmic antibiotic accumulation by enhancing uptake and reducing the efflux activity; 4) activation of non-specific protease activity or inhibition of protease activity; 5) inhibition of ATP production; 6) disruption of membrane integrity to cause cell lysis; 7) inhibition of the DosRST persistence pathway. Ab, antibiotics.

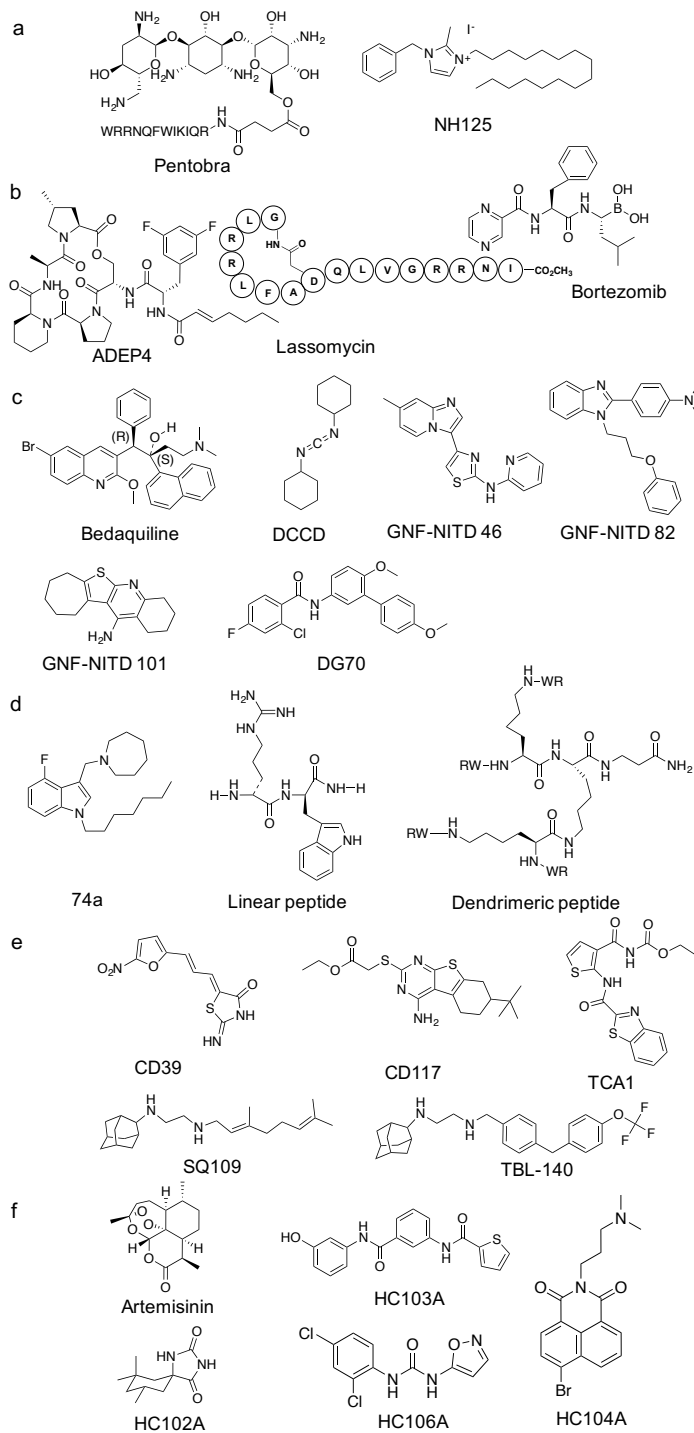


Figure 1.2. Structures of different classes of select inhibitors that kill persister cells. (a) Targeting bacterial membrane permeability; (b) targeting bacterial proteases; (c) inhibiting ATP synthesis; (d) disrupting bacterial membrane; (e) inhibiting bacterial cell wall synthesis; (f) inhibiting DosRST.

Enhancing antibiotic uptake promotes killing of persisters

One major reason that persister cells are tolerant to antibiotics is due to low cytoplasmic drug accumulation. Low metabolic and cellular transport activities of persister cells provide an excellent barrier for antibiotics to reach their cytoplasmic targets. The uptake of some classes of antibiotics, such as aminoglycosides and gentamicin, is an energy dependent process that requires a PMF. One approach to tackle this mechanism of antibiotic tolerance is to increase membrane permeability and promote entry of antibiotics into persister cells (Fig. 1.1). For example, a study by Cui *et al.* demonstrates that the membrane-active antibiotic colistin effectively eliminates class I *E. coli* persisters when used at higher concentrations (16). Moreover, using clinically relevant concentrations of colistin increases killing of persister cells in combination with gentamicin and ofloxacin. Enhanced accumulation of fluorescently-labeled gentamicin was observed following colistin treatment. Furthermore, Schmidt *et al.* have showed that conjugating tobramycin to a 12-amino acid peptide transporter uptake sequence, called Pentobra (Fig. 1.2), enabled effective killing of class I *E. coli* and *S. aureus* persister cells (17). The transporter sequence functions to permeabilize the bacterial membrane, enabling tobramycin to cross the persister cell membrane. In another study, Kim *et al.* (2015) used a fluorescence-based phenotypic screen to identify inhibitors that enhance cell membrane permeability, by monitoring changes in SYTOX green dye staining (18). Several inhibitors, including lysostaphin, nisin, and NH125, kill methicillin-resistant *S. aureus* (MRSA) persister cells by inducing cell membrane permeabilization (Fig. 1.2). NH125 is an imidazolium cation with a long fatty acid tail. To further improve the potency of NH125, analogs were synthesized (19), with alkylated and benzylated NH125 analogs showing enhanced potency against *S. aureus* persisters. These analogs also enhance antimicrobial activities when used in combination with other membrane-active agents, such as BAC-16 and daptomycin (19).

These studies suggest that targeting membrane permeability represents an effective strategy to kill persisters.

Another mechanism by which persister cells may develop antibiotic tolerance is by increasing the activity of efflux pumps. Recent research by Pu *et al.*, using a fluorescently labeled antibiotic penicillin termed BOCILLIN, demonstrated that BOCILLIN accumulation inside of class I *E. coli* persister cells is much lower than for the actively growing cells (20). Transcriptional analysis shows that the β -lactam antibiotics strongly induce the expression of numerous multi-drug efflux genes, such as *tolC*, in persister cells. This finding supports the notion that enhanced efflux pump activity in persister cells may be responsible for antibiotic tolerance. Supporting this model, a positive correlation is shown between *tolC* expression and persister cells. Deletion of *tolC* dramatically increases the accumulation of antibiotics inside the persister cells, suggesting TolC plays an important role to exclude the drugs from the persister cells. This finding supports the hypothesis that inhibiting the TolC efflux pump may function to enhance killing of class I persister cells by antibiotics. Indeed, it was observed that treating *E. coli* persister cells with TolC inhibitors, such as 1-(1-naphthylmethyl) piperazine and phenylalanine arginyl β -naphthylamide, decreased cell viability when bacteria were treated with carbencillin, cloxacillin, or nalidixic acid.

Targeting stationary phase respiration to inhibit persisters

When growing under aerobic conditions, persister cell populations increase as the bacterial cultures age. Studies conducted by Orman and Brynildsen (21) found a correlation between high redox activity, stationary phase respiration and class I persister formation. Redox Sensor Green (RSG) is a redox indicator that directly measures metabolic activity, with enhanced green fluorescence after reduction by bacterial reductases. Using RSG it was found that the population

of stationary phase cells with high redox activity is more likely to form class I persisters than the population with low redox activity. This high redox activity is also correlated with a high yield of non-growing cells, but inversely correlated with protein synthesis. For instance, persister cells with high redox activity have less activity of transcription and translation upon exposure to fresh medium. Therefore, it is suggested that the redox poise plays a decisive role in the increased formation of persister cells in stationary phase. It is further hypothesized that during stationary phase aerobic respiration is the major redox process, and inhibition of respiration decreases the population of persister cells. Indeed, treating the aerobically growing culture with potassium cyanide throughout stationary phase significantly reduces persister cells by up to 1,000-fold.

A role of respiration for survival of stationary phase persisters is further supported by genetic studies, where deletions of *E. coli* genes associated with metabolism caused low levels of persister cells, including the strains mutated in *sucB* that encodes for dihydrolipoyltranssuccinase, *mdh* for malate dehydrogenase, and *ubiF* for oxygenase involved in ubiquinone biosynthesis (21). These mutants exhibit significant perturbation of stationary phase respiration. Their initial protein synthesis is increased after re-inoculating into fresh medium. The indicated proteins are involved in generating reducing equivalents to power respiration, such as ubiquinol and NADH (21). The reducing power during stationary phase is mainly derived from acetate or catabolism of endogenous cellular components, such as phospholipids, ribosomes and proteins. It was found that cells with a deficiency of acetate consumption ($\Delta ackA\Delta poxB$) or phospholipid degradation ($\Delta fadD\Delta fadK$) have a similar level of persister cells as wild type (WT). However, the untreated stationary phase cells display reduced RNA integrity and protein level as compared to KCN-treated cells (21). This observation is consistent with previous observations that persisters have reduced transcription and translation. The mechanistic studies suggest that inhibiting stationary respiratory

activities prevents cells from digesting endogenous RNA and proteins, and leads cells to continue translation and replication. Additional studies have shown that inhibiting respiration of the stationary culture with nitric oxide also impairs persister formation (22). Like the cultures treated with KCN, the NO-treated culture also exhibits decreased RNA and protein degradation during stationary phase. Overall, these studies show that respiration is a critical process controlling persister formation, and they suggest this process can be targeted to inhibit bacterial persistence.

Targeting bacterial proteases to kill persisters

Recently, bacterial proteases, such as Clp system caseinolytic proteases (23), have generated interest as new targets for novel antibiotic development. The protease complex generally consists of a proteolytic core, ClpP, corresponding ATP-dependent AAA+ chaperone proteins and associated adaptor proteins (Fig. 1.1). The protease targets partially synthesized and misfolded proteins, as well as cleaving specific proteins with regulatory functions. Adaptor proteins assist with binding to protease substrates, which are unfolded by the chaperone proteins and then cleaved by ClpP.

Several inhibitors of Clp have been reported to kill class I persisters. For instance, a newly discovered series of ClpP activators, named acyldepsipeptides (ADEPs), are potent against a broad spectrum of bacteria (24). ADEPs activate ClpP by keeping its catalytic chamber open, allowing peptides and proteins to enter, and promoting uncontrolled protein degradation in bacterial cells. Furthermore, recent research shows that ADEP4 (Fig. 1.2) also has an effect on non-replicating persister cells (25). Instead of triggering specific proteolytic activity, ADEP4-bound ClpP is a nonspecific protease that causes excess breakdown of proteins. *S. aureus* persisters that survive ciprofloxacin treatment are eradicated by addition of ADEP4 (25). ADEP4 is also effective in

sterilizing stationary cultures treated with rifampicin, linezolid or ciprofloxacin, suggesting the compound enhances the killing of persister cells (25). Triggering nonspecific proteolytic activity is lethal to bacteria and is effective at eliminating both replicating and persister cells, indicating the idea that some essential processes can be targeted to kill persister cells

Several new protease inhibitors also have been reported to kill class II persisters. For instance, the new antibiotic lassomycin (Fig. 1.2) is reported to kill both growing and non-replicating Mtb by targeting the caseinolytic protease ClpC1P1P2 (26). Lassomycin binds to the ATPase domain of ClpC1 and increases its ATP hydrolysis activity, but also inhibits substrate translocation from ClpC1 to the proteolytic subunits ClpP1P2 of the complex. It decreases degradation of target cell proteins and is toxic to Mtb during stressful conditions. Additionally, the well-known human proteasome inhibitor, bortezomib (Fig. 1.2), has been shown to inhibit ClpP1P2 by covalently attaching via its boron atom to the hydroxyl group of serine at the catalytic triad (27). Bortezomib only potentiates Mtb to aminoglycoside treatment, suggesting that induction of protein mistranslation by aminoglycosides is toxic to Mtb if the proteasome is inhibited to remove incomplete translation products. To increase selectivity of bortezomib to anti-mycobacterial activity over inhibition of the human proteasome, the boronic acid warhead was changed to chloromethyl ketone (28). The newly synthesized analogs only display activity against mycobacterial ClpP1P2, but lack activity to the human proteasome. Moreover, a series of dipeptidyl boronate derivatives of bortezomib has also been synthesized (29). Structure-relationship studies reveal several compounds with improved anti-Mtb activity and selectivity for the mycobacterial ClpP1P2 protein. Compound 58 has good pharmacokinetic criteria, such as aqueous solubility and low cytotoxicity. Overall, these inhibitors show that ClpP protease is an attractive target that can be modulated via different mechanisms to kill bacterial persister cells.

Modulating intracellular ATP levels to kill persisters

Recent studies confirm a critical role of ATP in establishing persistence. For instance, Conlon *et al.* showed that *S. aureus* class I persister formation is directly linked to intracellular ATP levels (30), with stationary phase cultures showing significantly reduced ATP content (Fig. 1.1). Artificial reduction of ATP levels in an exponentially growing culture by adding arsenate increases antibiotic tolerance to rifampin, whereas increasing ATP concentration by supplementing tryptic soy broth medium with glucose causes a reduction in class I persister population during stationary phase (30). This phenomenon is also observed in another study in *E. coli* that shows a drop in intracellular ATP by treatment with arsenate led to antibiotic tolerance to ampicillin and ciprofloxacin (31). These two studies demonstrate that stochastic depletion of ATP intracellular concentration contributes significantly to persister cell formation. The drop in ATP level drives antibiotic tolerance because most antibiotic targets require ATP to function. Bacterial persister cells have thus evolved mechanisms to keep ATP at levels low enough to be viable, while still inducing persistence.

One effective strategy to eliminate class II bacterial persistence is to inhibit bacterial respiration and ATP synthesis (Fig. 1.1). It is hypothesized that during dormancy or NRP, bacteria still require some energy for survival, and further depletion of ATP synthesis will be lethal to persister cells. For instance, Rao *et al.* originally reported the intracellular ATP levels of Mtb rapidly decreases when entering NRP and then is maintained constant over 25 d of incubation in the Wayne model of hypoxia-driven NRP (32). Treating non-replicating Mtb bacilli with the F_0F_1 ATP synthase inhibitor bedaquiline (diarylquinoline) or DCCD (N,N-dicyclohexylcarbo-diimide) dramatically decreases the ATP content, and lowers cell viability (Fig. 1.2). Bedaquiline is also effective in killing Mtb in a mouse model of TB infection, and sterilizes bacteria in 2 months when

included with isoniazid and pyrazinamide treatment (33). The F_0F_1 ATP synthase is involved in the last step of ATP synthesis, and its function is driven by PMF. Disrupting PMF by inhibiting the membrane potential with valinomycin or disrupting the transmembrane proton concentration gradient with nigericin, also kills non-replicating Mtb (34). This indicates that energy production is required for survival, and decreasing the ATP concentration is lethal to class II persisters. Several inhibitors of ATP homeostasis in non-replicating Mtb were identified from high-throughput screening, including imidazopyridines (GNF-NITD 46), benzimidazole (GNF-NITD 82), and thieno[2,3-*b*]pyridin-4-amine (GNF-NITD 101) (Fig. 1.2) (35). All three classes of inhibitors show decreased ATP levels and bacterial survival of non-replicating Mtb. In another study, the biphenyl amide compound DG70 (Fig. 1.2) was identified from a screen that targeted non-replicating Mtb under nutrient-deprived conditions (36). DG70 kills both replicating and non-replicating Mtb and synergizes with other anti-mycobacterial drugs, including INH, bedaquiline and PA824. The compound was found to inhibit oxygen consumption and ATP biosynthesis. The resistant mutants show that this compound targets the MenG protein, which is involved in the last step of menaquinone biosynthesis. This finding is confirmed by biochemical studies showing that DG70 inhibited menaquinone biosynthesis. Overall, these findings suggest that DG70 inhibits replicating and non-replicating bacteria by inhibiting Mtb respiration.

Disrupting membrane integrity to kill persisters

Maintaining membrane integrity is essential for cell survival. Several studies have focused on discovering microbial membrane “disruptors” for controlling non-replicating microbes (Fig. 1.1). For instance, a recent screening conducted by Yang *et al.* has identified amphiphilic indole derivatives that target *Mycobacterium bovis* BCG membrane integrity (37). These novel

compounds cause BCG cell membrane depolarization and permeabilization in a time-dependent manner. The loss of membrane integrity by compound 74a is bactericidal and leads to a rapid killing of replicating cells, as well as effectively killing non-replicating bacilli in the Wayne model of hypoxia-driven NRP (Fig. 1.2). Boromycin is another example of how the cell membrane is a good target to kill persisters. This compound is a well-known polyether macrolide antibiotic that kills Gram-positive bacteria by functioning as a potassium ionophore. Studies demonstrate that boromycin has bactericidal activity against both replicating and non-replicating Mtb under the Wayne model of hypoxia-driven NRP (38). Like in Gram-positive bacteria, boromycin also causes a reduction of membrane potential in Mtb, as well as decreasing intracellular ATP level, suggesting it also acts as an ionophore in Mtb to collapse the potassium gradient across the membrane.

A screen to target non-replicating *S. aureus* identified the quinolone-derived compound HT61 as being more active against stationary phase non-replicating *S. aureus* (both methicillin sensitive *S. aureus* (MSSA) and MRSA) as compared to replicating *S. aureus* (39). It is also bactericidal in other Gram-positive bacteria, including *Streptococcus pyogenes*, *Streptococcus agalactiae*, and *Propionibacterium acnes*. Non-replicating *S. aureus* treated with HT61 exhibits more rapid depolarization of the cytoplasmic membrane as compared to replicating exponential-phase bacteria, and causes the cells to burst. HT61 also effectively kills non-replicating *S. aureus* in a murine skin model. HT61 potentiates killing of *S. aureus* with neomycin, gentamicin and mupirocin both *in vitro* and in an *in vivo* mouse model (40), suggesting that membrane integrity is important for bacterial survival.

Many new antibiotics that disrupt cell membranes have been discovered to eliminate persister populations. For instance, Chen *et al.* discovered that cationic peptides containing Trp/Arg are effective against both planktonic and biofilm-associated persister cell populations

(Fig. 1.2) (41). These peptides have been shown to penetrate and cause physical damage to the cell membrane as the mechanism of action in killing persister cells. Overall, these studies provide strong support for eradicating persister cell populations using agents that damage cellular membranes.

Inhibition of cell envelope biosynthesis potentiates killing of persisters by antibiotics

The Mtb cell envelope is composed of complex glycolipids that create a permeability barrier to the environment. The first-line antibiotic INH inhibits the enoyl-ACP reductase InhA after being activated by the catalase-peroxidase KatG to form an adduct with NAD. InhA is an essential protein involved in synthesis of mycolic acids in Mtb. Inhibition of InhA activity causes mycobacterial cell death. Efforts to discover novel InhA inhibitors that don't require an activator identified two compounds CD39 ((Z)-2-imino-5-((E)-3-(5-nitrofuranyl)allylidene)thiazolidin-4-one) and CD117 (tetrahydrobenzothienopyrimidine) (Fig. 1.2) (42). They are not only bactericidal against the growing *M. tuberculosis*, but also active against non-replicating bacilli grown under anaerobic conditions. This finding suggests these inhibitors have different mechanisms of action from INH, because isoniazid only kills replicating bacilli (32). Both compounds enhance anti-mycobacterial activity with INH and rifampin, and inhibit mycolic acids and fatty acid biosynthesis.

TCA1 is reported to inhibit DprE1, a decaprenylphosphoryl- β -D-ribofuranose oxidoreductase that is involved in cell wall biosynthesis, as well as MoeW, an enzyme involved in molybdenum cofactor synthesis (Fig. 1.2) (43). DprE1 and DprE2 (decaprenylphosphoryl-D-2-keto erythro pentose reductase) together catalyze the epimerization of decaprenylphosphoryl ribose to decaprenylphosphoryl arabinose (44). Decaprenylphosphoryl arabinose is the only

precursor of arabinogalactan and lipoarabinomannan polysaccharides of the mycobacterial cell envelope. Chemical inhibition of DprE1 abolishes biosynthesis of decaprenylphosphoryl arabinose, and causes cell lysis and bacterial death. There are numerous DprE1 inhibitors identified, including benzothiazinones, dinitrobenzamides, azaindoles (45), pyrazolopyridones (46), 2-carboxyquinoxalines (47), and pyrido-benzimidazole (48). However, TCA1 is the only inhibitor reported to effectively kill both replicating and non-replicating Mtb in a nutrient starvation model. TCA1 sterilizes Mtb cultures treated with INH or rifampin in about 3 weeks, and shows efficacy in acute and chronic TB mouse models. Interestingly, transcriptional profiling also showed that TCA1 downregulates the persistence genes involved in Mtb dormancy, including *rv3130c-rv3134c*, *fdxA* and *hspX*, suggesting TCA1 potentiates Mtb killing by antibiotics by inhibiting Mtb dormancy. The multiple functions of TCA1 differentiate it from other inhibitors.

The anti-mycobacterial compounds 1,2-ethylenediamine SQ109 and diphenylether-modified adamantyl 1,2-diamine TBL-140 have been shown to be bactericidal to replicating and non-replicating Mtb by targeting MmpL3 (Fig. 1.2) (49, 50). MmpL3 is a membrane-bound protein that acts as a flippase to translocate the mycolic acid precursor trehalose monomycolate (TMM) to the pseudoperiplasmic space, where TMM is further transported to the mycomembranes and modified into trehalose dimycolate (TDM) by Ag85 protein (51, 52). Treating Mtb cells with SQ109 and TBL-140 inhibits the transport activity of MmpL3, and results in accumulation of TMM in the cytoplasm and thus defective TDM biosynthesis. SQ109 also inhibits membrane potential and generation of the transmembrane proton gradient, while TBL-140 inhibits membrane potential (49, 50). SQ109 also potentiates killing of Mtb by first-line anti-tubercular drugs, including INH and rifampin (53).

Additionally, a new class of antibiotic called Art-175, which consists of a bacteriophage-encoded endolysin covalently attached to a transporting peptide, functions to kill class I persisters (54). The endolysin degrades the peptidoglycan, and is transported through the outer membrane of Gram-negative bacteria with assistance of the transporting peptide. It was shown that Art-175 is able to effectively kill both replicating *P. aeruginosa* and persister cells by penetrating the peptidoglycan layers of *P. aeruginosa* and causing rapid cell lysis. Overall, these findings support the idea that compounds inhibiting cell wall biosynthesis are a good approach for developing anti-persistence therapy.

Targeting two-component regulatory systems to inhibit bacterial persistence

Transcriptional regulators in bacterial pathogens often play essential roles to establish infection and evade host immunity. Anti-virulence therapies target virulence proteins that are not required for growth *in vitro*, but are necessary during infection. Targeting bacterial virulence is different from conventional antibiotics that directly kill bacteria, and may reduce selection for antibiotic resistant strains (55). The DosRST signaling pathway in Mtb has been implicated in Mtb persistence (Fig. 1.1). The primary focus of this dissertation was to determine if chemical inhibitors of the DosRST pathway could be discovered, and if so, could they function to inhibit Mtb persistence.

DosRST is a well-characterized two-component regulatory systems that functions to establish and maintain non-replicating persistence. It is composed of two histidine kinase sensors, DosS and DosT, and the cognate response regulator DosR (56), which regulates expression of approximately 50 genes in the DosR regulon (57). Mtb can sense a variety of environmental cues, including nitric oxide, carbon monoxide and oxygen, through DosS and DosT (57-61). All three

ligands of DosST are relevant for Mtb persistence. For instance, NO is often produced by NO synthase as an antibacterial agent to kill bacteria (62). CO is mainly produced by heme oxygenase 1 during the host immune response to influence anti-inflammatory and anti-apoptotic activities (63). Hypoxia is an important environmental stimulus to facilitate Mtb transition to the latent form. The center of caseous granulomas where Mtb resides during latent infection is highly hypoxic (64). Therefore, Mtb has evolved immune evasion strategies through its ability to sense environmental signals and then orchestrate appropriate genetic, metabolic, and physiologic responses to survive within the host.

Upon receiving the environmental signals, DosS/T catalyzes an ATP-dependent autophosphorylation at a conserved histidine and transmits the signal by phosphorylating DosR at an aspartate residue (61). Phosphorylated DosR is active and able to regulate transcription of the regulon (56, 65). DosS and DosT share extensive amino acid sequence similarity, ~61%, and have structural homology. Each contains two N-terminal GAF domains (cGMP, adenylyl cyclase, FhlA), a HisKA domain (histidine kinase phospho-acceptor) where a phosphoryl group-accepting histidine is located, and a C-terminal HATPase domain (histidine kinase-like ATPase) that is the ATP binding site (66, 67). The GAF domain functions as a small molecule binding regulatory domain that is present throughout prokaryotes and eukaryotes. Specifically, a *b*-type heme is embedded in the hydrophobic cavity of the GAF-A domain of DosS and DosT (68, 69). Even though DosS and DosT are heme-based sensor proteins sharing a similar structure, their biochemical mechanism of signal sensing is different. For instance, DosS is a redox and oxygen sensor and autoxidizes quickly under aerobic conditions (70). In contrast, DosT is a hypoxia sensor and has high affinity and sensitivity to O₂ (71). Both kinases sense O₂ or other ligands via heme, and are inactive when the heme group exists as either the Met (Fe³⁺) form (DosS) or the oxy (Fe²⁺-

O₂) form (DosT) in the presence of O₂. However, hypoxic conditions induce the conversion of DosS to the ferrous form and DosT to the deoxy form, activating the kinases (59, 68-70, 72). Therefore, DosS/T plays different roles in sensing the redox and oxygen status of the environment to turn on the DosR pathway.

In responding to the environmental cues, phosphorylated DosS/T triggers the induction of the DosR regulon and transitions Mtb into NRP. The non-replicating bacilli are problematic for two reasons: 1) they are naturally tolerant to most anti-mycobacterial drugs and are partially responsible for the required long course of TB therapy (32); and 2) they serve as a potential reservoir for transmitting infection once growth is resumed in favorable environmental conditions. Therefore, targeting DosRST can potentially inhibit Mtb from establishing and maintaining bacterial persistence.

The *in vitro* Wayne model has been employed to study hypoxia-driven NRP in Mtb. Bacteria are grown in a sealed screw cap tube with stirring. Oxygen levels diminish over time as bacteria grow in the culture. In the Wayne model, two distinct phases are observed in a time-dependent manner, including NRP1 (initiated at ~1% oxygen) and NRP2 (initiated at <0.06% oxygen). At NRP1, the bacilli cease replication and thicken their cell wall, while at NRP2 the bacilli become anaerobic-adapted bacteria and no longer increase in optical density (73).

The DosRST pathway is a potential therapeutic target because *in vitro* and *in vivo* studies have shown that Mtb is highly attenuated for survival during NRP in the absence of DosRST. For instance, in an *in vitro* rapid anaerobic dormancy model, a slightly modified version of the Wayne model with a higher stirring speed, deletion of *dosR* causes a significant loss of viability as bacilli fail to enter the NRP, and there is also a delay in recovery after re-inoculating the dormant cells into aerobic conditions (74). This finding suggests that DosR plays a functional role for Mtb to

enter and exit NRP, as well as survive during NRP. The $\Delta dosR$ mutant during NRP shows sharply reduced intracellular ATP and NAD, ~10-fold and ~50%-fold lower than WT, respectively (74). The $\Delta dosRS$ mutant also exhibits a growth defect in several animal models, including rabbits, guinea pigs, C3HeB/FeJ mice, and non-human primates (75-77). For instance, rabbits infected with the $\Delta dosRS$ mutant display significantly lower lung bacterial burdens at 8-week infection than those infected with WT. WT Mtb also stimulates formation of numerous intense and organized lesions in the lungs at week 5, whereas the mutant exhibits fewer lesions (75). In the guinea pig model of TB infection, $\Delta dosRS$ shows a 3-log reduction lung CFUs as compared to the WT at week 6. The mutant also causes less virulence, such as lack of formation of mature granulomas, while WT induces massive inflammation and lesions with central necrosis (75). Furthermore, in the C3HeB/FeJ mouse model of TB infection, infection with $\Delta dosS$ leads to 0.5- and 1.5-log lower lung CFUs than infection with WT at week 8 and 12, respectively (76). $\Delta dosS$ also results in 1-1.5 log less liver CFUs at week 12 and 15, respectively, as compared to WT. In the Naïve Indian rhesus macaques model of TB infection, all mutants, including $\Delta dosR$, $\Delta dosS$ and $\Delta dosST$, exhibit lower bacterial burden than WT (77). Specifically, the mutant strains have at least a 100-fold lower lung bacterial burden as compared to WT. Little or no TB-related pathology and granuloma formation are observed in the animals infected the mutant, while WT or complemented strains initiate formation of numerous granulomas with necrosis in the central area (77). All these animal models form well-organized hypoxia-associated granulomas when infected with Mtb, which mimics the pathology observed in humans quite well. The DosR-regulated genes also play a role in drug tolerance. For example, *tgsI* is a DosR-regulated gene that is highly induced during hypoxic conditions (56, 78, 79). It encodes a triacylglycerol (TAG) synthase, which is involved in

the last step of TAG biosynthesis. An *Mtb tgsI* mutant strain exhibits reduced tolerance to several antibiotics, such as isoniazid and ciprofloxacin, *in vitro* and *in vivo* (80, 81).

The *in vitro* and *in vivo* data confirm that DosRST is required for full virulence during *Mtb* infection and for survival during extended periods of hypoxia. Therefore, inhibiting DosRST may help reduce *Mtb* persistence and drug tolerance and shorten TB treatment. Based on the homology modeling of DosR, a DosR regulon inhibitor, a phenylcoumarin derivative, was found to inhibit DosR binding to DNA (82). Screening a phage display library allowed the discovery of short DosR mimetic peptides that inhibit the autophosphorylation activity of DosS (83). This dissertation describes the work toward the discovery and characterization of small molecules HC101A-HC106A (Fig. 1.2) that inhibit the DosRST signaling pathway, and shows that chemical inhibition of the DosRST pathway reduces *Mtb* persistence-associated physiologies, including TAG biosynthesis, survival and INH antibiotic tolerance. Mechanistic studies show a specific component of the DosRST pathway is targeted by each inhibitor through a distinct mechanisms. Both HC101A and HC106 target the sensor domain of DosS/T via different mechanisms, where HC101A modulates the redox status of DosS/T and alkylates the heme, and HC106A likely binds directly to the heme. HC102A and HC103A are proposed to target the kinase function of DosS/T by inhibiting their autophosphorylation activities. Biochemical assays indicates that HC104A functions by inhibiting DosR binding to promoter DNA. The long-term goal of these studies is to use these inhibitors, or other DosRST inhibitors, in combination with current TB drugs to eradicate persister populations and thus shorten the course of TB therapy.

Concluding remarks

Experimental evolution studies show that bacteria have the capacity to become tolerant to antibiotics as they evolve in the presence of these substances (84, 85). Phenotypic drug tolerance, driven by persisters, may facilitate the evolution of heritable drug resistance and represents a threat to the durable, long-term deployment of antibiotics. For instance, in *in vitro* evolution experiments, it was found that continued passaging of the surviving *E. coli* persisters in fresh medium with a high dose of ampicillin produces strains with high drug tolerance (84). It requires an extended time, measured by minimum duration for killing 99% of the population (86), to kill the evolved bacteria as compared to the WT strain. Imaging the division of single cells of stationary phase culture after passaging into fresh medium shows that evolved bacteria requires a longer time to initiate replication. This finding supports the hypothesis that an extended lag time or dormancy may protect the evolved bacteria from antibiotics. However, the evolved bacteria in the exponential phase of growth are more susceptible to antibiotic treatment than the stationary phase cultures. Thus drug tolerance is lag-time dependent, and this phenomenon is referred to as tolerance by lag (*tbl*) (84). Additionally, these high-tolerance bacteria also exhibit increased tolerance to other antibiotics, although they were evolved for ampicillin resistance, showing that they are not ampicillin specific. Genetic mutations were identified in the evolved strains, and introducing a WT copy of some genes decreased the lag times to be similar to WT, suggesting that mutant proteins have a role in the high tolerance, thus the encoded genes are referred to as *tbl* genes (84). These findings are clinically relevant because treatment of infectious disease with antibiotics exerts selection for high-tolerance bacteria, which may eventually reduce treatment effectiveness.

Persister cells are also associated with chronic infections and may drive drug resistance in chronic diseases, such as cystic fibrosis and tuberculosis. For example, it was found that strains isolated from cystic fibrosis patients infected with *P. aeruginosa* exhibit 100-fold greater numbers of persister cells (87). Moreover, studies have suggested that drug tolerance promotes the emergence of drug resistance. For instance, a recent *in vitro* experimental evolution experiment has demonstrated that passaging the surviving phenotypically drug-tolerant persisters in fresh medium with ampicillin promotes the evolution of genetically encoded drug resistance in mutant strains (88). Three different *E. coli* strains independently evolve cultures with increased minimum inhibitory concentration as compared with the parental strains, and each carries a mutation in the promoter of *ampC* that encodes β -lactamase. Further analysis shows that cultures become more phenotypically tolerant over time before evolving heritable drug resistance. The phenotype of high tolerance is not due to slow growth. Additional mutations in genes belonging to the “tolerome” are also present in the mutants with high tolerance. Without the platform of tolerance, mathematical models reveal a lower probability of establishing heritable resistance, suggesting that persistence and drug tolerance contribute significantly to the evolution of resistance. Therefore, bacterial persistence is a fundamental problem, and controlling bacterial persistence is an essential strategy to combat infectious disease and control drug resistance.

REFERENCES

REFERENCES

1. **Lewis K.** 2017. New approaches to antimicrobial discovery. *Biochem Pharmacol* **134**:87-98.
2. **Hobby GL, Meyer K, Chaffee E.** 1942. Observations on the mechanism of action of penicillin. *Proc Soc Exp Biol Med* **50**:281-285.
3. **Bigger J.** 1944. Treatment of Staphylococcal infections with penicillin by intermittent sterilisation. *The Lancet* **244**:497-500.
4. **Balaban NQ, Merrin J, Chait R, Kowalik L, Leibler S.** 2004. Bacterial persistence as a phenotypic switch. *Science* **305**:1622-1625.
5. **Kint CI, Verstraeten N, Fauvart M, Michiels J.** 2012. New-found fundamentals of bacterial persistence. *Trends Microbiol* **20**:577-585.
6. **Nathan C.** 2012. Fresh approaches to anti-infective therapies. *Sci Transl Med* **4**:140sr142.
7. **Gold B, Nathan C.** 2017. Targeting phenotypically tolerant *Mycobacterium tuberculosis*. *Microbiol Spectr* **5**:TBTB2-0031- 2016.
8. **Allison KR, Brynildsen MP, Collins JJ.** 2011. Metabolite-enabled eradication of bacterial persisters by aminoglycosides. *Nature* **473**:216-220.
9. **Prax M, Mechler L, Weidenmaier C, Bertram R.** 2016. Glucose augments killing efficiency of daptomycin challenged *Staphylococcus aureus* persisters. *PLoS One* **11**:e0150907.
10. **Marques CN, Morozov A, Planzos P, Zelaya HM.** 2014. The fatty acid signaling molecule cis-2-decenoic acid increases metabolic activity and reverts persister cells to an antimicrobial-susceptible state. *Appl Environ Microbiol* **80**:6976-6991.
11. **Lewis K.** 2007. Persister cells, dormancy and infectious disease. *Nat Rev Microbiol* **5**:48-56.
12. **Morones-Ramirez JR, Winkler JA, Spina CS, Collins JJ.** 2013. Silver enhances antibiotic activity against gram-negative bacteria. *Sci Transl Med* **5**:190ra181.
13. **Grant SS, Kaufmann BB, Chand NS, Haseley N, Hung DT.** 2012. Eradication of bacterial persisters with antibiotic-generated hydroxyl radicals. *Proc Natl Acad Sci U S A* **109**:12147-12152.

14. **Vilcheze C, Hartman T, Weinrick B, Jacobs WR, Jr.** 2013. *Mycobacterium tuberculosis* is extraordinarily sensitive to killing by a vitamin C-induced Fenton reaction. *Nat Commun* **4**:1-10.
15. **Vilcheze C, Hartman T, Weinrick B, Jain P, Weisbrod TR, Leung LW, Freundlich JS, Jacobs WR, Jr.** 2017. Enhanced respiration prevents drug tolerance and drug resistance in *Mycobacterium tuberculosis*. *Proc Natl Acad Sci U S A* **114**:4495-4500.
16. **Cui P, Niu H, Shi W, Zhang S, Zhang H, Margolick J, Zhang W, Zhang Y.** 2016. Disruption of membrane by colistin kills uropathogenic *Escherichia coli* persisters and enhances killing of other antibiotics. *Antimicrob Agents Chemother* **60**:6867-6871.
17. **Schmidt NW, Deshayes S, Hawker S, Blacker A, Kasko AM, Wong GC.** 2014. Engineering persister-specific antibiotics with synergistic antimicrobial functions. *ACS Nano* **8**:8786-8793.
18. **Kim W, Conery AL, Rajamuthiah R, Fuchs BB, Ausubel FM, Mylonakis E.** 2015. Identification of an antimicrobial agent effective against methicillin-resistant *Staphylococcus aureus* persisters using a fluorescence-based screening strategy. *PLoS One* **10**:e0127640.
19. **Basak A, Abouelhassan Y, Zuo R, Yousaf H, Ding Y, Huigens RW.** 2017. Antimicrobial peptide-inspired NH125 analogues: bacterial and fungal biofilm-eradicating agents and rapid killers of MRSA persisters. *Org Biomol Chem* **15**:5503-5512.
20. **Pu Y, Zhao Z, Li Y, Zou J, Ma Q, Zhao Y, Ke Y, Zhu Y, Chen H, Baker MA, Ge H, Sun Y, Xie XS, Bai F.** 2016. Enhanced efflux activity facilitates drug tolerance in dormant bacterial cells. *Mol Cell* **62**:284-294.
21. **Orman MA, Brynildsen MP.** 2015. Inhibition of stationary phase respiration impairs persister formation in *E. coli*. *Nat Commun* **6**:7983.
22. **Orman MA, Brynildsen MP.** 2016. Persister formation in *Escherichia coli* can be inhibited by treatment with nitric oxide. *Free Radic Biol Med* **93**:145-154.
23. **Brotz-Oosterhelt H, Sass P.** 2014. Bacterial caseinolytic proteases as novel targets for antibacterial treatment. *Int J Med Microbiol* **304**:23-30.
24. **Brotz-Oosterhelt H, Beyer D, Kroll HP, Endermann R, Ladel C, Schroeder W, Hinzen B, Raddatz S, Paulsen H, Henninger K, Bandow JE, Sahl HG, Labischinski H.** 2005. Dysregulation of bacterial proteolytic machinery by a new class of antibiotics. *Nat Med* **11**:1082-1087.
25. **Conlon BP, Nakayasu ES, Fleck LE, LaFleur MD, Isabella VM, Coleman K, Leonard SN, Smith RD, Adkins JN, Lewis K.** 2013. Activated ClpP kills persisters and eradicates a chronic biofilm infection. *Nature* **503**:365-370.

26. **Gavriš E, Sit CS, Cao S, Kandrór O, Spoering A, Peoples A, Ling L, Fetterman A, Hughes D, Bissell A, Torrey H, Akopian T, Mueller A, Epstein S, Goldberg A, Clardy J, Lewis K.** 2014. Lassomycin, a ribosomally synthesized cyclic peptide, kills *Mycobacterium tuberculosis* by targeting the ATP-dependent protease ClpC1P1P2. *Chem Biol* **21**:509-518.
27. **Moreira W, Ngan GJ, Low JL, Poulsen A, Chia BC, Ang MJ, Yap A, Fulwood J, Lakshmanan U, Lim J, Khoo AY, Flotow H, Hill J, Raju RM, Rubin EJ, Dick T.** 2015. Target mechanism-based whole-cell screening identifies bortezomib as an inhibitor of caseinolytic protease in mycobacteria. *MBio* **6**:e00253-00215.
28. **Moreira W, Santhanakrishnan S, Dymock BW, Dick T.** 2017. Bortezomib warhead-switch confers dual activity against mycobacterial caseinolytic protease and proteasome and selectivity against human proteasome. *Front Microbiol* **8**:1-6.
29. **Moreira W, Santhanakrishnan S, Ngan GJY, Low CB, Sangthongpitag K, Poulsen A, Dymock BW, Dick T.** 2017. Towards selective mycobacterial ClpP1P2 inhibitors with reduced activity against the human proteasome. *Antimicrob Agents Chemother* **61**:e02307-02316.
30. **Conlon BP, Rowe SE, Gandt AB, Nuxoll AS, Donegan NP, Zalis EA, Clair G, Adkins JN, Cheung AL, Lewis K.** 2016. Persister formation in *Staphylococcus aureus* is associated with ATP depletion. *Nat Microbiol* **1**:16051.
31. **Shan Y, Brown Gandt A, Rowe SE, Deisinger JP, Conlon BP, Lewis K.** 2017. ATP-dependent persister formation in *Escherichia coli*. *MBio* **8**:e02267-02216.
32. **Rao SP, Alonso S, Rand L, Dick T, Pethe K.** 2008. The protonmotive force is required for maintaining ATP homeostasis and viability of hypoxic, nonreplicating *Mycobacterium tuberculosis*. *Proc Natl Acad Sci U S A* **105**:11945-11950.
33. **Andries K, Verhasselt P, Guillemont J, Gohlmann HW, Neefs JM, Winkler H, Van Gestel J, Timmerman P, Zhu M, Lee E, Williams P, de Chaffoy D, Huitric E, Hoffner S, Cambau E, Truffot-Pernot C, Lounis N, Jarlier V.** 2005. A diarylquinoline drug active on the ATP synthase of *Mycobacterium tuberculosis*. *Science* **307**:223-227.
34. **Pethe K, Bifani P, Jang J, Kang S, Park S, Ahn S, Jiricek J, Jung J, Jeon HK, Cechetto J, Christophe T, Lee H, Kempf M, Jackson M, Lenaerts AJ, Pham H, Jones V, Seo MJ, Kim YM, Seo M, Seo JJ, Park D, Ko Y, Choi I, Kim R, Kim SY, Lim S, Yim SA, Nam J, Kang H, Kwon H, Oh CT, Cho Y, Jang Y, Kim J, Chua A, Tan BH, Nanjundappa MB, Rao SP, Barnes WS, Wintjens R, Walker JR, Alonso S, Lee S, Kim J, Oh S, Oh T, Nehrbaas U, Han SJ, No Z, et al.** 2013. Discovery of Q203, a potent clinical candidate for the treatment of tuberculosis. *Nat Med* **19**:1157-1160.
35. **Mak PA, Rao SP, Ping Tan M, Lin X, Chyba J, Tay J, Ng SH, Tan BH, Cherian J, Duraiswamy J, Bifani P, Lim V, Lee BH, Ling Ma N, Beer D, Thayalan P, Kuhén K,**

- Chatterjee A, Supek F, Glynn R, Zheng J, Boshoff HI, Barry CE, 3rd, Dick T, Pethe K, Camacho LR.** 2012. A high-throughput screen to identify inhibitors of ATP homeostasis in non-replicating *Mycobacterium tuberculosis*. *ACS Chem Biol* **7**:1190-1197.
36. **Sukheja P, Kumar P, Mittal N, Li SG, Singleton E, Russo R, Perryman AL, Shrestha R, Awasthi D, Husain S, Soteropoulos P, Brukh R, Connell N, Freundlich JS, Alland D.** 2017. A novel small-molecule inhibitor of the *Mycobacterium tuberculosis* demethylmenaquinone methyltransferase MenG is bactericidal to both growing and nutritionally deprived persister cells. *MBio* **8**:e02022-02016.
37. **Yang T, Moreira W, Nyantakyi SA, Chen H, Aziz DB, Go ML, Dick T.** 2017. Amphiphilic indole derivatives as antimycobacterial agents: structure-activity relationships and membrane targeting properties. *J Med Chem* **60**:2745-2763.
38. **Moreira W, Aziz DB, Dick T.** 2016. Boromycin kills mycobacterial persisters without detectable resistance. *Front Microbiol* **7**:1-7.
39. **Hu Y, Shamaei-Tousi A, Liu Y, Coates A.** 2010. A new approach for the discovery of antibiotics by targeting non-multiplying bacteria: a novel topical antibiotic for staphylococcal infections. *PLoS One* **5**:e11818.
40. **Hu Y, Coates AR.** 2013. Enhancement by novel anti-methicillin-resistant *Staphylococcus aureus* compound HT61 of the activity of neomycin, gentamicin, mupirocin and chlorhexidine: *in vitro* and *in vivo* studies. *J Antimicrob Chemother* **68**:374-384.
41. **Chen X, Zhang M, Zhou C, Kallenbach NR, Ren D.** 2011. Control of bacterial persister cells by Trp/Arg-containing antimicrobial peptides. *Appl Environ Microbiol* **77**:4878-4885.
42. **Vilcheze C, Baughn AD, Tufariello J, Leung LW, Kuo M, Basler CF, Alland D, Sacchetti JC, Freundlich JS, Jacobs WR, Jr.** 2011. Novel inhibitors of InhA efficiently kill *Mycobacterium tuberculosis* under aerobic and anaerobic conditions. *Antimicrob Agents Chemother* **55**:3889-3898.
43. **Wang F, Sambandan D, Halder R, Wang J, Batt SM, Weinrick B, Ahmad I, Yang P, Zhang Y, Kim J, Hassani M, Huszar S, Trefzer C, Ma Z, Kaneko T, Mdluli KE, Franzblau S, Chatterjee AK, Johnsson K, Mikusova K, Besra GS, Futterer K, Robbins SH, Barnes SW, Walker JR, Jacobs WR, Jr., Schultz PG.** 2013. Identification of a small molecule with activity against drug-resistant and persistent tuberculosis. *Proc Natl Acad Sci U S A* **110**:E2510-2517.
44. **Mikusova K, Huang H, Yagi T, Holsters M, Vereecke D, D'Haese W, Scherman MS, Brennan PJ, McNeil MR, Crick DC.** 2005. Decaprenylphosphoryl arabinofuranose, the donor of the D-arabinofuranosyl residues of mycobacterial arabinan, is formed via a two-step epimerization of decaprenylphosphoryl ribose. *J Bacteriol* **187**:8020-8025.

45. **Shirude PS, Shandil R, Sadler C, Naik M, Hosagrahara V, Hameed S, Shinde V, Bathula C, Humnabadkar V, Kumar N, Reddy J, Panduga V, Sharma S, Ambady A, Hegde N, Whiteaker J, McLaughlin RE, Gardner H, Madhavapeddi P, Ramachandran V, Kaur P, Narayan A, Guptha S, Awasthy D, Narayan C, Mahadevaswamy J, Vishwas KG, Ahuja V, Srivastava A, Prabhakar KR, Bharath S, Kale R, Ramaiah M, Choudhury NR, Sambandamurthy VK, Solapure S, Iyer PS, Narayanan S, Chatterji M.** 2013. Azaindoles: noncovalent DprE1 inhibitors from scaffold morphing efforts, kill *Mycobacterium tuberculosis* and are efficacious *in vivo*. *J Med Chem* **56**:9701-9708.
46. **Panda M, Ramachandran S, Ramachandran V, Shirude PS, Humnabadkar V, Nagalapur K, Sharma S, Kaur P, Guptha S, Narayan A, Mahadevaswamy J, Ambady A, Hegde N, Rudrapatna SS, Hosagrahara VP, Sambandamurthy VK, Raichurkar A.** 2014. Discovery of pyrazolopyridones as a novel class of noncovalent DprE1 inhibitor with potent anti-mycobacterial activity. *J Med Chem* **57**:4761-4771.
47. **Neres J, Hartkoorn RC, Chiarelli LR, Gadupudi R, Pasca MR, Mori G, Venturelli A, Savina S, Makarov V, Kolly GS, Molteni E, Binda C, Dhar N, Ferrari S, Brodin P, Delorme V, Landry V, de Jesus Lopes Ribeiro AL, Farina D, Saxena P, Pojer F, Carta A, Luciani R, Porta A, Zanoni G, De Rossi E, Costi MP, Riccardi G, Cole ST.** 2015. 2-Carboxyquinoxalines kill *Mycobacterium tuberculosis* through noncovalent inhibition of DprE1. *ACS Chem Biol* **10**:705-714.
48. **Warrier T, Kapilashrami K, Argyrou A, Ioerger TR, Little D, Murphy KC, Nandakumar M, Park S, Gold B, Mi J, Zhang T, Meiler E, Rees M, Somersan-Karakaya S, Porras-De Francisco E, Martinez-Hoyos M, Burns-Huang K, Roberts J, Ling Y, Rhee KY, Mendoza-Losana A, Luo M, Nathan CF.** 2016. N-methylation of a bactericidal compound as a resistance mechanism in *Mycobacterium tuberculosis*. *Proc Natl Acad Sci U S A* **113**:E4523-4530.
49. **Li W, Upadhyay A, Fontes FL, North EJ, Wang Y, Crans DC, Grzegorzewicz AE, Jones V, Franzblau SG, Lee RE, Crick DC, Jackson M.** 2014. Novel insights into the mechanism of inhibition of MmpL3, a target of multiple pharmacophores in *Mycobacterium tuberculosis*. *Antimicrob Agents Chemother* **58**:6413-6423.
50. **Foss MH, Pou S, Davidson PM, Dunaj JL, Winter RW, Pou S, Licon MH, Doh JK, Li Y, Kelly JX, Dodean RA, Koop DR, Riscoe MK, Purdy GE.** 2016. Diphenylether-Modified 1,2-Diamines with Improved Drug Properties for Development against *Mycobacterium tuberculosis*. *ACS Infect Dis* **2**:500-508.
51. **Tahlan K, Wilson R, Kastrinsky DB, Arora K, Nair V, Fischer E, Barnes SW, Walker JR, Alland D, Barry CE, 3rd, Boshoff HI.** 2012. SQ109 targets MmpL3, a membrane transporter of trehalose monomycolate involved in mycolic acid donation to the cell wall core of *Mycobacterium tuberculosis*. *Antimicrob Agents Chemother* **56**:1797-1809.

52. **Grzegorzewicz AE, Pham H, Gundi VA, Scherman MS, North EJ, Hess T, Jones V, Gruppo V, Born SE, Kordulakova J, Chavadi SS, Morisseau C, Lenaerts AJ, Lee RE, McNeil MR, Jackson M.** 2012. Inhibition of mycolic acid transport across the *Mycobacterium tuberculosis* plasma membrane. *Nat Chem Biol* **8**:334-341.
53. **Chen P, Gearhart J, Protopopova M, Einck L, Nacy CA.** 2006. Synergistic interactions of SQ109, a new ethylene diamine, with front-line antitubercular drugs *in vitro*. *J Antimicrob Chemother* **58**:332-337.
54. **Briers Y, Walmagh M, Grymonprez B, Biebl M, Pirnay JP, Defraigne V, Michiels J, Cenens W, Aertsen A, Miller S, Lavigne R.** 2014. Art-175 is a highly efficient antibacterial against multidrug-resistant strains and persists of *Pseudomonas aeruginosa*. *Antimicrob Agents Chemother* **58**:3774-3784.
55. **Johnson BK, Abramovitch RB.** 2017. Small molecules that sabotage bacterial virulence. *Trends Pharmacol Sci* **38**:339-362.
56. **Park HD, Guinn KM, Harrell MI, Liao R, Voskuil MI, Tompa M, Schoolnik GK, Sherman DR.** 2003. Rv3133c/dosR is a transcription factor that mediates the hypoxic response of *Mycobacterium tuberculosis*. *Mol Microbiol* **48**:833-843.
57. **Voskuil MI, Schnappinger D, Visconti KC, Harrell MI, Dolganov GM, Sherman DR, Schoolnik GK.** 2003. Inhibition of respiration by nitric oxide induces a *Mycobacterium tuberculosis* dormancy program. *J Exp Med* **198**:705-713.
58. **Vos MH, Bouzhir-Sima L, Lambry JC, Luo H, Eaton-Rye JJ, Ioanoviciu A, Ortiz de Montellano PR, Liebl U.** 2012. Ultrafast ligand dynamics in the heme-based GAF sensor domains of the histidine kinases DosS and DosT from *Mycobacterium tuberculosis*. *Biochemistry* **51**:159-166.
59. **Kumar A, Toledo JC, Patel RP, Lancaster JR, Jr., Steyn AJ.** 2007. *Mycobacterium tuberculosis* DosS is a redox sensor and DosT is a hypoxia sensor. *Proc Natl Acad Sci U S A* **104**:11568-11573.
60. **Ohno H, Zhu G, Mohan VP, Chu D, Kohno S, Jacobs WR, Jr., Chan J.** 2003. The effects of reactive nitrogen intermediates on gene expression in *Mycobacterium tuberculosis*. *Cell Microbiol* **5**:637-648.
61. **Roberts DM, Liao RP, Wisedchaisri G, Hol WG, Sherman DR.** 2004. Two sensor kinases contribute to the hypoxic response of *Mycobacterium tuberculosis*. *J Biol Chem* **279**:23082-23087.
62. **Gomez JE, McKinney JD.** 2004. *M. tuberculosis* persistence, latency, and drug tolerance. *Tuberculosis (Edinb)* **84**:29-44.

63. **Shiloh MU, Manzanillo P, Cox JS.** 2008. *Mycobacterium tuberculosis* senses host-derived carbon monoxide during macrophage infection. *Cell Host Microbe* **3**:323-330.
64. **Via LE, Lin PL, Ray SM, Carrillo J, Allen SS, Eum SY, Taylor K, Klein E, Manjunatha U, Gonzales J, Lee EG, Park SK, Raleigh JA, Cho SN, McMurray DN, Flynn JL, Barry CE, 3rd.** 2008. Tuberculous granulomas are hypoxic in guinea pigs, rabbits, and nonhuman primates. *Infect Immun* **76**:2333-2340.
65. **Wisedchaisri G, Wu M, Sherman DR, Hol WG.** 2008. Crystal structures of the response regulator DosR from *Mycobacterium tuberculosis* suggest a helix rearrangement mechanism for phosphorylation activation. *J Mol Biol* **378**:227-242.
66. **Sardiwal S, Kendall SL, Movahedzadeh F, Rison SC, Stoker NG, Djordjevic S.** 2005. A GAF domain in the hypoxia/NO-inducible *Mycobacterium tuberculosis* DosS protein binds haem. *J Mol Biol* **353**:929-936.
67. **Sivaramakrishnan S, de Montellano PR.** 2013. The DosS-DosT/DosR mycobacterial sensor system. *Biosensors* **3**:259-282.
68. **Cho HY, Cho HJ, Kim YM, Oh JI, Kang BS.** 2009. Structural insight into the heme-based redox sensing by DosS from *Mycobacterium tuberculosis*. *J Biol Chem* **284**:13057-13067.
69. **Podust LM, Ioanoviciu A, Ortiz de Montellano PR.** 2008. 2.3 A X-ray structure of the heme-bound GAF domain of sensory histidine kinase DosT of *Mycobacterium tuberculosis*. *Biochemistry* **47**:12523-12531.
70. **Ioanoviciu A, Yukl ET, Moenne-Loccoz P, de Montellano PR.** 2007. DevS, a heme-containing two-component oxygen sensor of *Mycobacterium tuberculosis*. *Biochemistry* **46**:4250-4260.
71. **Cho HY, Cho HJ, Kim MH, Kang BS.** 2011. Blockage of the channel to heme by the E87 side chain in the GAF domain of *Mycobacterium tuberculosis* DosS confers the unique sensitivity of DosS to oxygen. *FEBS Lett* **585**:1873-1878.
72. **Sousa EH, Tuckerman JR, Gonzalez G, Gilles-Gonzalez MA.** 2007. DosT and DevS are oxygen-switched kinases in *Mycobacterium tuberculosis*. *Protein Sci* **16**:1708-1719.
73. **Chao MC, Rubin EJ.** 2010. Letting sleeping dos lie: does dormancy play a role in tuberculosis? *Annu Rev Microbiol* **64**:293-311.
74. **Leistikow RL, Morton RA, Bartek IL, Frimpong I, Wagner K, Voskuil MI.** 2010. The *Mycobacterium tuberculosis* DosR regulon assists in metabolic homeostasis and enables rapid recovery from nonrespiring dormancy. *J Bacteriol* **192**:1662-1670.

75. **Converse PJ, Karakousis PC, Klinkenberg LG, Kesavan AK, Ly LH, Allen SS, Grosset JH, Jain SK, Lamichhane G, Manabe YC, McMurray DN, Nuermberger EL, Bishai WR.** 2009. Role of the dosR-dosS two-component regulatory system in *Mycobacterium tuberculosis* virulence in three animal models. *Infect Immun* **77**:1230-1237.
76. **Gautam US, McGillivray A, Mehra S, Didier PJ, Midkiff CC, Kisse RS, Golden NA, Alvarez X, Niu T, Rengarajan J, Sherman DR, Kaushal D.** 2015. DosS is required for the complete virulence of *Mycobacterium tuberculosis* in mice with classical granulomatous lesions. *Am J Respir Cell Mol Biol* **52**:708-716.
77. **Mehra S, Foreman TW, Didier PJ, Ahsan MH, Hudock TA, Kisse R, Golden NA, Gautam US, Johnson AM, Alvarez X, Russell-Lodrigue KE, Doyle LA, Roy CJ, Niu T, Blanchard JL, Khader SA, Lackner AA, Sherman DR, Kaushal D.** 2015. The DosR Regulon Modulates Adaptive Immunity and Is Essential for *Mycobacterium tuberculosis* Persistence. *Am J Respir Crit Care Med* **191**:1185-1196.
78. **Zheng H, Colvin CJ, Johnson BK, Kirchhoff PD, Wilson M, Jorgensen-Muga K, Larsen SD, Abramovitch RB.** 2017. Inhibitors of *Mycobacterium tuberculosis* DosRST signaling and persistence. *Nat Chem Biol* **13**:218-225.
79. **Rustad TR, Harrell MI, Liao R, Sherman DR.** 2008. The enduring hypoxic response of *Mycobacterium tuberculosis*. *PLoS One* **3**:e1502.
80. **Deb C, Lee CM, Dubey VS, Daniel J, Abomoelak B, Sirakova TD, Pawar S, Rogers L, Kolattukudy PE.** 2009. A novel in vitro multiple-stress dormancy model for *Mycobacterium tuberculosis* generates a lipid-loaded, drug-tolerant, dormant pathogen. *PLoS One* **4**:e6077.
81. **Baek SH, Li AH, Sasseti CM.** 2011. Metabolic regulation of mycobacterial growth and antibiotic sensitivity. *PLoS Biol* **9**:e1001065.
82. **Gupta RK, Thakur TS, Desiraju GR, Tyagi JS.** 2009. Structure-based design of DevR inhibitor active against nonreplicating *Mycobacterium tuberculosis*. *J Med Chem* **52**:6324-6334.
83. **Kaur K, Taneja NK, Dhingra S, Tyagi JS.** 2014. DevR (DosR) mimetic peptides impair transcriptional regulation and survival of *Mycobacterium tuberculosis* under hypoxia by inhibiting the autokinase activity of DevS sensor kinase. *BMC Microbiol* **14**:1-9.
84. **Fridman O, Goldberg A, Ronin I, Shores N, Balaban NQ.** 2014. Optimization of lag time underlies antibiotic tolerance in evolved bacterial populations. *Nature* **513**:418-421.
85. **Van den Bergh B, Michiels JE, Wenseleers T, Windels EM, Boer PV, Kestemont D, De Meester L, Verstrepen KJ, Verstraeten N, Fauvart M, Michiels J.** 2016. Frequency

of antibiotic application drives rapid evolutionary adaptation of *Escherichia coli* persistence. Nat Microbiol **1**:16020.

86. **Brauner A, Shores N, Fridman O, Balaban NQ.** 2017. An experimental framework for quantifying bacterial tolerance. Biophys J **112**:2664-2671.
87. **Mulcahy LR, Burns JL, Lory S, Lewis K.** 2010. Emergence of *Pseudomonas aeruginosa* strains producing high levels of persister cells in patients with cystic fibrosis. J Bacteriol **192**:6191-6199.
88. **Levin-Reisman I, Ronin I, Gefen O, Braniss I, Shores N, Balaban NQ.** 2017. Antibiotic tolerance facilitates the evolution of resistance. Science **355**:826-830.

CHAPTER 2 - Inhibitors of *Mycobacterium tuberculosis* DosRST signaling and persistence

This discovery and initial characterization of HC101A-HC103A presented in this chapter has been previously published:

Zheng H., Colvin C.J., Johnson B.K., Kirchhoff P.D., Wilson M., Jorgensen-Muga K., Larsen S.D., and Abramovitch R.B. (2017). Inhibitors of *Mycobacterium tuberculosis* DosRST signaling and persistence. *Nature Chemical Biology*, **13**, 218-225.

Author contributions for the study:

H.Z., C.J.C., B.K.J. and R.B.A. conducted high-throughput screen. H.Z. performed the Mtb physiology and biochemistry experiments. M.W. and S.D.L. synthesized chemical compounds; K.J.-M. contributed reagents. P.D.K. performed structural modeling.

Summary

The *Mycobacterium tuberculosis* (Mtb) DosRST two-component regulatory system promotes the survival of Mtb during non-replicating persistence (NRP). NRP bacteria help drive the long course of tuberculosis therapy, therefore, chemical inhibition of DosRST may inhibit the ability of Mtb to establish persistence and thus shorten treatment. Using a DosRST-dependent fluorescent Mtb reporter strain, a whole-cell phenotypic high-throughput screen of a ~540,000 compound small molecule library was conducted. The screen discovered novel inhibitors of the DosRST regulon, including three compounds that were subject to follow-up studies: artemisinin, HC102A and HC103A. Under hypoxia, all three compounds inhibit Mtb persistence associated physiologies, including triacylglycerol synthesis, survival and antibiotic tolerance. Artemisinin functions by disabling the heme-based DosS/T sensor kinases by oxidizing ferrous heme and generating heme-artemisinin adducts. In contrast, HC103A inhibits DosS and DosT autophosphorylation activity without targeting the sensor kinase heme.

Introduction

Mycobacterium tuberculosis (Mtb), the causative agent of tuberculosis (TB), can persist in the host for decades without causing disease symptoms (1). Mtb non-replicating persistence (NRP) is characterized by a gradual slowing of metabolic activity upon encountering pressures from the host immune system, including hypoxia, acidic pH or starvation (2-4). The DosRST two-component regulatory system plays an important role in Mtb NRP physiology (5). It is composed of two heme-based histidine sensor kinases, DosS and DosT, and the response regulator DosR, and strongly regulates the expression of approximately 50 genes known as the DosRST regulon (6-8). Mtb can sense host stimuli, including nitric oxide (NO), carbon monoxide (CO) and oxygen (O₂), through DosS and DosT (9), with DosS acting as an oxygen and redox sensor and DosT acting as an oxygen sensor (7, 9-11). During hypoxia-driven NRP, DosT is associated with initiating expression of the DosR regulon in response to hypoxia and DosS promotes sustained expression of the DosR regulon (12).

A fundamental challenge of current TB therapy is the long course of treatment. New drugs that shorten the course of therapy could revolutionize TB control. *dosR* mutants have reduced survival during hypoxia *in vitro* (13) and reduced virulence in rabbits, guinea pigs, non-human primates, and C3HeB/FeJ mice (14-16), animal models that generate hypoxic granulomas where DosR-dependent persistence is predicted to be required for survival. Additionally, disruption of a DosR regulated gene, *tgs1*, results in enhanced sensitivity of Mtb to antibiotics *in vitro* and during mouse infection (17). Therefore, chemical inhibition of the DosR regulon may stop the establishment and survival of persistent, drug-tolerant Mtb in the granuloma.

Whole-cell, phenotypic high-throughput screening (HTS) is a powerful tool in Mtb drug discovery. However, many important virulence targets are not accessible to whole-cell HTS

because the targets are only required during infection and not required *in vitro*. One method to address this shortcoming is to conduct a HTS of Mtb growing inside macrophages, which has been successfully employed to discover inhibitors specifically targeting physiology required during infection (18). An alternative approach is to use reporter strains that indicate the stimulation of a virulence pathway and then screening for inhibitors of a reporter signal, an approach that has been successfully employed to discover antivirulence compounds (19-23). The goal of this study was to conduct a reporter-based phenotypic HTS to discover chemical inhibitors of the DosRST regulon and Mtb persistence. Here we report the discovery and characterization of new chemical compounds that reduce expression of DosRST regulon genes, inhibit Mtb persistence-associated physiologies and directly inhibit the DosS/T sensor kinases.

Results

Discovery of DosRST regulon inhibitors

A whole-cell phenotypic high-throughput screen was conducted to identify small molecule inhibitors of DosRST. The CDC1551(*hspX'::GFP*) fluorescent reporter strain was previously reported to exhibit DosR-dependent GFP fluorescence that is induced by hypoxia and NO (24). Notably, the reporter is strongly induced under conditions of mild hypoxia (*e.g.* 2% O₂) where Mtb is capable of robust growth (24). *dosR* mutant strains grow well in rich medium until oxygen is almost fully consumed (5, 13), therefore, discovery of compounds that inhibit hypoxia-inducible reporter fluorescence, but leave growth unaffected, may be inhibitors of the DosRST pathway. To discover inhibitors of the DosRST regulon, the CDC1551(*hspX'::GFP*) reporter strain was used to screen a 540,288 compound library. The reporter strain was grown in rich medium with individual compounds (at a screening concentration of ~10 μM) in 384-well plates and incubated

for 6 d. Growth of Mtb causes the consumption of oxygen and promotes hypoxic conditions at the bottom of the well. GFP fluorescence and growth (as measured by optical density) were measured after 6 d incubation. For analysis of hits, fluorescence and growth inhibition were normalized at 100% or 0% inhibition based on rifampin and dimethyl sulfoxide (DMSO) controls, respectively. The Z-factor for the screen was 0.9 and the variation of controls was limited (Supplementary Fig. 2.1ab) confirming that the screen was robust. Hits were then distinguished based on their ability to specifically inhibit reporter fluorescence or as general inhibitors of Mtb growth. Putative DosRST pathway inhibitors were defined as compounds that exhibit >1.5-fold greater fluorescence inhibition as compared to growth inhibition ($p < 0.0003$, Supplementary Fig. 2.1c) with at least 35% fluorescence inhibition (Class 1 inhibitors, Fig. 2.1a). Fresh powders of several putative DosRST inhibitors were obtained and tested in secondary assays to confirm activity, and exclude compounds with GFP quenching activity and eukaryotic cytotoxicity. Six distinct scaffolds named HC101-HC106 (Fig. 2.1b) were confirmed as inhibitors of reporter fluorescence, while exhibiting no GFP quenching activity and limited eukaryotic cytotoxicity (e.g. half maximal effective concentration (EC_{50}) $>70 \mu\text{M}$ for eukaryotic cytotoxicity in murine bone marrow derived macrophages, Supplementary Table 2.1).

The most frequently identified scaffold from the primary screen was artemisinin (HC101A) and its analogs artemether, artesunate and dihydroartemisinin (DHA, Fig. 2.1a). This scaffold was identified as nine independent hits in the screen. Artemisinin and its analogs inhibit CDC1551(*hspX*::GFP) reporter fluorescence with an EC_{50} ranging from 1.2-3.7 μM (Fig. 2.1c, Supplementary Fig. 2.2a, Supplementary Table 2.1), while the growth inhibition EC_{50} is $>80 \mu\text{M}$, indicating a limited impact on growth. HC102A (**1**, (+/-) (5S,9R)-7,7,9-trimethyl-1,3-diazaspiro[4.5]decane-2,4-dione) was isolated as a singleton and inhibits *dosR*-dependent GFP

fluorescence with an EC₅₀ of 12.4 μM, while not inhibiting Mtb growth (e.g. a growth inhibition EC₅₀ >80 μM). HC103A (**2**, N-[3-[(3-hydroxyphenyl)carbamoyl]phenyl]thiophene-2-carboxamide) and the analog HC103B inhibit *dosR*-dependent GFP fluorescence with an EC₅₀ of 2.7 μM and 5.0 μM, respectively (Fig. 2.1c, Supplementary Fig. 2.2b) while not inhibiting growth (e.g. a growth inhibition EC₅₀ >80 μM). HC104A (**3**, 6-bromo-2-[3-(dimethylamino)propyl]benzo[de]isoquinoline-1,3-dione), HC105A (**4**, 9-ethyl-3-((4-(propylsulfonyl)piperazin-1-ium-1-yl)methyl)-9H-carbazol-9-ium oxalate) and HC106A (**5**, 1-(2,4-dichlorophenyl)-3-(1,2-oxazol-5-yl)urea) inhibit *dosR*-dependent GFP fluorescence with EC₅₀ of 2.8 μM, 12.7 μM and 6.9 μM respectively, while not inhibiting Mtb growth (e.g. a growth inhibition EC₅₀ >80 μM; Supplementary Fig. 2.2b and Supplementary Table 2.1). Artemisinin, HC102A and HC103A were selected for proof-of-concept follow-up experiments characterizing their ability to inhibit *dosRST* signaling. Both HC102A and HC103A were regenerated by organic synthesis and confirmed to have the activity of the commercially sourced compounds, thus confirming the assigned structures as the active structures (Supplementary Fig. 2.2cd).

The DosRST regulon is strongly induced by hypoxia and nitric oxide and composed of ~50 genes that are directly regulated by DosR (6). An additional >100 genes are also differentially expressed in a *dosR* mutant, possibly due to weak binding by DosR or indirect consequences of misregulated DosR regulon genes (8). To investigate the inhibitory mechanism of the compounds, RNAseq-based transcriptional profiling was undertaken on CDC1551 treated with 40 μM artemisinin, HC102A, HC103A or a DMSO control. The cultures were grown in standing flasks where growth causes the consumption of oxygen, and following 6 d of treatment RNA was isolated, sequenced and analyzed (25) (Supplementary Datasets 2.1-3). Artemisinin caused the strong downregulation of well-characterized DosR regulon genes, including *hspX*, *fdxA*, *tgsI*, and

dosRS (6) (Fig. 2.2a). Real-time PCR confirms the RNA-seq data with *hspX*, *tgsI* and *dosRS* showing 51-, 166-, and 37-fold inhibition by artemisinin, respectively (Supplementary Fig. 2.3a). Artemisinin inhibited 85 genes (>2-fold, $p < 0.05$) that are also repressed in the CDC1551($\Delta dosR$) mutant, accounting for greater than two-thirds of the 125 downregulated genes in the CDC1551($\Delta dosR$) mutant (Fig. 2.2b, Supplementary Dataset 2.1). Notably, artemisinin also inhibited 157 genes that are not modulated in the CDC1551($\Delta dosR$) mutant, suggesting the drug is also impacting DosRST-independent targets. HC102A and HC103A also inhibited DosRST regulon genes, however, in contrast to artemisinin, HC102A and HC103A showed greater specificity for inhibition of the DosRST regulon; for example, 48 out of 55 genes downregulated by HC102A and 76 out of 90 genes downregulated by HC103A are also downregulated in the CDC1551($\Delta dosR$) mutant (Fig. 2.2bc, Supplementary Fig. 2.3cd, Supplementary Dataset 2.1). These transcriptional profiles demonstrate that artemisinin, HC102A and HC103A inhibit induction of the core DosRST regulon.

To further assess the specificity of the compounds for inhibition of the DosRST pathway, a CDC1551($\Delta dosR$) mutant was treated with the compounds of interest, with the hypothesis that compounds specific for the DosRST pathway will not modulate gene expression in the CDC1551($\Delta dosR$) mutant. The CDC1551($\Delta dosR$) mutant treated with HC102A or HC103A, exhibited only 0 and 13 downregulated genes, respectively, confirming the on-target specificity of HC102A and HC103A (Fig. 2.2c, Supplementary Dataset 2.2). In contrast, the CDC1551($\Delta dosR$) mutant treated with artemisinin exhibited 69 downregulated genes (Fig. 2.2c, Supplementary Dataset 2.2), confirming substantial off-target activity for artemisinin. Overall, these data further support the hypothesis that artemisinin, HC102A and HC103A function to inhibit the core DosRST

regulon, with HC102A and HC103A showing strong specificity for the intended target of the DosRST regulon.

The DosRST pathway is also induced by NO and vitamin C (7, 11, 26) and it was examined if the inhibitors could suppress induction of the DosR pathway by these stimuli. CDC1551 was pre-treated with DHA, HC102A or HC103A for 1 d prior to induction with NO or vitamin C. As markers for the DosR regulon, the expression of three DosR regulated genes (*dosR*, *tgs1* and *hspX*) was monitored by real-time PCR. *dosR*, *hspX* and *tgs1*, were strongly up-regulated when Mtb was treated with vitamin C or NO-donor reagent, DETA-NONOate (Supplementary Fig. 2.3b). For example, vitamin C caused a 4-, 14- and 52-fold induction of *dosR*, *hspX* and *tgs1*, respectively, and NO caused an 491-, 373-, and 47-fold induction of *dosR*, *hspX* and *tgs1*, respectively. Pre-treatment with HC102A or HC103A strongly inhibited the induction of *dosR*, *hspX* and *tgs1* transcripts in response to both vitamin C and DETA-NONOate. For example, in HC102A and HC103A pretreated cells the *tgs1* transcript following treatment with DETA-NONOate is repressed 3-fold and 50-fold, respectively, whereas *tgs1* is induced >47-fold in the DMSO pretreated cells. Similarly, in vitamin C treated cells, the *tgs1* transcript is repressed 2-fold and 3-fold and in HC102A and HC103A pretreated cells, respectively, while induced >50 fold in the DMSO treated cells. DHA only weakly inhibited the induction of the DosR regulated genes by NO or vitamin C. In DHA pretreated cells, the *dosR*, *hspX* and *tgs1* transcripts remain induced by both vitamin C and DETA-NONOate treatments. Notably, the magnitude of the induction of the transcripts in response to DETA-NONOate is significantly reduced ~2-fold in DHA pretreated cells compared to the DMSO treatment, demonstrating partial inhibition of NO-dependent DosRST signaling by DHA. These data support the view that HC102A and HC103A act as broad inhibitors of the DosRST regulon in response to both hypoxia and redox environmental cues. In

contrast, artemisinin likely acts by a mechanism that is distinct from HC102A and HC103A, given its limited effectiveness to inhibit redox-mediated stimulation of the DosRST regulon.

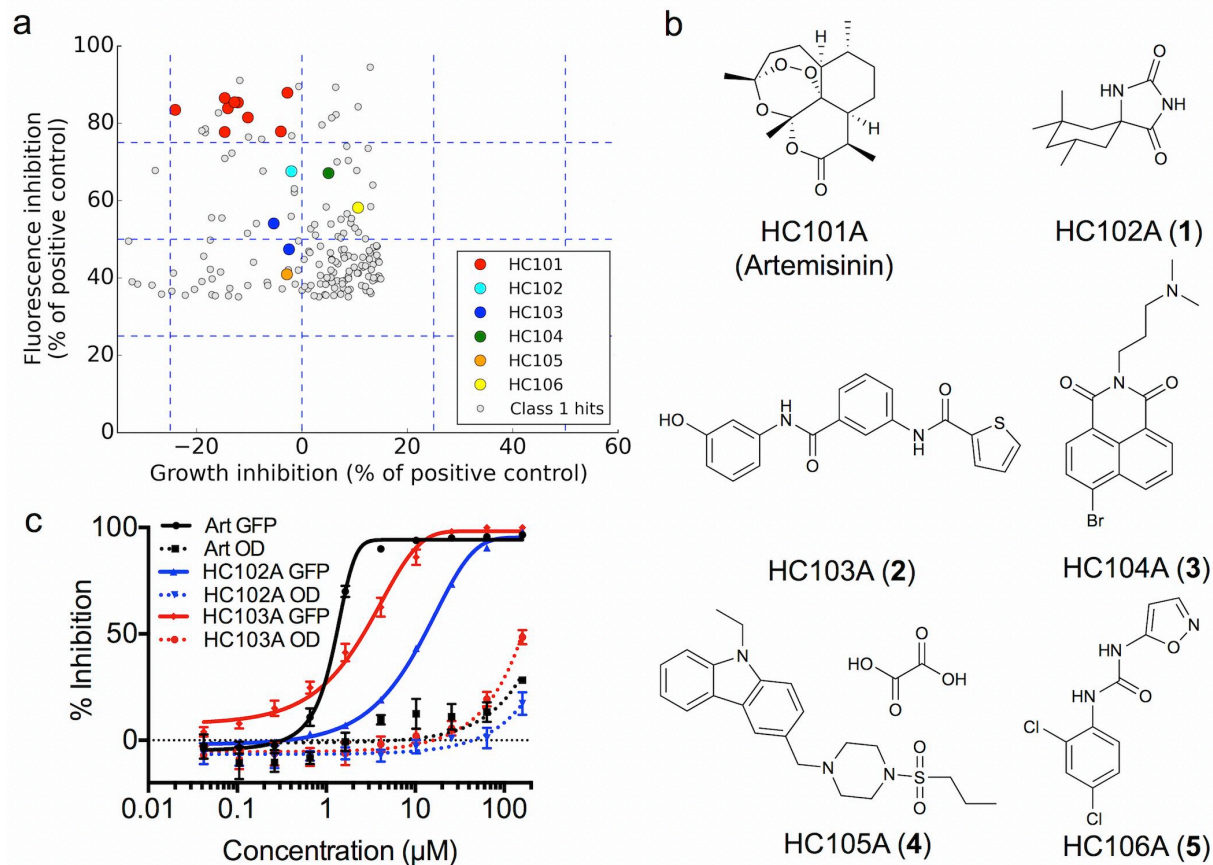


Figure 2.1. Discovery of inhibitors of the DosRST pathway. (a) Scatter plot of primary screening data showing compounds that inhibit CDC1551(*hspX*::GFP) reporter GFP fluorescence with limited impact on Mtb growth. Six distinct classes of compounds (HC101-HC106) are highlighted. (b) Structures of compounds confirmed to selectively inhibit CDC1551(*hspX*::GFP) reporter fluorescence. (c) Dose response curves for artemisinin (Art, HC101A), HC102A and HC103A inhibition of GFP fluorescence. Dose response curves for other characterized molecules are presented in Supplementary Fig. 2.1.

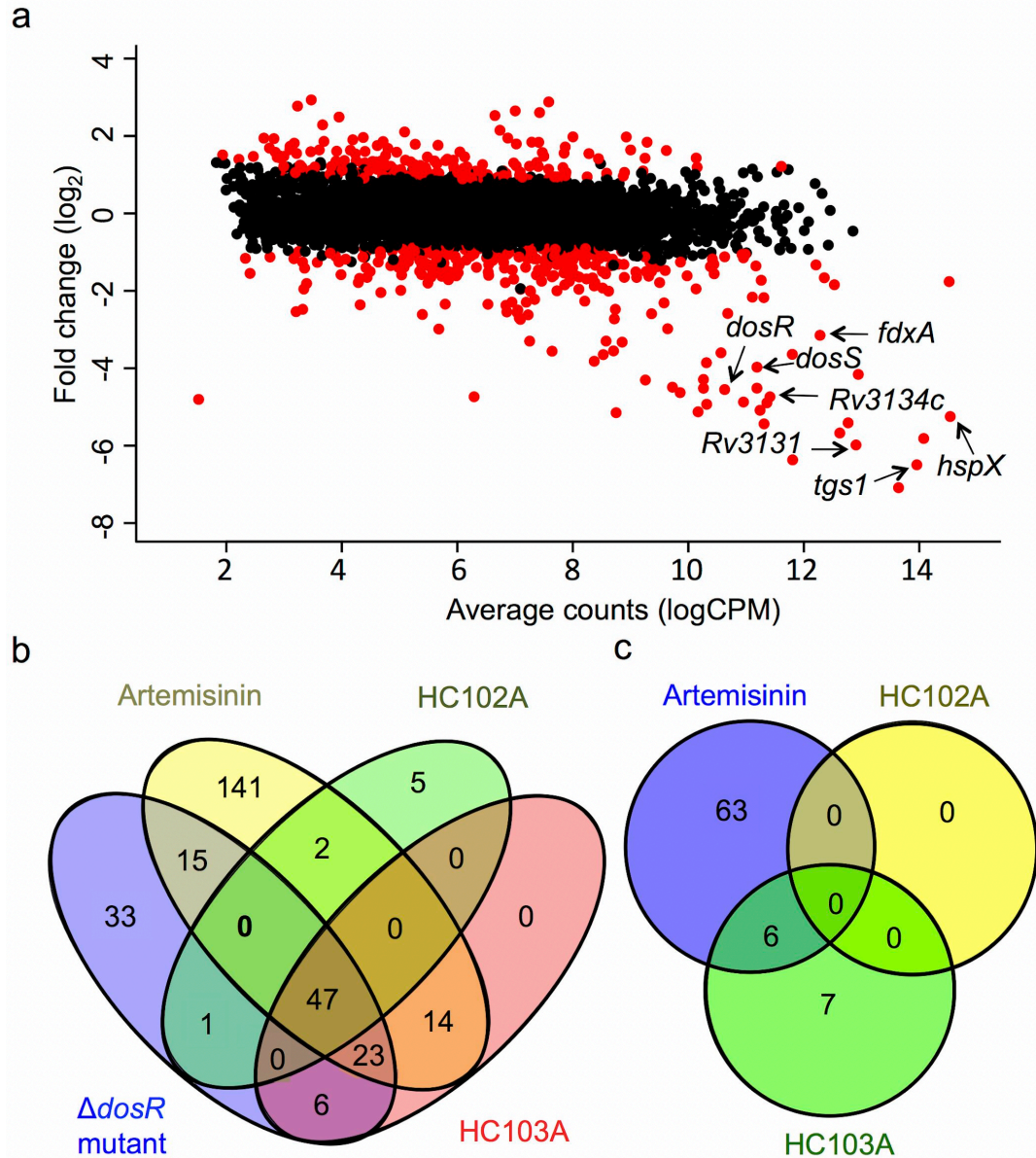


Figure 2.2. Transcriptional profiling shows artemisinin, HC102A and HC103A inhibit the core genes of the DosRST regulon during hypoxia. (a) Mtb differential gene expression in response to artemisinin. Genes in red have a p-value < 0.05. Indicated gene names include characterized DosR regulated genes. (b) Venn diagram showing genes that are downregulated (>2-fold, p < 0.05) in CDC1551 treated with artemisinin, HC102A or HC103A relative to a DMSO treated CDC1551 control. Also shown are genes downregulated (>2-fold, p < 0.05) in a DMSO treated CDC1551($\Delta dosR$) mutant strain relative to a DMSO treated CDC1551 control. (c) Venn diagram showing genes that are downregulated (>2-fold, p < 0.05) in a CDC1551 ($\Delta dosR$) mutant strain treated with artemisinin, HC102A or HC103A relative to a DMSO treated CDC1551($\Delta dosR$) control. The limited genes modulated by HC102A and HC103A confirm that these compounds are highly specific for the DosR regulon.

Artemisinin, HC102A and HC103A disrupt persistence

DosRST is required for several persistence-associated physiologies during hypoxia, including triacylglycerol (TAG) synthesis (3, 27) and survival (13). We hypothesized that artemisinin, HC102A or HC103A may target these physiologies and compared the activity of the inhibitors to a CDC1551($\Delta dosR$) mutant. Transcriptional profiling data in CDC1551 showed that the *tgsI* gene, which encodes for the TAG synthase involved in last step of TAG synthesis, is downregulated ~100 fold by artemisinin and ~20 and ~180 fold by HC102A and HC103A, respectively (Fig. 2.2 and Supplementary Fig. 2.3a, Supplementary Dataset 2.1). Therefore, we hypothesized that CDC1551 treated with artemisinin, HC102A or HC103A would be defective in TAG accumulation. To test this hypothesis, ^{14}C -labeled lipids were isolated from CDC1551($\Delta dosR$) mutant and WT CDC1551 treated with inhibitors or an equal volume of DMSO. The lipids were analyzed by thin layer chromatography and quantified. TAG accumulated in the DMSO-treated cells, whereas it was reduced 82% in the CDC1551($\Delta dosR$) mutant (Fig. 2.3a, Supplementary Fig. 2.4a). Treatment with artemisinin, HC102A and HC103A caused a 74%, 67% and 56% reduction in TAG accumulation, respectively (Fig. 2.3a, Supplementary Fig. 2.4a), thus providing functional evidence that the inhibitors are impacting persistence-associated lipid metabolism.

During NRP, the $\Delta dosR$ mutant has previously been shown to exhibit reduced intracellular survival as compared to WT bacteria (13). Using the hypoxic shift down model of NRP (27), we examined the impact of DHA, HC102A or HC103A on survival during NRP. Following 10 d of incubation in the hypoxic shift down assay, CDC1551 treated with 40 μM DHA, HC102A or HC103A, exhibited significantly reduced survival (70-80% reduction) as compared to the DMSO control (Fig. 2.3b). This reduction in survival is comparable to the CDC1551($\Delta dosR$) mutant relative to the DMSO treated WT control. The survival defect of the CDC1551($\Delta dosR$) mutant

was partially complemented in the CDC1551($\Delta dosR$) complemented strain, indicating that the observed survival defect is *dosR*-dependent. We also examined the impact of the inhibitors in the Mtb Erdman strain, to ensure the observed physiologies are not unique to the CDC1551 strain. Although minor differences between CDC1551 and Erdman existed, we observed that the inhibitors also significantly inhibited survival during NRP in the Erdman strain (Fig. 2.3b). The function of the inhibitors was examined in the hypoxic shift down assay in an 8 point dose response covering 1 μ M -100 μ M and percent viability relative to the DMSO treated control was examined following 10 d and 15 d treatment. Artemisinin, HC102A and HC103A exhibited dose dependent inhibition of viability in the hypoxic shift down model with all three compounds causing an ~50% reduction of viability at 10 μ M following 10 or 15 d of incubation (Fig. 2.3c and Supplementary Fig. 2.4b).

The DosR regulated gene *tgsI* has previously been shown to be required for Mtb tolerance to antibiotics during hypoxia (17, 28). Because the inhibitors strongly inhibit *tgsI* gene expression, we hypothesized these compounds may sensitize Mtb to isoniazid (INH). Using the hypoxic shift down assay, Mtb Erdman was pretreated with either 20 μ M or 40 μ M of artemisinin, HC102A or HC103A and following 2 d, the cells were treated again with the experimental inhibitors (for a combined treatment of 40 μ M or 80 μ M) in addition to INH over a dose response (1 μ M, 5 μ M, 25 μ M INH or a DMSO control). Following 10 and 15 d of INH treatment surviving bacteria were enumerated (Fig. 2.3d and Supplementary Fig. 2.4c). At day 10, treatment with artemisinin, HC102A or HC103A alone at 40 μ M or 80 μ M causes a significant reduction of survival ranging from a 3-fold to 30-fold decrease in surviving bacteria (Fig. 2.3d). Ten days post INH treatment, INH alone had minimal impact on Mtb survival, with ~100% viability at 1 μ M and 5 μ M INH and ~75% viability at 25 μ M INH (Fig. 2.3e), confirming that Mtb is tolerant to INH in the hypoxic

shift down assay. Treatment with 40 μ M artemisinin, HC102A or HC103A caused a significant ~30% reduction of Mtb viability in the presence of 5 μ M INH (Fig. 2.3e) relative to cultures not treated with INH, suggesting that the inhibitors inhibit INH tolerance. At day 15, similar trends were observed in reduction of Mtb survival and antibiotic tolerance in cultures treated with artemisinin, HC102A or HC103A (Supplementary Fig. 2.4cd). Notably, at day 15, treatment with 40 μ M artemisinin or HC103A caused a ~50% reduction of Mtb viability when treated with 5 μ M INH (Supplementary Fig. 2.4d), suggesting that the function of artemisinin and HC103A may be enhanced during longer periods of NRP.

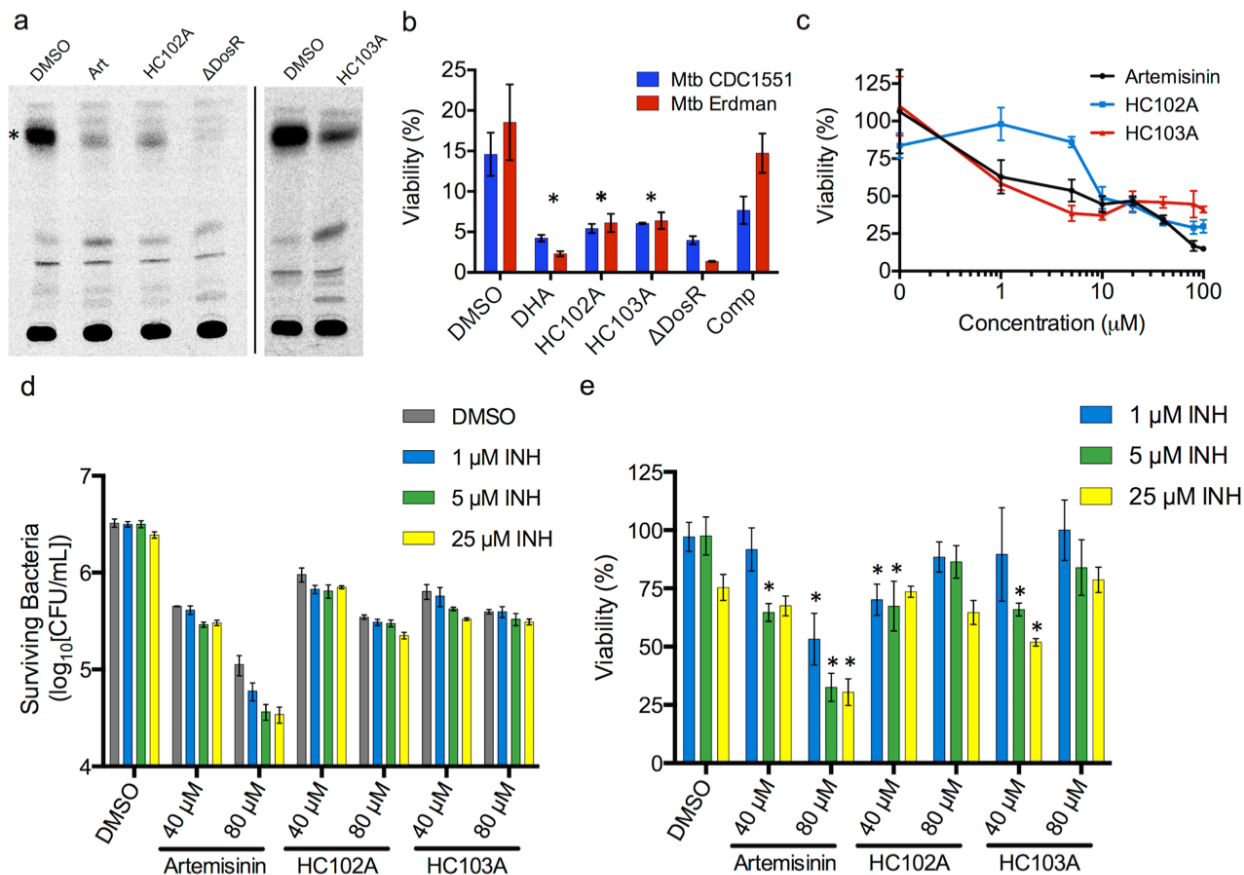


Figure 2.3. Artemisinin, HC102A and HC103A inhibit TAG synthesis, survival and isoniazid tolerance. (a) CDC1551 treated with compounds of interest (at 40 μ M) exhibits a 60-70% reduction of TAG accumulation, similar to the CDC1551(Δ *dosR*) mutant control. The position of TAG is indicated by the asterisk. (b) CDC1551 and Erdman strains treated with 40 μ M of the compounds of interest exhibit reduced survival following 10 d in the hypoxic shift down assay. CFUs were counted and percent survival calculated relative to the WT control at day 0. Differences between treated samples as compared to the DMSO control are significant (P -value <0.05 based on a t -test, marked with an asterisk). (c) Dose dependent inhibition of Mtb survival in the hypoxic shift down assay. Percent viability was calculated relative to viable bacteria in the DMSO control at day 10. (d) Following 10 d in the hypoxic shift down assay, treatment with artemisinin, HC102A or HC103A, with or without INH, significantly reduces bacterial survival relative to the respective DMSO controls (P -value <0.05 based on a t -test). (e) Artemisinin, HC102A and HC103A reduce INH tolerance in the hypoxic shift down assay. Percent viability at 1, 5 and 25 μ M INH was calculated relative to the 0 μ M INH control (using data in panel d). Significant inhibition of INH tolerance (marked with an asterisk, P -value <0.05 based on a t -test) is observed relative to the respective DMSO controls. For each panel, error bars represent the standard deviation and experiments were repeated at least twice with similar results.

Artemisinin targets DosS and DosT sensor kinase heme

Artemisinin is a first-line drug for treating malaria (29) and the mechanism of action has been extensively studied (29, 30). Evidence suggests that reductive cleavage of the artemisinin endoperoxide bridge is initiated by ferrous iron (Fe^{2+}) under reduced conditions, and generates a C4-centered radical. The radical form of artemisinin can alkylate heme and results in artemisinin-heme adduct formation (30, 31). Because DosS/T are also heme-containing proteins, we hypothesized that artemisinin interacts similarly with the heme in DosS/T leading to artemisinin-mediated inhibition of the DosRST regulon. Biochemical data suggest DosS is a redox sensor that autoxidizes quickly under aerobic conditions (32), whereas, DosT is a hypoxia sensor and has high affinity and sensitivity to O_2 (33). Both kinases sense environmental cues via heme, and are inactive when the heme group exists as either the Met (Fe^{3+}) form (in the case of DosS) or the oxy ($\text{Fe}^{2+}\text{-O}_2$) form (in the case of DosT) in the presence of O_2 ; the kinases are activated when DosS is in the ferrous form and DosT is in the deoxy form (11, 32, 34-36).

A UV-visible spectroscopy assay was employed to determine the interaction between DosS/T and artemisinin (11). DosS and DosT, purified under aerobic conditions, have Soret peaks at 409 nm and 412 nm, respectively (11) (Fig. 2.4ab). Reduction of the heme by dithionite (DTN) shifts the DosS/T Soret peaks to 430 nm. Treatment of DosS with artemisinin (purged of O_2) causes the Soret peak of DosS to gradually shift back to the original oxidized Soret peak. This indicates that artemisinin can function to modulate DosS redox status. Notably, treatment of DosT with artemisinin reduces the amplitude of the Soret peak, a response that has previously been shown to be associated with artemisinin-mediated degradation of heme (37, 38). The position of the peaks did not shift to the oxidized state in the DMSO treated proteins. Dose-response studies further show that artemisinin inhibits DosT at 50 μM (Fig. 2.5d), whereas artemisinin only causes the shift

of the reduced Soret peak of DosS at a much higher concentration of 400 μM (Supplementary Fig. 2.5a). This finding suggests that DosT is more sensitive to artemisinin than DosS and may explain why the artemisinins had weaker activity for the inhibition of the DosR pathway when stimulated by NO or vitamin C. Because the DosS/T kinases are active in the reduced form and inactive in the oxidized form (11), these data are consistent with artemisinin inhibiting DosS/T kinases by modulating their redox status (*e.g.* DosS at high concentrations) or causing degradation of the heme (*e.g.* DosT). To test the hypothesis that artemisinin can alkylate heme carried by the sensor kinase, DosS reaction samples treated with artemisinin or DMSO were subjected to LC-MS analysis. Molecules with masses of ~ 898 Da were identified in the artemisinin treated sample that are absent in the DMSO treated sample (Fig. 2.4c). This molecular weight corresponds to the sum of the masses of artemisinin (282 Da) and heme (616 Da), supporting the hypothesis that artemisinin alkylates the sensor kinase heme to form heme-artemisinin adducts (39). In a previous study, a structure of the artemisinin-alkylated heme with a mass of 898.3 was shown to involve alkylation of the heme at the α , β or δ positions with the iron in the ferric state (39). Notably, adducts of DosS peptides were not observed. Together, these findings support a mechanism of action where artemisinin directly targets the heme to inactivate the DosS and DosT sensor kinases. The UV-visible spectra and mass spectrometry data support differing mechanisms for DosS and DosT inactivation by artemisinin, with DosS alkylated-heme remaining intact but in the ferric state (39) and the DosT heme being degraded by artemisinin (37, 38). In both cases, these heme-artemisinin interactions would result in disabling the sensor functions of DosS/T.

Molecular modeling of DosS and DosT structures (34, 35) shows that the kinases have a channel through which the artemisinin may access and dock to the heme (Fig. 2.5a). To test this model, amino acid substitutions were generated along the channel in DosS/T, including E87L and

G117L in DosS or G85L and G115L in DosT, that are predicted to limit the ability of artemisinin to access the heme based on modeling conducted in this study and published studies (33). In the UV-visible spectroscopy assay, DosS (E87L) and DosS (G117L) exhibited similar overall spectra as WT DosS under aerobic conditions and treatment with DTN caused the Soret peak to shift to the reduced position (Fig. 2.5bc); thus, the heme in both mutant proteins retains the ability to respond to reduction by DTN. Notably, the DosS (E87L) and DosS (G117L) proteins were resistant to oxidation by 400 μ M artemisinin and the major Soret peak (430 nm) did not shift to the oxidized position following 60 min of treatment (Fig. 2.5bc). The analogous mutations of DosT, G85L and G115L, also exhibited similar overall spectrum as WT DosT under aerobic conditions, as well as in responding to DTN treatment (Fig. 2.5de and Supplementary Fig. 2.5b). However, the lower peak at 560 nm of deoxy-DosT (G115L) was maintained when treated with 100 μ M artemisinin as compared to WT DosT and DosT (G85L) (Fig. 2.5de and Supplementary Fig. 2.5b). The 560 nm peak is generated by merging two lower peaks at 538 nm and 575 nm together after DTN treatment (40). This peak is highly sensitive to oxygen or artemisinin treatment and disappears immediately upon exposure to oxygen or artemisinin (11, 37, 38). Additionally, the Soret peak in the G115L mutant is not reduced in a dose-dependent manner, as compared to the WT and G85L mutants (Fig 2.5de and Supplementary Fig. 2.5b), further supporting the DosT (G115L) protein exhibits artemisinin resistance.

The UV-visible spectroscopy data collectively support the notion that DosS E87L and G117L and DosT G115L substitutions may limit artemisinin from fully accessing the heme, thereby providing resistance to artemisinin. To test this hypothesis in *Mtb*, we transformed CDC1551 with a plasmid overexpressing the WT *dosT*, *dosT* (G85L) or *dosT* (G115L) genes and determined if artemisinin resistance is observed. The strains were grown in standing flasks to stimulate the

DosRST regulon and expression of DosRST regulon genes (*dosR*, *hspX*, *tgsl*) was examined by real-time PCR following 6 d of treatment with artemisinin over a dose response curve (Supplementary Fig. 2.6). Strains expressing WT *dosT* or *dosT* (*G85L*) exhibited EC₅₀ for artemisinin-mediated inhibition of DosR regulon genes of 0.2-0.3 μ M whereas, *dosT* (*G115L*) exhibited EC₅₀ of 1.0-1.6 μ M. (Fig. 2.5f and Supplementary Fig. 2.6). Therefore, the DosT (*G115L*) protein provides ~5 fold resistance to artemisinin and nearly full resistance at 1 μ M artemisinin (Fig. 2.5f). These biochemical and biological data confirm that artemisinin modulates the DosRST signaling by directly targeting the heme sensor carried by DosS and DosT histidine kinases.

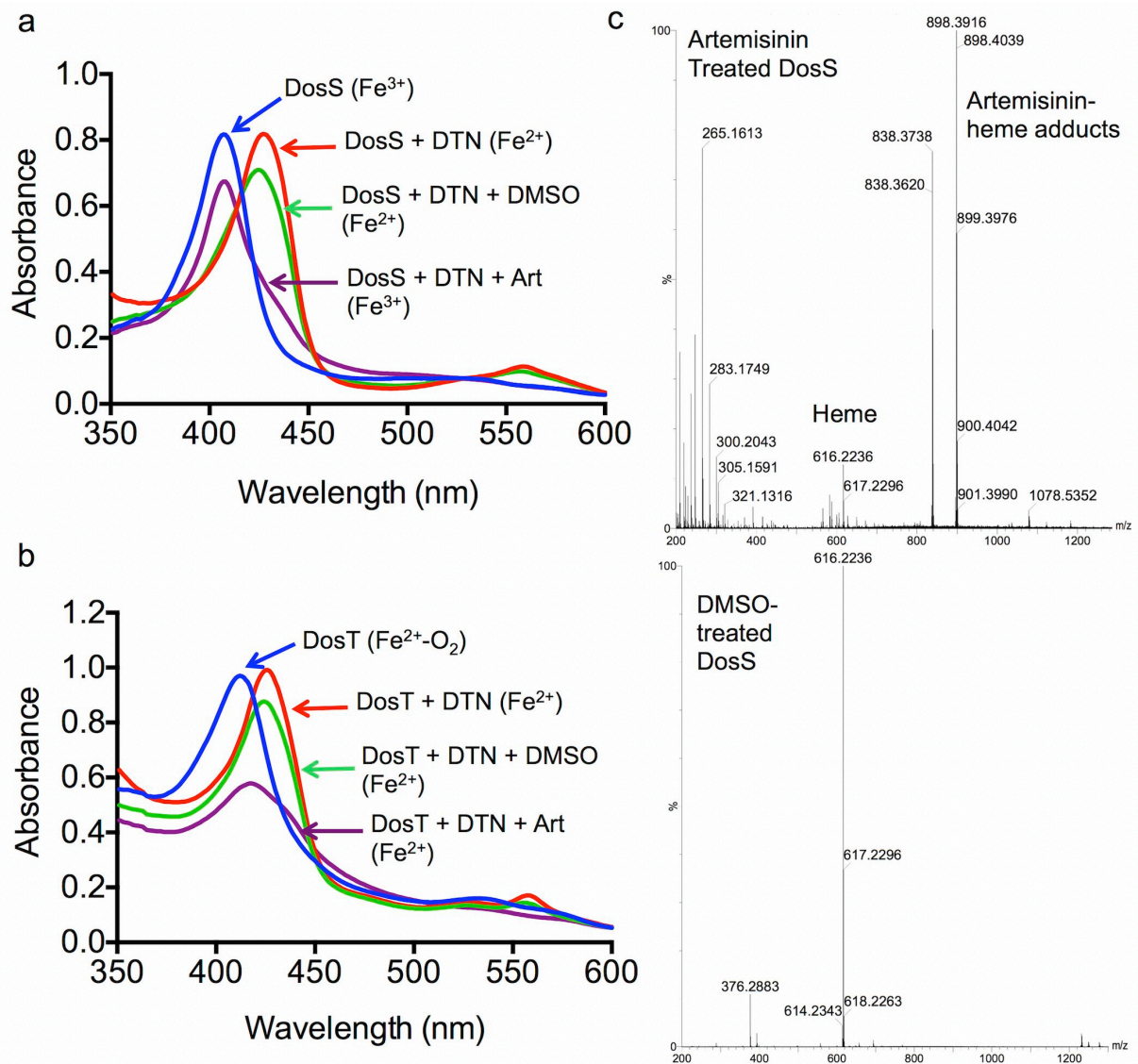


Figure 2.4. Artemisinin directly inhibits DosS and DosT by targeting sensor kinase heme. UV-visible spectra of DosS (panel a) and DosT (panel b) showing treatment with dithionite (DTN) reduces the heme (the “on” state for the kinases) and that artemisinin oxidizes or degrades the heme (“off” states of the kinases). (c) MS spectra showing the presence of peaks at ~898 Da that are present in artemisinin treated DosS samples, but absent in DMSO treated samples. This mass is the approximate combined mass of heme (616.487 Da) and artemisinin (282.332 Da) and is consistent with the formation of heme-artemisinin adducts. Experiments were repeated at least twice with similar results.

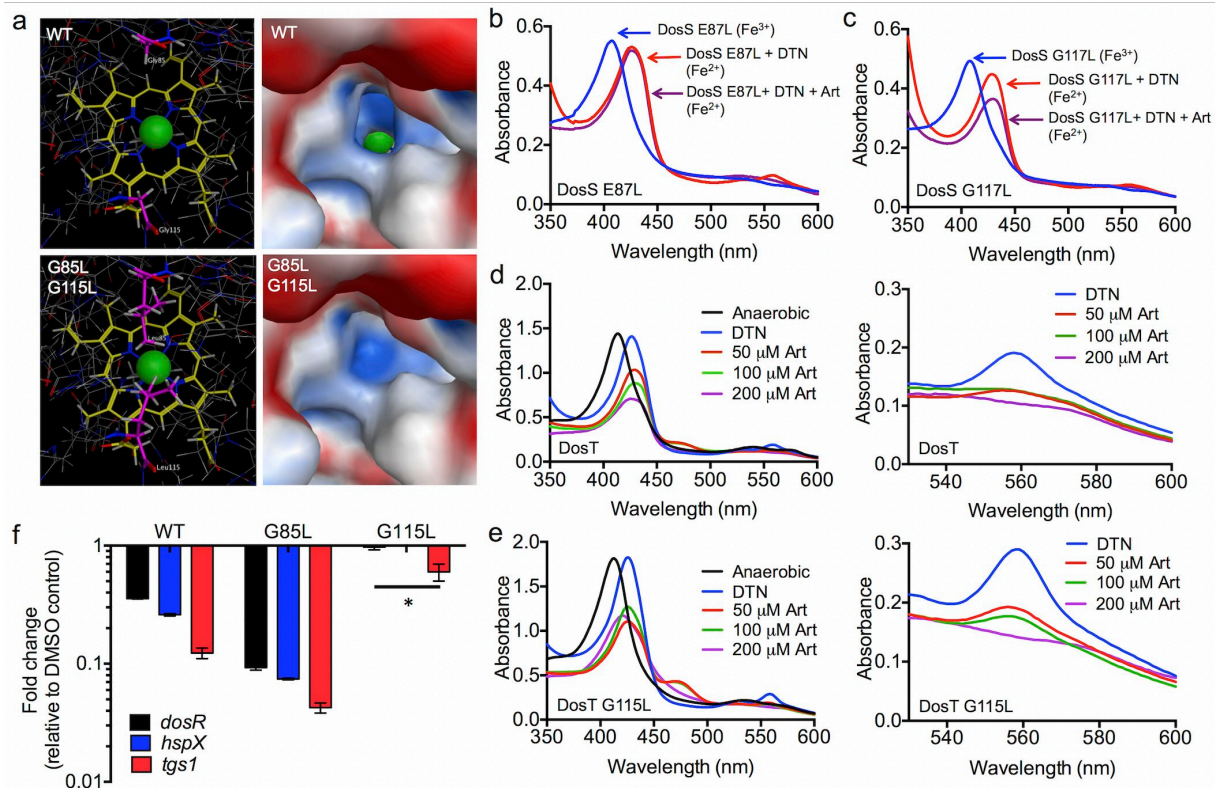


Figure 2.5. Amino acid substitutions in DosS or DosT promote resistance to artemisinin. (a) Molecular modeling indicates a channel exists in DosS and DosT through which artemisinin may access the heme. In WT DosT, the heme (colored yellow) and iron (green ball) are accessible to artemisinin via a channel. G85L and G115L substitutions are predicted to block this channel and access to the heme. (b and c) UV visible spectra show that DosS (G87L) and DosS (G117L) proteins can be reduced by the addition of dithionite (DTN) but are resistant to oxidation by artemisinin (Art). (d and e) WT DosT exhibits a dose-dependent decrease in the amplitude of the Soret peak at 430 nm (left side of panel d) and a loss of the peak at 560 nm (magnified in right side of panel d). In contrast, DosT (G115L) exhibits resistance to artemisinin because it does not exhibit a dose-dependent decrease in the 430 nm peak (left side of panel e) and the 560 nm peak is maintained at treatments of 50 and 100 μM artemisinin (right side of panel e). DosT (G85L) exhibits spectra similar to WT DosT (Supplementary Fig. 2.5B). (f) Overexpression of DosT (G115L) in CDC1551 provides artemisinin resistance. Mtb overexpressing WT DosT or DosT (G85L) exhibit strongly inhibited expression of DosR regulated genes (*dosR*, *hspX* and *tgs1*) in the presence of 1 μM artemisinin, while the strain overexpressing DosT (G115L) is resistant. Dose response curves are presented in Supplementary Fig. 2.6. Experiments were repeated at least twice with similar results.

HC103A inhibits DosS and DosT autophosphorylation

UV-visible spectroscopy studies showed that HC102A and HC103A have no impact on the redox status of DosS or DosT heme (Supplementary Fig. 2.7ab), suggesting these compounds function by a mechanism that is distinct from artemisinin. Given the strong specificity with which these compounds inhibit the DosRST regulon, we hypothesized that HC102A and HC103A may directly inhibit DosS/T autophosphorylation activity. To test this hypothesis, *in vitro* phosphorylation assays were performed as previously described (41). DosS and DosT were quickly phosphorylated within 30 s of initiating the assay by adding [γ - 32 P] ATP. The amount of phosphorylated protein increased over time consistent with previous reports (41). DosS treated with HC102A and HC103A showed decreased autophosphorylation activity (Fig. 2.6, Supplementary Fig. 2.8). Inhibition of DosS autophosphorylation activity increased in a dose-dependent manner with IC₅₀s of 1.9 μ M and 0.5 μ M for HC102A and HC103A, respectively. Notably, differences in maximal inhibition were observed, with ~60% and ~90% for HC102A and HC103A, respectively. DosT treated with HC103A also showed a dose-dependent inhibition of autophosphorylation and an IC₅₀ of ~5 μ M (Fig. 2.6). These findings support the proposal that HC103A functions by directly modulating DosS and DosT kinase activity.

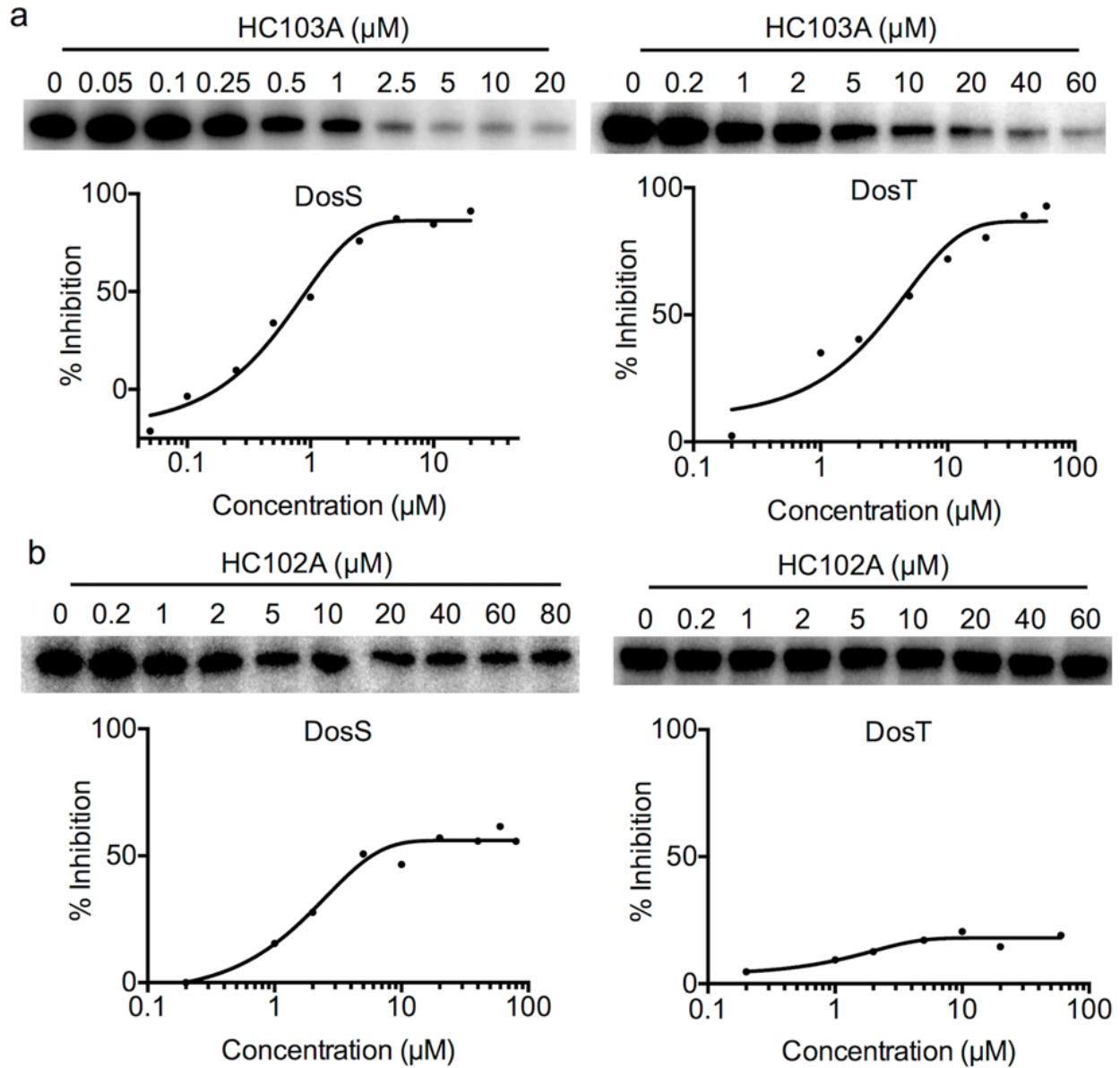


Figure 2.6. HC103A inhibits DosS and DosT autophosphorylation. Recombinant DosS or DosT was treated with HC103A (a) or HC102A (b) across a dose response curve. The autophosphorylation assay was incubated for 1 h, the proteins were blotted and the protein autophosphorylation was assessed by following exposure of the blot to a phosphor screen. HC102A and HC103A inhibit DosS autophosphorylation with IC_{50} of 1.9 μM and 0.5 μM , respectively. HC102A had limited impact on DosT autophosphorylation, whereas HC103A inhibited DosT autophosphorylation with an IC_{50} of ~ 5 μM . Experiments were repeated at least twice with similar results.

Discussion

In this study a CDC1551(*hspX*::GFP) fluorescent reporter strain was used as a synthetic phenotype for the targeted discovery of several compounds that inhibit the DosRST pathway. Treatment of Mtb with these compounds copies several phenotypes of a CDC1551(Δ *dosR*) mutant, including: downregulation of the core DosRST regulon, reduced TAG synthesis, and decreased survival during NRP. These findings provide proof-of-concept data that the high-throughput screen successfully identified inhibitors of the DosRST regulon and support further studies characterizing additional putative DosRST regulon inhibitors, including HC104-HC106, as well as uncharacterized putative hits from the primary screen. Several new chemical inhibitors of Mtb during NRP have been recently described. One promising target is the direct inhibition of ATP homeostasis by targeting the components of the electron transport chain or ATP synthase (27, 42-44). However, the approach of targeting the DosRST top-level regulators has the potential to inhibit multiple physiologies required for establishing or maintaining NRP and this multifactorial approach may broadly limit persistence in heterogeneous NRP-inducing environments. Using homology modeling, the discovery of a DosR regulon inhibitor that specifically inhibits DosR binding to target DNA (45) has been reported. Additionally, a screen for small molecules that modulate Esx-1 export, identified inhibitors that indirectly modulate the DosR regulon (46). However, to the best of our best knowledge, the newly discovered compounds represent novel inhibitors of the DosRST regulon with distinct mechanisms of action.

Both HC102A and HC103A appear to be remarkably specific for inhibiting the DosRST pathway. Indeed, no genes were downregulated (>2-fold, $p < 0.05$) in the CDC1551(Δ *dosR*) mutant treated with HC102A, supporting the idea that only DosR controlled pathways are targeted by HC102A. HC103A treatment of the CDC1551(Δ *dosR*) caused downregulation (>2-fold, $p < 0.05$)

of 13 genes. Several genes fell into related classes including: four arginine biosynthesis genes (*argC*, *argB*, *argJ* and *argF*), two acyl-(ACP) desaturases (*desA1* and *desA2*), two ferredoxins (*fdxC* and *fprB*), three PE-PPE genes (Rv0160c, Rv1386 and Rv1387), and an orphan response regulator (Rv0260c). This finding suggests that although HC103A is highly specific for the DosRST pathway other targets likely exist.

In contrast to HC102A and HC103A, artemisinin exhibits significant off-target activities, with 69 genes differentially regulated in the CDC1551(Δ *dosR*) mutant treated with this compound. Given that artemisinin has a reactive endoperoxide bridge, it is perhaps surprising that there are not a greater number of genes that are differentially regulated, as one might expect artemisinin to react with any proteins carrying reduced iron. The downregulated genes do not match genes regulated by ROS (47), suggesting that artemisinin is not promoting Fenton reactions and acting as an indiscriminate oxidant. Notably, it has been shown that when artemisinin is delivered into Mtb as a mycobactin–artemisinin conjugate it causes an intracellular burst of reactive oxygen via Fenton reactions that kills Mtb (48). Based on this finding, it is tempting to speculate that artemisinin alone cannot fully access the Mtb cytoplasm and is thus modulating membrane-associated proteins, such as DosS/T. Other membrane proteins that may interact with artemisinin (e.g. heme-bearing cytochromes) may be resistant to artemisinin if the heme is buried in the protein and not accessible to artemisinin. Structural analysis of the heme-embedded GAF domain of DosST shows that DosT has a wider channel than DosS that could potentially provide greater accessibility to artemisinin (34, 35). This suggestion is supported by our data that DosT is more sensitive to artemisinin than DosS and is consistent with artemisinins having limited ability to inhibit NO-mediated stimulation of the DosR regulon. Alternatively, DosS may be less sensitive to artemisinin than DosT due to differences in autooxidation rates, where DosS is more quickly

oxidized to the ferric state in the presence of oxygen (49). Autooxidized DosS in the ferric form would not react with artemisinin, resulting in the observed insensitivity. Collectively, we have shown this channel is susceptible to drugs with artemisinin as a proof-of-concept, therefore structure-based synthesis of compounds that block the heme-bearing channel of DosS and DosT may promote the development of additional novel inhibitors of Mtb persistence. The discovery that artemisinin inhibits Mtb persistence raises interesting questions about the use of artemisinin to treat malaria in individuals co-infected with malaria and Mtb, however, further studies will be required to determine the clinical significance of artemisinin-Mtb interactions.

Accession Codes:

The transcriptional profiling data have been submitted to the NCBI GEO database (accession no. GSE76566).

Materials and methods

Bacterial strains and growth conditions. Mtb strains CDC1551 and Erdman were used as indicated. CDC1551(Δ *dosR*) and Erdman(Δ *dosR*) mutants were constructed using gene replacement by homologous recombination (50) using methods as previously described (51). Deletions were confirmed by PCR and transcriptional profiling. All strains were cultured at 37°C and 5% CO₂ in standing, vented tissue culture flasks in 7H9 Middlebrook medium supplemented with 10% OADC (oleic acid albumin dextrose catalase) and 0.05% Tween-80. For *dosT* overexpression strains, the *dosT* gene was cloned under the control of the strong *hsp60* promoter in the pVV16 vector and transformed into CDC1551. *dosT* (*G85L*) and *dosT* (*G115L*) mutants

were generated using the QuickChange site directed mutagenesis approach (Agilent) in pVV16 and confirmed by sequencing.

High-throughput screening assay and data analysis. The HTS was conducted against two compound collections, the 211,655 compound ICCB-Longwood collection and the 328,633 compound NIH Molecular Libraries Program (MLP) collection, both provided by the ICCB at Harvard Medical School. The compounds were arrayed in 384-well clear bottom, black sided microtiter plates (Corning) at a final screening concentration of ~ 10 μ M. Two columns of each plate were left blank for positive and negative controls of 0.3 μ M rifampicin and DMSO alone, respectively. The *M. tuberculosis* CDC1551 (*hspX*::GFP) fluorescent reporter was grown to mid- to late-exponential phase in vented T-150 standing flasks in Middlebrook 7H9 (OADC) medium (buffered to pH 7.0 with 100 mM MOPS (3-morpholinopropanesulfonic acid)). The cultures were then re-suspended in 7H9 (OADC) pH 7.0 medium and dispensed into the 384-well assay plates utilizing a Cy-Bio Selma liquid handler robot to an OD₅₉₅ of 0.05. The plates were then placed in a Ziploc bag with a moistened paper towel (to limit evaporation) and incubated for 6 d at 37°C. Fluorescence and optical density (OD) readings were made on an EnSpire plate reader (Perkin Elmer, Inc.) at excitation and emission wavelengths of 488 and 509 nm as a top read, with the OD being taken at 595 nm as a bottom read.

Data analysis was performed utilizing an in-house developed computational tool written in Python. Raw fluorescence and optical density measurements were exported from the EnSpire plate reader (Perkin Elmer, Inc.) in plate format as comma-separated files. Measurements were then normalized as a function of percent inhibition compared to the negative (DMSO) control (see equation below).

$$NPI_{ijk} = \left\{ \frac{\beta_{ijk} - \bar{\mu}_{nk}}{\bar{\mu}_{nk} - \bar{\mu}_{pk}} \times 100 \mid \exists Z'_{jk} \geq 0.5; Z'_{jk} = 1 - \frac{3\sigma(\mu_{njk}) + 3\sigma(\mu_{pjk})}{\mu_{njk} - \mu_{pjk}} \right\}$$

The normalized percent inhibition (NPI) for fluorescence or optical density was calculated by subtracting the overall mean of the negative controls within the run ($\bar{\mu}_{nk}$) from the measured value (β), divided by the dynamic range and multiplied by 100. The overall means for the positive and negative controls within the run ($\bar{\mu}_{nk}$, $\bar{\mu}_{pk}$) were determined if there existed at least one plate in the run with a Z' greater than or equal to 0.5(52). ijk represents the i th value in the j th plate within the k th run. σ represents the standard deviation. Potential inhibitors of the DosRST regulon were defined as compounds with greater than 35% fluorescence inhibition, limited growth inhibition, and at least 1.5-fold selectivity in the fluorescence to growth inhibition ratio. To determine the statistical significance of the 1.5 fold selectivity cutoff, Z-scores were calculated for each experimental compound fluorescence inhibition:growth inhibition ratio relative to the negative controls and P-values were derived by testing against the null distribution. Due to the high number of tests, each P-value was false-discovery rate corrected (Supplementary Fig. 2.1c). These “class 1” compounds may be directly or indirectly inhibiting DosRST signaling. The Z-factors of the screens were 0.90 and 0.89 for the ICCB-L and MLP library screens, respectively (52).

For GFP quenching assays, the CDC1551 (*hspX*::GFP) reporter was grown under GFP-inducing conditions, aliquoted into 96 well plates, treated with a dose response of HC101A-HC106A and then the plates were immediately read for GFP fluorescence. GFP quenchers cause an inhibition of GFP fluorescence and none of the compounds exhibited GFP quenching activity. Cytotoxicity assays were conducted against three eukaryotic cells, primary C57Bl/6 murine derived macrophages (BMDMs), THP-1 and J774 cells. Macrophages were prepared as previously described (53) and seeded in white, opaque, 96 well plates (Corning) and treated for 3

d with the compounds treated with a 8-point dose response curve ranging from 400 μ M to 0.65 μ M. Following 3 d, viability was determined using the CellTiter-glo luminescent cell viability assay (Promega). Percent inhibition was normalized to a Triton X-100 positive control and a DMSO negative control. EC₅₀s were calculated using the GraphPad Prism software package (version 6). Each experiment included two technical replicates per plate and two biological replicates and error bars represent the standard deviation of the biological replicates. The experiment was repeated at least twice.

EC₅₀ determinations for HC101A-HC106 compounds were performed in clear bottom, black, 96 well plates (Corning), following methods similar to those described above for the HTS. Briefly, 200 μ L of the CDC1551(*hspX*::GFP) reporter was inoculated into each well at an initial OD of 0.05. The cells were treated for 6 d with compounds using an 8-point dose response curve ranging from 400 μ M to 0.65 μ M. The plates were then read for GFP fluorescence and optical density and percent inhibition was normalized to a rifampin positive control and DMSO negative control. EC₅₀s were calculated using the GraphPad Prism software package (version 6). Each experiment included two technical replicates per plate and two biological replicates and error bars represent the standard deviation of the biological replicates. The experiment was repeated at least twice.

Transcriptional profiling and data analysis. CDC1551 or CDC1551(*AdosR*) cultures were treated with 40 μ M artemisinin, HC102A, HC103A or DMSO (as a negative control) and grown at 37°C without shaking in T-25 vented, standing tissue culture flasks in 8 mL of 7H9 medium seeded at an initial OD of 0.1. The experiments were performed with two biological replicates. Following 6 d of incubation, total bacterial RNA was extracted and sequenced as described by Baker, Johnson

and Abramovitch (2). RNA-seq data were analyzed using the SPARTA software package (25).

Real-time PCR assays. For the NO and vitamin C sensitivity assays, CDC1551 was seeded at an initial density of 0.6 OD and treated with 80 μ M DHA, HC102A, or HC103A for 24 h, and then induced with 50 μ M DETA-NONOate or 2 mM vitamin C for 2 h. After treatment, total bacterial RNA was extracted as previously described (54). Transcripts of representative genes from the *dosR* regulon, including *dosR*, *hspX*, and *tgsI*, were quantified by RT-PCR using gene-specific primers as previously described (51). The experiment included three biological replicates and error bars represent the standard deviation from the mean. The experiment was repeated twice with similar results. For the artemisinin resistance assays, CDC1551 was seeded at an initial density of 0.1 and treated with 0.025 μ M - 20 μ M artemisinin for 6 d at 37 °C. Total RNA was extracted and RT-PCR quantification of DosR-regulated genes (*dosR*, *hspX* and *tgsI*) was conducted as described above. The experiment was repeated with three biological replicates with similar results. EC50s were calculated using the GraphPad Prism software package (version 6).

Triacylglycerol accumulation analysis. CDC1551 cultures were seeded at a density of 0.1 OD in 8 mL of 7H9 medium and treated with 40 μ M of artemisinin, HC102A, HC103A or DMSO. The cultures were radiolabeled by addition of 80 μ Ci of [1,2-¹⁴C] sodium acetate to the culture, which was then grown at 37°C in vented, standing, T-25 tissue culture flasks. Total lipid was extracted after 6 d incubation and analyzed in thin-layer chromatography (TLC), as previously described (51). Total extractable lipid ¹⁴C incorporation was determined using a scintillation counter, and 20,000 cpm was loaded for analysis in a 100-cm² high-performance TLC silica gel 60 aluminum sheet. To analyze TAG, the lipids were resolved in hexane-diethyl ether-acetic acid (80:20:1

[vol/vol/vol]) solvent system. The TLC was exposed to a phosphor screen for 3 d, imaged on a Typhoon imager and quantified by ImageJ (55). The experiment was repeated with two biological replicates with similar results.

NRP survival and antibiotic tolerance assays. The hypoxic shift down assay was used as a model for NRP and performed as previously described (27). CDC1551 or Erdman cultures were pelleted and resuspended in Dubos medium at OD₆₀₀ of 0.25, and inoculated in 24-well plates (1 mL/well). In the experiments presented in Figure 2.3b, cells were treated with 40 μ M artemisinin, HC102A or HC103A or equal volume of DMSO, and incubated in an anaerobic chamber (BD GasPakTM) for 12 d. Cultures become anaerobic within 48 h incubation as indicated by methylene blue turning to colorless, and consequently day 0 is considered after 48 h of incubation. Bacteria were plated on solid medium to enumerate CFUs at day 0 and day 10. Percent viability was determined by comparing surviving bacteria at day 10 relative to day 0. Experimental conditions were examined with three biological replicates and error bars represent the standard deviation from the mean. The dose response experiments (Fig. 2.3c and Supplementary Fig. 2.4b) were performed as described above with Mtb CDC1551 using an 8-point dose response covering 1-100 μ M and a DMSO control. CFUs were enumerated at day 10 and day 15 and percent viability was determined relative to the DMSO control at day 10 or day 15. The INH tolerance assays (Fig. 2.3d and Supplementary Fig. 2.4c) were performed as described above with the following modifications. Mtb Erdman was pretreated with 20 or 40 μ M artemisinin, HC102A or HC103A for 2 d in the hypoxic shift down assay and then the anaerobic chamber was opened and the cells were treated again with 20 or 40 μ M artemisinin, HC102A or HC103A (for a total treatment of 40 or 80 μ M). The cells were also treated with 1, 5 or 25 μ M INH or a DMSO control. The cells were incubated in the anaerobic

chamber for 10 or 15 d and CFUs were enumerated by plating on solid medium. To quantify INH tolerance, percent viability at 1, 5 and 25 μM INH was measured relative to the 0 μM INH control (DMSO control). These experiments were repeated at least twice with similar results.

DosS and DosT protein purification. The *dosS* (Rv3132c) and *dosT* (Rv2027c) genes were amplified from Mtb genomic DNA by PCR and cloned into the expression vector pET15b (Novagen Darmstadt, Germany). The DosS E87L and G117L substitutions and DosT G85L and G115L mutants were generated using the QuickChange site directed mutagenesis approach (Agilent) and confirmed by sequencing. The resulting constructs were confirmed by DNA sequencing. DosS/T protein expression in *E. coli* BL21(DE3) and purification via Co^{2+} column were performed as previously described (34). Briefly, the His₆-DosS or His₆-DosT were expressed in *E. coli* BL21(DE3) supplemented with hemin (30 mg/L) and induced by isopropyl 1-thio- β -D-galactopyranoside (IPTG, 1 mM) at 18°C for 20 h. Cell pellet was suspended in lysis buffer (50 mM sodium phosphate (pH 7.6), 10% glycerol, 200 mM sodium chloride, 1% Triton X-100, 0.5 mg/mL lysozyme, 0.1 mg/mL phenylmethylsulfonyl fluoride). The cell suspension was incubated with shaking at 37°C for 0.5 h and then sonicated. Soluble extract was applied to a Co^{2+} column (Clontech) and washed with washing buffers (with or without 20 mM imidazole in 50 mM sodium phosphate (pH 7.6), 10% glycerol, 500 mM sodium chloride). The recombinant proteins were eluted with 200 mM imidazole in the same buffer. The fractions containing the purified proteins were pooled together and dialyzed in 20 mM Tris-HCl, pH 7.5.

UV-visible spectroscopy assay and mass spectrometry. The absorption spectra of DosS (7.5 μM) and DosT (7.5 μM or 16.9 μM) were analyzed in a stoppered quartz cuvette by a DU800 spectrophotometer (Beckman Coulter). All reagents were degassed with argon in a sealed cuvette or vial prior to use. Proteins were also degassed, and then treated with 400 μM DTN. The UV-visible spectra were recorded before and after DTN treatment. Lastly, different concentration of artemisinin or an equal volume of DMSO was added to the reaction. The kinetic changes in the absorption spectra were recorded for 2 h. For mass spectrometry (MS) analysis, the proteins were subjected to pepsin digestion at 37°C for 30 min after the assay, and then analyzed by liquid chromatography MS (LC-MS). Sample analysis was carried out on Waters Xevo G2-XS QToF mass spectrometer (Milford, MA, USA) with an electrospray ionization positive mode. The parameters were: capillary voltage, 3 kV; sampling cone, 40 V; source temperature, 100 °C; desolvation temperature, 350 °C; cone gas flow, 25 L/h; desolvation gas flow, 600 L/h. Chromatographic separation was done in Waters ultra-performance liquid chromatograph (ACQUITY UPLC) system equipped with a Waters BEH C18 column (1.7 μM , 100x2.1 mm). The column temperature was kept at 30 °C. Solvents were (A) 0.1% (vol) folic acid in water, and (B) acetonitrile. The flow rate was 0.2 mL/min with following gradient: A/B = 99/1 to A/B = 70/30 in 8 min, then A/B = 1/99 for 10 min, and A/B = 99/1 for last 2 min. The acquisition mass range was 200-2,000 Da. The retention time for heme and heme-artemisinin adducts was between 10-11 min. The experiment was repeated with at least two biological replicates with similar results.

DosS and DosT autophosphorylation assay. The *in vitro* phosphorylation assays were performed as previously described (41). Briefly, 4 μL reaction contained 0.2 $\mu\text{g}/\mu\text{L}$ purified DosS or DosT

protein, 100 mM Tris-HCl, pH 8.0, 50 μ M KCl₂, 5 μ M MgCl₂ and 2.5 μ Ci/ μ L [γ -³²P] ATP (6000 Ci/mmol, PerkinElmer Life Science). The proteins were treated with a 9 or 10 point dose response curve of HC102A or HC103A and the reaction was incubated at RT for 1 h. All aliquots were analyzed in 4-12% gradient SDS-PAGE (Bio-Rad), and blotted to PVDF membrane. The blot was exposed to phosphor screen overnight and quantified by ImageJ (55). The experiment was repeated with three biological replicates with similar results.

Structural modeling of DosT and the G85L and G115L substituted proteins. Modeling of DosT was performed using the Molecular Operating Environment (MOE) software (Montreal, Canada). The structure for DosT (2VZW) was downloaded from the RCSB protein data bank. For DosT images, all of Chain B and its associated water molecules were deleted. For Chain A, all water molecules and the acetic acid were deleted. Heavy atoms were fixed and hydrogen atoms relaxed with energy minimization to a gradient of 0.001. Good parameters do not exist for the heme group. Sets were defined for the protein, heme, iron, and oxygen (O₂ ligand). Carbon atoms making up the heme were colored yellow. The iron atom of the heme was colored green as a large sphere. The oxygen atoms of the oxygen group were hidden from view in all of the remaining MOE files and pictures. Residues 85 and 115 were labeled and colored purple with heavy bonds. A “Molecular Surface” was created on the protein only. The surface was colored by electrostatics using Poisson-Boltzmann to compute the electrostatic field. The iron atom of the heme can be seen down the narrow gorge.

Chemical synthesis of HC102A (CCG-232500) and HC103A (CCG-257424). Please refer to Supplementary Notes.

Acknowledgements

High-throughput screening libraries and their preparation was supported by the New England Regional Center of Excellence (U54 AI057159) and the Institute of Chemistry and Cell Biology (ICCB) at Harvard Medical School. Mark Farrugia and Bob Hausinger provided support with the UV-visible spectroscopy experiments. The MSU RTSF provided technical support for the RNA-seq library preparation and sequencing. The Vahlteich Medicinal Chemistry Core is grateful for ongoing support from the Ella and Hans Vahlteich Fund and Beverly Vahlteich Delaney. We thank members of the Abramovitch lab for critical reading of the manuscript. This project was supported by start-up funding from Michigan State University and AgBioResearch, a grant from the NIH-NIAID (R21AI105867), and Grand Challenges Explorations awards (OPP1059227 and OPP1119065) from the Bill & Melinda Gates Foundation.

APPENDIX

APPENDIX

Supplementary Information Inhibitors of *Mycobacterium tuberculosis* DosRST signaling and persistence

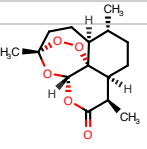
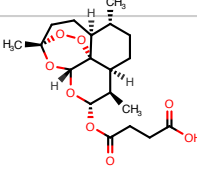
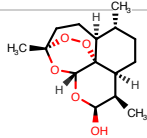
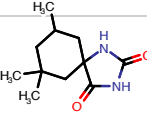
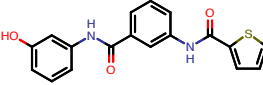
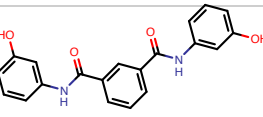
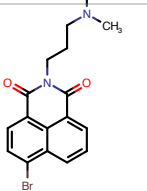
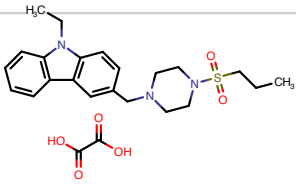
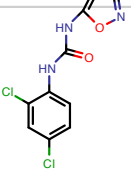
Supplementary Datasets

Supplementary Dataset 2.1. Differential gene expression data of WT Mtb treated with inhibitors and the DMSO treated DosR mutant

Supplementary Dataset 2.2. Differential gene expression data of the DosR mutant treated with the inhibitors.

Supplementary Dataset 2.3. Complete gene expression tables for transcriptional profiling experiments.

Supplementary Table 2.1. EC50 calculation of GFP fluorescence inhibition and eukaryotic cytotoxicity by DosR regulon inhibitors

Name	Structure	GFP FI (EC ₅₀ , μM)	Eukaryotic cytotoxicity (EC ₅₀ , μM)		
			BMDM	THP-1	J774
HC101A (Artemisinin)		1.2	>400	>400	>400
HC101B (Artesunate)		1.9	160.0	33.9	0.7
HC101C (Dihydroartemisinin)		3.7	100	18.8	0.4
HC102A		12.4	>400um	>400	>400
HC103A		2.7	>160	112	152
HC103B		5.0	179.8	91.1	204.6
HC104A		2.8	72.7	16.3	84.8
HC105A		12.7	235.8	90.5	57.2
HC106A		6.9	86	86	90

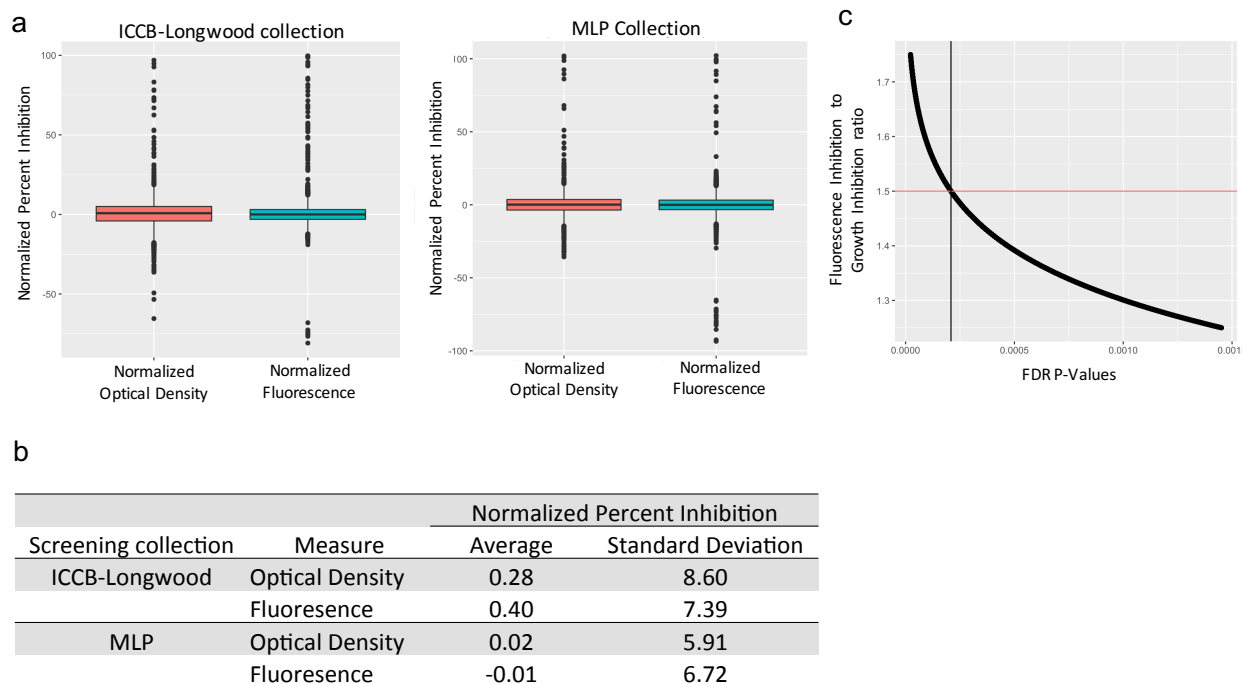
Supplementary Table 2.1. GFP fluorescence inhibition and eukaryotic cytotoxicity by DosR regulon inhibitors. For reporter fluorescence EC₅₀ determination, CDC1551(*hspX*::GFP)

Supplementary Table 2.1. (cont'd)

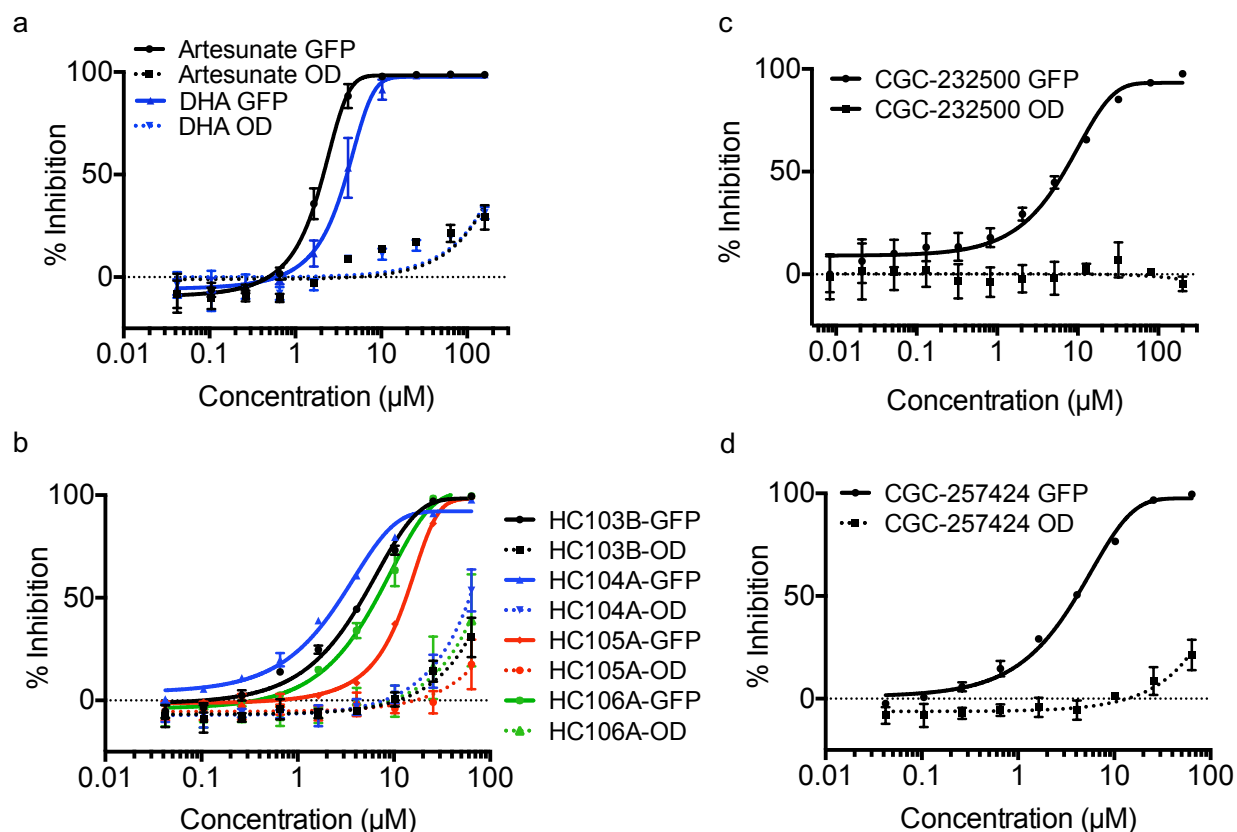
reporter was treated with compounds over an 8 point dose response curve ranging from 400 μM to 0.65 μM . Following 6 d of treatment, GFP fluorescence and optical density were measured. In all cases, no inhibition of growth was observed at the reported EC₅₀ for inhibition of GFP fluorescence. For eukaryotic cytotoxicity, macrophage cells including bone marrow derived macrophage (BMDM), THP-1 and J774, were tested with serial dilutions of DosR regulon inhibitors over an 8 point dose response curve ranging from 400 μM to 0.65 μM . Macrophages were incubated for 3 d and viability was determined using CellTiter-Glo (Promega) luminescent cell viability assay.

Category	Parameter	Description
Assay	Type of assay	Whole Cell Phenotypic Screen against a <i>M. tuberculosis</i> hypoxia-inducible fluorescent reporter strain
	Target	Inhibition of DosRST regulated reporter fluorescence. The intended targets were DosR (P95193), DosS (P95194) or DosT (O53473).
	Primary measurement	Inhibition of hypoxia-inducible reporter GFP fluorescence and with limited impact on reporter growth (measured by optical density)
	Key reagents	CDC1551 (<i>aprA</i> ::GFP) reporter strain
	Assay protocol	Described in methods section "High throughput screening and data analysis"
	Additional comments	Validation of reporter strain is published in Tan <i>et al.</i> , Plos Pathogens 2013, ref 26).
Library	Library size	540,288
	Library composition	Small molecules and known bioactives
	Source	Harvard Medical Schools Institute of Chemistry and Cell Biology's (ICCB) in house library (211,655 compounds) and the NIH MLP collection (328,633 compounds)
	Additional comments	Compound libraries described at: http://iccb.med.harvard.edu/libraries/compound-libraries/
Screen	Format	384-well optical plate
	Concentration(s) tested	~10 μ M in DMSO
	Plate controls	DMSO negative control, 0.3 μ M rifampin positive control
	Reagent/ compound dispensing system	Compounds were arrayed using Harvard's in house robotics platform. Reporter strain was added to the plates using a CyBio Selma Liquid handler.
	Detection instrument and software	Plates were read using a Perkin-Elmer Enspire plate reader.
	Assay validation/QC	Z'-Factors are calculated for each plate. Z'-factor for whole screen averaged 0.9.
	Correction factors	None
	Normalization	Percent inhibition relative to the positive and negative controls. See equation of page 17 in the methods section.
	Additional comments	The screen was conducted with a clinical strain of <i>M. tuberculosis</i> at Michigan State University in a BSL-3 HTS facility.
Post-HTS analysis	Hit criteria	>35% inhibition of reporter GFP fluorescence, and >1.5 fold inhibition of reporter fluorescence relative to optical density
	Hit rate	Remains to be fully determined, but below 0.01%.
	Additional assay(s)	GFP quenching; eukaryotic cytotoxicity in primary bone marrow macrophages and two macrophage like cell lines; EC ₅₀ determinations; RNA-seq; inhibition of Mtb survival during persistence; biochemical assays showing targeting of DosS or DosT using UV-visible spectroscopy or autophosphorylation assays.
	Confirmation of hit purity and structure	HC101 (artemisinin and analogs) are well characterized and were purchased from Sigma. For HC102A and HC103A, the commercial compounds were purchased from Enamine and Chembridge, respectively, and verified by chemists (see methods). HC102A and HC103A were also synthesized by organic chemists and confirmed in the whole cell and biochemical assays.
	Additional comments	

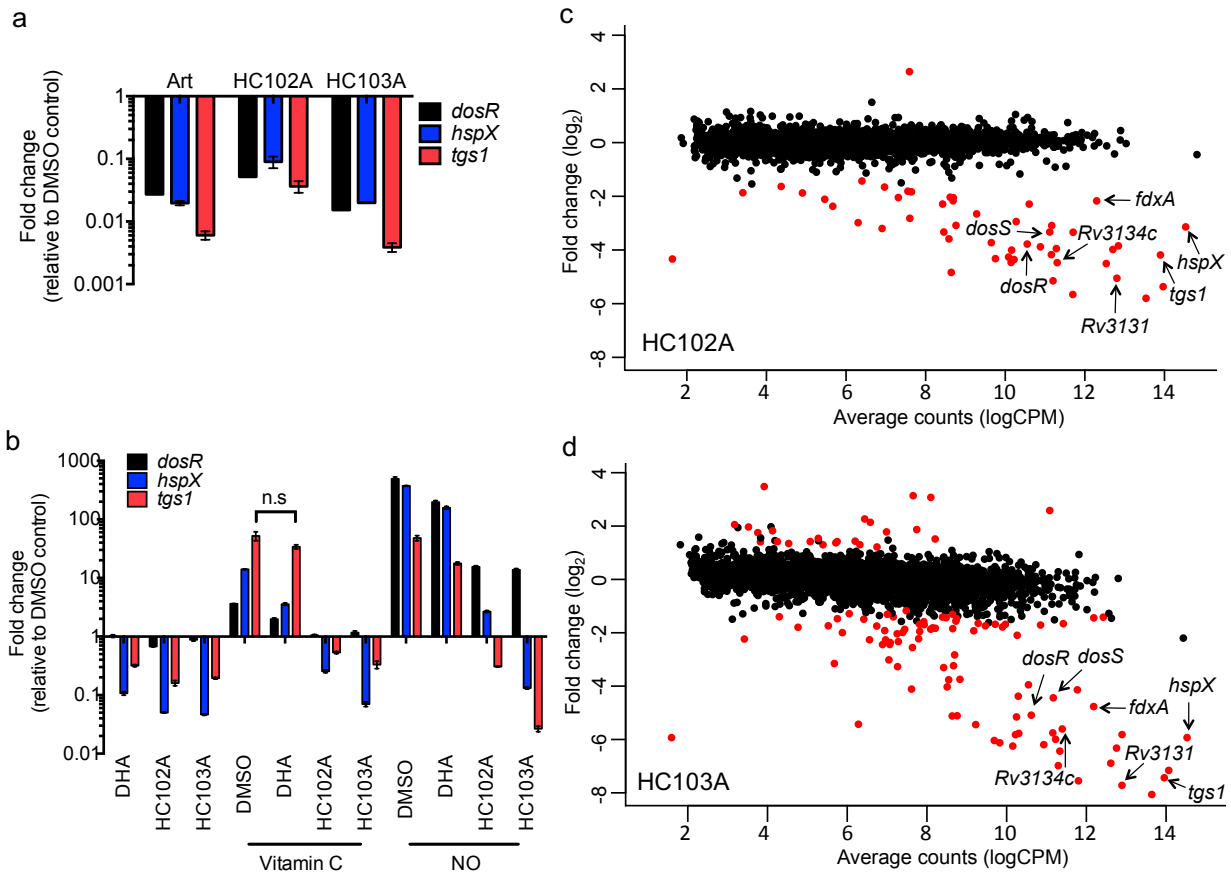
Supplementary Table 2.2. Small molecule screening data



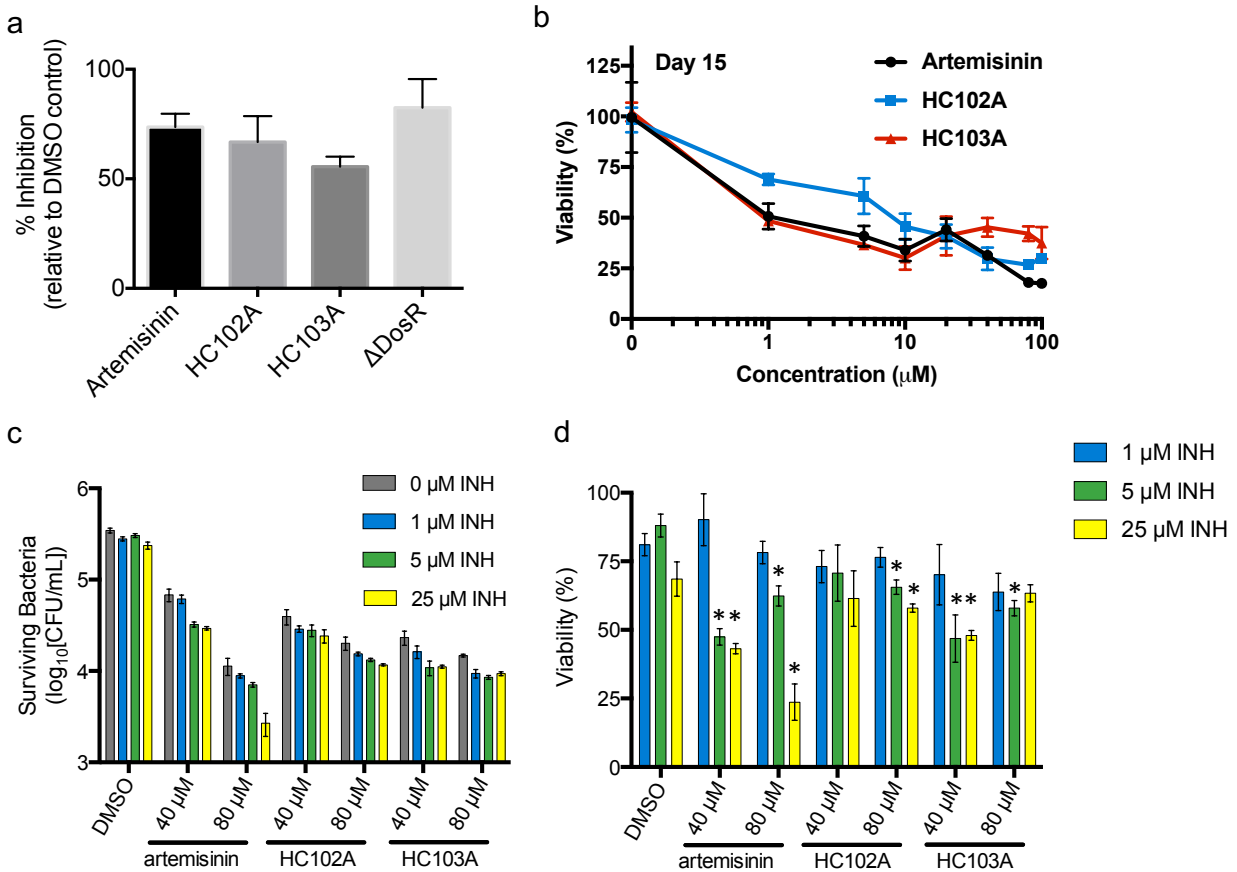
Supplementary Figure 2.1. Statistical analysis of HTS controls. (a) Box plots showing the variation of DMSO control wells (negative control) from the screens of the ICCB- Longwood and Molecular Libraries Program (MLP) collections. Boxes show the 25 and 75% quartiles and the whiskers are 1.5x the interquartile range (approximately 3 standard deviations away from the mean). The dots are considered “outliers”. (b) Table with the means and standard deviations from the DMSO controls. Along with the Z- factor of 0.9, tight clustering of the control wells around 0% inhibition for both fluorescence and optical density support robustness of the screen. (c) FDR p-values plotted vs. the fluorescence inhibition to growth inhibition ratios shows that the chosen 1.5-fold cut-off ratio (red line) is significant ($p < 0.0003$).



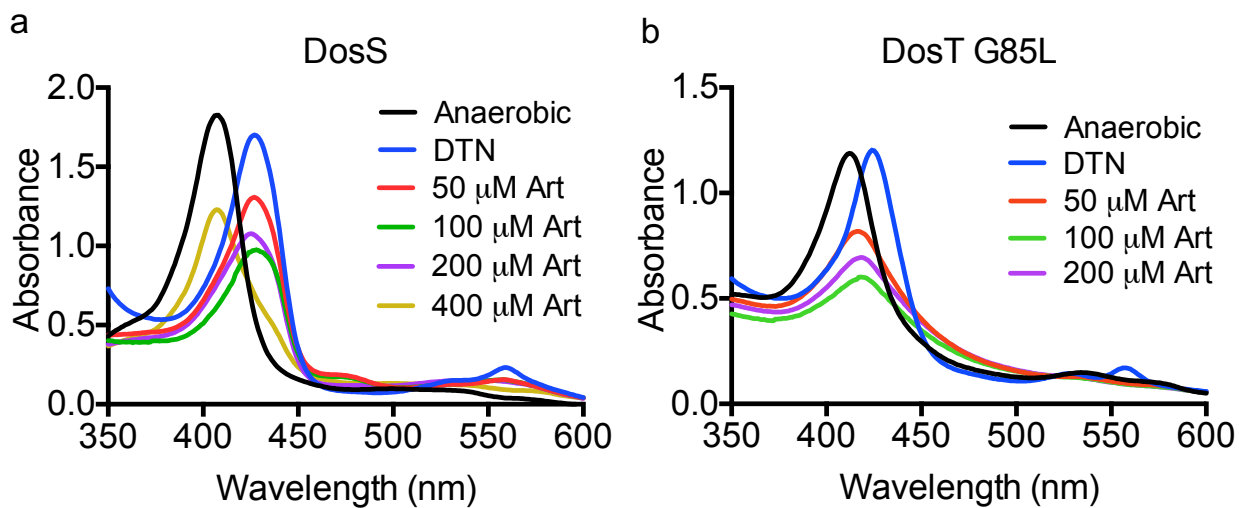
Supplementary Figure 2.2. Identification of inhibitors of the DosRST pathway. Dose response curves of GFP fluorescence inhibition of CDC1551(*hspX'*::GFP) reporter treated with DosRST regulon inhibitor compounds. **(a)** Artemisinin analogs, artesunate and dihydroartemisinin (DHA). **(b)** HC103B and HC104A-HC106A. **(c)** HC102A was generated by organic synthesis (CCG-2323500) and exhibited expected activity. **(d)** HC103A was generated by organic synthesis (CCG-257424) and exhibited expected activity. Error bars represent the standard deviation and experiments were repeated at least twice with similar results.



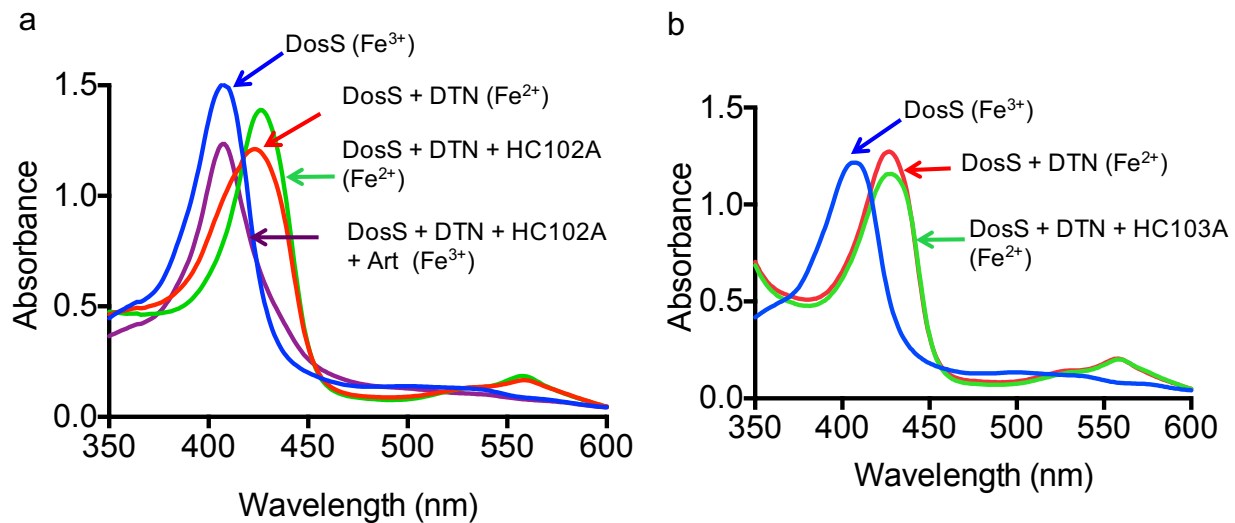
Supplementary Figure 2.3. Transcriptional profiling shows artemisinin, HC102A and HC103A inhibit the core genes of the DosRST regulon during hypoxia. (a) Inhibition of DosR regulon under hypoxic conditions by the DosR regulon inhibitors. *Mtb* treated with compounds of interest was grown at 37 °C without shaking for 6 d, and total RNA was extracted for RT-PCR quantification. RT-PCR shows three highly induced DosR regulon genes (*dosR*, *hspX* and *tgs1*) under hypoxia were repressed by the DosR regulon inhibitors. Error bars represent the standard deviation. (b) NO and Vitamin C assays. *Mtb* cells were pre-treated with compounds of interest for 24 h, and total RNA was extracted after inducing with NO or vitamin C for 2 h. HC102A and HC103A inhibited the induction of DosR regulon by NO and vitamin C, but DHA had little effect. In all cases, the difference in the drug treated samples compared to DMSO treated samples in response to vitamin C or NO is significant with a P -value <0.001 based on t -test, except those marked as non-significant (n.s.). Error bars represent the standard deviation. *Mtb* differential gene expression in response to HC102A (panel c) and HC103A (panel d). Genes in red have a p -value <0.05 , and indicated gene names are DosR regulated genes. The transcriptional analysis from different assays collectively confirm that the DosR pathway is the target of artemisinin, HC102A and HC103A. Experiments were repeated at least twice with similar results.



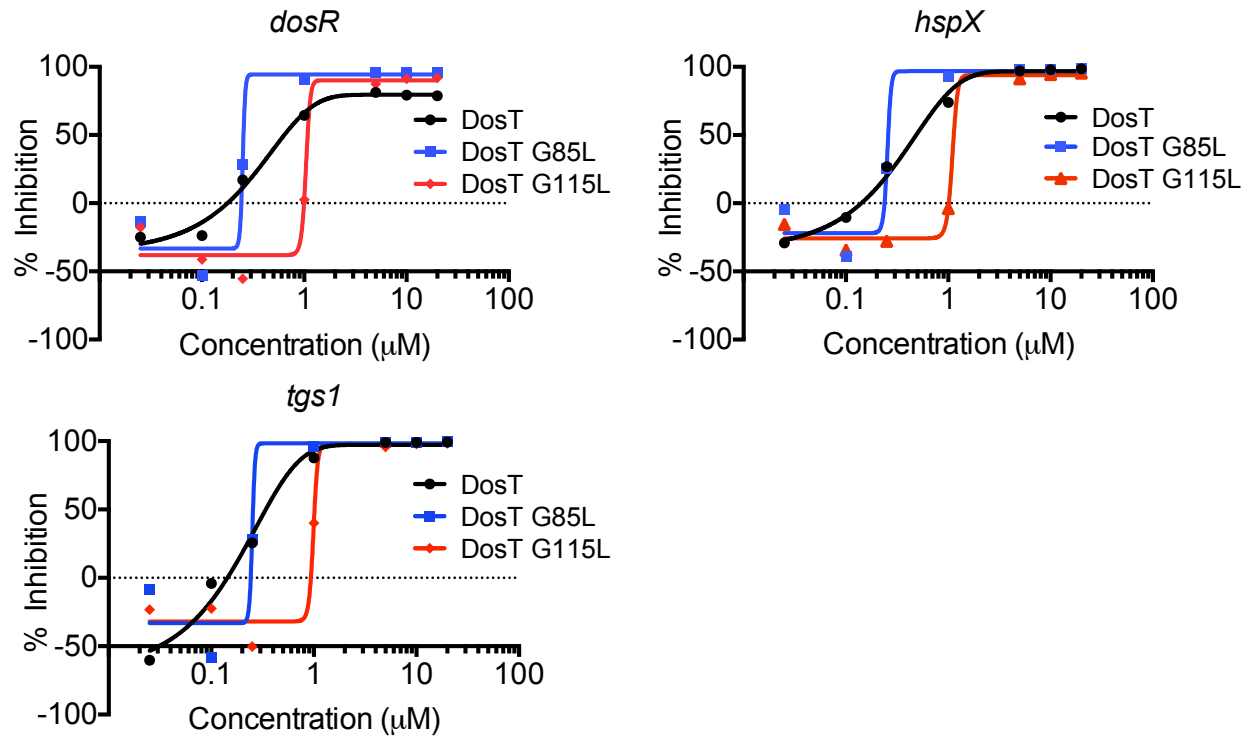
Supplementary Figure 2.4. Artemisinin, HC102A and HC103A inhibit TAG synthesis, survival and isoniazid tolerance during NRP. (a) Quantification of TAG accumulation for Mtb treated with compounds of interest shows that DosRST regulon inhibitors repress TAG synthesis to the level similar to Δ dosR mutant. Error bars represent the standard deviation. (b) Dose dependent inhibition of Mtb survival during NRP following 15 d of treatment. Percent viability was calculated relative to the viable bacteria in the DMSO control at day 15. Error bars represent the standard deviation of the mean. (c) Fifteen days of treatment with artemisinin, HC102A or HC103A, with or without INH, significantly reduces bacterial survival (P -value <0.05 based on a t -test) during NRP relative to the respective DMSO controls. (d) Fifteen days of treatment with artemisinin, HC102A and HC103A reduces isoniazid tolerance during NRP. To quantify INH tolerance, percent viability at 1, 5 and 25 μ M INH was measured relative to the 0 μ M INH control (DMSO control). Significant differences (marked with an asterisk, $p < 0.05$ based on a t -test) were calculated relative to the respective DMSO control sample. For example, cells treated with 5 μ M INH and artemisinin, HC102A and HC103A are significantly different from the DMSO control treated with 5 μ M INH. Experiments were repeated at least twice with similar results.



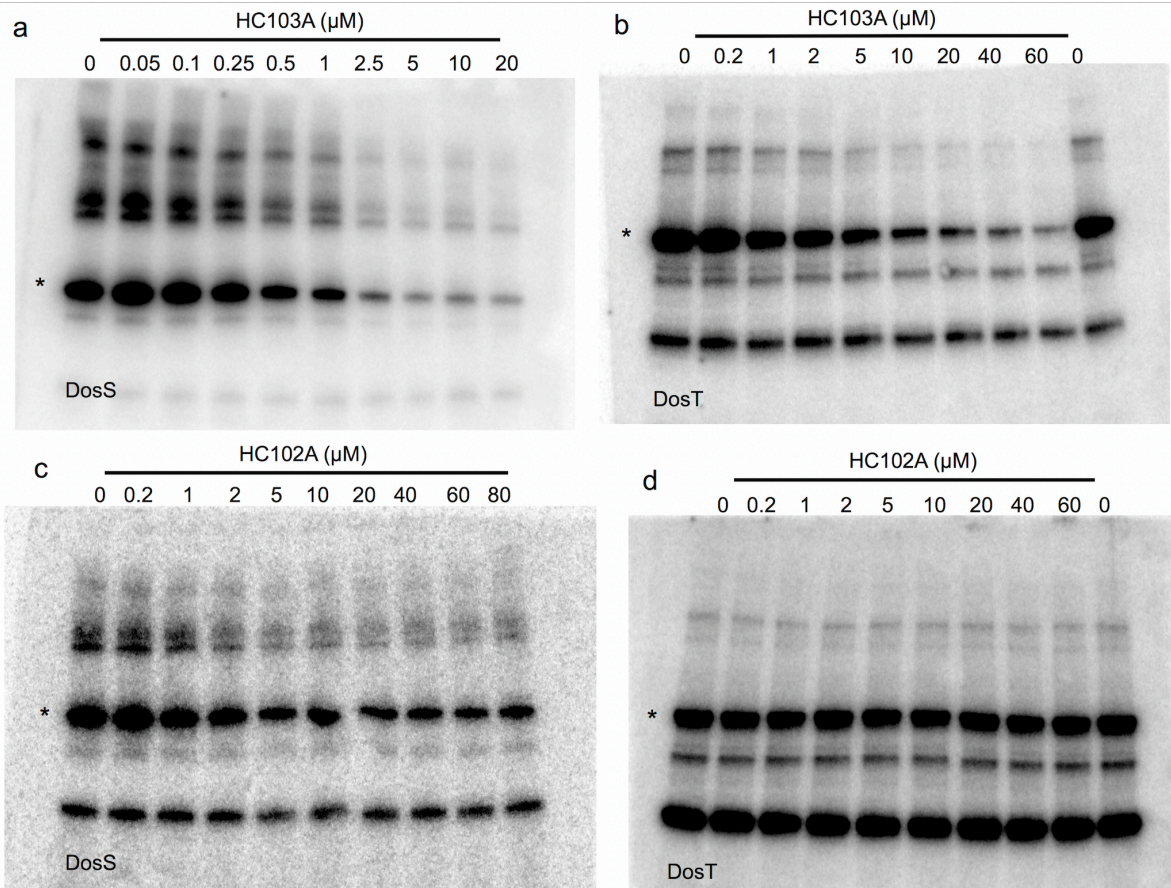
Supplementary Figure 2.5. Artemisinin directly modulates DosS and DosT (G85L) heme in a dose-dependent manner. UV-visible spectra of DosS (panel a) and DosT (G85L) (panel b) treated with different concentrations of artemisinin. Artemisinin modulated DosT heme at a lower concentration (50 μM , Figure 2.5d) than DosS heme (400 μM), confirming that DosT is more sensitive to artemisinin. DosT (G85L) exhibits a similar profile to WT DosT (Figure 2.5d)



Supplementary Figure 2.6. HC102A and HC103A do not modulate DosS redox. DosS treated with HC102A (panel a) or HC103A (panel b) shows a similar overall spectrum as the DMSO control. This result indicates that HC102A and HC103A has no effect in modulating redox status of DosS, and may inhibit DosR regulon by distinct mechanism.



Supplementary Figure 2.7. Substitutions in DosT provide resistance to artemisinin. Mtb was transformed with a replicating plasmid that overexpresses WT *dosT*, *dosT* (G85L) or *dosT* (G115L). Cells were treated with 0.025 µM - 20 µM artemisinin, and total RNA was extracted after 6 d incubation at 37 °C. RT-PCR quantification of DosR-regulated genes (*dosR*, *hspX* and *tgs1*) shows that strains expressing DosT (G115L) exhibited EC₅₀ for artemisinin-mediated inhibition of DosR regulon genes of 1.0-1.6 µM, which is ~5-fold more resistant than WT DosT or DosT (G85L) with EC₅₀ of 0.2-0.3 µM.



Supplementary Figure 2.8. Modulation of DosS and DosT kinase activities by HC102A and HC103A. Full western blots from which the cropped images in Figure 2.6 were generated. DosS and DosT protein is marked by the asterisk.

Supplementary Notes

Chemical synthesis of HC102A (CCG-232500) and HC103A (CCG-257424)

Powdered samples of commercially sourced HC102A and HC103A were analyzed by MS and combustion analysis and found to have a molecular formula consistent with the reported structures. 2D-NMR analysis confirmed **HC102A** to be the racemic (5S,9R)-7,7,9-trimethyl-1,3-diazaspiro[4.5]decane-2,4-dione (alpha) isomer. For **HC102A** synthesis (generating a compound designated CCG-232500), a mixture of 3,3,5-trimethylcyclohexan-1-one (1.1 g, 7.6 mmol) was treated with sodium cyanide (0.92 g, 18.8 mmol), and carbonic acid, diammonia salt (3.6 g, 37.5 mmol). EtOH (10 mL) and water (10 mL) were added and the resulting mixture was heated to 55 °C for 6 h. The mixture was cooled and then diluted with cold water, treated with conc. HCl (2 mL) and filtered. The collected solid was washed with water (2x) and triturated in hot methanol. The resulting solid was collected by filtration and dried under high vacuum overnight at room temp. (5S,9R)-7,7,9-trimethyl-1,3-diazaspiro[4.5]decane-2,4-dione was obtained as a white solid (0.53 g, 2.5 mmol, 32%). HPLC system A ($t_R = 5.6$ min). $^1\text{H NMR}$ (400 MHz, DMSO- d_6) δ 10.63 (s, 1H), 8.09 (s, 1H), 1.83 (d, $J = 9.3$ Hz, 1H), 1.44 (dd, $J = 13.3, 7.1$ Hz, 2H), 1.32 (dd, $J = 32.7, 13.7$ Hz, 2H), 1.14 (t, $J = 12.9$ Hz, 1H), 0.96 (s, 3H), 0.92 – 0.62 (m, 7H). ESI-MS m/z 209.1 (M-H⁺). For HC103A synthesis (generating a compound designated CCG-257424), first 3-amino-N-(3-hydroxyphenyl)benzamide was synthesized. To a solution of 3-aminobenzoic acid (1 g, 7.3 mmol), 3-aminophenol (0.88 g, 8.0 mmol) and HOBt (1.3 g, 8.7 mmol) in dry DMF cooled to 0 °C was added EDC (1.6 g, 8.75 mmol). The resulting solution was allowed to warm to room temperature and stirred overnight. The reaction was diluted with water and washed with satd. NaHCO_3 , satd. NaCl solution and dried over MgSO_4 . After filtration, the organic layer was concentrated in vacuo and purified by flash chromatography (CombiFlash, $\text{CH}_2\text{Cl}_2/\text{MeOH}$

gradient). 3-amino-N-(3-hydroxyphenyl)benzamide was obtained as an amorphous solid (0.24 g, 7.29 mmol, 14.4 % yield). ¹H NMR (400 MHz, DMSO-d₆) (Rotomers) δ 10.18 (m, *J* = 51.4, 10.6 Hz, 1H), 9.90 (s, 1H), 9.35 (m, 2H), 8.25 (s, 1H), 7.95 (m, 1H), 7.83 – 7.34 (m, 2H), 6.82 – 6.32 (m, 2H). 5.2 (s, 2H). To synthesize CGC257424, to a solution of 3-amino-N-(3-hydroxyphenyl)benzamide (0.2 g, 0.87 mmol), EDC (0.20 g, 1.1 mmol), and HOBT (0.16 g, 1.0 mmol) in dry DMF cooled to 0 °C was added thiophene-2-carboxylic acid (0.12 g, 0.96 mmol) followed by catalytic 4-dimethylaminopyridine. The resulting solution was allowed to warm to room temperature and stir overnight. The reaction was diluted with water and washed with satd. NaHCO₃, satd. NaCl solution and dried, MgSO₄. The organic layer was filtered and concentrated in vacuo. Flash chromatography (CH₂Cl₂/MeOH) was used to obtain N-(3-((3-hydroxyphenyl)carbamoyl)phenyl)thiophene-2-carboxamide as a white solid (0.06 g, 0.17 mmol, 20.2 % yield). HPLC system A (*t_R* = 5.8 min). ¹H NMR (400 MHz, DMSO-d₆) δ 10.04 (s, 1H), 9.62 (s, 1H), 8.91 (s, 1H), 8.13 (t, *J* = 1.9 Hz, 1H), 8.02 – 7.90 (m, 2H), 7.59 (d, *J* = 17.2 Hz, 2H), 7.50 (dd, *J* = 4.9, 1.2 Hz, 1H), 7.38 – 7.29 (m, 2H), 7.11 – 6.97 (m, 2H), 6.47 (dt, *J* = 8.3, 1.4 Hz, 1H). ESI-MS *m/z* 339.0 (M+H⁺).

Starting materials were purchased from Fisher, Sigma-Aldrich Lancaster, Fluka or TCI-America and were used without purification. All reaction solvents were purchased from Fisher and used as received. Reactions were monitored by TLC using precoated silica gel 60 F254 plates. Silica gel chromatography was performed by flash chromatography using silica gel (220-240 mesh) obtained from Silicycle or via medium pressure liquid chromatography on a CombiFlash instrument. NMR spectra were recorded on a Varian 400 MHz spectrometer. Chemical shifts are reported in δ (parts per million), by reference to the hydrogenated residues of deuterated solvent as internal standard CDCl₃; δ = 7.28 (¹H NMR). Mass spectra were recorded on a Micromass

LCT time-of-flight instrument utilizing the electrospray ionization mode. The purity of the compounds was assessed via analytical reversed-phase high-performance liquid chromatography with a gradient of 10% acetonitrile/water to 90% acetonitrile/water over 6 min (“System A”, C18 column, 3.5 μm , 4.6x100 mm, 254 nm).

REFERENCES

REFERENCES

1. **Gengenbacher M, Kaufmann SH.** 2012. *Mycobacterium tuberculosis*: success through dormancy. *FEMS Microbiol Rev* **36**:514-532.
2. **Baker JJ, Johnson BK, Abramovitch RB.** 2014. Slow growth of *Mycobacterium tuberculosis* at acidic pH is regulated by *phoPR* and host-associated carbon sources. *Mol Microbiol* **94**:56-69.
3. **Wayne LG, Sohaskey CD.** 2001. Nonreplicating persistence of *Mycobacterium tuberculosis*. *Annu Rev Microbiol* **55**:139-163.
4. **Betts JC, Lukey PT, Robb LC, McAdam RA, Duncan K.** 2002. Evaluation of a nutrient starvation model of *Mycobacterium tuberculosis* persistence by gene and protein expression profiling. *Mol Microbiol* **43**:717-731.
5. **Boon C, Dick T.** 2002. *Mycobacterium bovis* BCG response regulator essential for hypoxic dormancy. *J Bacteriol* **184**:6760-6767.
6. **Park HD, Guinn KM, Harrell MI, Liao R, Voskuil MI, Tompa M, Schoolnik GK, Sherman DR.** 2003. Rv3133c/dosR is a transcription factor that mediates the hypoxic response of *Mycobacterium tuberculosis*. *Mol Microbiol* **48**:833-843.
7. **Voskuil MI, Schnappinger D, Visconti KC, Harrell MI, Dolganov GM, Sherman DR, Schoolnik GK.** 2003. Inhibition of respiration by nitric oxide induces a *Mycobacterium tuberculosis* dormancy program. *J Exp Med* **198**:705-713.
8. **Galagan JE, Minch K, Peterson M, Lyubetskaya A, Azizi E, Sweet L, Gomes A, Rustad T, Dolganov G, Glotova I, Abeel T, Mahwinney C, Kennedy AD, Allard R, Brabant W, Krueger A, Jaini S, Honda B, Yu WH, Hickey MJ, Zucker J, Garay C, Weiner B, Sisk P, Stolte C, Winkler JK, Van de Peer Y, Iazzetti P, Camacho D, Dreyfuss J, Liu Y, Dorhoi A, Mollenkopf HJ, Drogaris P, Lamontagne J, Zhou Y, Piquenot J, Park ST, Raman S, Kaufmann SH, Mohny RP, Chelsky D, Moody DB, Sherman DR, Schoolnik GK.** 2013. The *Mycobacterium tuberculosis* regulatory network and hypoxia. *Nature* **499**:178-183.
9. **Ioanoviciu A, Meharena YT, Poulos TL, Ortiz de Montellano PR.** 2009. DevS oxy complex stability identifies this heme protein as a gas sensor in *Mycobacterium tuberculosis* dormancy. *Biochemistry* **48**:5839-5848.
10. **Vos MH, Bouzahir-Sima L, Lambry JC, Luo H, Eaton-Rye JJ, Ioanoviciu A, Ortiz de Montellano PR, Liebl U.** 2012. Ultrafast ligand dynamics in the heme-based GAF sensor domains of the histidine kinases DosS and DosT from *Mycobacterium tuberculosis*. *Biochemistry* **51**:159-166.

11. **Kumar A, Toledo JC, Patel RP, Lancaster JR, Jr., Steyn AJ.** 2007. *Mycobacterium tuberculosis* DosS is a redox sensor and DosT is a hypoxia sensor. Proc Natl Acad Sci U S A **104**:11568-11573.
12. **Honaker RW, Leistikow RL, Bartek IL, Voskuil MI.** 2009. Unique roles of DosT and DosS in DosR regulon induction and *Mycobacterium tuberculosis* dormancy. Infect Immun **77**:3258-3263.
13. **Leistikow RL, Morton RA, Bartek IL, Frimpong I, Wagner K, Voskuil MI.** 2010. The *Mycobacterium tuberculosis* DosR regulon assists in metabolic homeostasis and enables rapid recovery from nonrespiring dormancy. J Bacteriol **192**:1662-1670.
14. **Converse PJ, Karakousis PC, Klinkenberg LG, Kesavan AK, Ly LH, Allen SS, Grosset JH, Jain SK, Lamichhane G, Manabe YC, McMurray DN, Nuermberger EL, Bishai WR.** 2009. Role of the dosR-dosS two-component regulatory system in *Mycobacterium tuberculosis* virulence in three animal models. Infect Immun **77**:1230-1237.
15. **Gautam US, McGillivray A, Mehra S, Didier PJ, Midkiff CC, Kisse RS, Golden NA, Alvarez X, Niu T, Rengarajan J, Sherman DR, Kaushal D.** 2015. DosS is required for the complete virulence of *Mycobacterium tuberculosis* in mice with classical granulomatous lesions. Am J Respir Cell Mol Biol **52**:708-716.
16. **Mehra S, Foreman TW, Didier PJ, Ahsan MH, Hudock TA, Kisse R, Golden NA, Gautam US, Johnson AM, Alvarez X, Russell-Lodrigue KE, Doyle LA, Roy CJ, Niu T, Blanchard JL, Khader SA, Lackner AA, Sherman DR, Kaushal D.** 2015. The DosR Regulon modulates adaptive immunity and is essential for *Mycobacterium tuberculosis* persistence. Am J Respir Crit Care Med **191**:1185-1196.
17. **Baek SH, Li AH, Sasseti CM.** 2011. Metabolic regulation of mycobacterial growth and antibiotic sensitivity. PLoS Biol **9**:e1001065.
18. **VanderVen BC, Fahey RJ, Lee W, Liu Y, Abramovitch RB, Memmott C, Crowe AM, Eltis LD, Perola E, Deininger DD, Wang T, Locher CP, Russell DG.** 2015. Novel inhibitors of cholesterol degradation in *Mycobacterium tuberculosis* reveal how the bacterium's metabolism is constrained by the intracellular environment. PLoS Pathog **11**:e1004679.
19. **Rasko DA, Moreira CG, Li de R, Reading NC, Ritchie JM, Waldor MK, Williams N, Taussig R, Wei S, Roth M, Hughes DT, Huntley JF, Fina MW, Falck JR, Sperandio V.** 2008. Targeting QseC signaling and virulence for antibiotic development. Science **321**:1078-1080.
20. **Rasko DA, Sperandio V.** 2010. Anti-virulence strategies to combat bacteria-mediated disease. Nat Rev Drug Discov **9**:117-128.

21. **Anthouard R, DiRita VJ.** 2013. Small-molecule inhibitors of toxT expression in *Vibrio cholerae*. *MBio* **4**.
22. **Ng WL, Perez L, Cong J, Semmelhack MF, Bassler BL.** 2012. Broad spectrum pro-quorum-sensing molecules as inhibitors of virulence in vibrios. *PLoS Pathog* **8**:e1002767.
23. **Johnson BK, Colvin CJ, Needle DB, Mba Medie F, Champion PA, Abramovitch RB.** 2015. The carbonic anhydrase inhibitor ethoxzolamide inhibits the *Mycobacterium tuberculosis* PhoPR regulon and Esx-1 secretion and attenuates virulence. *Antimicrob Agents Chemother* **59**:4436-4445.
24. **Tan S, Sukumar N, Abramovitch RB, Parish T, Russell DG.** 2013. *Mycobacterium tuberculosis* responds to chloride and pH as synergistic cues to the immune status of its host cell. *PLoS Pathog* **9**:e1003282.
25. **Johnson BK, Scholz MB, Teal TK, Abramovitch RB.** 2016. SPARTA: Simple program for automated reference-based bacterial RNA-seq transcriptome analysis. *BMC Bioinformatics* **17**:66.
26. **Taneja NK, Dhingra S, Mittal A, Naresh M, Tyagi JS.** 2010. *Mycobacterium tuberculosis* transcriptional adaptation, growth arrest and dormancy phenotype development is triggered by vitamin C. *PLoS One* **5**:e10860.
27. **Mak PA, Rao SP, Ping Tan M, Lin X, Chyba J, Tay J, Ng SH, Tan BH, Cherian J, Duraiswamy J, Bifani P, Lim V, Lee BH, Ling Ma N, Beer D, Thayalan P, Kuhen K, Chatterjee A, Supek F, Glynn R, Zheng J, Boshoff HI, Barry CE, 3rd, Dick T, Pethe K, Camacho LR.** 2012. A high-throughput screen to identify inhibitors of ATP homeostasis in non-replicating *Mycobacterium tuberculosis*. *ACS Chem Biol* **7**:1190-1197.
28. **Deb C, Lee CM, Dubey VS, Daniel J, Abomoelak B, Sirakova TD, Pawar S, Rogers L, Kolattukudy PE.** 2009. A novel in vitro multiple-stress dormancy model for *Mycobacterium tuberculosis* generates a lipid-loaded, drug-tolerant, dormant pathogen. *PLoS One* **4**:e6077.
29. **Krishna S, Bustamante L, Haynes RK, Staines HM.** 2008. Artemisinins: their growing importance in medicine. *Trends Pharmacol Sci* **29**:520-527.
30. **Selmecki K, Robert A, Claparols C, Meunier B.** 2004. Alkylation of human hemoglobin A0 by the antimalarial drug artemisinin. *FEBS Lett* **556**:245-248.
31. **Robert A, Dechy-Cabaret O, Cazelles J, Meunier B.** 2002. From mechanistic studies on artemisinin derivatives to new modular antimalarial drugs. *Acc Chem Res* **35**:167-174.

32. **Ioanoviciu A, Yukl ET, Moenne-Loccoz P, de Montellano PR.** 2007. DevS, a heme-containing two-component oxygen sensor of *Mycobacterium tuberculosis*. *Biochemistry* **46**:4250-4260.
33. **Cho HY, Cho HJ, Kim MH, Kang BS.** 2011. Blockage of the channel to heme by the E87 side chain in the GAF domain of *Mycobacterium tuberculosis* DosS confers the unique sensitivity of DosS to oxygen. *FEBS Lett* **585**:1873-1878.
34. **Podust LM, Ioanoviciu A, Ortiz de Montellano PR.** 2008. 2.3 A X-ray structure of the heme-bound GAF domain of sensory histidine kinase DosT of *Mycobacterium tuberculosis*. *Biochemistry* **47**:12523-12531.
35. **Cho HY, Cho HJ, Kim YM, Oh JI, Kang BS.** 2009. Structural insight into the heme-based redox sensing by DosS from *Mycobacterium tuberculosis*. *J Biol Chem* **284**:13057-13067.
36. **Sousa EH, Tuckerman JR, Gonzalez G, Gilles-Gonzalez MA.** 2007. DosT and DevS are oxygen-switched kinases in *Mycobacterium tuberculosis*. *Protein Sci* **16**:1708-1719.
37. **Messori L, Gabbiani C, Casini A, Siragusa M, Vincieri FF, Bilia AR.** 2006. The reaction of artemisinins with hemoglobin: a unified picture. *Bioorg Med Chem* **14**:2972-2977.
38. **Zhang S, Gerhard GS.** 2008. Heme activates artemisinin more efficiently than hemin, inorganic iron, or hemoglobin. *Bioorg Med Chem* **16**:7853-7861.
39. **Robert A, Coppel Y, Meunier B.** 2002. Alkylation of heme by the antimalarial drug artemisinin. *Chem Commun (Camb)*:414-415.
40. **Sivaramakrishnan S, de Montellano PR.** 2013. The DosS-DosT/DosR mycobacterial sensor system. *Biosensors* **3**:259-282.
41. **Roberts DM, Liao RP, Wisedchaisri G, Hol WG, Sherman DR.** 2004. Two sensor kinases contribute to the hypoxic response of *Mycobacterium tuberculosis*. *J Biol Chem* **279**:23082-23087.
42. **Koul A, Vranckx L, Dendouga N, Balemans W, Van den Wyngaert I, Vergauwen K, Gohlmann HW, Willebrords R, Poncelet A, Guillemont J, Bald D, Andries K.** 2008. Diarylquinolines are bactericidal for dormant mycobacteria as a result of disturbed ATP homeostasis. *J Biol Chem* **283**:25273-25280.
43. **Pethe K, Bifani P, Jang J, Kang S, Park S, Ahn S, Jiricek J, Jung J, Jeon HK, Cechetto J, Christophe T, Lee H, Kempf M, Jackson M, Lenaerts AJ, Pham H, Jones V, Seo MJ, Kim YM, Seo M, Seo JJ, Park D, Ko Y, Choi I, Kim R, Kim SY, Lim S, Yim SA, Nam J, Kang H, Kwon H, Oh CT, Cho Y, Jang Y, Kim J, Chua A, Tan BH, Nanjundappa MB, Rao SP, Barnes WS, Wintjens R, Walker JR, Alonso S, Lee S,**

- Kim J, Oh S, Oh T, Nehrbass U, Han SJ, No Z, et al.** 2013. Discovery of Q203, a potent clinical candidate for the treatment of tuberculosis. *Nat Med* **19**:1157-1160.
44. **Li W, Upadhyay A, Fontes FL, North EJ, Wang Y, Crans DC, Grzegorzewicz AE, Jones V, Franzblau SG, Lee RE, Crick DC, Jackson M.** 2014. Novel insights into the mechanism of inhibition of MmpL3, a target of multiple pharmacophores in *Mycobacterium tuberculosis*. *Antimicrob Agents Chemother* **58**:6413-6423.
45. **Gupta RK, Thakur TS, Desiraju GR, Tyagi JS.** 2009. Structure-based design of DevR inhibitor active against nonreplicating *Mycobacterium tuberculosis*. *J Med Chem* **52**:6324-6334.
46. **Rybniker J, Chen JM, Sala C, Hartkoorn RC, Vocat A, Benjak A, Boy-Rottger S, Zhang M, Szekely R, Greff Z, Orfi L, Szabadkai I, Pato J, Keri G, Cole ST.** 2014. Anticytolytic screen identifies inhibitors of mycobacterial virulence protein secretion. *Cell Host & Microbe* **16**:538-548.
47. **Boshoff HI, Myers TG, Copp BR, McNeil MR, Wilson MA, Barry CE, 3rd.** 2004. The transcriptional responses of *Mycobacterium tuberculosis* to inhibitors of metabolism: novel insights into drug mechanisms of action. *J Biol Chem* **279**:40174-40184.
48. **Miller MJ, Walz AJ, Zhu H, Wu C, Moraski G, Mollmann U, Tristani EM, Crumbliss AL, Ferdig MT, Checkley L, Edwards RL, Boshoff HI.** 2011. Design, synthesis, and study of a mycobactin-artemisinin conjugate that has selective and potent activity against tuberculosis and malaria. *J Am Chem Soc* **133**:2076-2079.
49. **Kim MJ, Park KJ, Ko IJ, Kim YM, Oh JI.** 2010. Different roles of DosS and DosT in the hypoxic adaptation of Mycobacteria. *J Bacteriol* **192**:4868-4875.
50. **Sander P, B S, Bottger E.** 2001. Gene Replacement in *Mycobacterium tuberculosis* and *Mycobacterium bovis* BCG Using *rpsL* as a Dominant Negative Selectable Marker, vol 54. Humana Press, Totowa, NJ.
51. **Abramovitch RB, Rohde KH, Hsu FF, Russell DG.** 2011. *aprABC*: a *Mycobacterium tuberculosis* complex-specific locus that modulates pH-driven adaptation to the macrophage phagosome. *Mol Microbiol* **80**:678-694.
52. **Zhang JH, Chung TD, Oldenburg KR.** 1999. A Simple Statistical Parameter for Use in Evaluation and Validation of High Throughput Screening Assays. *J Biomol Screen* **4**:67-73.
53. **Johnson BK, Abramovitch RB.** 2015. Macrophage infection models for *Mycobacterium tuberculosis*. *Methods Mol Biol* **1285**:329-341.

54. **Rohde KH, Abramovitch RB, Russell DG.** 2007. *Mycobacterium tuberculosis* invasion of macrophages: linking bacterial gene expression to environmental cues. *Cell Host Microbe* **2**:352-364.
55. **Schneider CA, Rasband WS, Eliceiri KW.** 2012. NIH Image to ImageJ: 25 years of image analysis. *Nat Methods* **9**:671-675.

CHAPTER 3 - Chemical inhibition of the *Mycobacterium tuberculosis* DosRST two-component regulatory system by targeting sensor kinase heme and response regulator DNA binding

This work is in preparation for journal submission. Contributions and authors for the work described below:

Huiqing Zheng, Bilal Aleiwi, Edmund Ellsworth, and Robert B. Abramovitch

H.Z., E.E. and R.B.A conceived the experiments. H.Z. performed the Mtb physiology and biochemistry experiments. B.A. synthesized the analogs. E.E. directed the medicinal chemistry optimizations.

Summary

Mycobacterium tuberculosis (Mtb) possesses a two-component regulatory system, DosRST, that enables Mtb to sense host immune cues and establish a state of non-replicating persistence (NRP). NRP bacteria are tolerant to several anti-mycobacterial drugs and are thought to play a role in the long course of tuberculosis (TB) therapy. Therefore, small molecules that inhibit Mtb from establishing or maintaining NRP could reduce the reservoir of drug tolerant bacteria and function as an adjunct therapy to reduce treatment time. Previously, we reported the discovery of six novel chemical inhibitors of DosRST, named HC101A-106A, from a whole cell, reporter-based phenotypic high-throughput screen. Here, we report functional and mechanism of action studies of HC104A and HC106A. RNAseq transcriptional profiling shows that the compounds downregulate genes of the DosRST regulon. Both compounds reduce hypoxia-induced triacylglycerol synthesis by ~50%. HC106A inhibits Mtb survival during hypoxia-induced NRP, however, HC104A did not inhibit survival during NRP. An electrophoretic mobility assay shows that HC104A inhibits DosR DNA binding in a dose-dependent manner, indicating that HC104A may function by directly targeting DosR. In contrast, UV-visible spectroscopy studies suggest HC106A directly targets the histidine kinase heme, via a mechanism that is distinct from the oxidation and alkylation of heme previously observed with artemisinin (HC101A). Synergistic interactions were observed when DosRST inhibitors were examined in pair-wise combinations with the strongest potentiation observed between artemisinin paired with HC102A, HC103A, or HC106A. Our data collectively show that the DosRST pathway can be inhibited by multiple distinct mechanisms.

Introduction

Mycobacterium tuberculosis (Mtb) is the causative agent of tuberculosis (TB). Mtb is an intracellular pathogen that can latently infect the host without causing disease symptoms (1). During chronic infection, it can establish a dormant state known as non-replicating persistence (NRP) where Mtb modulates its metabolism in response to environmental and host immune cues, such as hypoxia, acidic pH, and nutrient starvation (2, 3). DosRST is a two-component regulatory system that regulates Mtb persistence (4-6). It consists of two sensor histidine kinases, DosS and DosT, and the cognate response regulator DosR, which regulates expression of about 50 genes in the DosRST regulon (6-8). The pathway can be induced by host intracellular stimuli, such as nitric oxide (NO), carbon monoxide (CO) and hypoxia, through DosS and DosT (9-11). DosS is an oxygen and redox sensor, whereas DosT acts as an oxygen sensor (12-14). Both kinases sense ligands via the heme group, and are inactive when the heme exists as either the Met (Fe^{3+}) form (DosS) or the oxy ($\text{Fe}^{2+}\text{-O}_2$) form (DosT) in the presence of O_2 (13). However, hypoxic conditions activate the kinases by inducing the conversion of DosS to the ferrous form and DosT to the deoxy form. Therefore, DosS/T play overlapping and distinct roles in sensing the redox status and oxygen level of the environment to turn on the DosR pathway (11, 15).

Non-replicating bacilli are naturally tolerant to many anti-mycobacterial drugs, such as isoniazid (INH) that only kills replicating Mtb (16-18). During TB infection, the disease presents as a spectrum of replicating and non-replicating bacteria; the NRP population of bacteria are thought to be responsible, in part, for the 6-month long course of TB treatment. This long antibiotic regimen makes controlling the TB epidemic challenging and has likely contributed to the evolution of drug-resistant Mtb strains. Therefore, there exists an urgent need to identify new strategies to treat the disease, with a particular focus on discovering new ways to shorten the course of TB

therapy. Targeting the DosRST pathway is a promising strategy, because *dosRST* mutants are attenuated in *in vitro* models of hypoxia-driven NRP (19) and in animal models that generate hypoxic granulomas, including non-human primates, guinea pigs, and C3HeB/FeJ mouse models of TB infection (4, 20-22). Furthermore, deletion of DosR-regulated gene *tgsl*, which is involved in triacylglycerol (TAG) synthesis, causes reduced antibiotic tolerance (23, 24). Therefore, inhibiting the DosRST pathway and killing the reservoir of NRP bacteria may function to narrow the spectrum of TB disease and shorten the course of TB therapy.

In an effort to discover the new chemical probes that inhibit Mtb persistence, we previously performed a whole cell phenotypic high-throughput screening (HTS) of a >540,000 compound library using the DosRST regulon reporter strain CDC1551 (*hspX'::GFP*) (25). We discovered six compounds that inhibit the DosR-dependent, hypoxia-induced GFP fluorescence. In the previous report, we showed that the HC101, HC102 and HC103 series functioned to inhibit NRP associated physiologies, including TAG accumulation, survival during hypoxia and isoniazid tolerance. Mechanism of action studies showed that the HC101 series, composed of artemisinin and related analogs, functioned by oxidizing and alkylating the DosS and DosT heme. HC102 and HC103 did not modulate the DosS/T heme, and were instead found to inhibit sensor kinase autophosphorylation. Here, we report the characterization of two additional compounds, HC104A and HC106A. Transcriptional and biochemical analysis demonstrate that both compounds function to downregulate the DosRST pathway and inhibit persistence associated physiologies. Biochemical studies show HC104A and HC106A function by distinct mechanisms of action, with HC104A inhibiting DosR DNA binding and HC106A interacting with DosS and DosT heme to block environmental sensing. Studies examining the pair-wise interactions between the five DosRST inhibitors revealed synergistic interactions, including strong potentiating interactions of

artermisinin and HC106A. Structure activity relationship studies of HC106 identified functional groups of HC106A that are required for activity and enabled optimization of HC106 potency to nanomolar effective concentrations against whole cell Mtb.

Results

Inhibition of the DosR regulon by HC104A and HC106A

Characterization studies were undertaken with two putative DosRST regulon inhibitors, HC104A and HC106A (Fig. 3.1a) (25). Half-maximal effective concentration (EC_{50}) studies using the CDC1551 (*hspX'::GFP*) DosRST-dependent fluorescent reporter strain, show that HC104A and HC106A inhibit DosRST-dependent GFP fluorescence with EC_{50} values of 9.8 μ M and 2.48 μ M, respectively (Fig. 3.1b and 3.1c). The compounds have minimal impact on Mtb growth, suggesting they are also potential DosRST inhibitors, as DosRST is not required for survival under the conditions of mild hypoxia used in the reporter-based assay. RNA-seq-based transcriptional profiling was undertaken to determine if the DosRST regulon was inhibited by the compounds. Mtb was treated with 40 μ M HC104A, HC106A or dimethyl sulfoxide (DMSO) control for 6 d in a standing flask, and following incubation RNA was extracted, sequenced and analyzed for differential gene expression relative to the DMSO control. As a control for the DosR regulon, transcriptional profiling was also previously conducted on a DMSO treated CDC1551(Δ *dosR*) mutant strain (25). The transcriptional profiles showed that the genes strongly repressed by HC104A and HC106A (>2-fold; $q < 0.05$) are from the *dosR* regulon (Fig. 3.2a-c, Supplementary Dataset 3.1, 3.3). HC106A exhibited a remarkably strong reduction of gene expression, with transcripts for *tgsI* and *hspX* being almost undetectable by RNA-seq following HC106A treatment. Interestingly, while HC106A broadly inhibited genes of the DosRST regulon, HC104A only

strongly inhibited part of the DosR regulon, with the strongest inhibition reserved for *hspX*, the promoter used to drive reporter fluorescence in the screen. These RNA-seq results were validated by semi-quantitative RT-PCR, with HC104A causing downregulation of *dosR*, *hspX*, and *tgs1* *in vitro* by 6-, 570- and 13-fold, respectively; whereas HC106A downregulated these three genes by 49-, 1360-, and 1424-fold, respectively (Supplementary Fig. 3.1), with *hspX* and *tgs1* transcripts being below the level of detection by qRT-PCR.

Comparisons of transcriptional profiles from the inhibitor treated wild type (WT) Mtb strain to a CDC1551(Δ *dosR*) mutant strain showed that there are a total of 26 genes and 53 genes from *dosR* regulon inhibited by HC104A and HC106A, respectively. Notably, HC104A and HC106A have an additional 119 genes and 35 genes repressed that were not repressed in the CDC1551(Δ *dosR*) mutant strain (Fig. 3.2c). This observation suggested that these two compounds exhibit some DosR-independent activities. To confirm the specificity of the compounds, RNA-seq was also performed on CDC1551(Δ *dosR*) mutant background (Supplementary Dataset 3.2-3) treated with HC104A or HC106A. This analysis identified 171 genes and 51 genes that are downregulated (>2-fold; $q < 0.05$) by HC104A and HC106A, respectively (Fig. 3.2d). This finding indicates that HC104A and HC106A impact other targets beside DosR regulon, with HC106A showing greater on-target specificity than HC104A. Based on these findings, we conclude that: 1) HC106A strongly and specifically inhibits the DosRST regulon; and 2) HC104A strongly inhibits a portion of the DosRST regulon, with several notable off-target activities.

To assess the impact of the inhibitors on the DosRST pathway on intracellular Mtb, murine bone marrow-derived mouse macrophages were infected with Mtb and treated with 40 μ M HC104A and HC106A for 48 h. Total bacterial RNA was isolated and analyzed by RT-PCR for *hspX* and *tgs1* gene differential expression. The results demonstrate that the induction of *hspX* and

tgsI were inhibited 185- and 10-fold by HC104A and 6- and 4-fold by HC106A, respectively (Fig. 3.3a). These findings confirm that HC104A and HC106A can access Mtb inside the macrophage, however, the reduced repression of the pathway by HC106A as compared to broth culture, suggests that the molecule may not be able to efficiently target intracellular Mtb.

The DosRST pathway is also induced by redox signals such as vitamin C and NO (25). To examine whether HC104A and HC106A can repress the induction of DosRST pathway by vitamin C or NO, Mtb cells were pretreated with HC104A or HC106A for 24 h followed by vitamin C or NO induction for 2 h. The expression of DosR-regulated genes (*hspX* and *tgsI*) was examined by real time-PCR. Vitamin C and DETA-NONOate (NO donor) strongly induced *hspX* and *tgsI* as previously reported ((25), Fig. 3.3b). For instance, vitamin C induced *hspX* and *tgsI* by 2162- and 58-fold, respectively; whereas DETA-NONOate upregulated *hspX* and *tgsI* 3024- and 113-fold, respectively (Fig. 3.3b). Mtb cells pretreated with HC106A showed strong inhibition of *hspX* and *tgsI* induction by vitamin C and DETA-NONOate. For example, HC106A inhibited the *hspX* and *tgsI* transcripts by 78- and 14-fold following vitamin C treatment, respectively, and 362- and 151-fold following DETA-NONOate treatment. Following vitamin C treatment, HC104 showed inhibition of *hspX* by 3.4-fold and no effect on *tgsI*, or 302- and 6.6-fold inhibition of *hspX* and *tgsI* following DETA-NONOate treatment. These findings show that HC104A and HC106A act as inhibitors of the DosRST pathway in response to hypoxia and redox signals.

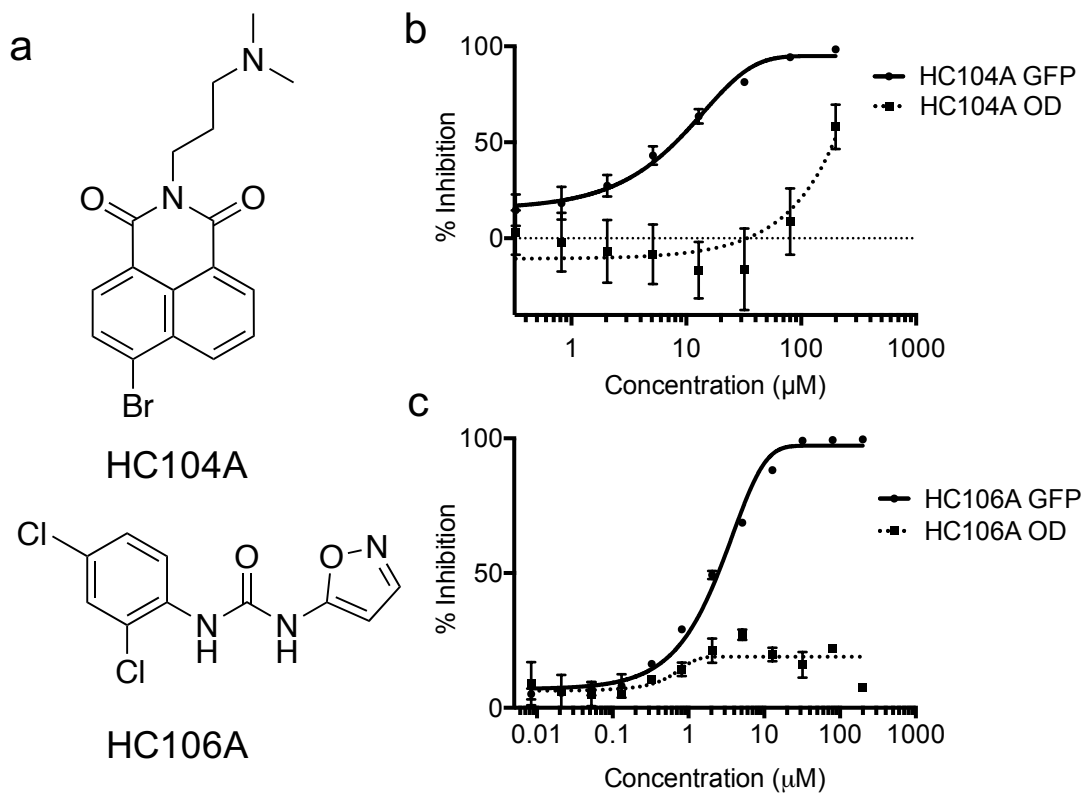


Figure 3.1. HC104A and HC106A inhibit DosRST reporter fluorescence. (a) Chemical structures of HC104A and HC106A. HC104A (b) and HC106A (c) inhibited DosR-driven GFP fluorescence signal in a dose-dependent manner, while having minimal impact of Mtb growth. The EC_{50} values of fluorescence inhibition for HC104A and HC106A are 9.8 μ M and 2.5 μ M, respectively.

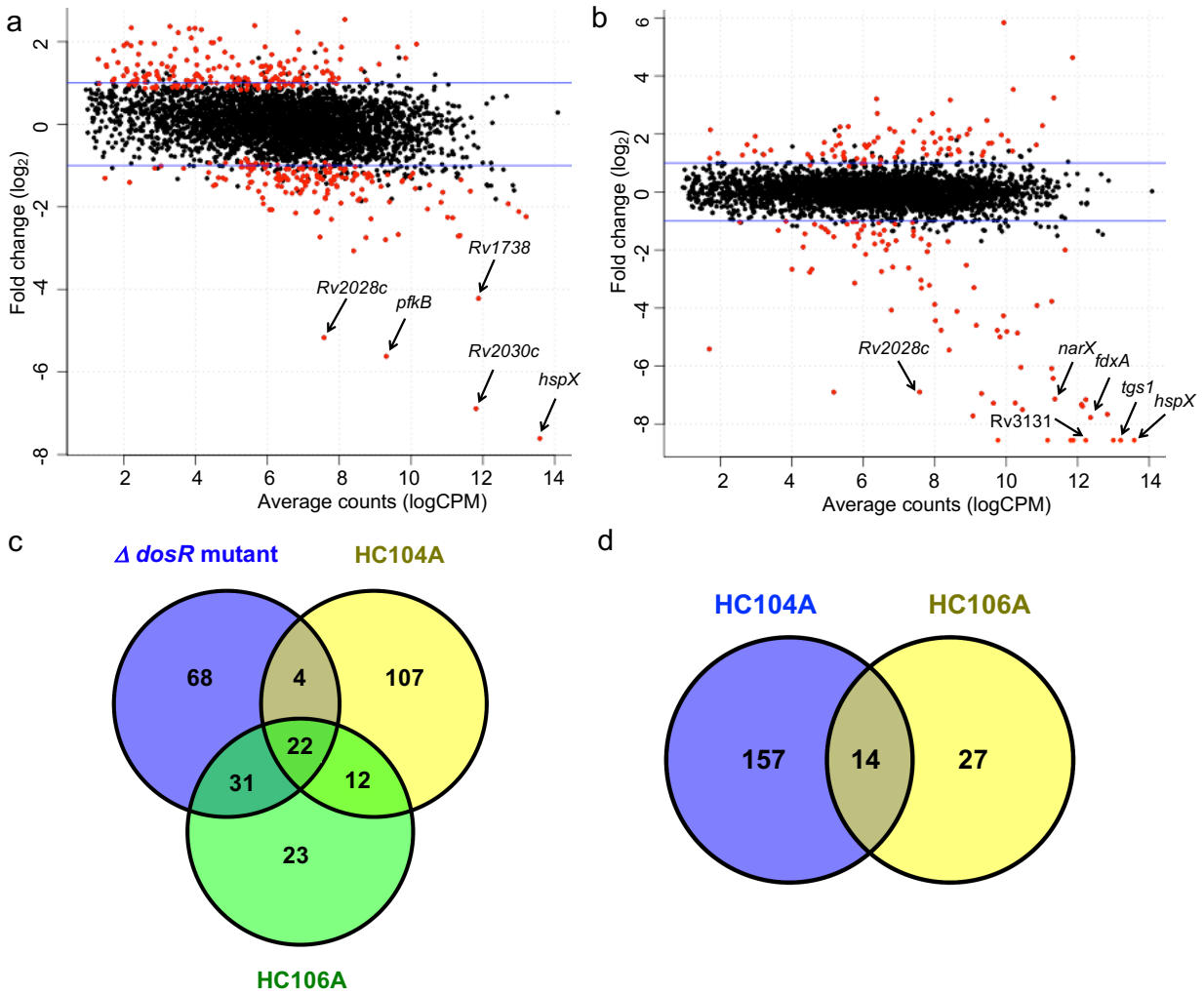


Figure 3.2. Transcriptional profiling shows HC104A and HC106A inhibited DosR regulon during hypoxia. Magnitude-amplitude plots showing differential gene expression of Mtb cells treated with 40 μM HC104A (**a**) or HC106A (**b**). The labeled genes represent selected genes that belong to the DosRST regulon. The red dots represent genes with significant differential expression, $q < 0.05$. (**c**) A Venn diagram for the downregulated genes (>2 -fold; $q < 0.05$) of WT CDC1551 treated with HC104A or HC106A compared to that of CDC1551 (ΔdosR). (**d**) Venn diagram for downregulated genes (>2 -fold; $q < 0.05$) of CDC1551 (ΔdosR) treated with HC104A or HC106A.

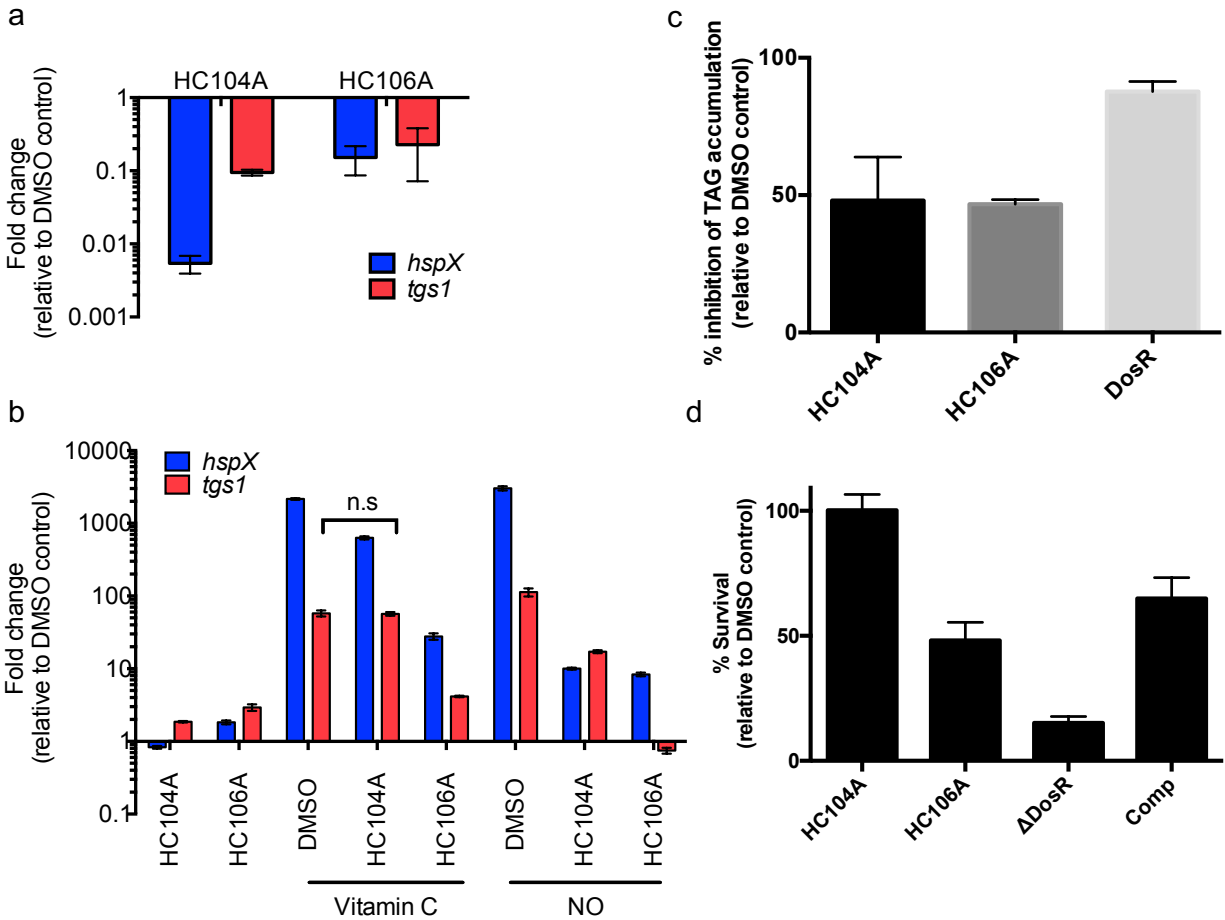


Figure 3.3. Inhibition of DosR regulon and persistence-associated physiologies by HC104A and HC106A. (a) Inhibition of DosR regulon in murine macrophages infected with Mtb and treated with HC104A and HC106A for 48 h. Bacterial RNA was isolated after incubation, and the differential gene expression of *hspX* and *tgs1* bone-marrow derived were quantified by qRT-PCR. The error bars represent the standard derivation of three biological replicates. (b) HC104A and HC106A inhibit DosR regulon induction by vitamin C and NO. Cells were pretreated with the compounds or DMSO for 24 h, and induced with vitamin C or NO for 2 h. Total bacterial RNA was isolated, and the transcripts of DosR-regulated genes, *hspX* and *tgs1*, were quantified by qRT-PCR. The difference in the drug treated samples compared to DMSO treated samples in response to vitamin C or NO are significant with a P -value <0.001 based on a t -test, except the one marked as non-significant (n.s.). The error bars represent the standard deviation of three replicates. The experiment was repeated twice with similar results. (c) Inhibition of TAG accumulation of Mtb treated with HC104A or HC106A. Mtb cells were treated with 40 μ M of the compounds and labeled with [1,2- 14 C] sodium acetate for 6 d. Total lipid was isolated and analyzed by TLC. TAG accumulation was quantified from the TLC. The error bars represent the standard derivation of two biological replicates. (d) Mtb cell survival during NRP when treated with HC104A or HC106A during NRP. Mtb cells were pretreated with 40 μ M of compounds for 48 h in an anaerobic chamber, and continued incubation for 10 d. Surviving bacteria were enumerated on 7H10 agar. The error bars represent the standard derivation of three biological replicates. The experiment was repeated twice with similar results.

Inhibition of Mtb persistence-associated physiologies

Mtb accumulates TAG during hypoxia (25-27). DosR directly regulates *tgs1*, which encodes a TAG synthase that is involved in the last step of TAG biosynthesis and is required for TAG accumulation during hypoxia (28). Transcriptional profiling showed that HC104A and HC106A repress expression of *tgs1*. Based on this transcriptional profiling, we hypothesized these two compounds may inhibit TAG biosynthesis during NRP. To test our hypothesis, Mtb cells were radiolabeled with ^{14}C -acetate and treated with HC104A or HC106A for 6 d. Lipids were isolated and analyzed by thin layer chromatography (TLC). As previously observed, DMSO treated CDC1551(Δ *dosR*) mutant displayed a strong (87%) reduction of TAG accumulation as compared to DMSO treated WT (Fig. 3.3c and Supplementary Fig. 3.2). Mtb cells treated with HC104A or HC106A showed a ~50% reduction of TAG accumulation, supporting our hypothesis that the compounds can inhibit TAG biosynthesis.

DosRST has been previously reported to be required for survival during NRP, where deletion of DosR causes greatly reduced survival during prolonged hypoxic stress (19). The impact of HC104A and HC106A on Mtb survival during NRP was examined using the hypoxic shift-down model (25). Mtb survival was examined following 10 d of treatment with the compounds at 40 μM . The Δ *dosR* mutant control had 15% survival relative to DMSO, and was partially complemented, supporting the proposal that survival during hypoxia is DosR dependent. Mtb cells treated with HC106A displayed 50% survival relative to DMSO control (Fig. 3.3d), whereas, HC104A had no impact on Mtb survival during NRP, an observation that suggests the portion of the DosR regulon inhibited by HC104A is not essential for survival during NRP.

HC104A inhibits DosR DNA binding

There are several potential targets of HC104A and HC106A to directly inhibit DosRST signaling, including: 1) direct inhibition of DosS/T sensor kinase activity, 2) modulation of the heme in the sensor, or 3) inhibition of DosR binding of DNA. To investigate the biochemical mechanisms of action of HC104A and HC106A, inhibition of DosS autophosphorylation was initially evaluated. The DosS protein was treated with different concentrations of HC104A and HC106A from 10 μ M to 40 μ M, or with 40 μ M HC103A as a positive control that was previously discovered to be a DosS/T autophosphorylation inhibitor (25). As previously observed, HC103A strongly inhibited DosS autophosphorylation, but HC104A and HC106A had no inhibitory activity (Supplementary Fig. 3.3). This suggests HC104A and HC106A are not directly inhibiting DosS/T autophosphorylation activity.

Next, a UV-visible spectroscopy assay was employed to investigate if HC104A targets to the heme of the sensor kinase DosS. Treatment of DosS protein with the reducing agent dithionite (DTN) caused a shift of the Soret peak from 403 nm to 430 nm as previously described (13, 25). Addition of HC104A to reduced DosS did not shift the peak to the oxidized position, suggesting that HC104A does not modulate DosS heme redox (Supplementary Fig. 3.4). Together, these data indicate that HC104A does not inhibit DosRST signaling by targeting sensor kinase autophosphorylation or heme and supported examining DosR as a potential target.

Inspection of the HC104A structure revealed it had significant similarity to the compound virstatin (29). Virstatin is an anti-virulence compound that inhibits *Vibrio cholera* cholera toxin production by targeting the transcription regulator ToxT (29). Virstatin inhibits ToxT protein dimerization and subsequently interferes with DNA binding, thereby inhibiting the transcription of downstream genes involved in toxin production. Based on the similarity of chemical structure

between HC104A and viristatin, we hypothesized that HC104A may be targeting DosR, and interfering with DNA binding. To test this hypothesis, an electrophoretic mobility shift assay (EMSA) was employed to investigate the impact of HC104A on DosR DNA binding. Recombinant DosR protein, ranging from 0.5 μM to 4 μM , was treated with 40 μM HC104A or a DMSO control and tested for binding to fluorescently labeled *hspX* promoter DNA. In the DMSO treated control, DosR bound promoter DNA beginning at a concentration 2 μM DosR protein (Fig. 3.4a). Treating the reaction containing 2 μM DosR protein with HC104A significantly inhibited DNA binding by ~22-fold compared to DMSO control (Fig. 3.4b). To further characterize the impact of HC104A on DosR binding of DNA, a dose-response study was performed. Reactions containing 2 μM recombinant DosR proteins were treated with different concentrations of HC104A or viristatin ranging from 1 – 80 μM . HC104A inhibited DosR binding of DNA beginning at 10 μM HC104A. The fraction of free DNA increased as HC104A concentration increased (Fig. 3.4c). For example, the fraction of free DNA was 72%, 89%, 92%, 96% and 100% for 20 μM , 30 μM , 40 μM , 60 μM and 80 μM HC104A, respectively, whereas DMSO control had 15% free DNA (Fig. 3.4d). Thus, HC104A significantly inhibits DosR-DNA binding in a dose-dependent manner. Reactions treated with viristatin had no impact on DosR binding of DNA (Supplementary Fig. 3.5a). Consistent with these observations, viristatin did not have any impact on DosRST signaling in the whole cell Mtb fluorescence reporter assay (Supplementary Fig. 3.5b). These findings support the hypothesis that HC104A may function by inhibiting DosR DNA binding activity and has an activity that is distinct from the related molecule viristatin.

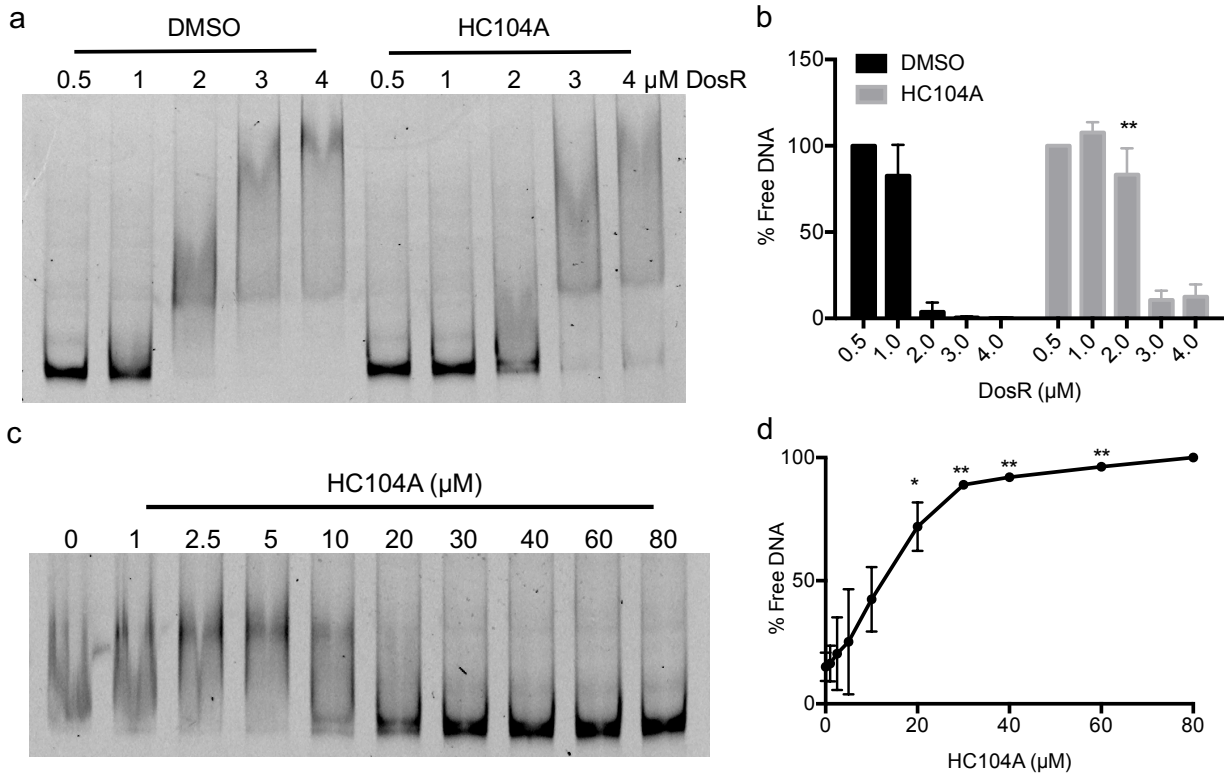


Figure 3.4. Inhibition of DosR DNA-binding by HC104A. (a) DosR protein ranging from 0.5 μM to 4 μM was treated with DMSO or 40 μM HC104A and binding to the *hspX* promoter was examined by EMSA. HC104A inhibits DosR DNA binding at 2 μM concentration. (b) The free DNA of each reaction was quantified in ImageJ and the percentage of free DNA was normalized using reactions containing 0.5 μM DosR as 100% free DNA. Differences between reactions containing 2 μM DosR treated with DMSO or HC104A are significant (** P value <0.005 based on a t -test). The error bars represent the standard derivation of two biological replicates. (c) Dose-dependent impact of HC104A on DosR DNA binding. DosR protein at 2 μM was treated with HC104A at concentrations from 1 μM to 80 μM . (d) The free DNA of each reaction was also quantified in ImageJ with the percentage of free DNA is normalized using the reaction containing 80 μM HC104A as 100% free DNA. The differences between treated reactions as compared to DMSO control are significant. (* P value <0.05 and ** P value <0.005 based on a t -test). The error bars represent the standard derivation of two biological reps.

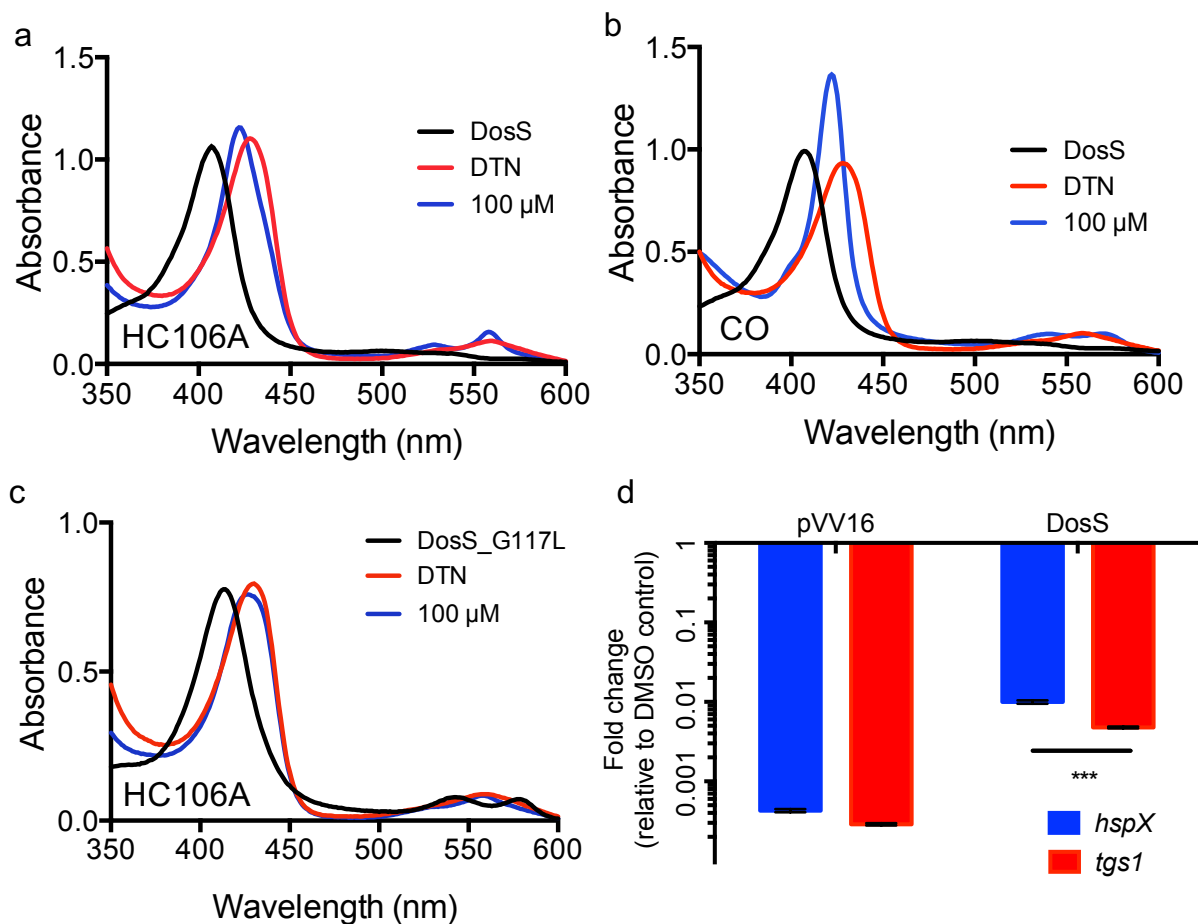


Figure 3.5. Interactions between HC106A and DosS heme. WT DosS protein was treated with dithionite (DTN) and then 100 μ M HC106A (a) or 100 μ M pf CORM-2 (a CO donor) (b). The UV-visible spectra of the two treatments exhibited a shift of the Soret peak to a common position of 422 nm. (c) DosS with a G117L amino acid substitution, that is predicted to block the heme exposing channel, provides resistance to HC106A. The spectrum of the mutant protein did not change, after HC106A treatment, indicating resistance to HC106A. (d) Overexpression of DosS protein promotes resistance to HC106A treatment in Mtb. Mtb cells with the pVV16 empty vector or the DosS overexpression plasmid were treated with 20 μ M HC106A for 6 d. Bacterial RNA was isolated for analysis of the differential gene expression of *hspX* and *tgs1* and analyzed by qRT-PCR. Overexpression of DosS caused 23- and 16.5-fold increase of *hspX* and *tgs1* transcripts, respectively, compared to the empty vector control (***) P value <0.0001 based on a t -test). The error bar represents the standard derivation of the mean for three technical replicates. The experiments were repeated twice with a similar result.

HC106A modulates DosS heme

DosS and DosT have a channel that exposes the heme to the environment and enables interactions with gases (30, 31). This channel is an Achilles heel that can be targeted by small molecules. Previously, it was shown that the artemisinin modulates DosS/T by oxidizing and alkylating heme carried by the kinases (25). UV-visible spectroscopy studies were conducted to examine if HC106A modulated DosS heme. Recombinant DosS was purified from *E. coli*, degassed and the change of DosS heme spectrum was monitored under anaerobic conditions by UV-visible spectroscopy. Treating DosS with the reducing agent dithionite (DTN) caused the Soret peak to shift to 430 nm as shown previously (13, 25). HC106A was added to the reaction following DTN treatment to observe the impact on the DosS heme UV-visible spectrum. HC106A caused the DosS Soret peak to immediately shift to 422 nm, where the peak was stably maintained for 2 h (Fig. 3.5a). This spectrum shift is different from artemisinin, where under identical conditions, artemisinin causes the DosS Soret peak to gradually shift back to the oxidized state at 403 nm (25). These findings show that HC106A may also interact with sensor kinase heme, but via a mechanism that is distinct from artemisinin-heme interactions.

The Soret peak at 422 nm is consistent with previously described spectra that are observed when DosS heme interacts with NO or CO (13). To confirm this observation, DosS was treated with 100 μ M CORM-2 (a CO donor) which caused a shift of the Soret peak to 422 nm, similar to what was observed for HC106A (Fig. 3.5b). This finding supports a hypothesis that HC106A may also be directly binding to the heme. Notably, CO activates DosS kinase function, whereas HC106A functions to inactivate the regulon, demonstrating that the impact of heme binding by CO or HC106A has differing impacts on the sensor kinase switch.

Amino acid substitutions in the channel exposing the DosS heme to the environment, such as DosS E87L or G117L, can limit access of artemisinin to modulate heme (25). To support the hypothesis that HC106A directly targets DosS heme, we tested the impact of these amino acid substitutions on HC106A/DosS heme interactions. Treating DosS(E87L) with HC106A exhibited a profile similar to wild type DosS with the Soret peak shifting to 422 nm (Supplementary Fig. 3.6). However, DosS(G117L) had no change to the overall spectrum after HC106A treatment (Fig. 3.5c). This finding indicates that DosS(G117L) is resistant to HC106A, and confirms that HC106A accesses the heme via a similar mechanism as artemisinin.

To confirm DosS is a target of HC106A in Mtb, we examined the impact of overexpressing DosS protein in Mtb. If DosS is the target of HC106A, overexpression may reduce the effectiveness of HC106A. WT DosS protein was constitutively expressed from the *hsp60* promoter in Mtb. The vector control showed that both *hspX* and *tgsI* genes were downregulated by HC106A by 2331- and 3470-fold, respectively (Fig. 3.5d). Overexpressing DosS provided significant resistance to HC106A, with *hspX* and *tgsI* showing 23- and 16.5-fold less inhibition, respectively, relative to the empty vector control. This observation of resistance in Mtb is consistent with the biochemical data supporting the view that DosS is a direct target of HC106A.

Synergistic interactions between DosRST inhibitors

With multiple distinct inhibitory activities of the HC101A, HC102A, HC103A, HC104A and HC106A, we sought to examine if potentiating or antagonistic interactions existed between the molecules, when targeting the DosRST pathway. To examine these interactions, checkboard assays were performed with pairwise comparisons of artemisinin (HC101A), HC102A, HC103A, HC104A and HC106A. CDC1551 (*hspX*::GFP) was treated with combinations of two compounds

ranging from 50 μM to 0.08 μM in 96-well plates. DosR-driven GFP fluorescence and optical density were measured following 6 d of treatment. The Combination Index (CI) was calculated for each drug pair based on the Chou-Talalay method in the CompuSyn software package (32, 33), where CI values of < 1 , $= 1$ and >1 indicate synergistic, additive or antagonistic interactions, respectively. Among all 64 compound pairs, artemisinin combined with HC102A, HC103A, HC104A and HC106, showed 46, 49, 41, and 50 combinations that have $\text{CI} < 1$, respectively (Fig. 3.6). Notably, some CI values are below 0.1 when artemisinin was paired with HC102A, HC103A or HC106A combinations. Example dose response curves illustrate these synergistic interactions (Fig. 3.6). Several other pairwise comparisons also demonstrated synergy (Supplementary Fig. 3.7), however, in general, these interactions had CI between 1 and 0.1, supporting weaker synergistic interactions, as compared to combinations with artemisinin. Overall, these studies provide the evidence that the inhibitors function by distinct mechanisms and may be combined to improve potency.

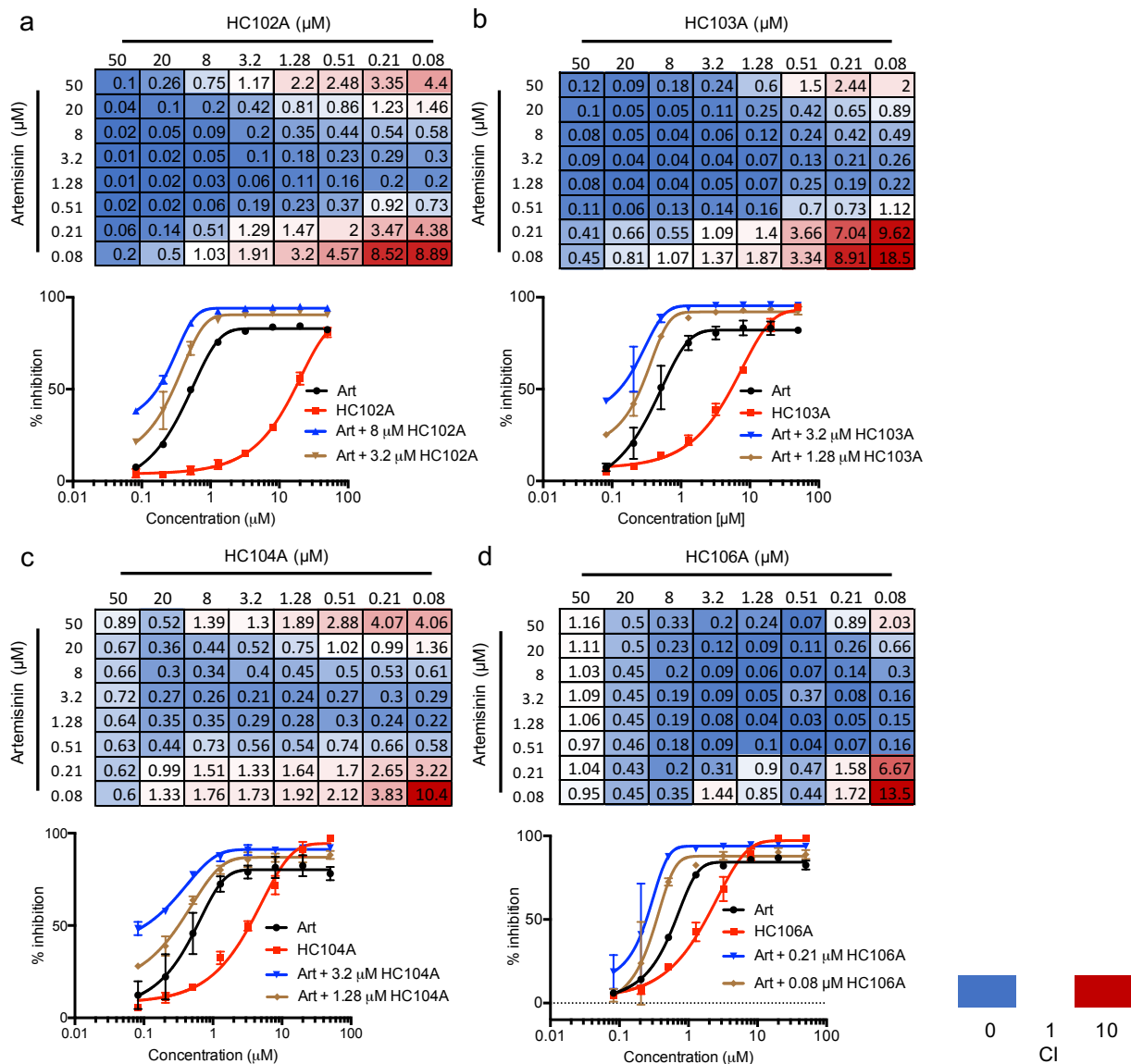


Figure 3.6. Synergistic interactions between DosRST inhibitors. CDC1551 (*hspX*::GFP) was treated with pairwise combinations of two compounds at concentrations of 50 μM to 0.08 μM . GFP fluorescence was measured and used to calculate percentage inhibition. The data were analyzed in the CompuSyn software to determine the combination index (CI) for the panel of each drug combination, including (a) artemisinin and HC102A; (b) artemisinin and HC103A; (c) artemisinin and HC104A; and (d) artemisinin and HC106A. Example EC₅₀ curves are presented with individual compounds or a selected synergistic combination to illustrate the potentiating interactions.

Structure-activity relationship study for HC104A and HC106

We conducted a catalog search for HC104 and HC106 analogs and obtained 10 commercial analogs for each series to define initial structure activity relationships (SAR). For HC104A we observed that a bromine in the 5-position is required for activity and that the R2 dimethylamine group is not required (Supplementary Table 3.1). For example, HC104B is identical to HC104A except for the removal of the bromine (R1), which results in a complete loss of activity in the whole cell assay. Whereas, replacement of the R2 group with a methyl (HC104G) results in an active compound, although ~5-fold less active than HC104A. Although not highly potent, its ligand efficiency, cLogD and druglikeness are in the range of what would be considered acceptable to good as a starting point for further manipulation. For HC106A (Supplementary Table 3.2), catalog SAR work led to new understandings of the nature of the series. We first found that the simple removal of an ortho chloro on the “A” ring of HC106A leads to ~ 2-fold enhanced activity, with an EC₅₀ in the whole cell Mtb assay for DosRST inhibition of 1.33 μM (HC106F). It was also found that the use of an alternative isomer of the isoxazole had no activity (HC106C).

To further understand the SAR of the HC106 series, additional analogs were synthesized to examine the need of the central urea functionality and whether modifications can be tolerated (Supplementary Table 3.3). A pyridyl analog (MSU-41425), designed to replace the isoxazole also demonstrated no activity as was the symmetrical 4-chloroaniline derived urea (MSU-41324). However, the bis-isoxazole urea (MSU-39444) provides an EC₅₀ of 1.7 μM, indicating that the isoxazole is important for binding. Isoxazoles are unique among heterocycles in that they exist in multiple tautomeric forms as supported by initial NMR studies (34). We next explored the need of one of the -NHs of the urea, capping it with a methyl (MSU-39451), integrating it into a ring for conformational restriction (MSU-39453), and replacing with a methylene unit

(MSU-39449). In all cases, reduced activity (0.5 - 1 log) was observed but not all activity was lost. Thus, HC106A is a potent whole cell inhibitor of the DosRST pathway, with flexibility to be improved via SAR.

To further test the SAR, we conducted a Topliss Tree evaluation of the “A-ring” aniline (35). To reliably prepare the derivatives, we explored and established a general preparation (Supplementary Fig. 3.8). This route is preferred relative to alternative approaches for its cleanliness, yields and ease of purification, usually by trituration. It is also anticipated that it will allow access to future derivatives. Using HC106F and HC106A as starting points, we prepared the 3,4-dichloro and 3-chloro derivatives (MSU-39452 and MSU-39445, respectively). Both the 3- and 4-chloro derivatives demonstrated greater activity than 3,4-dichloro (MSU-39452). We found that replacing the 4-chlorophenyl ring with pyridyl analogs (MSU-39448 and MSU-39450) lead to increased activity. Focusing on 4-position derivatives, we found that fluoro (MSU-39446), bromo (MSU-41464) and methoxy (MSU-39447), as electron p-orbital donating substituents, also lead towards increased activity. Para-t-butyl phenyl (MSU-41442), also did the same. Electron withdrawing substituents, such as 4-CO₂Me (MSU-4165), 4-trifluoromethyl (MSU-41463) and biphenyl (MSU-41443) saw similar activity. Overall, several analogs were discovered with significantly ~4-fold enhanced potency, with several inhibitors having whole cell DosRST inhibitory EC₅₀ below 1 μM, including EC₅₀ of 0.63 μM, 0.61 μM, 0.54 μM and 0.75 μM for MSU-33189, -39447, -39446, and -39455, respectively. The parent analog HC106A had an EC₅₀ of 2.48 μM. Kinetic solubility assays were conducted for selected analogs and all exhibited excellent aqueous solubility greater than >100 μM, except for MSU-41443 (Supplementary Table 3.3). This finding shows that the urea group present in the HC106A does not have a detrimental impact on HC106 aqueous solubility.

Overall, the nanomolar whole cell potency, flexible SAR and excellent solubility, confirm that the HC106 series is a suitable series for continued optimizations to identify a drug-like lead compound.

Discussion

DosRST is a two-component regulatory system required for Mtb environmental sensing, adaptation, and persistence. By using a fluorescent reporter strain CDC1551 (*hspX'::GFP*), we have previously discovered small molecule inhibitors of DosRST, named HC101A-HC106A, from the whole-cell phenotypic HTS. Here, we report the characterizations of HC104A and HC106A as DosRST inhibitors. Both compounds downregulated genes in the DosR regulon, and inhibited TAG biosynthesis. HC106A also reduced Mtb survival during NRP.

In a UV-visible spectroscopy assay, we observed that HC106A interacts with the heme of sensor kinase DosS. The UV-visible spectrum of HC106A-treated DosS is similar to those of CO- or NO-treated DosS. The overlap between the CO and HC106A spectra supports that HC106A may also directly bind to the heme of DosS. Interestingly, CO activates sensor kinases, whereas HC106A inhibits them. This could be due to the difference in conformational changes induced by CO and HC106A, or binding of HC106A may lock the sensor kinases into an inactive state. Furthermore, the DosS G117L substitution, recombinant DosS blocks the heme exposing channel, provides resistance to HC106A. This means that, similar to artemisinin, this channel is also important for the activity of HC106A. These findings provide additional evidence that the heme-exposing channel in DosS/T can be exploited by small molecules to prevent or inhibit the heme from sensing signals and to disrupt signal transduction of a two-component regulatory system. To

our knowledge, these two distinct mechanisms of actions are novel mechanisms to inhibit the DosRST pathway.

Mechanistic studies via EMSA indicates that HC104A may function by targeting DosR and inhibiting DosR DNA binding. Virstatin had no effect on DosR DNA binding and no impact on the DosRST signaling in whole cells, showing that although both compounds share a similar structure, they function by distinct mechanisms. From the catalog SAR study, we found that the bromine group is required for the compound. Virstatin does not have the bromine, and the R-group is butyric acid instead of dimethylamine. These two differences are enough to differentiate the activity of the compounds. Moreover, transcriptional profiling shows that the most repressed genes by HC104A are from the DosR regulon, providing additional evidence that HC104A is somewhat selective for DosR regulated genes. Interestingly, the genes most downregulated by HC104A, including *hspX*, *Rv2030c*, *pfkB*, and *Rv2028c*, are from the same operon under control of *hspX* promoter, which is strongly induced by DosR in hypoxia. This result suggests that HC104A is more specific to target *hspX* operon genes as compared to other DosR regulated genes. This finding leads to the speculation that HC104A may be more efficient to prevent DosR binding to the *hspX* promoter than the other DosR promoters. HC104A may fit better in the pocket in the interface of DosR-*hspX*' complex. This postulation also supports the idea that HC104A may not have an impact on DosR protein dimerization, which would lead to universal downregulation of DosR-regulated genes. Detailed characterizations of HC104A on inhibiting DosR dimerization and promoter binding specificity is the subject of ongoing characterizations.

This study together with the previous report reveals multiple distinct inhibitory mechanisms for the five compounds, HC101A-104A, HC106A. Four out five compounds, HC101A-HC103A and HC106A, are proposed to function by targeting the sensor kinases

DosRST. Furthermore, these four compounds are effective at decreasing Mtb survival during NRP in hypoxic-shift down assay. In contrast, the compound targeting DosR, HC104A, had no impact on Mtb survival during NRP. This result is consistent with a previous report that showed only the $\Delta dosS$ mutant exhibits a survival defect in the C3HeB/FeJ mouse model (22). Notably, the *dosR* mutant strain used in our study is also lacking *dosS* expression due to polar impacts of the deletion, supporting the hypothesis that the reduced survival during NRP may be dependent on DosS. Alternatively, we noted that HC104A only inhibits a portion of the DosR regulon with only 26 genes being downregulated. This finding suggests that the DosR regulated genes that are inhibited by HC104A (Fig. 3.2, and Supplementary Dataset 3.1, 3.3) are not required for DosRST-dependent persistence during NRP or not sufficiently inhibited to have an impact on survival.

The transcriptional profiling data showed off-target impacts in the treated *dosR* mutant strain. These effects may be due to inhibition of DosS/T signaling that functions independent of the response regulator. Several recent studies have demonstrated the occurrence of cross-interactions between histidine kinases and response regulators in Mtb. For instance, Lee *et al.* shows that DosT can interact with the other non-cognate response regulators, including NarL and PrrA (36). Our transcriptional profiling of the compound treated *dosR* mutant strain suggests that some genes downregulated by HC101A, HC103A and HC106A may be DosS-dependent but DosR-independent (Supplementary Fig 3.9). In the prior study, six genes are similarly regulated between artemisinin and HC103A in the treated *dosR* mutant strain, including Rv0260c that encodes a putative response regulator (25). HC106A and HC103A share four differentially regulated genes in the *dosR* mutant, including *argC*, *argJ*, *argB*, and *argF*, which are genes involved in arginine biosynthesis. Our data presented here and in the literature point to the possibility that DosST modulate gene expression independently of DosR.

The synergy studies show significant synergistic interactions between artemisinin, HC102A, HC103A, HC104, or HC106A. Moreover, artemisinin exhibited the greatest synergistic activities with HC102A, HC103A or HC106A, indicating that inhibition of histidine kinases by a second inhibitor can lead to synergistic inhibition of the DosRST pathway. This interaction could be due to both sensor kinases being required for full induction of the DosR regulon, where DosT responds early during hypoxia and DosS further induces the regulon at later times (37), and it is possible that the inhibitors have different affinities for DosS or DosT. Thus, multiple inhibitors could inhibit both DosS and DosT better than an inhibitor alone. Interestingly, artemisinin shows the greatest synergism with HC106A. Both compounds are proposed to target the heme of DosS/T, but through different mechanisms. This finding shows that both inhibitors can enter the channel of DosST to interact with the heme and do so without antagonizing interactions.

The identification of new antibacterial agents and tuberculosis drugs has been associated with the realization that these compounds can occupy a different region of chemical space relative to drugs in most other therapeutic areas. Series HC106 is easily in the range of the characteristics for compounds currently in use, in development and anti-TB compounds. Series HC104 needs further exploration to fully assess its suitability. The physicochemical properties of a drug, such as solubility and permeability, impact its oral bioavailability as these factors influence absorption, distribution, metabolism, and excretion. Series HC106 demonstrates excellent aqueous solubility (Table 3.3, with compounds generally having solubility >100 μ M). The melting points of most of the compounds in the series and the corresponding cLogP are also supportive appropriate solubility. The ability of an anti-TB drug to reach its target site is greatly hampered by the highly impermeable Mtb cell envelope. Both series (HC104 and HC106) demonstrate low micromolar and nanomolar whole cell EC₅₀ values, suggesting adequate cell wall permeability. SAR studies

of HC106 show that there remain significant opportunities for optimization of HC106 for potency and drug properties and future studies will be focused on such optimizations.

Materials and methods

Bacterial strains and growth conditions. Mtb CDC1551, CDC1551 ($\Delta dosR$) strains were used in this study. All cultures were grown at 37°C and 5% CO₂ in 7H9 Middlebrook medium supplemented with 10% OADC (oleic acid albumin dextrose catalase) and 0.05% Tween-80 in standing, vented tissue culture flasks, unless stated otherwise.

EC₅₀ assays. The assay was performed as previously described (25). Briefly, the (*hspX*::GFP) reporter strain culture was diluted to an OD₆₀₀ of 0.05 in fresh 7H9 media, pH 7.0, and 200 μ L of diluted culture was aliquoted in clear-bottom, black, 96-well plates (Corning). Cells were treated with an 8-point (2.5-fold) dilution series ranging from 200 μ M – 0.32 μ M. For the structure relationship studies for the HC106 series, a 12-point (2.5-fold) dilution series of HC106 analogs ranging from 200 μ M – 8.4 nM were used. GFP fluorescence and optical density were measured following 6 d incubation. Percentage fluorescence and growth inhibitions were normalized to a rifampin-positive control (100% inhibition) and DMSO-negative control (0% inhibition). EC₅₀ values were calculated for each compound using GraphPad Prism software package (version 6). Each experiment was performed with two technical replicates per plate and two biological replicates, and the error bar represents the s.d. of the biological replicates. Experiments were performed twice with similar results.

Transcriptional profiling and data analysis. Transcriptional profiling studies were conducted as previously described in Zheng *et al.* (25). Briefly, CDC1551 or CDC1551 ($\Delta dosR$) cultures were treated with 40 μ M HC104A, HC106A or DMSO control for 6 d. The starting OD₆₀₀ was 0.1 in 8 mL of 7H9 medium in standing T25 vented tissue culture flasks. Bacterial growth consumes oxygen and stimulates the DosRST pathway. The total bacterial RNA from two biological replicates was isolated and prepared for sequencing as previously described (38). The RNA-seq data were processed and analyzed using the SPARTA software package (39).

Real-time PCR assays. The vitamin C and NO assays were performed as previously described (25). Briefly, cultures at an OD₆₀₀ of 0.6 were pretreated with 80 μ M HC104A, HC106A or a DMSO control for 24 h, and induced with 50 μ M DETA-NONOate or 20 mM vitamin C for 2 h. For the HC106A resistance assays, CDC1551 was transformed with the empty replicating plasmid pVV16 or the plasmid expressing *dosS* from the strong *hsp60* promoter (pVV16-DosS), and treated with 20 μ M HC106A for 6 d. Total bacterial RNA was isolated and differential gene expression of DosR-regulated genes, including *hspX* and *tgsl*, was quantified. The experiment was performed in three technical replicates and error bars represent the s.d from the mean. The experiment was repeated twice with similar results. To examine Mtb gene expression in macrophages, murine bone-marrow derived macrophages were isolated as previously described (40) and seeded in T75 vented, tissue culture flasks. Macrophages were infected with CDC1551 with multiplicity of infection ratio of 1:20 as previously described (40). After infection, the flasks were treated with 40 μ M HC104A or HC106A or DMSO for 48 h, with three individual flasks for each treatment. Total bacterial RNA was isolated after treatment, and the transcripts of DosR-

controlled genes (*hspX* and *tgsI*) were quantified in RT-PCR. The experiment was conducted with three biological replicates. The error bar represents the s.d. of the biological replicates.

TAG biosynthesis. The lipid labelling and TAG TLCs were performed as previously described (25). Briefly, CDC1551 was cultured at an initial OD₆₀₀ of 0.1 and radiolabeled with 8 μ Ci of [1,2-¹⁴C] sodium acetate in T25 vented tissue culture flasks. The cultures were treated with 40 μ M HC104A, HC106A or DMSO for 6 d at 37°C. CDC1551 (Δ *dosR*) and *dosRS* complement strains were also examined. Total lipids were extracted and ¹⁴C incorporation was determined by scintillation counting. 20,000 c.p.m. of total lipids were analyzed by TLC using silica gel 60 aluminum sheets (EMD Millipore). To determine TAG accumulation, the lipids were developed in hexane-diethyl ether-acetic acid (80:20:1; vol/vol/vol) solvent system. The TLC was exposed to a phosphor screen for 3 d, and imaged on a Typhoon imager and TAG was quantified using ImageJ software (41). The experiment was repeated twice with similar results, and the error bar represents the s.d. of two biological replicates.

NRP survival assays. Survival during NRP was examined using the hypoxic shift down assays as previously described (25, 42). Briefly, CDC1551 cells were treated with 40 μ M HC104A, HC106A or DMSO control in a 24-well plate (1 mL/well). CDC1551 (Δ *dosR*) and *dosRS* complement strains were also examined. Plates were incubated in an anaerobic chamber (BD GasPak) for 12 d. It took 48 h for cultures to become anaerobic, as monitored by a methylene blue control. Bacterial CFUs were numerated on 7H10 agar plates following incubation. The experiment was repeated twice with similar results.

DosR protein purification. *DosR* full length protein was purified as previously described (43). Briefly, the *dosR* gene (Rv3133c) was cloned into pET15b (Novagen Darmstadt, Germany) using the primer set: forward primer 5'-TTTCATATGGTGGTAAAGGTCTTCTTGGTCGATGAC-3'; reverse primer 5'-TTTGGATCCTCATGGTCCATCACCGGGTGG-3'. The His₆-*DosR* protein was expressed in *E. coli* BL21(DE3) strain. The culture was grown to OD₆₀₀ 0.5-0.6, and induced with 1 mM IPTG for 6.5 h at 29°C. The cell pellet was suspended in lysis buffer (20 mM Tris-HCl, pH 8.0, 10% glycerol, 500 mM NaCl, 0.5 mg/ml lysozyme and 0.1 mg/ml PMSF), and incubated at 37°C for 30 min. The soluble fraction of lysate was collected after centrifugation and applied to a TALON metal affinity Co²⁺ column (Clontech). The column was washed twice with washing buffer (20 mM Tris-HCl, pH 8.0, 10% glycerol, 500 mM NaCl) without imidazole, then with 20 mM imidazole. The protein was eluted with the same buffer containing 300 mM imidazole. The fractions with the most *DosR* protein (as determined by SDS-PAGE) were pooled together for dialysis in 25 mM Tris-HCl, pH 8.0. The final protein concentration was determined using a Qubit kit (Invitrogen).

Electrophoretic mobility assay. The assay is fluorescence-based using 6-carboxyfluorescein (6FAM) labeled 385 bp probe from the *hspX* promoter. In designing the primer set, 6FAM was added to the 5' ends of forward and reverse primers. The *hspX* probe was synthesized via PCR using the primer set: forward primer 5'-6FAM-CAACTGCACCGCGCTCTTGATG-3'; reverse primer 5'-6FAM-CATCTCGTCTTCCAGCCGCATCAAC-3'. The probe was purified by Qiagen PCR purification kit. The *DosR* protein was pre-phosphorylated in 10 µL of phosphorylation buffer (40 mM Tris-HCl, pH 8.0, 5 mM MgCl₂, 50 mM lithium potassium acetyl phosphate), and incubated at room temperature for 30 min. The protein was then transferred to binding buffer in a

final volume of 20 μ L (final concentration, 25 mM Tris-HCl, pH 8.0, 0.5 mM EDTA, 20 mM KCl, 6 mM MgCl₂, 10 nM probe, 1 μ g poly-dI-dC (Sigma Aldrich)), and treated with HC104A or an equal volume of DMSO or virstatin (Santa Cruz Biotech). Two different assays were performed. Firstly, different DosR protein concentrations from 0.5 μ M to 4 μ M were treated with 40 μ M. Second, dose response assays were performed with 2 μ M DosR treated with different concentrations of HC104A or virstatin from 1 μ M to 80 μ M. After incubating on ice for 30 min, the reactions were terminated by adding 1 μ L 80% glycerol, and loaded on a native 5% Tris/Borate/EDTA (TBE) polyacrylamide gel. The gel was run at 50 V, for 5-6 h at 4°C in 1X TBE buffer, and was imaged using a Typhoon scanner with appropriate filters that can detect fluorescence at excitation = 495 nm, emission = 520 nm. Binding of the unbound probe was quantified using ImageJ (41). The assay was repeated at least twice with similar results. The error bar represents the s.d. of two biological replicates.

UV-visible spectroscopy assay. DosS and mutant proteins were purified and analyzed as previously described (25). Briefly, 7.5 μ M of recombinant DosS protein was deoxygenated with argon gas in a sealed cuvette. The protein was reduced with 400 μ M DTN for 20 min. The reaction was then treated with 100 μ M HC106A, 400 μ M HC104A, 100 μ M CORM-2 (tricarbonyldichlororuthenium (II) dimer) or equal volume of DMSO. The UV-visible spectra were recorded for kinetic changes over 2 h. The experiment was repeated at least twice with similar results.

Checkboard synergy studies. The reporter strain CDC1551 (*hspX::GFP*) was treated with pairs of DosRST inhibitors from 50 μ M – 0.08 μ M in 96-well plates, including HC101A-HC104A and

HC106A. GFP fluorescence and OD₆₀₀ were measured after 6 d incubation. The percentage of fluorescence inhibition (FI) and growth inhibition were calculated for each drug pair, with limited growth inhibition observed. The FI data was utilized for further analysis of interactions using CompuSyn software (32). The Combination Index (CI) value was calculated for each drug pair according to the Chou-Talalay method, which is based on the Median-Effect equation derived from the Mass-Action Law principle (33, 44). The resulting CI values provide quantitative determination of drug interactions, including synergism (CI < 1), additive effect (C = 1), and antagonism (C > 1).

Autophosphorylation assay. The DosS autophosphorylation assay was performed as previously described (25). Recombinant DosS protein was treated with 10 μM, 20 μM or 40 μM of HC104A, or HC106A. DMSO and 40 μM HC103A were also included as positive and negative controls, respectively.

Kinetic solubility assay. The assay was performed with 7-point (2-fold) dilutions from 200 μM - 3.125 μM for HC106 analogs. Mebendazole, benxarotene and aspirin were also included as controls. The drug dilutions were added to PBS, pH 7.4, with the final DMSO concentration of 1%, and incubated at 37 °C for 2 h. The absorbance at 620 nm was measured for each drug dilution to estimate of the compound solubility. Three replicates were examined for each dilution.

Acknowledgements

The MSU RTSF provided technical support for the RNA-seq library preparation and sequencing. This project was supported by start-up funding and a Molecular Discovery Grant from Michigan

State University, AgBioResearch, a grant from the NIH-NIAID (R21AI105687) and Grand Challenges Explorations grants from the Bill and Melinda Gates Foundation (OPP1059227 and OPP1119065).

APPENDIX

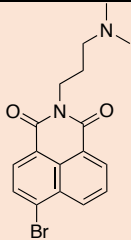
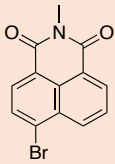
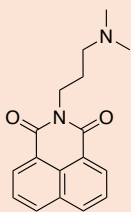
APPENDIX

Supplementary information

Supplementary Dataset 3.1. Differential gene expression data of WT Mtb treated with inhibitors

Supplementary Dataset 3.2. Differential gene expression data of the DosR mutant treated with the inhibitors.

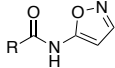
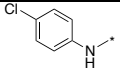
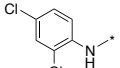
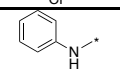
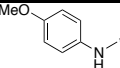
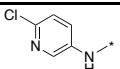
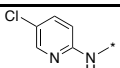
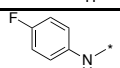
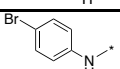
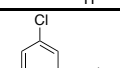
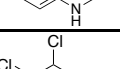
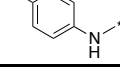
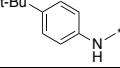
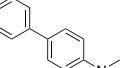
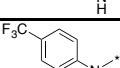
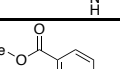
Supplementary Dataset 3.3. Complete gene expression tables for transcriptional profiling experiments.

Compound			
ID#	HC104A	HC104G	HC104B
MW (g/mole)	361.2	290.1	282.3
EC ₅₀ (μM)	9.8	43.8	>200
Ligand Efficiency	0.34	0.36	0.26
CLogP (cLogD at pH 7.4)	3.0 (0.55)	2.3 (2.4)	2.9 (-0.24)
Druglikeness	4.4	0.55	6.2

Supplementary Table 3.1. Structure and properties of HC104 series. Catalog structure activity relationship study performed for HC104 analogs with different R-groups. The reporter strain CDC1551 (*hspX'::GFP*) was treated across doses of each analog from 200 μM to 0.328 μM. The EC₅₀ values of fluorescence inhibition calculated for each analog to determine their potency. The other chemical properties of the analogs are also included.

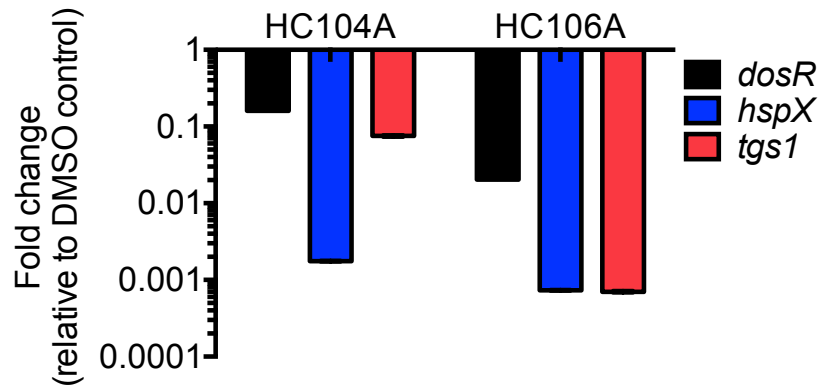
ID#	Compound	EC ₅₀ (μM)	ID#	Compound	EC ₅₀ (μM)
HC106F		1.33	MSU-41324		>200
HC106A		2.48	MSU-39449		5.2
HC106C		>200	MSU-39451		4.14
MSU-39450		1.95	MSU-39453		16.62
MSU-39444		1.7	MSU-41422		>200
MSU-41425		>200			

Supplementary Table 3.2. Initial SAR studies of the HC106 series. The HC106 analogs with different R-groups were synthesized or purchased. The reporter strain CDC1551 (*hspX'::GFP*) was treated with across doses of each analog from 200 μM to 0.328 μM. The EC₅₀ values of fluorescence inhibition calculated for each analog to determine their potency.

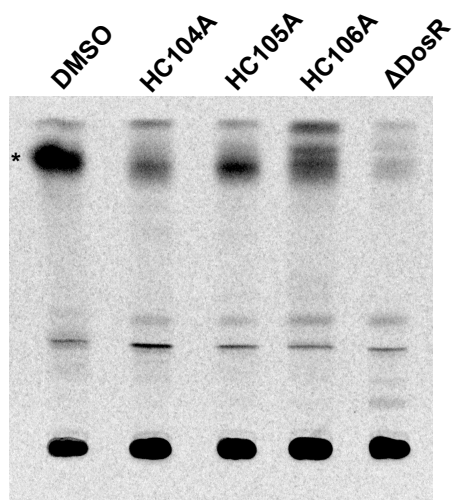
								
ID#	Compound R =	EC ₅₀ (μM)	MW (g/mol)	TPSA (ang ²)	Ligand Efficiency (LE)	m.p. (°C)	cLogP	Solubility (μM)
HC106F		1.33	237.6	63	0.54	183	2.2	>200
HC106A		2.48	272.1	63		164		110
MSU-33189		0.63	203.1	63	0.40	183-184	1.6	
MSU-39447		0.61	233.2	72	0.36	166-167	1.5	>100
MSU-39448		1.42	238.6	75	0.38	158-159	1.3	
MSU-39450		1.95	238.6	75	0.38	122-123	1.3	
MSU-39446		0.54	221.2	63	0.38	176-177	1.7	>100
MSU-41464		1.2	282.1	67		183-184	2.3	
MSU-39445		0.75	237.6	63	0.37	159 (dec)	2.1	>100
MSU-39452		2.47	272.1	63	0.36	164	2.8	
MSU-41442		2.08	259.3	63		163	3.1	>100
MSU-41443		11.2	279.3	63		193	3.2	14
MSU-41463		1.67	271.2	67		178	2.4	
MSU-41465		1.16	261.2	94		194	1.5	
MSU-41462		1.12	217.2	67		128-130	1.3	

Supplementary Table 3.3. Initial Topliss Tree evaluation of “A-ring” aniline of series HC106.

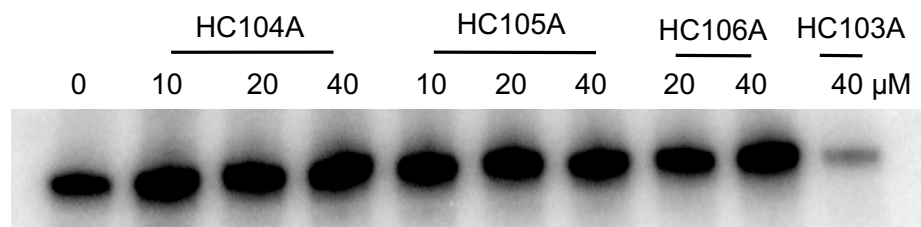
The HC106 analogs with different R-groups were synthesized. The reporter strain CDC1551 (*hspX'::GFP*) was treated with across doses of each analog from 200 μM to 0.328 μM. The EC₅₀ values of fluorescence inhibition were calculated for each analog to determine their potency. The other chemical properties of the analogs are also included. Kinetic solubility was experimentally determined.



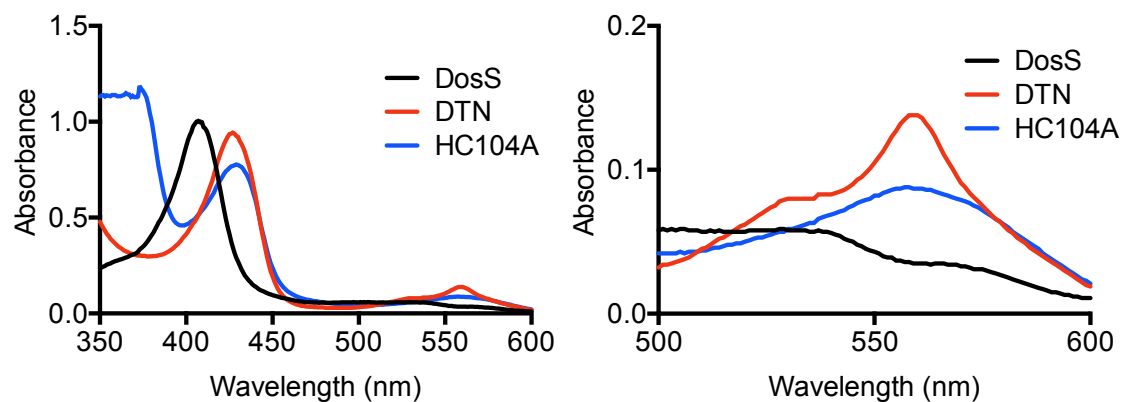
Supplementary Figure 3.1. Inhibition of the DosR regulon by HC104 and HC106A during hypoxia. Mtb cells were treated with 40 μ M compounds for 6 d, and total bacterial RNA was isolated. The DosR regulated genes, *dosR*, *hspX*, and *tgs1* were quantified in qRT-PCR. The error bars represent the standard derivation of three replicates. The experiment was repeated at least twice with similar results.



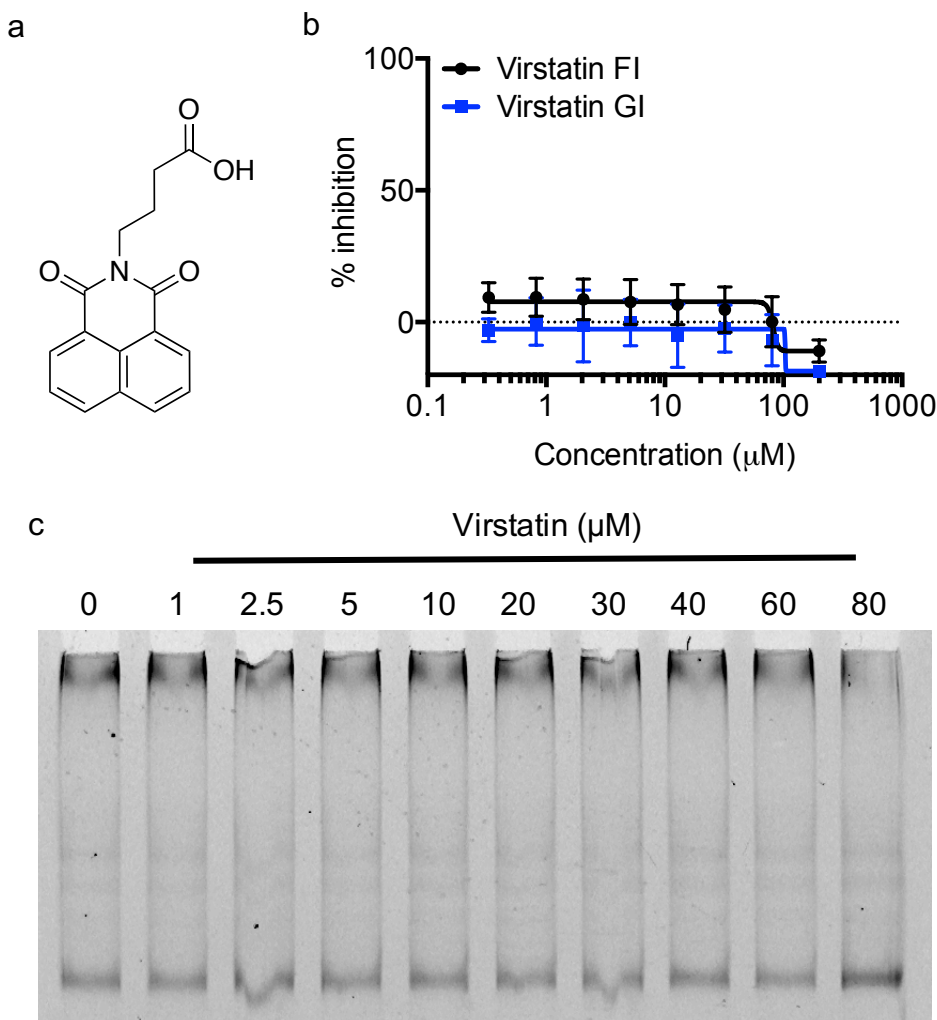
Supplementary Figure 3.2. TLC of TAG reduction in *Mtb* treated with HC104A and HC106A. *Mtb* cells were treated with 40 μ M of the compounds and labeled with [1,2- 14 C] sodium acetate in T25 vented tissue culture flasks for 6 d. Total lipid was isolated and analyzed BY TLC. The experiment was repeated twice with similar results.



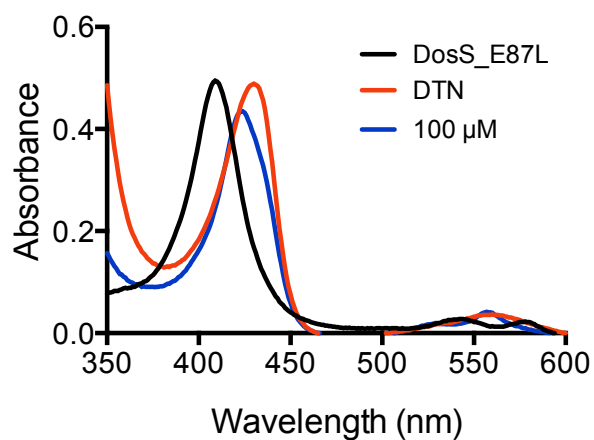
Supplementary Figure 3.3. Autoradiograph examining the impact of HC104A and HC106A on DosS autophosphorylation. DosS protein was treated with 10 μ M, 20 μ M or 40 μ M of the compounds, with DMSO and HC103A as positive and negative controls, respectively. The results show that HC104A and HC106A have no effect on DosS autophosphorylation.



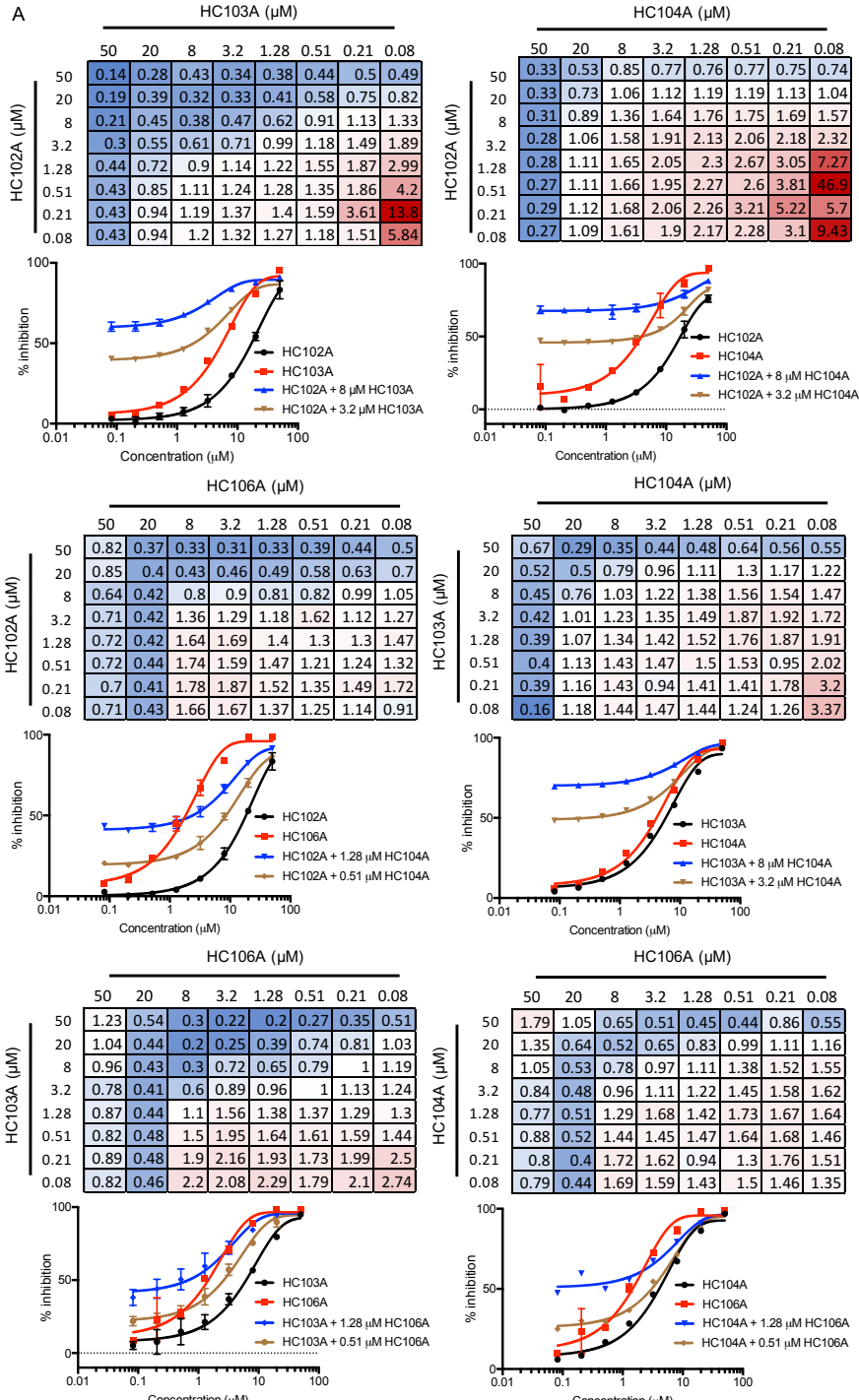
Supplementary Figure 3.4. Investigation of interaction between HC104A and DosS. WT DosS treated with 400 μ M HC104A shows no impact on shifting of the Soret peak in the UV-visible spectroscopy assay. The experiment was repeated at least twice with similar results.



Supplementary Figure 3.5. The impact of virstatin on DosR DNA-binding and DosRST signaling in *Mtb*. (a) Chemical structure of virstatin. (b) Dose-response curve of virstatin shows no effect on inhibition of *Mtb* DosR-driven GFP fluorescence. (c) DosR protein at 2 μM was treated with 9 point dose response of virstatin from 1 μM to 80 μM . The reactions were analyzed on native PAGE gel. The experiment was repeated at least twice with similar results.



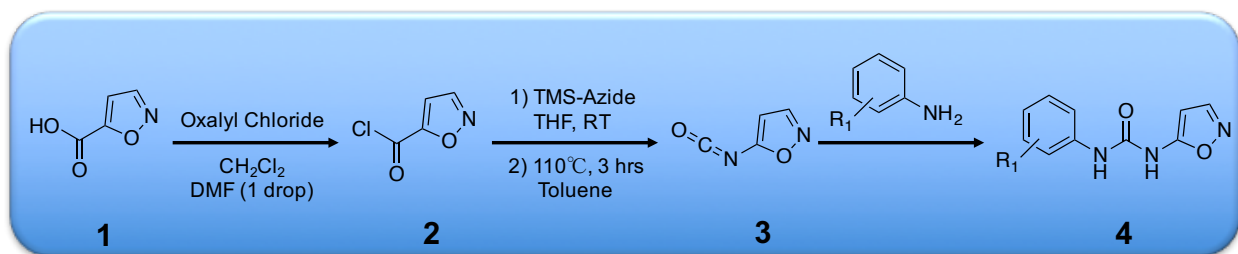
Supplementary Figure 3.6. Investigating the interaction between HC106A and DosS heme. DosS E87L protein was treated with 100 μ M HC106A after being reduced with DTN. The UV-visible spectra were recorded after each treatment, and showed no change on the overall spectrum compared to WT protein. The experiment was repeated at least twice with similar results.



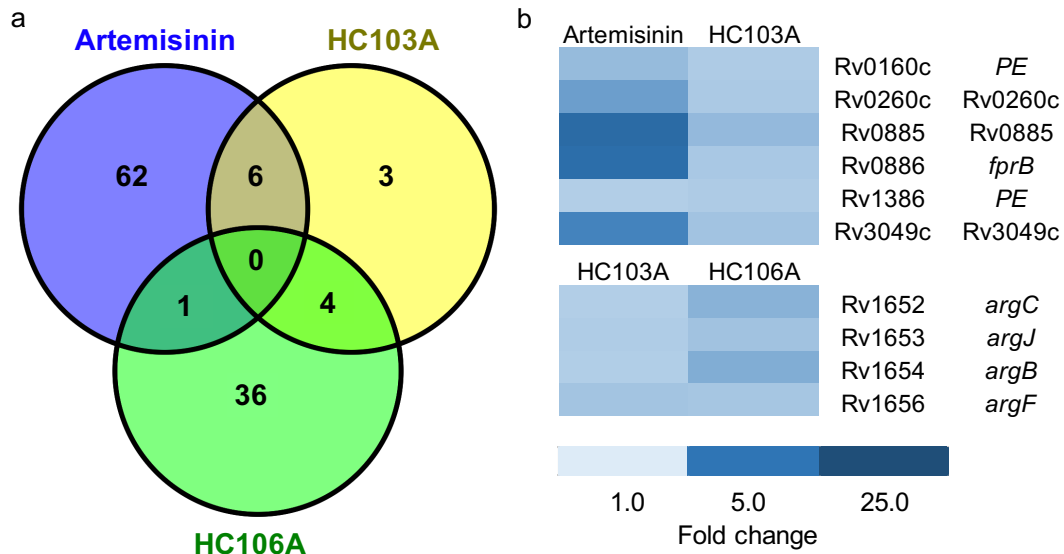
Supplementary Figure 3.7. Checkerboard assays examining paired interactions of DosRST inhibitors. CDC1551 (*hspX'::GFP*) was treated with different combination of two compounds from 50 μM to 0.08 μM. GFP fluorescence was measured and used to calculate percentage inhibition. The data were analyzed in the CompuSyn software to determine the combination index (CI) for the panel of each drug combination, including (a) artemisinin and HC104A; (b) HC102A and HC103A; (c) HC102A and HC104A; (d) HC102A and HC106A; (e) HC103A and HC104A; (f) HC103A and

Supplementary Figure 3.7. (cont'd)

HC106A; (g) HC104A and HC106A. Selected dose response curves are presented to illustrate synergistic interactions. The experiment was repeated twice with similar results.



Supplementary Figure 3.8. Synthetic scheme for the HC106 analogs.



Supplementary Figure 3.9. Comparison between artemisinin, HC103 and HC106 for interactions. (a) Venn diagram for the downregulated genes (>2-fold; $q < 0.05$) of CDC1551 ($\Delta dosR$) treated with artemisinin, HC103A, or HC106A. **(b)** Overlap exists between artemisinin and HC103A or HC103A and HC106A differentially expressed genes (downregulated >2X, $q < 0.05$). The heatmaps represent the commonly downregulated genes between the two compounds.

Experimental procedures for urea formation

Formation of acyl chloride 2. To a stirred solution of isoxazole acid **1** (1 eq.) in dry tetrahydrofuran (THF, 0.4 M) under N₂ atmosphere was added oxalyl chloride (1.5 eq.) dropwise over 5-10 min followed by dimethylformamide (DMF) (cat.) and the reaction mixture was continued to stir at room temperature. Upon completion, the reaction mixture was concentrated into a residue *in vacuo* and the residue was dissolved in THF and concentrated again to ensure the removal of excess oxalyl chloride. The crude acyl chloride **2** was used directly in the next step without further purification.

Formation of acyl azide and rearrangement into isocyanate 3. The crude acyl chloride **2** was dissolved in THF (0.4 M) and stirred at room temperature under N₂ atmosphere. Trimethylsilyl (TMS) azide (2 eq.) was added dropwise over 5 min and stirring was continued. Upon completion of the reaction, the mixture was diluted with ethyl acetate (0.4 M) and quenched with H₂O (0.4 M). The two layers were separated, and the organic layer was dried over anhydrous Na₂SO₄ and filtered. The ethyl acetate solvent was swapped into toluene (0.1 M) by the addition of toluene followed by removal of the ethyl acetate *in vacuo*. Care was taken not to concentrate the toluene. The toluene acyl azide solution was heated at reflux conditions under N₂ atmosphere for 4 h to give the desired isocyanate **3** which was used as a solution in toluene in the next step.

Formation of urea 4. The crude isocyanate solution in toluene was mixed with different amines (1.5 eq.) and stirred at room temperature overnight. Isolation of the ureas was done by diluting the reaction mixture with hexanes, stirring for few hours and filtration of the formed precipitate. The solid material was washed with hexanes and dried under high vacuum. The urea products usually do not require further purifications. All products were analyzed by ¹H NMR and high-resolution mass spectrometry.

Synthesis of MSU-41422 (amide) from acyl chloride 2. Acyl chloride 2 (1 eq.) was dissolved in dichloromethane (DCM, 0.2 M) and 4-chloroaniline (1.2 eq.) was added. The reaction mixture was stirred at room temperature overnight. The reaction mixture was concentrated *in vacuo* and the residue was purified by flash column chromatography.

Synthesis of MSU-39449. A slurry of aaa (0.10 g, 0.60 mmoles) in 2.0 mL of DCM was treated with oxalyl chloride (0.12 mL, 0.9 mmoles) and 1 drop of DMF. The mixture (with gas evolution) gradually became homogeneous and was stirred for 30 min. The mixture was concentrated *in vacuo*, diluted with 5 mL of DCM and again concentrated *in vacuo*, the process repeated three times. The resulting residue was again dissolved in DCM (2 mL) and treated with 5-aminoisoxazole (0.030 g., 0.36 mmoles), followed by pyridine (0.48 mL, 0.6 mmoles). The mixture was then allowed to stir overnight. The mixture was then quenched with 1.0 N HCl and extracted with DCM. The organic layers were combined, washed with saturated KHCO₃, dried with Na₂SO₄ and concentrated *in vacuo*. Medium pressure liquid chromatography (SiO₂, 100% DCM to 3% methanol / DCM) to provide a solid (0.023 g).

MSU-39444. ¹H NMR (500 MHz, DMSO-*d*₆) δ 10.54 (s, 2H), 8.44 (d, *J* = 1.9 Hz, 2H), 6.11 (d, *J* = 2.0 Hz, 2H).

MSU-39449. ¹H NMR (500 MHz, DMSO-*d*₆) δ 11.91 (s, 1H), 8.41 (s, 1H), 7.39 (d, *J* = 2.0 Hz, 2H), 7.35 (d, *J* = 2.0 Hz, 2H), 6.19 (s, 1H), 3.73 (s, 2H).

MSU-39445. ¹H NMR (500 MHz, DMSO-*d*₆) δ 10.41 (s, 1H), 9.14 (s, 1H), 8.40 (d, *J* = 2.0 Hz, 1H), 7.82 – 7.58 (m, 1H), 7.31 (dd, *J* = 4.9, 1.8 Hz, 2H), 7.07 (dt, *J* = 6.4, 2.3 Hz, 1H), 6.06 (d, *J* = 1.9 Hz, 1H).

MSU-39452. ¹H NMR (500 MHz, DMSO-*d*₆) δ 10.50 (s, 1H), 9.23 (s, 1H), 8.51 – 8.28 (m, 1H), 7.86 (d, *J* = 2.5 Hz, 1H), 7.64 – 7.43 (m, 1H), 7.37 (dd, *J* = 8.9, 2.5 Hz, 1H), 6.26 – 5.80 (m, 1H).

MSU-39447. ^1H NMR (500 MHz, DMSO- d_6) δ 8.83 (s, 1H), 8.43 – 8.29 (m, 1H), 7.36 (d, J = 8.4 Hz, 2H), 6.86 (d, J = 8.6 Hz, 2H), 6.00 (d, J = 1.9 Hz, 1H), 3.70 (s, 3H).

MSU-39451. ^1H NMR (500 MHz, DMSO- d_6) δ 10.13 (s, 1H), 8.34 (d, J = 1.9 Hz, 1H), 7.56 – 7.41 (m, 2H), 7.41 – 7.22 (m, 2H), 6.04 (d, J = 2.0 Hz, 1H), 3.25 (s, 3H).

MSU-39453. ^1H NMR (500 MHz, DMSO- d_6) δ 10.49 (s, 1H), 8.41 (d, J = 1.9 Hz, 1H), 7.84 (d, J = 8.7 Hz, 1H), 7.27 (dt, J = 2.3, 1.1 Hz, 1H), 7.18 (dt, J = 8.8, 1.6 Hz, 1H), 6.14 (d, J = 1.9 Hz, 1H), 4.13 (dd, J = 9.1, 8.2 Hz, 2H), 3.17 (t, J = 8.6 Hz, 2H).

MSU-39448. ^1H NMR (500 MHz, DMSO- d_6) δ 10.55 (s, 1H), 9.25 (s, 1H), 8.64 – 8.24 (m, 2H), 7.98 (d, J = 8.6 Hz, 1H), 7.45 (d, J = 8.6 Hz, 1H), 6.08 (d, J = 18.1 Hz, 1H).

MSU-39450. ^1H NMR (500 MHz, DMSO- d_6) δ 11.00 (s, 1H), 9.66 (s, 1H), 8.42 (d, J = 1.9 Hz, 1H), 8.34 (d, J = 2.6 Hz, 1H), 7.96 – 7.79 (m, 1H), 7.73 (d, J = 8.9 Hz, 1H), 6.10 (q, J = 2.7, 2.2 Hz, 2H).

MSU-39446. ^1H NMR (500 MHz, DMSO- d_6) δ 10.24 (s, 1H), 8.90 (s, 1H), 8.38 (d, J = 1.9 Hz, 1H), 7.54 – 7.37 (m, 2H), 7.26 – 7.02 (m, 2H), 6.03 (d, J = 2.0 Hz, 1H).

MSU-41422. ^1H NMR (500 MHz, Chloroform- d) δ 8.41 (d, J = 1.8 Hz, 1H), 8.26 (s, 1H), 7.71 – 7.52 (m, 2H), 7.44 – 7.33 (m, 2H), 7.06 (d, J = 1.8 Hz, 1H).

MSU-41324. ^1H NMR (500 MHz, DMSO- d_6) δ 9.91 (s, 1H), 9.50 (s, 1H), 8.31 (d, J = 2.6 Hz, 1H), 7.85 (dd, J = 9.0, 2.7 Hz, 1H), 7.67 (d, J = 8.9 Hz, 1H), 7.39 – 7.30 (m, 2H).

MSU-41425. ^1H NMR (500 MHz, DMSO- d_6) δ 8.83 (s, 1H), 7.53 – 7.39 (m, 2H), 7.39 – 7.16 (m, 2H).

MSU-41443. ^1H NMR (500 MHz, DMSO- d_6) δ 10.36 (d, J = 28.4 Hz, 1H), 9.13 (d, J = 45.7 Hz, 1H), 8.40 (d, J = 1.9 Hz, 1H), 7.70 – 7.59 (m, 5H), 7.59 – 7.49 (m, 3H), 7.43 (t, J = 7.7 Hz, 3H), 7.32 (t, J = 7.4 Hz, 1H), 6.06 (d, J = 1.9 Hz, 1H).

MSU-41442. ^1H NMR (500 MHz, DMSO- d_6) δ 10.15 (s, 1H), 8.77 (s, 1H), 8.38 (d, $J = 1.9$ Hz, 1H), 7.44 – 7.27 (m, 4H), 6.03 (d, $J = 2.0$ Hz, 1H), 1.25 (s, 9H).

MSU-33189. ^1H NMR (500 MHz, DMSO- d_6) δ 10.20 (s, 1H), 8.85 (s, 1H), 8.39 (d, $J = 1.9$ Hz, 1H), 7.54 – 7.37 (m, 2H), 7.35 – 7.21 (m, 2H), 7.02 (t, $J = 7.4$ Hz, 1H), 6.04 (d, $J = 1.9$ Hz, 1H).

MSU-33231. ^1H NMR (500 MHz, DMSO- d_6) δ 10.29 (s, 1H), 9.01 (s, 1H), 8.39 (d, $J = 1.9$ Hz, 1H), 7.56 – 7.41 (m, 2H), 7.41 – 7.27 (m, 2H), 6.05 (d, $J = 1.9$ Hz, 1H).

MSU-41462. ^1H NMR (500 MHz, DMSO- d_6) δ 10.18 (s, 1H), 8.31 (d, $J = 2.0$ Hz, 1H), 7.43 – 7.07 (m, 3H), 6.92 (s, 1H), 5.94 (d, $J = 1.9$ Hz, 1H), 4.30 (d, $J = 6.0$ Hz, 2H).

MSU-41463. ^1H NMR (500 MHz, DMSO- d_6) δ 10.39 (s, 1H), 9.29 (s, 1H), 8.41 (d, $J = 1.9$ Hz, 1H), 7.67 (d, $J = 1.0$ Hz, 4H), 6.08 (d, $J = 1.9$ Hz, 1H).

MSU-41464. ^1H NMR (500 MHz, DMSO- d_6) δ 10.29 (s, 1H), 9.01 (s, 1H), 8.39 (d, $J = 1.9$ Hz, 2H), 7.50 – 7.45 (m, 1H), 7.45 – 7.40 (m, 1H), 6.05 (s, 1H).

MSU-41465. ^1H NMR (500 MHz, DMSO- d_6) δ 10.38 (s, 1H), 9.27 (s, 1H), 8.41 (d, $J = 2.0$ Hz, 1H), 8.00 – 7.79 (m, 2H), 7.66 – 7.48 (m, 2H), 6.08 (d, $J = 1.9$ Hz, 1H), 3.81 (s, 3H).

REFERENCES

REFERENCES

1. **Boon C, Dick T.** 2012. How *Mycobacterium tuberculosis* goes to sleep: the dormancy survival regulator DosR a decade later. *Future Microbiol* **7**:513-518.
2. **Rustad TR, Sherrid AM, Minch KJ, Sherman DR.** 2009. Hypoxia: a window into *Mycobacterium tuberculosis* latency. *Cell Microbiol* **11**:1151-1159.
3. **Wayne LG, Sohaskey CD.** 2001. Nonreplicating persistence of *Mycobacterium tuberculosis*. *Annu Rev Microbiol* **55**:139-163.
4. **Mehra S, Foreman TW, Didier PJ, Ahsan MH, Hudock TA, Kisse R, Golden NA, Gautam US, Johnson AM, Alvarez X, Russell-Lodrigue KE, Doyle LA, Roy CJ, Niu T, Blanchard JL, Khader SA, Lackner AA, Sherman DR, Kaushal D.** 2015. The DosR Regulon Modulates Adaptive Immunity and Is Essential for *Mycobacterium tuberculosis* Persistence. *Am J Respir Crit Care Med* **191**:1185-1196.
5. **Hudock TA, Foreman TW, Bandyopadhyay N, Gautam US, Veatch AV, LoBato DN, Gentry KM, Golden NA, Cavigli A, Mueller M, Hwang SA, Hunter RL, Alvarez X, Lackner AA, Bader JS, Mehra S, Kaushal D.** 2017. Hypoxia sensing and persistence genes are expressed during the intragranulomatous survival of *Mycobacterium tuberculosis*. *Am J Respir Cell Mol Biol* **56**:637-647.
6. **Dasgupta N, Kapur V, Singh KK, Das TK, Sachdeva S, Jyothisri K, Tyagi JS.** 2000. Characterization of a two-component system, devR-devS, of *Mycobacterium tuberculosis*. *Tuber Lung Dis* **80**:141-159.
7. **Park HD, Guinn KM, Harrell MI, Liao R, Voskuil MI, Tompa M, Schoolnik GK, Sherman DR.** 2003. Rv3133c/dosR is a transcription factor that mediates the hypoxic response of *Mycobacterium tuberculosis*. *Mol Microbiol* **48**:833-843.
8. **Saini DK, Malhotra V, Dey D, Pant N, Das TK, Tyagi JS.** 2004. DevR-DevS is a bona fide two-component system of *Mycobacterium tuberculosis* that is hypoxia-responsive in the absence of the DNA-binding domain of DevR. *Microbiology* **150**:865-875.
9. **Voskuil MI, Schnappinger D, Visconti KC, Harrell MI, Dolganov GM, Sherman DR, Schoolnik GK.** 2003. Inhibition of respiration by nitric oxide induces a *Mycobacterium tuberculosis* dormancy program. *J Exp Med* **198**:705-713.
10. **Kumar A, Deshane JS, Crossman DK, Bolisetty S, Yan BS, Kramnik I, Agarwal A, Steyn AJ.** 2008. Heme oxygenase-1-derived carbon monoxide induces the *Mycobacterium tuberculosis* dormancy regulon. *J Biol Chem* **283**:18032-18039.

11. **Lee JM, Cho HY, Cho HJ, Ko IJ, Park SW, Baik HS, Oh JH, Eom CY, Kim YM, Kang BS, Oh JI.** 2008. O₂- and NO-sensing mechanism through the DevSR two-component system in *Mycobacterium smegmatis*. *J Bacteriol* **190**:6795-6804.
12. **Sousa EH, Tuckerman JR, Gonzalez G, Gilles-Gonzalez MA.** 2007. DosT and DevS are oxygen-switched kinases in *Mycobacterium tuberculosis*. *Protein Sci* **16**:1708-1719.
13. **Kumar A, Toledo JC, Patel RP, Lancaster JR, Jr., Steyn AJ.** 2007. *Mycobacterium tuberculosis* DosS is a redox sensor and DosT is a hypoxia sensor. *Proc Natl Acad Sci U S A* **104**:11568-11573.
14. **Ioanoviciu A, Yukl ET, Moenne-Loccoz P, de Montellano PR.** 2007. DevS, a heme-containing two-component oxygen sensor of *Mycobacterium tuberculosis*. *Biochemistry* **46**:4250-4260.
15. **Kim MJ, Park KJ, Ko IJ, Kim YM, Oh JI.** 2010. Different roles of DosS and DosT in the hypoxic adaptation of Mycobacteria. *J Bacteriol* **192**:4868-4875.
16. **Rao SP, Alonso S, Rand L, Dick T, Pethe K.** 2008. The protonmotive force is required for maintaining ATP homeostasis and viability of hypoxic, nonreplicating *Mycobacterium tuberculosis*. *Proc Natl Acad Sci U S A* **105**:11945-11950.
17. **Adams KN, Takaki K, Connolly LE, Wiedenhof H, Winglee K, Humbert O, Edelstein PH, Cosma CL, Ramakrishnan L.** 2011. Drug tolerance in replicating mycobacteria mediated by a macrophage-induced efflux mechanism. *Cell* **145**:39-53.
18. **Grant SS, Kaufmann BB, Chand NS, Haseley N, Hung DT.** 2012. Eradication of bacterial persisters with antibiotic-generated hydroxyl radicals. *Proc Natl Acad Sci U S A* **109**:12147-12152.
19. **Leistikow RL, Morton RA, Bartek IL, Frimpong I, Wagner K, Voskuil MI.** 2010. The *Mycobacterium tuberculosis* DosR regulon assists in metabolic homeostasis and enables rapid recovery from nonrespiring dormancy. *J Bacteriol* **192**:1662-1670.
20. **Converse PJ, Karakousis PC, Klinkenberg LG, Kesavan AK, Ly LH, Allen SS, Grosset JH, Jain SK, Lamichhane G, Manabe YC, McMurray DN, Nuermberger EL, Bishai WR.** 2009. Role of the dosR-dosS two-component regulatory system in *Mycobacterium tuberculosis* virulence in three animal models. *Infect Immun* **77**:1230-1237.
21. **Gautam US, Mehra S, Kaushal D.** 2015. *in-vivo* gene signatures of *Mycobacterium tuberculosis* in C3HeB/FeJ Mice. *PLoS One* **10**:e0135208.
22. **Gautam US, McGillivray A, Mehra S, Didier PJ, Midkiff CC, Kisse RS, Golden NA, Alvarez X, Niu T, Rengarajan J, Sherman DR, Kaushal D.** 2015. DosS is required for

- the complete virulence of *Mycobacterium tuberculosis* in mice with classical granulomatous lesions. *Am J Respir Cell Mol Biol* **52**:708-716.
23. **Deb C, Lee CM, Dubey VS, Daniel J, Abomoelak B, Sirakova TD, Pawar S, Rogers L, Kolattukudy PE.** 2009. A novel in vitro multiple-stress dormancy model for *Mycobacterium tuberculosis* generates a lipid-loaded, drug-tolerant, dormant pathogen. *PLoS One* **4**:e6077.
 24. **Basak A, Abouelhassan Y, Zuo R, Yousaf H, Ding Y, Huigens RW.** 2017. Antimicrobial peptide-inspired NH125 analogues: bacterial and fungal biofilm-eradicating agents and rapid killers of MRSA persisters. *Org Biomol Chem* **15**:5503-5512.
 25. **Zheng H, Colvin CJ, Johnson BK, Kirchhoff PD, Wilson M, Jorgensen-Muga K, Larsen SD, Abramovitch RB.** 2017. Inhibitors of *Mycobacterium tuberculosis* DosRST signaling and persistence. *Nat Chem Biol* **13**:218-225.
 26. **Daniel J, Deb C, Dubey VS, Sirakova TD, Abomoelak B, Morbidoni HR, Kolattukudy PE.** 2004. Induction of a novel class of diacylglycerol acyltransferases and triacylglycerol accumulation in *Mycobacterium tuberculosis* as it goes into a dormancy-like state in culture. *J Bacteriol* **186**:5017-5030.
 27. **Sirakova TD, Dubey VS, Deb C, Daniel J, Korotkova TA, Abomoelak B, Kolattukudy PE.** 2006. Identification of a diacylglycerol acyltransferase gene involved in accumulation of triacylglycerol in *Mycobacterium tuberculosis* under stress. *Microbiology* **152**:2717-2725.
 28. **Baek SH, Li AH, Sasseti CM.** 2011. Metabolic regulation of mycobacterial growth and antibiotic sensitivity. *PLoS Biol* **9**:e1001065.
 29. **Hung DT, Shakhnovich EA, Pierson E, Mekalanos JJ.** 2005. Small-molecule inhibitor of *Vibrio cholerae* virulence and intestinal colonization. *Science* **310**:670-674.
 30. **Podust LM, Ioanoviciu A, Ortiz de Montellano PR.** 2008. 2.3 A X-ray structure of the heme-bound GAF domain of sensory histidine kinase DosT of *Mycobacterium tuberculosis*. *Biochemistry* **47**:12523-12531.
 31. **Cho HY, Cho HJ, Kim YM, Oh JI, Kang BS.** 2009. Structural insight into the heme-based redox sensing by DosS from *Mycobacterium tuberculosis*. *J Biol Chem* **284**:13057-13067.
 32. **Chou T, Martin N.** 2005. CompuSyn for drug combinations: PC software and user's guide: a computer program for quantitation of synergism and antagonism in drug combinations, and the determination of IC50 and ED50 and LD50 values.
 33. **Chou TC, Talalay P.** 1984. Quantitative analysis of dose-effect relationships: the combined effects of multiple drugs or enzyme inhibitors. *Adv Enzyme Regul* **22**:27-55.

34. **Boulton AJ, Katritzky AR.** 1961. The tautomerism of heteroaromatic compounds with five-membered rings—I: 5-hydroxyisoxazoles-isoxazol-5-ones. *Tetrahedron* **12**:41-50.
35. **Topliss JG.** 1972. Utilization of operational schemes for analog synthesis in drug design. *Journal of Medicinal Chemistry* **15**:1006-1011.
36. **Lee HN, Jung KE, Ko IJ, Baik HS, Oh JI.** 2012. Protein-protein interactions between histidine kinases and response regulators of *Mycobacterium tuberculosis* H37Rv. *J Microbiol* **50**:270-277.
37. **Honaker RW, Leistikow RL, Bartek IL, Voskuil MI.** 2009. Unique roles of DosT and DosS in DosR regulon induction and *Mycobacterium tuberculosis* dormancy. *Infect Immun* **77**:3258-3263.
38. **Baker JJ, Johnson BK, Abramovitch RB.** 2014. Slow growth of *Mycobacterium tuberculosis* at acidic pH is regulated by phoPR and host-associated carbon sources. *Mol Microbiol* **94**:56-69.
39. **Johnson BK, Scholz MB, Teal TK, Abramovitch RB.** 2016. SPARTA: Simple Program for Automated reference-based bacterial RNA-seq Transcriptome Analysis. *BMC Bioinformatics* **17**:66.
40. **Johnson BK, Abramovitch RB.** 2015. Macrophage infection models for *Mycobacterium tuberculosis*. *Methods Mol Biol* **1285**:329-341.
41. **Schneider CA, Rasband WS, Eliceiri KW.** 2012. NIH Image to ImageJ: 25 years of image analysis. *Nat Methods* **9**:671-675.
42. **Mak PA, Rao SP, Ping Tan M, Lin X, Chyba J, Tay J, Ng SH, Tan BH, Cherian J, Duraiswamy J, Bifani P, Lim V, Lee BH, Ling Ma N, Beer D, Thayalan P, Kuhen K, Chatterjee A, Supek F, Glynn R, Zheng J, Boshoff HI, Barry CE, 3rd, Dick T, Pethe K, Camacho LR.** 2012. A high-throughput screen to identify inhibitors of ATP homeostasis in non-replicating *Mycobacterium tuberculosis*. *ACS Chem Biol* **7**:1190-1197.
43. **Vashist A, Prithvi Raj D, Gupta UD, Bhat R, Tyagi JS.** 2016. The alpha10 helix of DevR, the *Mycobacterium tuberculosis* dormancy response regulator, regulates its DNA binding and activity. *Febs j* **283**:1286-1299.
44. **Chou TC.** 2010. Drug combination studies and their synergy quantification using the Chou-Talalay method. *Cancer Res* **70**:440-446.

CHAPTER - 4 HC2091 kills *Mycobacterium tuberculosis* by targeting the MmpL3 mycolic acid transporter

This work has been submitted to Antimicrobial Agents and Chemotherapy and is currently under peer-review. Contributions and authors for the work described below:

Huiqing Zheng, Garry B. Coulson, Elizabeth R. Haiderer and Robert B. Abramovitch

H.Z., G.B.C and R.B.A conceived the experiments. H.Z. performed the Mtb physiology and biochemistry experiments. G.B.C. performed initial characterization and secondary assays prioritizing HC2091 for study. E.R.H conducted the spectrum of activity studies cherry-pick of the compounds.

Summary

Tuberculosis, caused by the intracellular pathogen *Mycobacterium tuberculosis* (Mtb), is a deadly disease that requires a long course of treatment. The emergence of drug resistant strains has been driven efforts to discover new small molecules that can kill the bacterium. Here we report characterizations of the compound HC2091 that kills Mtb in a time- and dose-dependent manner *in vitro*, as well as killing Mtb in macrophages. Whole genome sequencing of mutants that are spontaneously resistant to HC2091 identified single nucleotide variants in the *mmpL3* mycolic acid transporter gene. HC2091 resistant mutants do not exhibit cross-resistance with the well-characterized MmpL3 inhibitor SQ109, suggesting a distinct mechanism of interaction with MmpL3. Additionally, HC2091 does not modulate bacterial membrane potential or kill non-replicating Mtb, thus acting differently from other known MmpL3 inhibitors. RNA-seq transcriptional profiling and lipid profiling of Mtb treated with HC2091 or SQ109 show that both compounds target a similar pathway. HC2091 has a dissimilar chemical structure from previously described MmpL3 inhibitors, supporting that HC2091 is a new class of MmpL3 inhibitor.

Introduction

Mycobacterium tuberculosis (Mtb) is the causative agent of tuberculosis (TB). Standard TB therapy requires months long treatment with four drugs, isoniazid, rifampin, pyrazinamide, and ethambutol. However, with the evolution and spread of drug resistant Mtb, currently available therapies have become inadequate to control multi-drug resistance and extensively drug resistant TB. Therefore, discovery efforts focused on identifying new antibiotics is critical for the long-term control of TB disease. Several new classes of compounds that kill Mtb, by inhibiting new targets, have been discovered in recent years (1), including inhibitors of the MmpL3 mycolic acid transporter.

MmpL3 (Mycobacterium membrane protein Large 3) has proven to be a common target of small molecule inhibitors of mycobacterial growth identified by high-throughput screens (2, 3). MmpL3 is a membrane transporter belonging to the resistance, nodulation, and division superfamily. It is a mycolic acid flippase (4) that moves trehalose monomycolate (TMM) to the pseudoperiplasmic space, from where TMM is further modified to trehalose dimycolate (TDM) and incorporated into the mycomembrane (5, 6). Initial genetic studies suggested that *mmpL3* may be essential, including the absence of mutants in high density transposon mutant library (7, 8) and an inability to generate deletion mutants by homologous recombination (6, 9). Mtb and *M. smegmatis* *mmpL3* knockdown strains provide genetic evidence that *mmpL3* is required for survival both *in vitro* and *in vivo* in a mouse TB infection model (3, 10-12). Depletion of MmpL3 arrests bacterial cell division and causes rapid cell death. This phenotype makes MmpL3 an attractive therapeutic target and supports efforts to characterize small molecules targeting MmpL3. Reported MmpL3 inhibitors include a highly diverse collection of chemical classes: 1,2-ethylenediamine, SQ109 (13); diphenylether-modified adamantyl 1,2-diamine, TBL-140 (14);

indole-2-carboxamide, NITD-304 and NITD-349 (15-17); adamantyl ureas, AU1235 (6, 18); 1,5-diarylpyrrole, BM212 (19, 20); benzimidazole, C215 (21); tetrahydropyrazo[1,5-a]pyrimidine-3-carboxamide, THPP-2 (22) and N-benzyl-6',7'-dihydro-spiro[piperidine-4,4'-thieno[3,2-c]pyrans (23) and N-[(4-methoxyphenyl)methyl]-5-(4-methylphenyl)-7-(trifluoromethyl)-1,5,6,7-tetrahydropyrazolo[1,5-a]pyrimidine-3-carboxamide, Compound 2 (24). MmpL3 inhibitors decrease TDM synthesis due to ineffective transport of precursor TMM. Additionally, several MmpL3 inhibitors decrease intracellular ATP concentration and reduce the protein motive force (PMF) by disrupting membrane potential (14, 25, 26), however, this activity is not universally shared by compounds targeted MmpL3. We previously performed a high-throughput phenotypic screen of a >200,000 compound library for inhibitors of Mtb PhoPR and DosRST two-component regulatory systems (27, 28), and as part of these screens we also identified compounds that inhibited Mtb growth. Through a series of high-throughput secondary assays, the compound HC2091 was identified in both screens as an inhibitor of Mtb growth with no detectable macrophage cytotoxicity, supporting its continued study. Here we report that HC2091 is an MmpL3 inhibitor that kills Mtb *in vitro* and in macrophages.

Results

HC2091 kills Mtb in vitro and in macrophages

HC2091 (N-[2-(4-chlorophenyl)ethyl]-4-thiophen-2-yloxane-4-carboxamide; Fig. 4.1a) inhibits Mtb growth with a half maximal effective concentration (EC₅₀) of 6.4 μM (Fig. 4.1b). The structure is distinct from other previously identified MmpL3 inhibitors, however it does share a carboxamide group that is present in indolecarboxamides and THPP, suggesting this functional group may be associated with activity. The spectrum of activity of HC2091 was

examined in *M. smegmatis* and other non-mycobacteria. HC2091 was active against *M. smegmatis* with a growth inhibition EC₅₀ of 20 µM, but had no impact on other tested Gram-negative or -positive bacteria (Supplementary Table 4.1), supporting the notion that HC2091 inhibits a mycobacterium specific target.

Dose- and time- dependent killing of Mtb by HC2901 was examined by treating Mtb for 7 d across a 0.25 µM to 80 µM dose response curve, and enumerating CFUs (Fig. 4.1c). At concentrations below 1 µM HC2091 had no effect on growth, at 5 µM HC2091 was bacteriostatic and above 10 µM HC2091 was bactericidal with an ~3 log reduction of CFU at day 7, relative to dimethyl sulfoxide (DMSO) treated controls. Killing of Mtb was observed beginning at 2 d of treatment. Collectively these data indicate that HC2091 bactericidal activity is dose and time dependent. Furthermore, HC2091 did not show any cytotoxicity against primary murine bone-marrow derived macrophages up to concentrations of 200 µM (Supplementary Table 4.2) and was fully soluble in a kinetic solubility assay (Supplementary Table 4.3).

The observed high solubility and low cytotoxicity properties of HC2091 suggested that the compound could kill Mtb in macrophages. To examine the activity of HC2091 against intracellular Mtb, murine bone marrow derived macrophages were infected with Mtb and treated with HC2091 across a 6-point dose response curve from 1 µM to 40 µM. Bacterial CFUs were enumerated at various timepoints over 6 d of treatment. Consistent with the potency in broth culture (Figure 4.1c), bacterial growth inhibition was observed at concentrations of 5 µM and greater, with a 1 log reduction of CFUs compared to the DMSO control (Fig. 4.2a). These data show that HC2091 can kill intracellular Mtb.

During infection, Mtb can present as a spectrum of disease, with some bacteria actively replicating and others existing in a state of non-replicating persistence (NRP). Non-replicating

bacteria are often tolerant to antibiotics and we sought to determine if HC2091 could kill them. Using the hypoxic-shift down model of NRP to examine HC2091 activity (29), Mtb cells were pre-incubated in an anaerobic chamber for 48 h to promote NRP, and then treated with HC2091 from 0.5 μ M to 80 μ M for 5 and 10 d. As a positive control, cells were treated with 10 μ M and 20 μ M SQ109, which has been shown to kill Mtb during NRP. To show that the bacteria were drug tolerant, cells were treated with 5 μ M and 25 μ M isoniazid (INH), which is less effective against NRP bacteria. It was observed that HC2091, like INH, does not kill NRP Mtb. In contrast, SQ109 reduced Mtb CFUs by 1 log at day 5 and 2 logs at day 10. This supports the hypothesis that HC2091 is inactive against non-replicating Mtb cells and likely acts in a manner unique from that of SQ109.

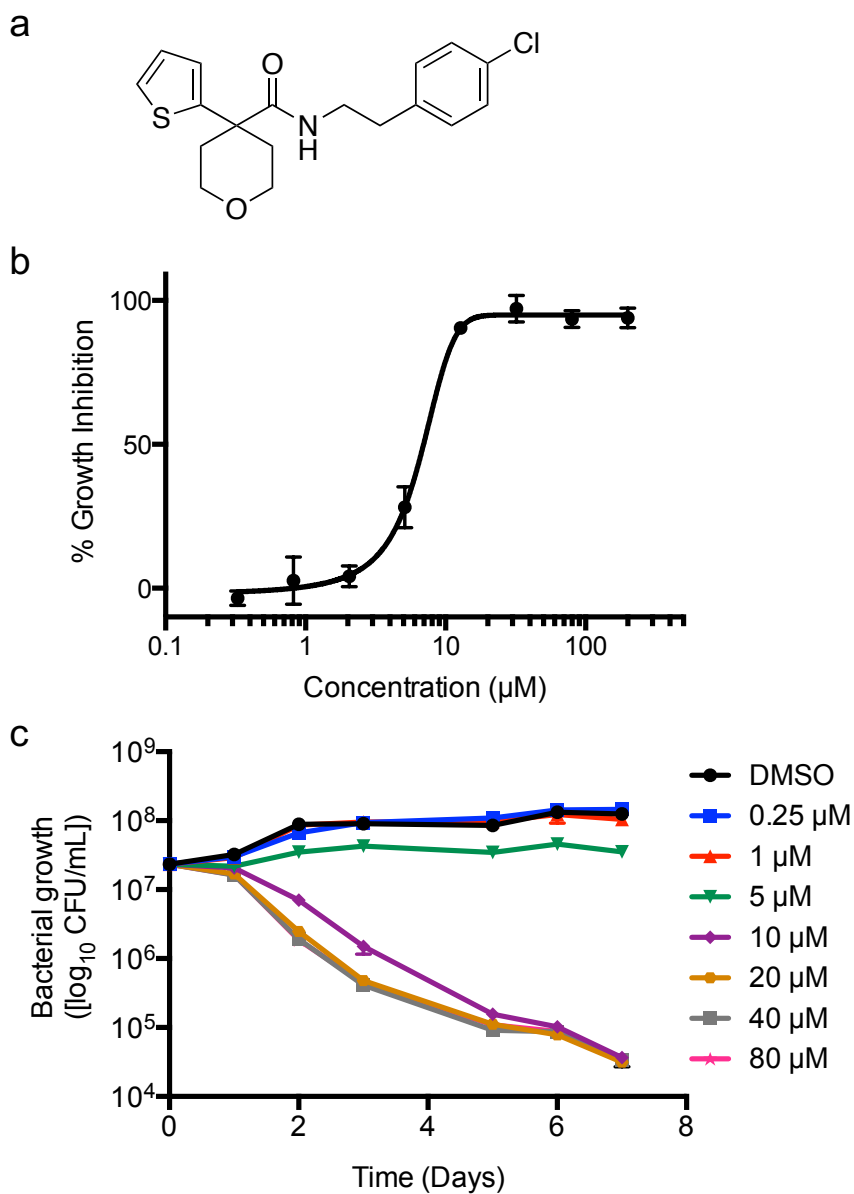


Figure 4.1. HC2091 is bactericidal to Mtb. (a) Chemical structure of HC2091; (b) HC2091 inhibits Mtb growth with EC₅₀ value of 6.4 µM; (c) HC2091 kills Mtb in a dose- and time- dependent manner. The error bars represent the standard deviation of three technical replicates. The experiment was repeated twice with similar results.

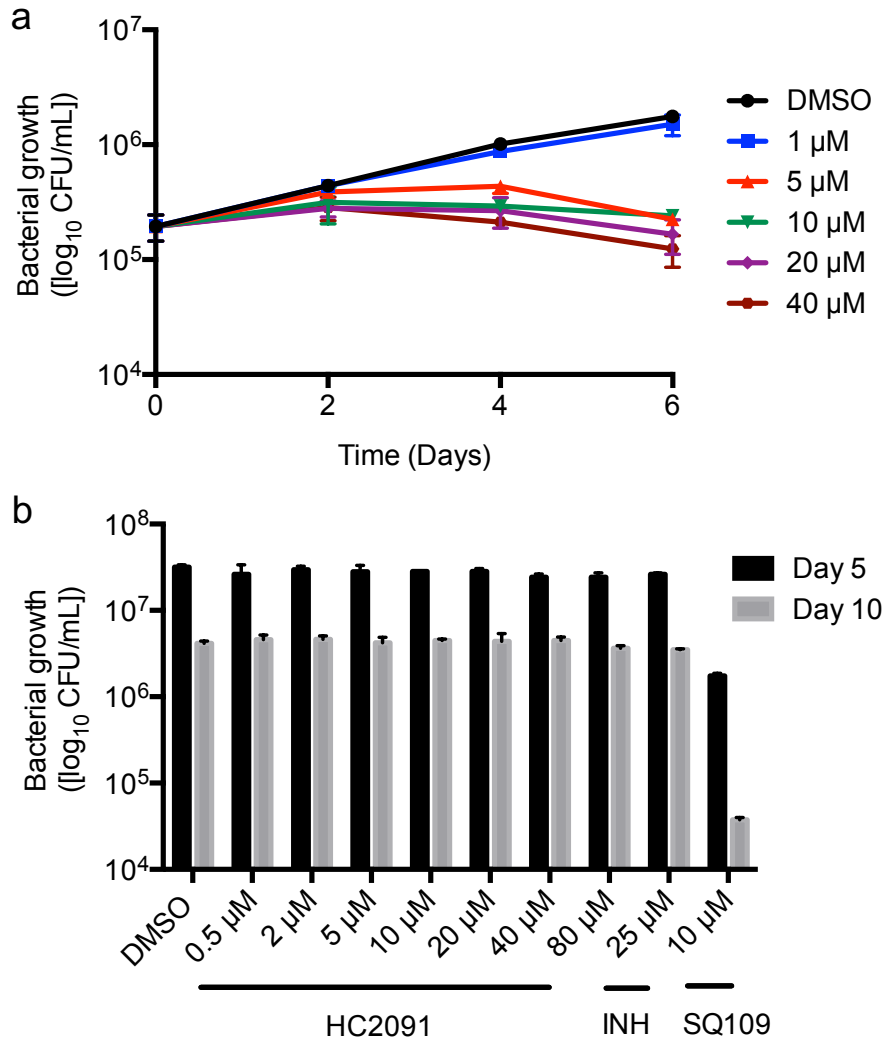


Figure 4.2. HC2091 is active against intracellular Mtb and inactive against non-replicating Mtb. (a) Mtb-infected murine bone marrow derived macrophages were treated with doses of HC2091 ranging from 1 μ M to 40 μ M. CFUs were enumerated on 7H10 agar plates at the indicated days post infection. (b) The impact of HC2091 on non-replicating Mtb was characterized using the hypoxic shift-down assay (29). SQ109 and INH were used as controls. Both experiments were repeated twice with similar results and the error bars represent the standard deviation of three technical replicates.

HC2091 resistant strains have mutations in mmpL3

To identify the potential target of HC2091, 10^{10} Mtb cells were plated on 7H10 plates containing 10 μ M HC2091. Putative spontaneous resistant mutants were isolated and purified and EC_{50} values were determined for 23 mutants to confirm their resistance to HC2091. All mutants exhibited 8- to 30- fold increased resistance to HC2091 compared to WT (Supplemental Fig. 4.1). Whole genome sequences for eleven mutants were obtained to discover the potential target of HC2091. Using a GATK-based analysis pipeline, single nucleotide variants in each mutant were identified. All of the sequenced mutants harbored mutations in the *mmpL3* gene (Table 4.1). Notably, four amino acid substitutions were concentrated in the region of amino acid 643-670 (Supplementary Fig. 4.2), which is a distinct region from where many other *mmpL3* resistance mutations have been identified. This observation suggests that cross-resistance may not be observed with other MmpL3 inhibitors. To test this hypothesis, the EC_{50} of SQ109 was examined in several of the HC2091 mutants. HC2091 resistant mutants exhibited a small 1- to 3- fold enhanced resistance to SQ109 (Table 4.1), as compared to a greater than 10-fold resistance to HC2091. This observation suggests HC2091 may target a different region of MmpL3 than SQ109 and other MmpL3 inhibitors where the HC2091 resistant alleles have not been isolated.

Mutant clones	SNV location	Nucleotide change	Quality	Amino acid changes	HC2091 EC ₅₀ (μM)	SQ109 EC ₅₀ (μM)
WT	N/A	N/A	N/A	N/A	6.4	0.95
#01/17	245733	CTG -> CCG	3030/3503	L567P	40-45	2.2
#02	245506	GTG -> ATG	2491	V643M	>100	3.77
#03	245488	ATG -> CTG	3441	M649L	>100	1.03
#04/14/16	245503	TTC -> CTC	2899/3179/ 3662	F644L	>100	3.75
#05/06/12	245424	ACC -> AAC	2685/2474/ 2191	T670N	>100	1.02
#23	245335	GCC -> ACC	2615	A700T	>100	2.5

Table 4.1. Identification of HC2091 resistance mutations. Whole genome sequencing of selected HC2091 resistant strains identified single nucleotide variants (SNVs) in *mmpL3* in all of the sequenced mutants. The mutants did not show cross resistance with SQ109.

Inhibition of mycolic acid biosynthesis by HC2091

A primary function of MmpL3 is to export TMM from the cytoplasm for mycomembrane formation (4-6). To assess the impact of HC2091 on biosynthesis of mycolic acids, Mtb cells were grown in the presence of ^{14}C -acetate and treated with HC2091. Radiolabelled total lipids were isolated and analyzed by thin layer chromatography (TLC, Fig. 4.3a). TDM accumulation in HC2091-treated Mtb was decreased in a dose dependent manner, with a 66% reduction of TDM relative to a DMSO control when treated with 40 μM HC2091 (Fig. 4.3b). Consistent with the mechanism of an MmpL3 inhibitor, the TDM-precursor TMM accumulated in all of the treatments. The results are consistent with previous reports that TDM biosynthesis is inhibited due to blockage of the exporting precursor TMM (5, 6). Modulation of mycolic acid accumulation provides further evidence supporting that MmpL3 is the target of HC2091.

Transcriptional analysis of Mtb treated with HC2091 and SQ109

Transcriptional profiling was undertaken to define pathways that are regulated by HC2091. Mtb cells were treated with 10 μM HC2091 or SQ109 for 24 h, and total bacterial RNA was isolated. HC2091 at this concentration and time point was observed to have a defined impact on Mtb transcriptional profiling with 11 genes downregulated (>2 -fold, $q < 0.05$, Fig. 4.4ab and Supplementary Database 4.1-2). These genes completely overlapped with genes downregulated by treatment with SQ109, suggesting that both compounds are targeting the same pathway (Fig. 4.4c). The most highly repressed genes include Rv1886c (*fbpB*) and Rv2244 (*acpM*) both of which are involved in cell wall mycolic acid biosynthesis. The RNA-seq data show that HC2091 and SQ109 likely inhibit the same target. Given the limited number of genes regulated by HC2091, it is likely that HC2091 does not have other strong activities independent of targeting MmpL3.

HC2091 has no effect on Mtb membrane potential.

Several MmpL3 inhibitors inhibit the mycobacterial membrane potential, including SQ109, BM212, TBL-140, indolecarboxamides, AUs, and THPPs (14, 22). Additionally, specific *mmpL3* mutations have been shown to modulate membrane potential (30). We next sought to determine if HC2091 had any impact on Mtb membrane potential. Using the ratiometric membrane potential reporter dye DiOC₂, kinetic changes of membrane potential were monitored for 1 h after treatment with doses of HC2091, at 5 μ M, 20 μ M and 80 μ M, or treatment with SQ109 and carbonyl cyanide *m*-chlorophenyl hydrazone (CCCP) as positive controls. The results showed that the fluorescence ratio was decreased over time with CCCP and SQ109 treatments (Supplementary Figure 4.3), consistent with the previous reports that these two compounds inhibit Mtb membrane potential. However, for HC2091 treatments, the fluorescence ratio was stable and similar to the DMSO control. These data support the idea that HC2091 does not impact on Mtb membrane potential.

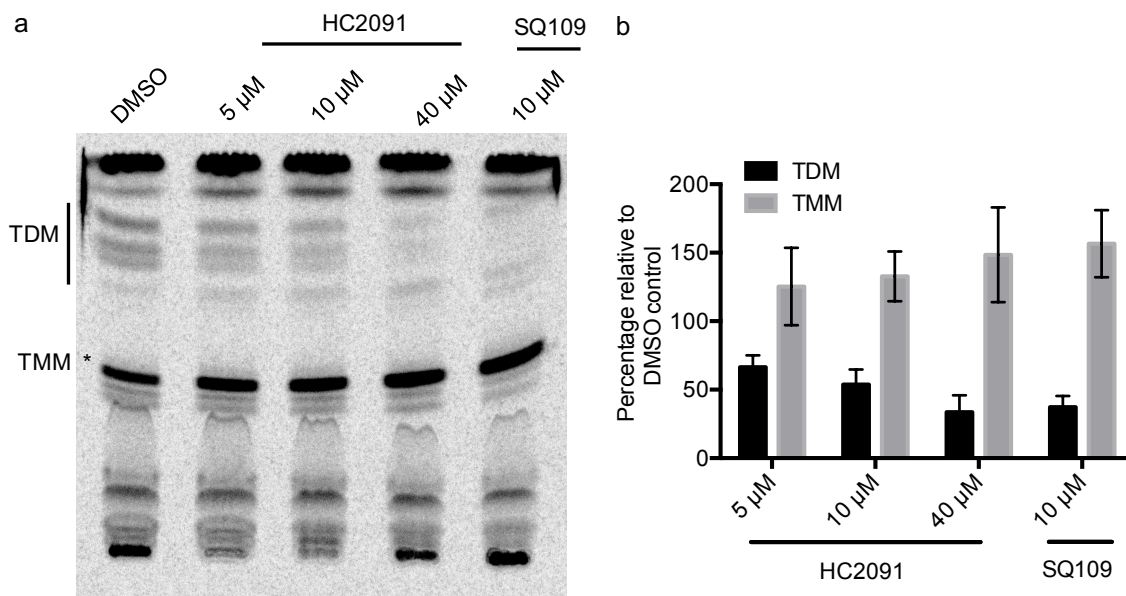


Figure 4.3. HC2091 inhibits TDM accumulation. (a) Mtb cells were treated with HC2091 or SQ109 and lipids were labeled with ^{14}C -acetate for 6 d. Lipids were isolated and analyzed by TLC. (b) Quantification of TDM and TMM accumulation for Mtb cells treated with HC2091 or SQ109 as controls. The error bars represent the standard deviation of two biological replicates.

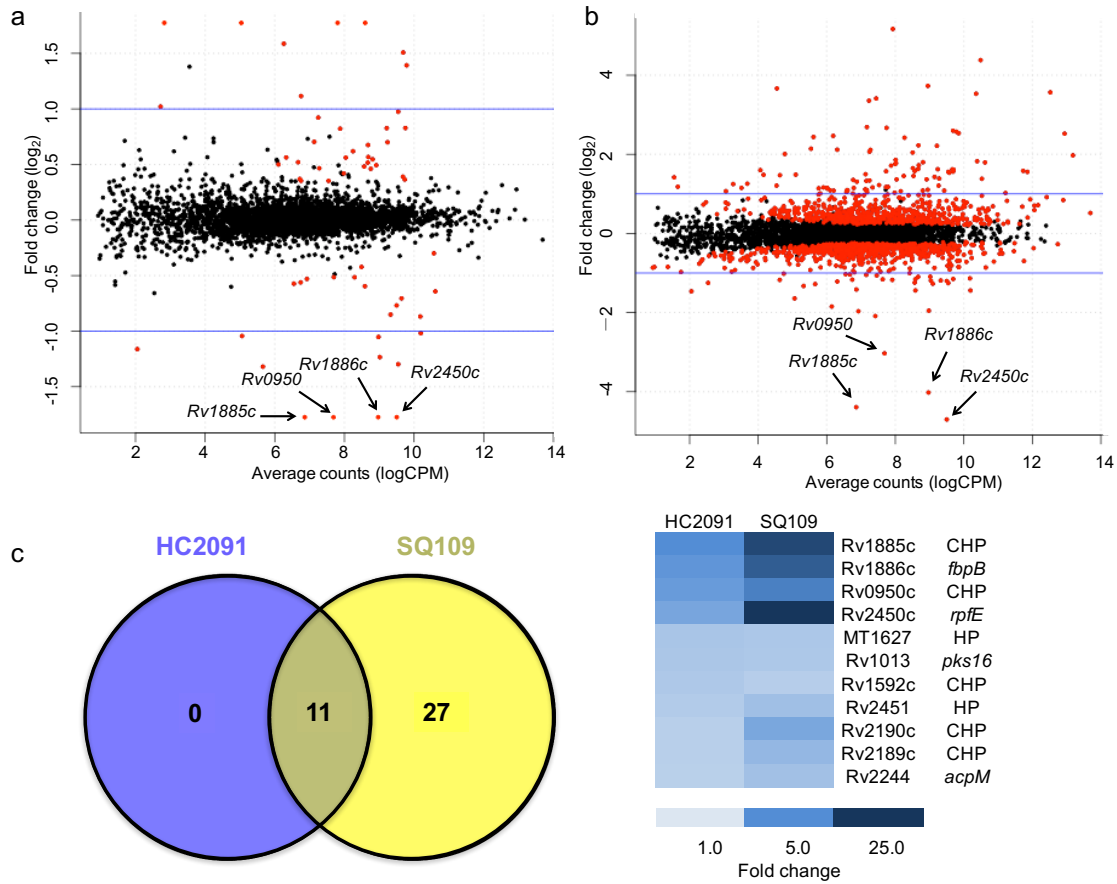


Figure 4.4. Shared transcriptional profiles between HC2091 and SQ109. Transcriptional profiling of Mtb cells treated with HC2091 (a) or SQ109 (b). Cells were treated with 10 μ M of the compounds for 24 h. The genes in red are significantly differentially regulated ($q < 0.05$). (c) Overlap exists between the HC2091 and SQ109 differentially expressed genes (downregulated $>2X$, $q < 0.05$). The heatmap represents the 11 commonly downregulated genes. CHP, conserved hypothetical protein; HP, hypothetical protein.

Structure-activity relationship studies

A small-scale structure-activity relationship (SAR) study of HC2091 was conducted using 24 commercially available compounds to identify the functional group/s of the compound responsible for its activity. Mtb was treated with a dose response profile from 0.32 μM to 200 μM , growth was measured after 6 d incubation and EC_{50} values were determined for each analog (Fig. 4.6). We observed that HC2091M, N, W had a similar activity to HC2091A, with EC_{50} values are 9.7 μM , 10 μM , and 8.5 μM , respectively. HC2091D, E, F have EC_{50} values of 33 μM , 22 μM , and 35 μM , respectively. HC2091G, J, L have EC_{50} values of 81.3 μM , 66.8 μM , and 63.8 μM , respectively. HC2091I and K were inactive (>200 μM). Comparing the activity of HC2091A to HC2091E shows that the extra carbon linker to the benzene ring improves the activity. Additional observations include that a chloride (HC2091E) at the para-position had higher activity as compared to a fluoride (HC2091J), with EC_{50} of 21.9 μM and 66.8 μM , respectively. However, other functional groups, such as trifluoromethyl, ethyl, and isobutyl, provided activity similar to the primary hit HC2091A. Eukaryotic cytotoxicity was determined for HC2091A, M, N, W (Supplemental Table 4.2) and toxicity was >200 μM for HC2091A, M, and N and 80 μM for HC2091W, suggesting that the analogs have limited macrophage cytotoxicity. Analogs HC2091A, M and N were also soluble in water at concentrations of >200 μM (Supplementary Fig. 4.3). Overall, these initial SAR studies indicate that there exists opportunities to improve the HC2091 for potency or pharmacokinetic properties, as several distinct analogs of HC2091 exhibited activity, cytotoxicity and solubility properties comparable to the parent compound.

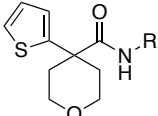
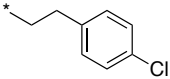
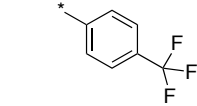
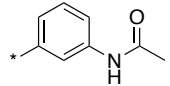
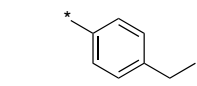
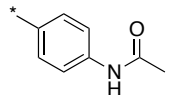
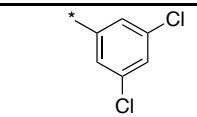
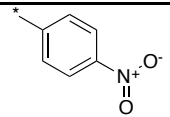
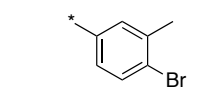
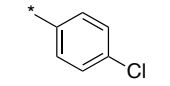
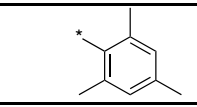
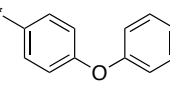
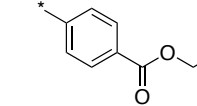
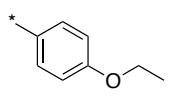
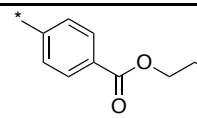
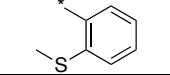
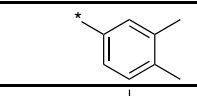
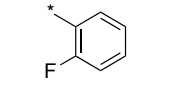
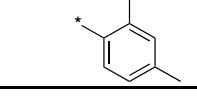
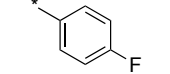
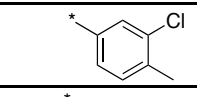
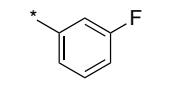
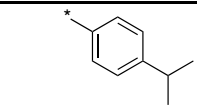
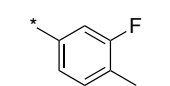
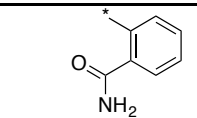
					
Analogs	R	EC ₅₀ (μM)	Analogs	R	EC ₅₀ (μM)
A		6.4	M		9.7
B		200	N		10
C		200	O		200
D		32.7	P		200
E		21.9	Q		200
F		34.4	R		200
G		81.3	S		121
H		200	T		200
I		200	U		200
J		66.8	V		200
K		200	W		8.5
L		63.8	X		200

Table 4.2. HC2091 Structure activity relationship study. Analogs of HC2091 were purchased from commercial sources and EC₅₀ values were calculated for each analog. The primary hit HC2091A has EC₅₀ value of 6 μM. Three analogs with a similar EC₅₀ value as HC2091A were identified, including HC2091M, N, W.

Discussion

This study describes the identification of a new class of MmpL3 inhibitor. HC2091 has several features that distinguish it from other MmpL3 inhibitors, including a distinct chemical structure, limited impact on membrane potential, resistance amino acid substitutions clustered in the MmpL3 C-terminus, and high solubility. In contrast to SQ109, HC2091 has no effect on non-replicating Mtb, consistent with its lack of impact on membrane potential, which is essential for Mtb survival during NRP (31). HC2091 resistant mutants do not show cross-resistance with SQ109, and HC2091 does not impact the membrane potential, suggesting that HC2091 is a distinct anti-mycobacterial agent from SQ109. Whole genome sequencing of HC2091 resistant mutants strongly suggests that HC2091 targets MmpL3. This conclusion is further supported by the phenotype of decreasing TDM accumulation observed by TLC. Analogs of HC2091A were identified from an SAR study, showing that optimization of this molecule is possible with additional chemistry efforts. Such optimizations could include increased potency and improvements to pharmacokinetic properties, such as replacing the thiophene group which may be prone to *in vivo* metabolism (32).

MmpL3 has the essential function of exporting mycolic acids to the mycomembrane. *mmpL3* knockdown studies show that MmpL3 is essential to Mtb and required for virulence in a mouse model of TB infection (10, 11). Therefore, MmpL3 is an attractive drug target for new TB therapies. Several MmpL3 inhibitors have been discovered recently, with a variety of distinct chemical structures. None of the known MmpL3 inhibitors known to date share the structure of HC2091. It is apparent that MmpL3 is particularly susceptible to chemical inhibition, however, it is unclear why it is such a common target in whole cell phenotypic screens. One possibility is that the mutations in *mmpL3* are enough to offset the activity of the compound on other targets. For

instance, THPP was originally discovered and characterized as an MmpL3 inhibitor based on spontaneous resistance-conferring mutations and phenotypes. Later research, however, showed that it actually targets EchA6, which is predicted to be an enoyl-coenzyme A (CoA) hydrolase (33). This result raises the question of whether other putative MmpL3 inhibitors are actually targeting to MmpL3 or have other targets. Further biochemical studies are needed to characterize these compounds to define their direct interaction and modulation of the MmpL3 protein, such as a recent demonstration that BM212 directly binds and inhibits MmpL3 (4).

In membrane potential studies, MmpL3 inhibitors, including SQ109, BM212, indolecarboxamides, AUs, and THPPs, were all reported to disrupt membrane potential (22), which abolishes PMF-driven translocation processes, including TMM translocation via MmpL3. To further support the requirement of PMF for TMM translocation, the impacts of known PMF inhibitors, CCCP and valinomycin, on TDM synthesis were examined (22). The results showed CCCP caused 3.7-fold decrease in TDM biosynthesis, while there was 10-fold increase in TMM accumulation (22). Similar effects were also observed when Mtb was treated with valinomycin. This may explain why these MmpL3 inhibitors have broader targets, as PMF is required for many cellular functions.

HC2091 exhibited a very narrow transcriptional response when treated with HC2091, however, the genes that were regulated overlapped with SQ109. These observations support the hypothesis that MmpL3 may be the primary target of HC2091. Additionally, HC2091 has no impact on non-replicating Mtb, while other MmpL3 inhibitors, including SQ109, DA5, BM212, THPP-2 have significant impact on killing non-replicating Mtb. It is not known whether MmpL3 is required for Mtb survival during NRP, whereas agents that target electron transport and membrane potential are known to kill NRP bacteria (29, 31, 34). However, it is known that cell

wall synthesis, including mycolic acid biosynthesis, is reduced during NRP, therefore it is reasonable to postulate that the translocation of TMM is minimal, and inhibition of MmpL3, without disrupting PMF, is not lethal to non-replicating Mtb. Therefore, the impact on non-replicating Mtb by other MmpL3 inhibitors may not be due to inhibition of TDM synthesis, but rather due to disruption of PMF. Overall, HC2091 represents a new class of MmpL3 inhibitor with distinct chemical and physiological properties that support its continued study as a potential new anti-mycobacterial agent.

Materials and methods

Bacterial strains and growth conditions. Mtb strain CDC1551 was used for this study. It was cultured in 7H9 Middlebrook medium (supplemented with 10% OADC (oleic acid dextrose catalase) and 0.05% Tween-80) at 37°C and 5% CO₂ in standing vented tissue culture flasks. *M. smegmatis* was grown in Luria-Bertani (LB) broth with standing at 37°C. Non-mycobacterial strains include *S. aureus* strains Wichita (29213) or Seattle (25923), *E. coli* (Migula) Castellani and Chalmers, *P. aeruginosa* (Schroeter) Migula, *P. vulgaris* Hauser emend Judicial Commission, and *E. faecalis* (Andrewes and Horder) Schleifer and Kilpper-Balz. All of non-mycobacterial strains were grown in LB broth with shaking at 37°C with the exception of *E. faecalis*, which was grown in brain heart infusion medium in standing flasks at 37°C.

EC₅₀ determination and spectrum of activity in other mycobacteria and non-mycobacteria. Mtb cultures were grown to mid-exponential phase, diluted into fresh 7H9 medium to an OD₆₀₀ of 0.05, and 200 µL of diluted culture was aliquoted to wells of a 96-well plate and treated with an 8-point (2.5-fold) dilution series of HC2091 ranging from 200 µM-0.32 µM. Optical density (OD₆₀₀) was

measured after 6 d of incubation, and growth of cultures was normalized based on OD₆₀₀ relative to the 0.3 μM rifampin (100% growth inhibition) and DMSO (0% growth inhibition) controls. The EC₅₀ values were calculated using the GraphPad Prism software package (version 6).

To examine the spectrum of activity of HC2091, the EC₅₀ of HC2091 was also determined against *M. smegmatis* and other non-mycobacteria, including *S. aureus*, *E. coli*, *P. aeruginosa*, *P. vulgaris*, and *E. faecalis*. Tests were performed in 96-well plates in LB broth shaking at 37°C, with the exception of *E. faecalis*, which was grown in brain heart infusion medium in standing flasks at 37°C, and *M. smegmatis*, which was also grown standing at 37°C. Culture was diluted to a starting OD₆₀₀ of 0.05. Bacteria were incubated in the presence of an 8-point (2-fold) dilution series of HC2091 ranging from 200 μM - 1.5 μM for 6-8 h, except for *M. smegmatis*, which was incubated for 60 h. Growth was monitored using by measuring OD₆₀₀ and normalized based on kanamycin (100% growth inhibition) and DMSO (0% growth inhibition) controls with the exception of *P. aeruginosa*, for which tobramycin was used as the control for 100% growth inhibition. The experiments were performed with three technical replicates per plate and two biological replicates. EC₅₀ values were calculated based on a variable slope, four-parameter non-linear least squares regression model in the GraphPad Prism software package (ver. 6).

Bactericidal activity of HC2091. Mtb cells were initially cultured to an OD₆₀₀ 0.1 in 7H9 media in standing T25 tissue culture flasks, and incubated at 37°C. The cultures were treated with different doses of HC2091 from 0.25 μM to 80 μM including a DMSO control. At each indicated time point, 100 μL of culture was removed from the flasks, and 10-fold serial dilutions were performed and bacterial CFUs were enumerated by dilution plating on 7H10 agar plates. Bactericidal activity of the compound was determined by comparing bacterial CFUs after

treatment to the initial inoculum. The experiments were performed with three technical replicates per treatment and two biological replicates.

Activity of HC2091 against intracellular Mtb. Murine bone-marrow derived macrophages were seeded in 24-well plates before infection as previously described (35). Macrophages were infected with Mtb at a multiplicity of infection ratio of 1:2 for 1 h. Mtb-infected macrophages were then treated with indicated doses of HC2091 with a DMSO control. Culture medium was changed every 2 d with fresh antibiotics added at each medium change. Macrophages were lysed by adding 0.1% Tween-80 in water. Viable Mtb cells were dilution plated on 7H10 agar medium and enumerating CFUs. The experiment was performed with three technical replicates per treatment and two biological replicates.

Whole genome sequencing to identify the target of HC2091. Mtb cells were grown to late-exponential phase with an OD₆₀₀ of ~1.0, 10¹⁰ cells were plated on 7H10 agar medium supplemented with 10 μM HC2091. The plates were incubated at 37°C until isolated resistant colonies were observed. Spontaneous resistant mutants were isolated, cultured and dilution plated to purify single colonies. EC₅₀ values were determined as described above. Genomic DNA from eleven resistant mutants with different EC₅₀ values were submitted for whole genome sequencing, and results were analyzed using a GATK based workflow as previously described (36, 37).

Mycolic acid accumulation analysis. Mtb cells were diluted to OD₆₀₀ of 0.1 in 8 mL of 7H9 medium in standing T-25 tissue culture flasks. Cells were radiolabeled by adding 8 μCi of [1,2-¹⁴C] sodium acetate to the culture. Cultures were treated with the indicated doses of HC2091,

SQ109 or a DMSO control for 24 h at 37°C. Total lipid was extracted and analyzed in thin-layer chromatography (TLC), as previously described (38). Total extractable lipid ¹⁴C incorporation was determined in scintillation counting, and 20,000 c.p.m. (counts per minute) were spotted on a 100-cm² high-performance TLC silica gel 60 aluminum sheet (EMD Millipore). A chloroform-methanol-water (20:4:0.5, vol/vol/vol) solvent system was used to resolve lipids to analyze mycolic acid accumulation. The TLC was exposed to a phosphor screen for 3 d, imaged on a Typhon imager and lipids were quantified by ImageJ (39). The experiment was repeated with two biological replicates with similar results.

Transcriptional profiling and data analysis. Mtb cells were inoculated to an initial OD₆₀₀ of 0.1 in 8 mL 7H9 medium. Cell were treated with 10 μM HC2091, SQ109 or DMSO for 24 h and grown at 37°C and 5% CO₂ without shaking in T-25 tissue culture flasks. Total bacterial RNA from two biological replicates was extracted and sequenced as previously described (38). RNA-seq data were analyzed in the SPARTA software package (40). Transcriptional profiling data is available at the GEO Database (GEO accession number GSE107485).

Membrane potential. The membrane potential assay was performed as previously described (14). Briefly, CDC1551 cells were labeled with 30 μM DiOC₂ (diethyloxacarbocyanine iodide, ThermoScientific) in 1 mL PBS, pH 7.4, supplemented with 50 mM KCl, and incubated at 37°C for 15 min. Cells were washed twice and suspended in PBS at final concentration of 0.2 OD₆₀₀, 200 μL of labeled cells were aliquoted to 96-well plates, and treated with 20 μM SQ109, or 5 μM, 20 μM, and 80 μM HC2091. A DMSO negative control and a 25 μM CCCP (Sigma Aldrich) positive controls were also included in the assay. Each treatment included 4 replicates per plate.

The kinetics of fluorescence (excitation = 485 nm, emission = 610 nm / 515 nm) was measured every 2 min for 60 min. The red / green (610 nm / 515 nm) fluorescence intensity ratio was calculated and used to quantify membrane potential. The experiment was repeated at least twice with similar result. The error bars represent the standard deviation of four replicates.

Structure activity relationship (SAR) and eukaryotic cytotoxicity of HC2091. HC2091 analogs with different chemical properties were purchased from ChemDiv for catalog SAR studies. The EC₅₀ values of compounds B-X were calculated by using 8-point (2.5-fold) dilution series ranging from 200-0.32 μ M as described above. Eukaryotic cytotoxicity of HC2091 and its selected analogs were examined as previously described (28). Briefly, mouse bone marrow derived macrophages were seeded in 96-well plates and grown at 37°C with 5% CO₂ in medium without antibiotics. After overnight incubation, cells were treated with a dilution series of the compounds from 200 - 0.32 μ M, and continued incubation for 4 d at 37°C with 5% CO₂. Cell viability was assessed using the CellTiter Glo luciferase reagent (Promega). The data were normalized with the 1% Triton X-100 (100% toxicity) and DMSO (0% toxicity) controls. EC₅₀ and half-maximal cell toxicity concentration (CC₅₀) values were calculated in the GraphPad Prism software package (version 6).

Kinetic solubility assay. The solubility assay was performed with 7-point (2-fold) dilutions from 200 μ M - 3.125 μ M for HC2091 analogs. Mebendazole, benxarotene and aspirin were also included as controls. The drug dilutions were added to PBS, pH 7.4, with the final DMSO concentration of 1%, and incubated at 37 °C for 2 h. The absorbance at 620 nm was measured for each drug dilution to estimate the compound solubility. Three replicates were done for each dilution.

Acknowledgements

We thank Edmund Ellsworth and the MSU Chemical Biology and Medicinal Chemistry Core for conducting the kinetic solubility assays. The MSU RTSF provided technical support for the RNA-seq library preparation and sequencing. This project was supported by start-up funding from Michigan State University, AgBioResearch, grants from the NIH-NIAID (R21AI105687 and R01AI116605) and Grand Challenges Explorations grants from the Bill and Melinda Gates foundation (OPP1059227 and OPP1119065) and the Jean P. Schultz Endowed Biomedical Research Fund at the MSU College of Human Medicine.

APPENDIX

APPENDIX

Supplementary information

Supplementary Dataset 4.1. Differential gene expression data of WT Mtb treated with inhibitors

Supplementary Dataset 4.2. Complete gene expression tables for transcriptional profiling experiments.

Bacterial strain	EC₅₀ (μM)
<i>E. coli</i>	> 200
<i>E. faecalis</i>	> 200
<i>M. smegmatis</i>	20
<i>P. aeruginosa</i>	> 200
<i>P. vulgaris</i>	> 200
<i>S. aureus</i> 25923	> 200
<i>S. aureus</i> 29213	> 200

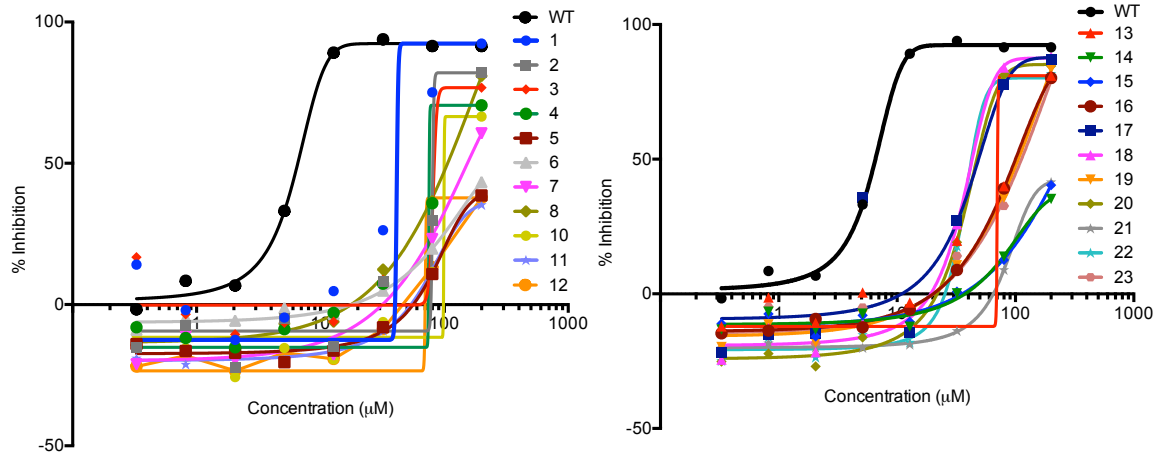
Supplementary Table 4.1. Spectrum of activity of HC2091. The EC₅₀ studies were performed for the mycobacteria and non-mycobacteria. Cells were treated with a dose from 200 μM to 0.32 μM, and the optical density was measured after time that allowed for bacterial growth. The EC₅₀ values were calculated for each strain. The experiment was repeated twice with similar results.

HC2091 analogs	EC₅₀ (μM)
A	> 200
M	> 200
N	>200
W	> 80

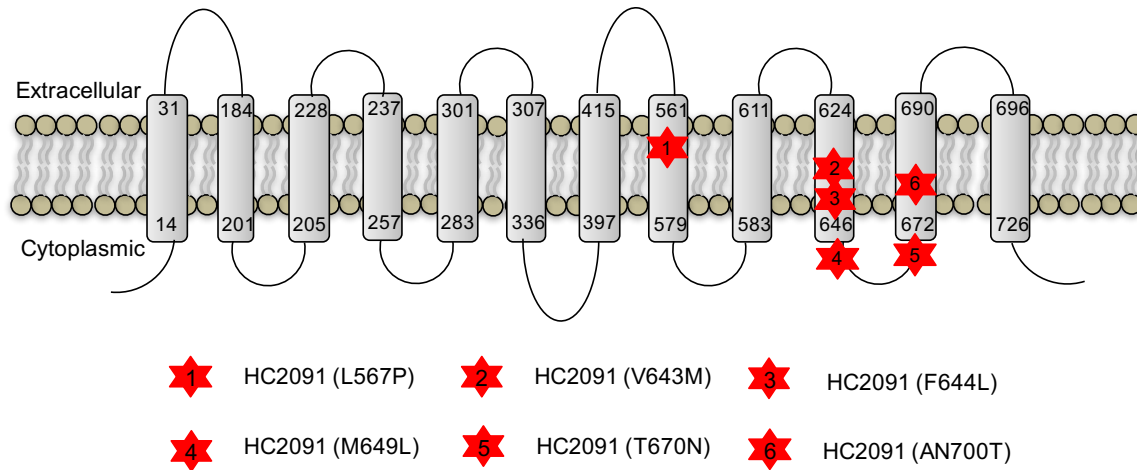
Supplementary Table 4.2. Cytotoxicity of HC2091 analogs. Murine bone-marrow derived macrophages were treated with a series of (2.5-fold) dilutions of HC2091 analogs ranging from 200 μM to 0.32 μM for 4 d. Cell survival was measured with CellTiter-Glo (Promega).

Compound Name	Solubility (μM)
Mebendazole	37.0
Benxarotene	23.8
Aspirin	>100
HC2091A	> 200
HC2091M	> 200
HC2091N	>200
HC2091W	161.8

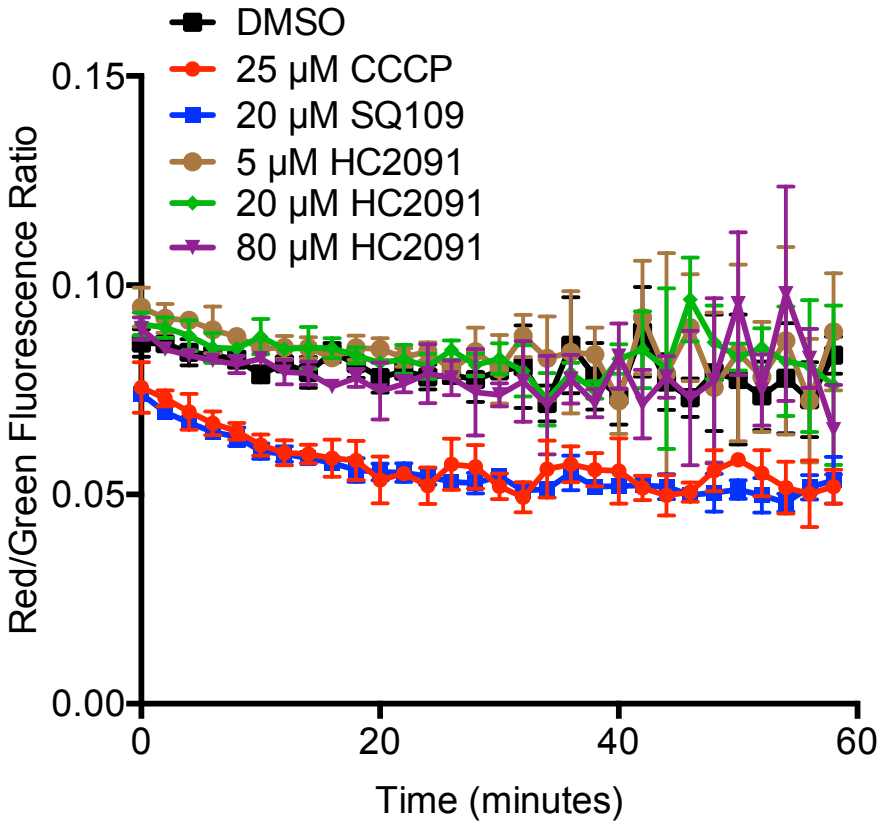
Supplementary Table 4.3. Solubility of HC2091 analogs. The assay was performed with 7-point (2-fold) dilutions from 200 μM - 3.125 μM for HC2091 analogs. Mebendazole, benxarotene and aspirin were also included as controls. The absorbance at 620 nm was measured for each drug dilution to estimate of the compound solubility. The experiment was repeated with three replicates.



Supplementary Figure 4.1. Dose-response curves for HC2091 resistant mutants. Each mutant was treated with a series of (2.5-fold) dilutions of HC2091 ranging from 200 μM to 0.32 μM for 6 d, and the OD_{600} was measured after allowing 6 d for growth. The experiment was repeated twice with similar results.



Supplementary Figure 4.2. The map of HC2091 resistance substitutions on the MmpL3 protein. Six different single mutations on *mmpL3* were identified from whole genome sequencing of HC2091 spontaneous resistant mutants. The majority of the amino acid substitutions are located in the C-terminus of the protein. The model of MmpL3 protein was derived from the PHYRE2 protein fold recognition server (41).



Supplementary Figure 4.3. Impact of HC2091 on Mtb membrane potential. Mtb cells were labeled with DiOC₂ and treated with 20 μM SQ109, or 5 μM, 20μM, and 80μM HC2091. DMSO-negative and CCCP-positive controls were also included. The red / green (610 nm / 515 nm) fluorescence intensity ratio was calculated for each treatment over 60 min. SQ109 and CCCP showed reduced fluorescence intensity ratio, while HC2091 maintained the curve similar to DMSO control, suggesting HC2091 has no impact on Mtb membrane potential. The experiment was repeated twice with similar results. The error bars represent the standard deviation of four technical replicates.

REFERENCES

REFERENCES

1. **Hoagland DT, Liu J, Lee RB, Lee RE.** 2016. New agents for the treatment of drug-resistant *Mycobacterium tuberculosis*. *Adv Drug Deliv Rev* **102**:55-72.
2. **Poce G, Consalvi S, Biava M.** 2016. MmpL3 inhibitors: diverse chemical scaffolds inhibit the same target. *Mini Rev Med Chem* **16**:1274-1283.
3. **Belardinelli JM, Yazidi A, Yang L, Fabre L, Li W, Jacques B, Angala SK, Rouiller I, Zgurskaya HI, Sygusch J, Jackson M.** 2016. Structure-function profile of MmpL3, the essential mycolic acid transporter from *Mycobacterium tuberculosis*. *ACS Infect Dis* **2**:702-713.
4. **Xu Z, Meshcheryakov VA, Poce G, Chng SS.** 2017. MmpL3 is the flippase for mycolic acids in mycobacteria. *Proc Natl Acad Sci U S A* **114**:7993-7998.
5. **Tahlan K, Wilson R, Kastrinsky DB, Arora K, Nair V, Fischer E, Barnes SW, Walker JR, Alland D, Barry CE, 3rd, Boshoff HI.** 2012. SQ109 targets MmpL3, a membrane transporter of trehalose monomycolate involved in mycolic acid donation to the cell wall core of *Mycobacterium tuberculosis*. *Antimicrob Agents Chemother* **56**:1797-1809.
6. **Grzegorzewicz AE, Pham H, Gundi VA, Scherman MS, North EJ, Hess T, Jones V, Gruppo V, Born SE, Kordulakova J, Chavadi SS, Morisseau C, Lenaerts AJ, Lee RE, McNeil MR, Jackson M.** 2012. Inhibition of mycolic acid transport across the *Mycobacterium tuberculosis* plasma membrane. *Nat Chem Biol* **8**:334-341.
7. **Lamichhane G, Tyagi S, Bishai WR.** 2005. Designer arrays for defined mutant analysis to detect genes essential for survival of *Mycobacterium tuberculosis* in mouse lungs. *Infect Immun* **73**:2533-2540.
8. **Griffin JE, Gawronski JD, Dejesus MA, Ioerger TR, Akerley BJ, Sassetti CM.** 2011. High-resolution phenotypic profiling defines genes essential for mycobacterial growth and cholesterol catabolism. *PLoS Pathog* **7**:e1002251.
9. **Domenech P, Reed MB, Barry CE, 3rd.** 2005. Contribution of the *Mycobacterium tuberculosis* MmpL protein family to virulence and drug resistance. *Infect Immun* **73**:3492-3501.
10. **Li W, Obregon-Henao A, Wallach JB, North EJ, Lee RE, Gonzalez-Juarrero M, Schnappinger D, Jackson M.** 2016. Therapeutic potential of the *Mycobacterium tuberculosis* mycolic acid transporter, MmpL3. *Antimicrob Agents Chemother* **60**:5198-5207.

11. **Degiacomi G, Benjak A, Madacki J, Boldrin F, Provvedi R, Palu G, Kordulakova J, Cole ST, Manganelli R.** 2017. Essentiality of mmpL3 and impact of its silencing on *Mycobacterium tuberculosis* gene expression. *Sci Rep* **7**:43495.
12. **Rock JM, Hopkins FF, Chavez A, Diallo M, Chase MR, Gerrick ER, Pritchard JR, Church GM, Rubin EJ, Sasseti CM, Schnappinger D, Fortune SM.** 2017. Programmable transcriptional repression in mycobacteria using an orthogonal CRISPR interference platform. *Nat Microbiol* **2**:16274.
13. **Sacksteder KA, Protopopova M, Barry CE, 3rd, Andries K, Nacy CA.** 2012. Discovery and development of SQ109: a new antitubercular drug with a novel mechanism of action. *Future Microbiol* **7**:823-837.
14. **Foss MH, Pou S, Davidson PM, Dunaj JL, Winter RW, Pou S, Licon MH, Doh JK, Li Y, Kelly JX, Dodean RA, Koop DR, Riscoe MK, Purdy GE.** 2016. Diphenylether-Modified 1,2-Diamines with Improved Drug Properties for Development against *Mycobacterium tuberculosis*. *ACS Infect Dis* **2**:500-508.
15. **Rao SP, Lakshminarayana SB, Kondreddi RR, Herve M, Camacho LR, Bifani P, Kalapala SK, Jiricek J, Ma NL, Tan BH, Ng SH, Nanjundappa M, Ravindran S, Seah PG, Thayalan P, Lim SH, Lee BH, Goh A, Barnes WS, Chen Z, Gagaring K, Chatterjee AK, Pethe K, Kuhen K, Walker J, Feng G, Babu S, Zhang L, Blasco F, Beer D, Weaver M, Dartois V, Glynne R, Dick T, Smith PW, Diagana TT, Manjunatha UH.** 2013. Indolcarboxamide is a preclinical candidate for treating multidrug-resistant tuberculosis. *Sci Transl Med* **5**:214ra168.
16. **Stec J, Onajole OK, Lun S, Guo H, Merenbloom B, Vistoli G, Bishai WR, Kozikowski AP.** 2016. Indole-2-carboxamide-based MmpL3 inhibitors show exceptional antitubercular activity in an animal model of tuberculosis infection. *J Med Chem* **59**:6232-6247.
17. **Lun S, Guo H, Onajole OK, Pieroni M, Gunosewoyo H, Chen G, Tipparaju SK, Ammerman NC, Kozikowski AP, Bishai WR.** 2013. Indoleamides are active against drug-resistant *Mycobacterium tuberculosis*. *Nat Commun* **4**:2907.
18. **Scherman MS, North EJ, Jones V, Hess TN, Grzegorzewicz AE, Kasagami T, Kim IH, Merzlikin O, Lenaerts AJ, Lee RE, Jackson M, Morisseau C, McNeil MR.** 2012. Screening a library of 1600 adamantyl ureas for anti-*Mycobacterium tuberculosis* activity in vitro and for better physical chemical properties for bioavailability. *Bioorg Med Chem* **20**:3255-3262.
19. **La Rosa V, Poce G, Canseco JO, Buroni S, Pasca MR, Biava M, Raju RM, Porretta GC, Alfonso S, Battilocchio C, Javid B, Sorrentino F, Ioerger TR, Sacchettini JC, Manetti F, Botta M, De Logu A, Rubin EJ, De Rossi E.** 2012. MmpL3 is the cellular target of the antitubercular pyrrole derivative BM212. *Antimicrob Agents Chemother* **56**:324-331.

20. **Deidda D, Lampis G, Fioravanti R, Biava M, Porretta GC, Zanetti S, Pompei R.** 1998. Bactericidal activities of the pyrrole derivative BM212 against multidrug-resistant and intramacrophagic *Mycobacterium tuberculosis* strains. *Antimicrob Agents Chemother* **42**:3035-3037.
21. **Stanley SA, Grant SS, Kawate T, Iwase N, Shimizu M, Wivagg C, Silvis M, Kazyanskaya E, Aquadro J, Golas A, Fitzgerald M, Dai H, Zhang L, Hung DT.** 2012. Identification of novel inhibitors of *M. tuberculosis* growth using whole cell based high-throughput screening. *ACS Chem Biol* **7**:1377-1384.
22. **Li W, Upadhyay A, Fontes FL, North EJ, Wang Y, Crans DC, Grzegorzewicz AE, Jones V, Franzblau SG, Lee RE, Crick DC, Jackson M.** 2014. Novel insights into the mechanism of inhibition of MmpL3, a target of multiple pharmacophores in *Mycobacterium tuberculosis*. *Antimicrob Agents Chemother* **58**:6413-6423.
23. **Remuinan MJ, Perez-Herran E, Rullas J, Alemparte C, Martinez-Hoyos M, Dow DJ, Afari J, Mehta N, Esquivias J, Jimenez E, Ortega-Muro F, Fraile-Gabaldon MT, Spivey VL, Loman NJ, Pallen MJ, Constantinidou C, Minick DJ, Cacho M, Rebollo-Lopez MJ, Gonzalez C, Sousa V, Angulo-Barturen I, Mendoza-Losana A, Barros D, Besra GS, Ballell L, Cammack N.** 2013. Tetrahydropyrazolo[1,5-a]pyrimidine-3-carboxamide and N-benzyl-6',7'-dihydrospiro[piperidine-4,4'-thieno[3,2-c]pyran] analogues with bactericidal efficacy against *Mycobacterium tuberculosis* targeting MmpL3. *PLoS One* **8**:e60933.
24. **Ioerger TR, O'Malley T, Liao R, Guinn KM, Hickey MJ, Mohaideen N, Murphy KC, Boshoff HI, Mizrahi V, Rubin EJ, Sasseti CM, Barry CE, 3rd, Sherman DR, Parish T, Sacchettini JC.** 2013. Identification of new drug targets and resistance mechanisms in *Mycobacterium tuberculosis*. *PLoS One* **8**:e75245.
25. **Feng X, Zhu W, Schurig-Briccio LA, Lindert S, Shoen C, Hitchings R, Li J, Wang Y, Baig N, Zhou T, Kim BK, Crick DC, Cynamon M, McCammon JA, Gennis RB, Oldfield E.** 2015. Antiinfectives targeting enzymes and the proton motive force. *Proc Natl Acad Sci U S A* **112**:E7073-7082.
26. **Li K, Schurig-Briccio LA, Feng X, Upadhyay A, Pujari V, Lechartier B, Fontes FL, Yang H, Rao G, Zhu W, Gulati A, No JH, Cintra G, Bogue S, Liu YL, Molohon K, Orlean P, Mitchell DA, Freitas-Junior L, Ren F, Sun H, Jiang T, Li Y, Guo RT, Cole ST, Gennis RB, Crick DC, Oldfield E.** 2014. Multitarget drug discovery for tuberculosis and other infectious diseases. *J Med Chem* **57**:3126-3139.
27. **Johnson BK, Colvin CJ, Needle DB, Mba Medie F, Champion PA, Abramovitch RB.** 2015. The carbonic anhydrase inhibitor ethoxzolamide inhibits the *Mycobacterium tuberculosis* PhoPR regulon and Esx-1 secretion and attenuates virulence. *Antimicrob Agents Chemother* **59**:4436-4445.

28. **Zheng H, Colvin CJ, Johnson BK, Kirchhoff PD, Wilson M, Jorgensen-Muga K, Larsen SD, Abramovitch RB.** 2017. Inhibitors of *Mycobacterium tuberculosis* DosRST signaling and persistence. *Nat Chem Biol* **13**:218-225.
29. **Mak PA, Rao SP, Ping Tan M, Lin X, Chyba J, Tay J, Ng SH, Tan BH, Cherian J, Duraiswamy J, Bifani P, Lim V, Lee BH, Ling Ma N, Beer D, Thayalan P, Kuhen K, Chatterjee A, Supek F, Glynn R, Zheng J, Boshoff HI, Barry CE, 3rd, Dick T, Pethe K, Camacho LR.** 2012. A high-throughput screen to identify inhibitors of ATP homeostasis in non-replicating *Mycobacterium tuberculosis*. *ACS Chem Biol* **7**:1190-1197.
30. **McNeil MB, Dennison D, Parish T.** 2017. Mutations in MmpL3 alter membrane potential, hydrophobicity and antibiotic susceptibility in *Mycobacterium smegmatis*. *Microbiology* **163**:1065-1070.
31. **Rao SP, Alonso S, Rand L, Dick T, Pethe K.** 2008. The protonmotive force is required for maintaining ATP homeostasis and viability of hypoxic, nonreplicating *Mycobacterium tuberculosis*. *Proc Natl Acad Sci U S A* **105**:11945-11950.
32. **Jaladanki CK, Taxak N, Varikoti RA, Bharatam PV.** 2015. Toxicity originating from thiophene containing drugs: exploring the mechanism using quantum chemical methods. *Chem Res Toxicol* **28**:2364-2376.
33. **Cox JA, Abrahams KA, Alemparte C, Ghidelli-Disse S, Rullas J, Angulo-Barturen I, Singh A, Gurcha SS, Nataraj V, Bethell S, Remuinan MJ, Encinas L, Jervis PJ, Cammack NC, Bhatt A, Kruse U, Bantscheff M, Futterer K, Barros D, Ballell L, Drewes G, Besra GS.** 2016. THPP target assignment reveals EchA6 as an essential fatty acid shuttle in mycobacteria. *Nat Microbiol* **1**:15006.
34. **Pethe K, Bifani P, Jang J, Kang S, Park S, Ahn S, Jiricek J, Jung J, Jeon HK, Cechetto J, Christophe T, Lee H, Kempf M, Jackson M, Lenaerts AJ, Pham H, Jones V, Seo MJ, Kim YM, Seo M, Seo JJ, Park D, Ko Y, Choi I, Kim R, Kim SY, Lim S, Yim SA, Nam J, Kang H, Kwon H, Oh CT, Cho Y, Jang Y, Kim J, Chua A, Tan BH, Nanjundappa MB, Rao SP, Barnes WS, Wintjens R, Walker JR, Alonso S, Lee S, Kim J, Oh S, Oh T, Nehrbass U, Han SJ, No Z, et al.** 2013. Discovery of Q203, a potent clinical candidate for the treatment of tuberculosis. *Nat Med* **19**:1157-1160.
35. **Johnson BK, Abramovitch RB.** 2015. Macrophage infection models for *Mycobacterium tuberculosis*. *Methods Mol Biol* **1285**:329-341.
36. **Williams EA, Mba Medie F, Bosserman RE, Johnson BK, Reyna C, Ferrell MJ, Champion MM, Abramovitch RB, Champion PA.** 2017. A nonsense mutation in *Mycobacterium marinum* that is suppressible by a novel mechanism. *Infect Immun* **85**:e00653-16

37. **McKenna A, Hanna M, Banks E, Sivachenko A, Cibulskis K, Kernytsky A, Garimella K, Altshuler D, Gabriel S, Daly M, DePristo MA.** 2010. The Genome Analysis Toolkit: a MapReduce framework for analyzing next-generation DNA sequencing data. *Genome Res* **20**:1297-1303.
38. **Baker JJ, Johnson BK, Abramovitch RB.** 2014. Slow growth of *Mycobacterium tuberculosis* at acidic pH is regulated by *phoPR* and host-associated carbon sources. *Mol Microbiol* **94**:56-69.
39. **Schneider CA, Rasband WS, Eliceiri KW.** 2012. NIH Image to ImageJ: 25 years of image analysis. *Nat Methods* **9**:671-675.
40. **Johnson BK, Scholz MB, Teal TK, Abramovitch RB.** 2016. SPARTA: Simple program for automated reference-based bacterial RNA-seq transcriptome analysis. *BMC Bioinformatics* **17**:66.
41. **Kelley LA, Mezulis S, Yates CM, Wass MN, Sternberg MJE.** 2015. The Phyre2 web portal for protein modeling, prediction and analysis. *Nature Protocols* **10**:845.

CHAPTER 5 – Concluding Remarks

Bacterial persistence is increasingly recognized as a threat to human health, as it may contribute to infectious disease treatment failure. Although currently available antibiotics are effective at killing replicating bacteria, the remaining persisters or non-replicating bacteria that survive antibiotic treatment represent a reservoir that can promote disease relapse. Additionally, survival of persisters can select for the evolution of drug-resistant bacterial strains, which further exacerbates the control of infectious diseases. Therefore, bacterial persistence is a fundamental problem in infectious disease research. Approaches for controlling bacterial persistence or eradicating the survivors of drug treatment represent important new avenues for drug development. This dissertation demonstrates new discoveries that may be applied to control bacterial persistence.

Mycobacterium tuberculosis (Mtb) is an excellent pathogen to study bacterial persistence because Mtb is well-known for shifting its physiology to a non-replicating persistence (NRP) state to survive in stressful environmental conditions. Although Mtb is a strict aerobe, it can remain viable for years in anaerobic conditions during dormancy (1). Non-replicating Mtb naturally tolerates many anti-mycobacterial drugs (2), and is a driving force of the long course of TB therapy. Therefore, one strategy to shorten and improve TB treatment is to inhibit Mtb from establishing and maintaining NRP.

Mtb uses the DosRST two-component regulatory system to promote NRP and enable it to establish and maintain a chronic infection. DosRST is not required *in vitro* under conditions of mild hypoxia, but is required for full virulence *in vivo* (1). Animal model studies show that deletion of *dosR* significantly reduces Mtb survival in different animal species that form hypoxic granulomas, including C3Heb/FeJ mice, non-human primates, and guinea pigs, suggesting the

DosRST pathway is a valid drug target (3-5). This dissertation presents a new approach to target the DosRST pathway using small molecule inhibitors discovered from whole cell phenotypic high-throughput screening (HTS). The reporter strain CDC1551 (*hspX'::GFP*) was used to screen for compounds that inhibit DosR-driven GFP fluorescence under hypoxic conditions, while having minimal impact on Mtb growth (Chapter 2). Six novel molecules HC101A-HC106A with distinct chemical structures were identified and characterized as DosRST inhibitors. To our knowledge, these are the first small molecules that inhibit the DosRST pathway by the presented mechanisms. The success of this HTS validates the use of a reporter strain to screen for virulence inhibitors. A series of physiology studies show that DosRST inhibitors can inhibit persistence-associated physiologies, including triacylglycerol biosynthesis, survival and antibiotic tolerance, providing proof-of-concept evidence that inhibiting Mtb from establishing or maintaining persistence is an effective way to kill Mtb (Chapter 2-3).

Biochemical studies revealed novel mechanisms of action for the compounds (Chapter 2-3). HC101A is the first-line antimalarial drug artemisinin that targets DosS/T heme, by modulating the heme iron redox state and alkylating the heme carried by the sensor histidine kinases. Interestingly, HC106A also interacts with the heme of DosS/T, likely by directly binding to the ferrous ion in a manner similar to natural ligands, such as carbon monoxide (CO) and nitric oxide (NO). Although both HC101A and HC106A target the heme of DosST, their inhibitory mechanisms are distinct. This result demonstrates that the heme is particularly vulnerable to chemical modulation to repress the DosRST pathway. This dissertation further shows that HC102A and HC103A may target the kinase domains of DosST by inhibiting their autophosphorylation activity, although further genetic and biochemical studies are required to define the precise mechanism of action. HC104A disrupts DosR DNA binding activity, without

modulating sensor kinase heme or autophosphorylation activity. Overall, these mechanistic studies demonstrate there are multiple mechanisms by which chemical probes can disrupt DosRST signaling.

This dissertation also shows that characterization of small molecules can be applied as chemical biology tools to study protein structure and function. For instance, modeling of the protein DosT with artemisinin revealed a channel on the protein that artemisinin can access to interact with the heme. To support the modeling results, amino acid substitutions E85L and G115L in DosS or G87L and G117L in DosT were tested in biochemical assays and shown to block the channel and provide resistance to artemisinin (Chapter 2). This study provides evidence that the channel is important for the protein function and can be targeted by small molecules and thus opens the door to screen for or design small molecules that target this channel. For instance, any molecules that can enter the channel and block it or modulate the heme may efficiently inactivate the protein DosS/T from sensing host signals. Moreover, HC106A binds to the ferrous ion of the heme like CO or NO (Chapter 3). Interestingly, CO or NO binding of heme activates the protein (6), whereas HC106A presumably inactivates the protein. Future structural biology comparisons examining conformational changes of DosS/T induced by the binding of HC106A, CO or NO can be performed to elucidate the mechanism of kinase activation. This information is important because the structural profiles can be used to design drugs that lock the protein in the inactive form via simulation. Furthermore, incorporating the protein channel information and ligand binding, more novel drugs can be designed to target the sensor domains of heme-based histidine kinases.

This study also supports the hypothesis that other heme-based sensor kinases may also be targeted by similar mechanisms. For instance, the newly discovered NO sensor, NosP, is a heme-containing sensor protein that regulates biofilm formation and quorum sensing in many bacteria,

including *Pseudomonas aeruginosa*, *Vibrio cholera*, *Legionella pneumophila* and *Shewanella oneidensis* (7, 8). Binding of NO to NosP inhibits the activity of the associated histidine kinase, and thus blocks phosphate flux to activate the signaling pathways. NtrY/NtrX is the two-component system that regulates gene expression of a nitrogen respiration enzyme in *Brucella abortus* (9). This system functions more like DosRST, where NtrY is a redox sensor that employs the heme group in the PAS domain to sense the environmental cues, including NO, CO and oxygen level. It can be quickly oxidized in the presence of oxygen, whereas it is activated under low oxygen level to induce the NtrX regulon. RcoM is a single-component transcriptional regulator that induces the CO oxidation operon in responding to CO in *Burkholderia xenovorans* (10). It has a PAS sensor domain in the N-terminus, and a LytTR DNA-binding domain in the C-terminus. The heme group of RcoM can bind to CO to activate the protein for binding to the targeted genes. In the future, we hope to examine the impact of heme-targeting molecules on these diverse environmental sensors.

Two-component regulatory systems play essential roles in bacterial signaling, and are often required for bacterial pathogenesis. Many inhibitors have been discovered and proven as an effective way to control bacterial pathogenesis (11-13). An early study found the chemical inhibitors of the AlgR2/AlgR1 two-component regulatory system that is involved in the regulation of alginate production in *P. aeruginosa* (14). These inhibitors repressed autophosphorylation activity of AlgR2, analogous to how we propose HC102A and HC103A may inhibit DosST, and another inhibitor targeted DNA-binding activity of AlgR1, analogous to how we think HC104A may target DosR. They have therapeutic potential to treat *P. aeruginosa* infections in cystic fibrosis patients (14). Another notable inhibitor, LED209, was found to have a broad spectrum of activity against multiple Gram-negative bacteria by inhibiting the conserved histidine kinase,

QseC (15). QseC can activate multiple response regulators that control the induction of the locus enterocyte effacement, as well as Shiga toxin production in different bacterial species. Animal studies show that LED209 significantly improves survival of mice infected with *Salmonella typhimurim* and *Francisella tularensis* (16). Ethoxzolamide was discovered as an inhibitor of the PhoPR system involved in sensing several environmental cues, such as acidic pH and chloride (17). Mtb treated with ethoxzolamide have reduced virulence lipid production, as well as inhibition of the Esx-1 secretion system. Mice treated with ethoxzolamide also have reduced bacterial burdens following TB infection. Together, data presented in this dissertation, along with these other examples support the conclusion that two-component regulatory systems are good drug targets to treat pathogenic bacteria to control infectious diseases.

Additionally, this dissertation discovered an impact of artemisinin on Mtb. The recent advances in antimalarials have identified several novel synthetic endoperoxides that are effective as antimalarials (18-22). It would be interesting to see if those synthetic endoperoxides also have an impact on modulating the DosRST signaling pathway. Furthermore, modification of the chemical structure to become more TB specific would be ideal, so there is reduced overlap between malaria and TB treatments. Co-infection of malaria and TB is not commonly reported, but cases have been described in some developing countries (23). Given the high prevalence of latent TB in the developing world, it is highly likely many individuals with malaria are chronically infected with TB. Findings from this dissertation raise potential concerns about the impact of artemisinin treatment on TB in co-infected patients. It is unknown whether treating co-infected patients with artemisinin to cure malaria has any impact on latent TB. There might exist a risk that artemisinin treatment can reactivate Mtb from dormancy by inhibiting the DosRST pathway.

Lastly, this dissertation describes the discovery and characterization of another compound, HC2091, that kills Mtb by targeting MmpL3 (Chapter 4). Many MmpL3 inhibitors have been reported in the literature, however many of the previously discovered inhibitors have liabilities including poor solubility (24, 25). HC2091 exhibits no cross-resistance with the well characterized MmpL3 inhibitor SQ109, and the HC2091 resistance mutations are observed in distinct areas of the gene. Together, these data suggest that the compounds might use different mechanisms to inhibit MmpL3. HC2091 has high solubility (>200 μ M) and low cytotoxicity, characteristics that support continued studies of HC2091 as a candidate for treating TB disease. Further efforts to optimize potency and ascertain drug metabolism and pharmacokinetic properties of HC2091 are required to determine if it could be pursued as a potential TB therapeutic.

There remain significant future studies that will need to be undertaken to follow up the research presented in this dissertation. This dissertation presents the initial discovery and characterization of the DosRST inhibitors HC101A-HC106A, and shows that these inhibitors reduce Mtb survival and antibiotic tolerance *in vitro*. However, in order to further develop these inhibitors, several additional experiments are required. For instance, testing DosRST inhibitors in TB infection animal models, such as C3Heb/FeJ mice, and specifically examining the ability of these compounds to reduce Mtb survival and antibiotic tolerance. Large scale structure-function relationship studies should be performed for the compounds discovered in this dissertation, including DosRST inhibitors and HC2091, in order to optimize their potency and pharmacokinetic properties and to prioritize compounds for animal efficacy studies.

This dissertation presents chemical biology based approaches to define novel mechanisms of inhibiting the Mtb two-component regulatory system DosRST. The studies provide proof-of-concept evidence supporting our original hypothesis that inhibiting Mtb from establishing NRP

via chemical inhibition of the DosRST pathway will reduce Mtb survival and antibiotic tolerance. In addition, I have shown multiple, distinct mechanisms of action for the inhibitors to repress DosRST signaling. This work has furthered our understanding of how to target two-component regulatory systems that are important for virulence. Moreover, I discovered an MmpL3 inhibitor that is effective against Mtb. Together, these studies advance our knowledge of Mtb physiology and biochemistry. The findings support new avenues to combat this deadly disease and, thus, this research has the potential to improve TB treatment and global health.

REFERENCES

REFERENCES

1. **Leistikow RL, Morton RA, Bartek IL, Frimpong I, Wagner K, Voskuil MI.** 2010. The *Mycobacterium tuberculosis* DosR regulon assists in metabolic homeostasis and enables rapid recovery from nonrespiring dormancy. *J Bacteriol* **192**:1662-1670.
2. **Rao SP, Alonso S, Rand L, Dick T, Pethe K.** 2008. The protonmotive force is required for maintaining ATP homeostasis and viability of hypoxic, nonreplicating *Mycobacterium tuberculosis*. *Proc Natl Acad Sci U S A* **105**:11945-11950.
3. **Converse PJ, Karakousis PC, Klinkenberg LG, Kesavan AK, Ly LH, Allen SS, Grosset JH, Jain SK, Lamichhane G, Manabe YC, McMurray DN, Nuermberger EL, Bishai WR.** 2009. Role of the dosR-dosS two-component regulatory system in *Mycobacterium tuberculosis* virulence in three animal models. *Infect Immun* **77**:1230-1237.
4. **Gautam US, McGillivray A, Mehra S, Didier PJ, Midkiff CC, Kisse RS, Golden NA, Alvarez X, Niu T, Rengarajan J, Sherman DR, Kaushal D.** 2015. DosS is required for the complete virulence of *Mycobacterium tuberculosis* in mice with classical granulomatous lesions. *Am J Respir Cell Mol Biol* **52**:708-716.
5. **Mehra S, Foreman TW, Didier PJ, Ahsan MH, Hudock TA, Kisse R, Golden NA, Gautam US, Johnson AM, Alvarez X, Russell-Lodrigue KE, Doyle LA, Roy CJ, Niu T, Blanchard JL, Khader SA, Lackner AA, Sherman DR, Kaushal D.** 2015. The DosR regulon modulates adaptive immunity and is essential for *Mycobacterium tuberculosis* persistence. *Am J Respir Crit Care Med* **191**:1185-1196.
6. **Kumar A, Toledo JC, Patel RP, Lancaster JR, Jr., Steyn AJ.** 2007. *Mycobacterium tuberculosis* DosS is a redox sensor and DosT is a hypoxia sensor. *Proc Natl Acad Sci U S A* **104**:11568-11573.
7. **Hossain S, Boon EM.** 2017. Discovery of a novel nitric oxide binding protein and nitric-oxide-responsive signaling pathway in *Pseudomonas aeruginosa*. *ACS Infect Dis* **3**:454-461.
8. **Williams DE, Nisbett LM, Bacon B, Boon E.** 2017. Bacterial heme-based sensors of nitric oxide. *Antioxid Redox Signal* **00**:1-16.
9. **Carrica Mdel C, Fernandez I, Marti MA, Paris G, Goldbaum FA.** 2012. The NtrY/X two-component system of *Brucella* spp. acts as a redox sensor and regulates the expression of nitrogen respiration enzymes. *Mol Microbiol* **85**:39-50.
10. **Kerby RL, Youn H, Roberts GP.** 2008. RcoM: a new single-component transcriptional regulator of CO metabolism in bacteria. *J Bacteriol* **190**:3336-3343.

11. **Gotoh Y, Eguchi Y, Watanabe T, Okamoto S, Doi A, Utsumi R.** 2010. Two-component signal transduction as potential drug targets in pathogenic bacteria. *Curr Opin Microbiol* **13**:232-239.
12. **Matsushita M, Janda KD.** 2002. Histidine kinases as targets for new antimicrobial agents. *Bioorg Med Chem* **10**:855-867.
13. **Johnson BK, Abramovitch RB.** 2017. Small molecules that sabotage bacterial virulence. *Trends Pharmacol Sci* **38**:339-362.
14. **Roychoudhury S, Zielinski NA, Ninfa AJ, Allen NE, Jungheim LN, Nicas TI, Chakrabarty AM.** 1993. Inhibitors of two-component signal transduction systems: inhibition of alginate gene activation in *Pseudomonas aeruginosa*. *Proc Natl Acad Sci U S A* **90**:965-969.
15. **Rasko DA, Moreira CG, Li de R, Reading NC, Ritchie JM, Waldor MK, Williams N, Taussig R, Wei S, Roth M, Hughes DT, Huntley JF, Fina MW, Falck JR, Sperandio V.** 2008. Targeting QseC signaling and virulence for antibiotic development. *Science* **321**:1078-1080.
16. **Curtis MM, Russell R, Moreira CG, Adebessin AM, Wang C, Williams NS, Taussig R, Stewart D, Zimmermann P, Lu B, Prasad RN, Zhu C, Rasko DA, Huntley JF, Falck JR, Sperandio V.** 2014. QseC inhibitors as an antivirulence approach for Gram-negative pathogens. *MBio* **5**:e02165.
17. **Johnson BK, Colvin CJ, Needle DB, Mba Medie F, Champion PA, Abramovitch RB.** 2015. The carbonic anhydrase inhibitor ethoxzolamide inhibits the *Mycobacterium tuberculosis* PhoPR regulon and Esx-1 secretion and attenuates virulence. *Antimicrob Agents Chemother* **59**:4436-4445.
18. **Charman SA, Arbe-Barnes S, Bathurst IC, Brun R, Campbell M, Charman WN, Chiu FC, Chollet J, Craft JC, Creek DJ, Dong Y, Matile H, Maurer M, Morizzi J, Nguyen T, Papastogiannidis P, Scheurer C, Shackelford DM, Sriraghavan K, Stingelin L, Tang Y, Urwyler H, Wang X, White KL, Wittlin S, Zhou L, Vennerstrom JL.** 2011. Synthetic ozonide drug candidate OZ439 offers new hope for a single-dose cure of uncomplicated malaria. *Proc Natl Acad Sci U S A* **108**:4400-4405.
19. **Vennerstrom JL, Arbe-Barnes S, Brun R, Charman SA, Chiu FC, Chollet J, Dong Y, Dorn A, Hunziker D, Matile H, McIntosh K, Padmanilayam M, Santo Tomas J, Scheurer C, Scorneaux B, Tang Y, Urwyler H, Wittlin S, Charman WN.** 2004. Identification of an antimalarial synthetic trioxolane drug development candidate. *Nature* **430**:900-904.
20. **O'Neill PM, Amewu RK, Nixon GL, Bousejra ElGarah F, Mungthin M, Chadwick J, Shone AE, Vivas L, Lander H, Barton V, Muangnoicharoen S, Bray PG, Davies J, Park BK, Wittlin S, Brun R, Preschel M, Zhang K, Ward SA.** 2010. Identification of a

- 1,2,4,5-tetraoxane antimalarial drug-development candidate (RKA 182) with superior properties to the semisynthetic artemisinins. *Angew Chem Int Ed Engl* **49**:5693-5697.
21. **Rudrapal M, Chetia D.** 2016. Endoperoxide antimalarials: development, structural diversity and pharmacodynamic aspects with reference to 1,2,4-trioxane-based structural scaffold. *Drug Des Devel Ther* **10**:3575-3590.
 22. **O'Neill PM, Amewu RK, Charman SA, Sabbani S, Gnadig NF, Straimer J, Fidock DA, Shore ER, Roberts NL, Wong MH, Hong WD, Pidathala C, Riley C, Murphy B, Aljayoussi G, Gamo FJ, Sanz L, Rodrigues J, Cortes CG, Herreros E, Angulo-Barturen I, Jimenez-Diaz MB, Bazaga SF, Martinez-Martinez MS, Campo B, Sharma R, Ryan E, Shackelford DM, Campbell S, Smith DA, Wirjanata G, Noviyanti R, Price RN, Marfurt J, Palmer MJ, Copple IM, Mercer AE, Ruecker A, Delves MJ, Sinden RE, Siegl P, Davies J, Rochford R, Kocken CHM, Zeeman AM, Nixon GL, Biagini GA, Ward SA.** 2017. A tetraoxane-based antimalarial drug candidate that overcomes Pfk13-C580Y dependent artemisinin resistance. *Nat Commun* **8**:15159.
 23. **Li XX, Zhou XN.** 2013. Co-infection of tuberculosis and parasitic diseases in humans: a systematic review. *Parasit Vectors* **6**:1-12.
 24. **Jia L, Tomaszewski JE, Hanrahan C, Coward L, Noker P, Gorman G, Nikonenko B, Protopopova M.** 2005. Pharmacodynamics and pharmacokinetics of SQ109, a new diamine-based antitubercular drug. *Br J Pharmacol* **144**:80-87.
 25. **Jia L, Noker PE, Coward L, Gorman GS, Protopopova M, Tomaszewski JE.** 2006. Interspecies pharmacokinetics and in vitro metabolism of SQ109. *Br J Pharmacol* **147**:476-485.